



Dean, Robert Thomas Gregory (2014) *An investigation into cellular stress pathways in Hodgkin lymphoma*. PhD thesis.

<http://theses.gla.ac.uk/5225/>

Copyright and moral rights for this work are retained by the author

A copy can be downloaded for personal non-commercial research or study, without prior permission or charge

This work cannot be reproduced or quoted extensively from without first obtaining permission in writing from the author

The content must not be changed in any way or sold commercially in any format or medium without the formal permission of the author

When referring to this work, full bibliographic details including the author, title, awarding institution and date of the thesis must be given

Enlighten:Theses
<http://theses.gla.ac.uk/>
theses@gla.ac.uk

An investigation into cellular stress pathways in Hodgkin lymphoma

Robert Thomas Gregory Dean

BSc (Hons), MRes

Submitted in fulfilment of the requirements for the Degree of Doctor of Philosophy

Institute of Infection, Immunity and Inflammation

College of Medical, Veterinary and Life Sciences

University of Glasgow

April 2014

© Robert Dean, 2014

Abstract

Hodgkin lymphoma (HL) is one of the most common haematological malignancies in the Western world. Although HL responds favourably to cytotoxic therapy in the majority of cases, late side-effects such as secondary malignancies and cardiovascular disease are becoming of great concern, particularly in younger patients. The current challenges are to maintain treatment efficacy whilst reducing side-effects and to develop biomarkers to predict response to treatment(s). Protein degradation pathways in HL cells have remained largely unstudied in this malignancy and represent an opportunity for more targeted therapy. This thesis describes the activities of protein degradation pathways in HL-derived cell lines and their sensitivities to inhibition. The results suggest that the use of proteasome and HDAC6 inhibitors, alone or in combination, may be of clinical benefit in the treatment of HL in the future. The presence of p62 was used to monitor protein handling stress; however, its diverse expression patterns in HL-derived cell lines and in paraffin-embedded HL biopsy material preclude its use as an informative biomarker in HL. p62 was found to traffic between the cytoplasm and nucleus in HL-derived cell lines and its association with a DNA damage marker in both cellular compartments implicate it as a chaperone for the cytoplasmic degradation of nuclear proteins. A previously unreported nuclear expression of the lysosomal enzyme cathepsin B in HL-derived cell lines was identified, and this may have implications for the aberrant transcriptional profile of these cells given the regulatory activities of other members of this family of cysteine proteases. The non-lymphoid origin of the HD-MyZ cell line, a putative HL-derived cell line, was corroborated by phenotypic differences in protein handling pathways in comparison to accepted HL-derived cell lines. The activities and insensitivity to inhibition of protein handling pathways in this cell line suggest that it will be an interesting model for studying alternative protein degradation pathways. The presence of a number of small cell populations with cancer stem cell (CSC)-like characteristics was confirmed in HL-derived cell lines and, although these populations require further characterisation, this has implications for HL patients who suffer relapse.

Table of Contents

Abstract	2
Table of Contents	3
List of Tables	7
List of Figures	8
Acknowledgements	11
Author Declaration	12
Symbols and Abbreviations	13
Chapter 1. Introduction	20
1.1 The Cell Biology of Hodgkin lymphoma	21
1.1.1 Hodgkin Lymphoma	21
1.1.2 Cellular origin of HL.....	21
1.1.3 Transcriptional reprogramming	23
1.1.4 Epigenetic silencing.....	24
1.1.5 Interactions with the immune system	25
1.1.6 Constitutively active signalling pathways.....	29
1.1.6.1 The NFkB pathway in HL.....	29
1.1.6.2 JAK/STAT signalling in HL.....	32
1.1.6.3 ERK/MAPK and Akt signalling pathways	34
1.1.7 HL-derived cell lines and mouse models.....	36
1.1.7.1 HL-derived cell lines	36
1.1.7.2 Animal models of HL.....	38
1.1.8 Current treatments of HL.....	39
1.1.8.1 Treatment Options	39
1.1.8.2 Side-effects.....	41
1.1.8.3 Novel agents against HL.....	41
1.2 Protein degradation pathways	42
1.2.1 Ubiquitin	42
1.2.2 The Proteasome.....	44
1.2.3 Protein aggregation and aggresome formation	48
1.2.4 Autophagy	49
1.2.5 p62/ Sequestosome 1 (SQSTM1)	54
1.2.6 Autophagy and disease.....	59

1.3	Summary	61
1.4	Aims.....	62
Chapter 2. Materials and Methods.....		63
2.1	Suppliers and Manufacturers	64
2.2	Consumables.....	66
2.3	Equipment.....	67
2.4	Cell Culture	67
2.5	Cell counts with Trypan Blue dye exclusion.....	69
2.6	Cryopreservation of Cells.....	69
2.7	Immunocytochemistry	70
2.7.1	Solutions	70
2.7.2	Procedure.....	70
2.8	Immunohistochemistry (IHC)	72
2.9	SDS-PAGE and Western blot	73
2.9.1	Solutions	73
2.9.2	Cell lysis	75
2.9.3	Protein separation	75
2.9.4	Western blotting	76
2.9.5	Membrane stripping and re-probing for loading controls	76
2.10	Drug Treatments for ICH/western blotting	77
2.11	Chymotrypsin-like Proteasome activity	78
2.12	Autophagy activity	79
2.13	Viability assay.....	80
2.14	Mitochondrial permeability.....	80
2.15	Statistical analysis	811
2.16	Cell cycle analysis using propidium iodide (PI).....	81
2.17	Detection of CD30, CD20 and CD27 by flow cytometry	81
2.18	Side population analysis by Hoechst 33342 dye exclusion	82
2.19	Side population analysis by Vybrant® DyeCycle Violet	82
2.20	ALDEFLUOR™ assay	833
2.21	Measurement of reactive oxygen species (ROS)	83
2.22	Fluorescence-activated cell sorting	83
2.22.1	FACS of Hoechst 33342 stained SP cells.....	844
2.22.2	FACS of Vybrant® DyeCycle Violet stained SP cells.....	84
2.22.3	FACS of ROS ^{low} and ROS ^{hi} cells.....	84

Chapter 3. p62 expression in HL-derived cell lines and in patient sections 866

3.1	Summary	877
3.2	Introduction	888
3.3	Results.....	900
3.3.1	Basal p62 expression in HL-derived cell lines	900
3.3.2	p62 staining in patient sections	933
3.3.3	Nucleo-cytoplasmic shuttling of p62.....	955
3.3.4	Proteasome inhibition in HL-derived cell lines.....	977
3.4	Discussion	101

Chapter 4. Protein handling pathways in HL-derived cell lines 105

4.1	Summary	106
4.2	Introduction	107
4.3	Results.....	110
4.3.1	Basal proteasome and autophagy activity in HL-derived cell lines..	110
4.3.2	Evidence of mitophagy in HL-derived cell lines	113
4.3.3	Evidence of polarised protein degradation in HL-derived cell lines .	119
4.3.4	Proteasome inhibition in HL-derived cell lines.....	125
4.3.5	Autophagy inhibition in HL-derived cell lines	127
4.3.6	HDAC6 inhibition in HL-derived cell lines	130
4.3.7	Nuclear targets of p62.....	134
4.3.8	BML-281 causes DSBs in prophase-like cells.....	138
4.3.9	Dual protein-handling pathway inhibition.....	140
4.3.10	Mechanism of cell death following proteasome- and HDAC6- inhibition	141
4.4	Discussion	144
4.4.1	Proteasome activity does not directly correlate with sensitivity to proteasome inhibition.....	144
4.4.2	Sequestration of p62 into aggregates correlates with cell death in the L-540 cell line.....	144
4.4.3	Cytoplasmic aggregates of p62 were found to increase under conditions of increased and stalled autophagic flux.....	145
4.4.4	Non-reciprocal compensation of pathway activity.....	146
4.4.5	A unique constitutively nuclear fraction of p62 was identified in L-1236 cells.....	147
4.4.6	Spatial restriction of p62 expression in L-428 cells was not due to its role in mitophagy	148
4.4.7	Evidence of polarisation of protein handling in L-428 cells.....	148

4.4.8	HDAC6 inhibition provoked a mitotic phenotype associated with DNA damage.....	150
4.4.9	Combined proteasome and HDAC6 inhibition was the most effective cytotoxic drug combination	151
Chapter 5. Further examination of the HD-MyZ cell line.....		153
5.1	Summary	154
5.2	Introduction	155
5.3	Results.....	158
5.3.1	Parkin appears to localise with microtubules.....	158
5.3.2	Withaferin A treatment.....	168
5.3.3	The effect of WFA on vimentin	170
5.3.4	The effect of WFA on p62 distribution	176
5.4	Discussion	180
Chapter 6. Putative cancer stem cells in HL-derived cell lines		188
6.1	Summary	189
6.2	Introduction	190
6.3	Results.....	198
6.3.1	CD30 ⁻ CD20 ⁺ CD27 ⁺ Cells in KM-H2 and L-428	198
6.3.2	Hoechst 33342 Side Population	200
6.3.3	DyeCycle Violet (DCV) Side population	202
6.3.4	ALDEFLUOR™ Assay	207
6.3.5	Reactive Oxygen Species	208
6.4	Discussion	214
Chapter 7. Concluding Remarks.....		219
7.1	Concluding remarks.....	220
References.....		227

List of Tables

Table 1-1 HL-derived cell lines.....	38
Table 1-2 Ann Arbor staging system for HL.....	40
Table 1-2 Components of the 26S proteasome and their known functions.....	47
Table 2-1 Suppliers and Manufacturers.....	64
Table 2-2 Equipment and suppliers.....	67
Table 2-3 Commonly used media and buffers.....	68
Table 2-4 Buffers used for immunocytochemistry.....	70
Table 2-5 Antibodies used for immunocytochemistry.....	71
Table 2-6 Buffers and gel recipes used for SDS-PAGE and western blotting.....	73
Table 2-7 Antibodies used for western blotting.....	77

List of Figures

Figure 1-1 HRS cell interactions with the cellular microenvironment	27
Figure 1-2 NF κ B signalling pathway in HL	31
Figure 1-3 The JAK-STAT signalling pathway in HL	33
Figure 1-4 ERK/MAPK and AKT signalling through tyrosine receptor kinases	35
Figure 1-5 Components of the 26S Proteasome.....	45
Figure 1-6 The three forms of autophagy.....	51
Figure 1-7 Autophagosome biogenesis	53
Figure 1-8 Representation of organisation of the functional domains of p62	56
Figure 3-1 p62 expression in HL-derived cell lines as measured by immunocytochemistry.	911
Figure 3-2 p62 expression in HL-derived cell lines as measured by western blotting.	922
Figure 3-3 p62 staining patterns in HL patient biopsy material.	944
Figure 3-4 p62 is trapped in the nucleus following Leptomycin B treatment.	966
Figure 3-5 Examples of p62 localisation with PML bodies in Leptomycin B treated KM-H2 cells.....	977
Figure 3-6 p62 distribution following proteasome inhibition.	999
Figure 3-7 Effect of Bortezomib on proteasome activity.....	100
Figure 4-1 Basal proteasome and autophagy activity in HL-derived cell lines. ...	112
Figure 4-2 p62 “fleck” in KM-H2 cells.....	114
Figure 4-3 Distribution of mitochondria in KM-H2 and L-428 cells.	115
Figure 4-4 MitoTracker™-retaining mitochondria can accumulate in an MTOC-like distribution	116
Figure 4-5 Parkin expression in KM-H2 and L-428.	118
Figure 4-6 Distribution of mitochondria, p62 and LAMP2 in L-428.....	120
Figure 4-7 Vimentin and Tom20 distribution in HL-derived cell lines.	122
Figure 4-8 γ -tubulin and Tom20 distribution in HL-derived cell lines.....	123
Figure 4-9 LAMP2 and TARC distribution in HL-derived cell lines.....	124
Figure 4-10 Effect of Bortezomib on proteasome activity, cell viability and autophagy activity.	126
Figure 4-11 Proteasome inhibition results in G2/M arrest in KM-H2 cells.	127

Figure 4-12 p62 distribution following autophagy inhibition.....	129
Figure 4-13 Effect of Bafilomycin A1 on cell viability and proteasome activity. ...	130
Figure 4-14 p62 distribution following HDAC6 inhibition.	131
Figure 4-15 Effect of HDAC6 inhibition on cell viability.	132
Figure 4-16 Effects of BML-281 on acetylated tubulin and histone H3.	133
Figure 4-17 K48-linked polyubiquitinated proteins are found mostly in the nuclei of HL-derived cell lines, which also contain high levels of DNA damage.	135
Figure 4-18 p62 juxtaposes and co-localises with γ H2AX puncta in KM-H2 and L- 1236.....	137
Figure 4-19 BML-281 causes DSBs in mitotic cells.	139
Figure 4-20 Effect of dual proteasome and autophagy or HDAC6 inhibition on cell viability.	141
Figure 4-21 Confirmation of cell death following proteasome and HDAC6 inhibition.	143
Figure 5-1 Parkin expression in HD-MyZ	159
Figure 5-2 Distribution of vimentin and microtubules in HD-MyZ	161
Figure 5-3 HD-MyZ is no more susceptible to Paclitaxel than other HL-derived cell lines	162
Figure 5-4 Vimentin expression in HD-MyZ	163
Figure 5-5 Partially condensed chromatin in HD-MyZ.....	164
Figure 5-6 Cathepsin B expression in HL-derived cell lines.....	165
Figure 5-7 Cathepsin B does not change after interference with protein handling pathways.....	166
Figure 5-8 Discrepancies in vimentin cleavage products	167
Figure 5-9 Effects of WFA on cell viability and cell cycle status.....	169
Figure 5-10 WFA targets vimentin in HD-MyZ but not other HL-derived cell lines	171
Figure 5-11 Effect of WFA on vimentin expression in HD-MyZ.....	173
Figure 5-12 Effect of WFA on vimentin expression in L-540 and KM-H2	174
Figure 5-13 Effect of WFA on vimentin expression in L-428	175
Figure 5-14 Effect of WFA on p62 expression in L-540 and KM-H2	177
Figure 5-15 Effect of WFA on p62 expression in L-428 and HD-MyZ	178

Figure 5-16 Effect of WFA on p62 in HD-MyZ and on K48-linked polyubiquitin levels.....	179
Figure 6-1 Example of side population analysis.....	192
Figure 6-2 Example of ALDEFLUOR™ analysis.....	193
Figure 6-3 CD30 ⁺ but not CD20 ⁺ or CD27 ⁺ cells were detected in the KM-H2 cell line.	199
Figure 6-4 CD20 ⁺ and CD27 ⁺ cells were not detected in the L-428 cell line.	200
Figure 6-5 SP cells were identified in the KM-H2 cell line using Hoechst 33342 dye efflux.	202
Figure 6-6 Vybrant® DyeCycle Violet SP cells were detected in the L-428 cell line.	203
Figure 6-7 Vybrant® DyeCycle Violet SP was detected in the KM-H2 cell line...	204
Figure 6-8 No differences were observed in the expression of PML, γH2AX, Tom20, Vimentin or p62 in SP vs non-SP cells.....	206
Figure 6-9 A small population of ALDH ^{hi} cells were identified in the L-428 and L-1236 cell lines.....	207
Figure 6-10 ROS expression is not cell size dependent	208
Figure 6-11 ROS ^{low} cells in L-428 and L-1236 cell lines tend to be smaller cells while ROS ^{hi} cells are heterogeneous in size.....	209
Figure 6-12 ALDH ^{hi} cells displayed heterogeneous ROS levels	211
Figure 6-13 ROS ^{low} cells do not fall within the ALDH ^{hi} population in the L-428 cell line.	212
Figure 6-14 ROS ^{low} cells do not fall within the ALDH ^{hi} population in the L-1236 cell line.	213

Acknowledgements

This thesis would not have been possible without the help and support of a number of individuals. Firstly, I'd like to thank my supervisor Dr. Tina Rich for her invaluable guidance throughout the duration of this project. I'm truly grateful for all of her advice and support, without which this work would not have been possible. I'd also like to thank my co-supervisor Professor Ruth Jarrett for her help and advice during the course of this project and during the writing up process.

I'd like to thank all of the members of the LRF Virus Centre, past and present, Dr. Alice Gallagher, Ms. Annette Lake, Dr. Katrina Farrell, Dr. Karen McAuley (and Maisie!), Ms. Leslie Shield, and Mrs. Shauna Crae, for all of their help and for creating such a friendly and enjoyable working environment. In particular, I'd like to thank Ms. Dorothy Montgomery for all of her help and support in dealing with cell and flow cytometry dramas.

From the MacRoberts Lab, I'd like to thank Mrs. Elizabeth Gault, Mr. Edward Dornan and Dr. Mary Donaldson for all of their assistance and support. I'd also like to thank my assessors Dr. Anna Kilbey, Dr. Julia Edgar and Professor Iain Morgan for their advice and constructive comments during the assessment process.

Thanks go to the Veterinary Diagnostic Services at the University of Glasgow Veterinary School, particularly Mrs. Lynn Stevenson and Ms. Lynn Oxford, for the immunohistochemical staining of the paraffin-embedded HL biopsy samples.

Finally, I'm extremely grateful for the support of all my friends and family. Thanks for keeping me relatively sane and getting me through the last year, I couldn't have done it without you.

Author Declaration

I declare that this thesis is the result of my own work and has not been submitted for any other degree at the University of Glasgow or any other institution. Collaborative work is acknowledged where present.

Signature _____

Printed name _____

Date _____

Symbols and Abbreviations

List of Symbols

α	Alpha
β	Beta
γ	Gamma
ϵ	Epsilon
κ	Kappa
μl	Micro litre
μg	Micro gram
μM	Micro molar
$^{\circ}\text{C}$	Degrees centigrade
w/v	Weight per volume

List of Abbreviations

3-MA	3-methyladenine
ABF1	Autonomously replicating sequence binding factor 1
ABVD	Adriamycin (doxorubicin), Bleomycin, Vinblastine, Dacarbazine
AIRAPL	Arsenite-inducible RNA-associated protein-like protein
ALDH	Aldehyde dehydrogenase
ALIS	Aggresome-like inducible structure
AML	Acute myeloid leukaemia
AMP	Adenosine monophosphate
AMPK	AMP-activated protein kinase
aPKC	Atypical protein kinase C
APRIL	A proliferation-inducing ligand
ATG	Autophagy related gene
ATP	Adenosine triphosphate
BAA ⁻	BODIPY aminoacetate

BAAA	BODIPY aminoacetylaldehyde
BAD	Bcl-2 associated agonist of cell death
BAFF	B-cell activating factor
Bcl-2	B-cell lymphoma 2
BCMA	B cell maturation antigen
BEACOPP	Bleomycin, Etoposide, Adriamycin (Doxorubicin), Cyclophosphamide, Oncovin (Vincristine), Prednisone, Procarbazine
Bob1	B cell oct-binding protein 1
BODIPY	Boron-dipyrromethene
BRCA1	Breast cancer 1, early onset
BSA	Bovine serum albumin
CCCP	Carbonyl cyanide 3-chlorophenylhydrazone
CCL	Chemokine (C-C motif) ligand
CD	Cluster of differentiation
CDKN2C	Cyclin-dependent kinase inhibitor 2C
CDP/Cux	CCAAT-displacement protein/Cut homeobox
CHEK2	Checkpoint kinase 2
CIC	Cancer initiating cell
CIC	Cancer-initiating cell
CMA	Chaperone-mediated autophagy
CML	Chronic myeloid leukaemia
CQ	Chloroquine
CSC	Cancer stem-like cell
CSF-1	Colony stimulating factor 1
CYLD	Cylindromatosis
DAPI	4',6-diamidino-2-phenylindole
Ddi1	DNA damage-inducible protein 1
DDR2	Discoidin domain receptor 2
DEAB	Diethylamino-benzaldehyde
dH ₂ O	distilled H ₂ O
DISC	Death inducing signalling complex
DMSO	dimethylsulphoxide
DNA	Deoxyribonucleic acid

DR	Death receptor
DSB	Double strand break
Dsk2	Ubiquitin domain-containing protein Dsk2
DUB	Deubiquitinating enzyme
EBF	Early B cell factor
EBV	Epstein-Barr Virus
EDTA	ethylenediaminetetraacetic acid
EPHB1	Ephrin receptor B1
ER	Endoplasmic reticulum
ERK	Extracellular signal-regulated kinase
FACS	Fluorescence-activated cell sorting
FBS	Foetal bovine serum
FETF	Freedom from treatment failure
GAB1	GRB2-associated binding protein 1
GAN	Giant axonal neuropathy
GAPDH	glyceraldehyde 3-phosphate dehydrogenase
GATA3	GATA-binding protein 3
GC	Germinal centre
GDP	Guanosine diphosphate
GM-CSF	Granulocyte-macrophage colony-stimulating factor
GPX	Glutathione peroxidase
GRB2	Growth factor receptor bound protein 2
GTP	Guanosine triphosphate
GTPase	Guanosine triphosphatase
H	Hodgkin cell
HCQ	Hydroxychloroquine
HDAC	Histone deacetylase
HDM2	Human double minute 2 homolog
HGF	Hepatocyte growth factor
HL	Hodgkin lymphoma
HRP	Horseradish peroxidase
HRS	Hodgkin/Reed-Sternberg cell
HSC	Haematopoietic stem cell

Hsc70	Heat shock cognate protein 70
ID2	Inhibitor of DNA binding 2
IFN	Interferon
Ig	Immunoglobulin
IKK	I κ B kinase
IL	Interleukin
IRF8	IFN regulatory factor 8
I κ B	Inhibitor of NF κ B
JAK	Janus kinase
K	Lysine
KEAP1	Kelch-like ECH-associated protein 1
KIR	KEAP1 interacting region
KLF4	Kruppel-like factor 4
LAMP-2A	lysosome-associated membrane protein 2A
LC3	Light chain 3
LIR	LC3 interacting region
LMB	Leptomycin B
LMP1	latent membrane protein 1
LT	Lymphotoxin
MAP3K14	Mitogen-activated protein kinase kinase kinase 14
MAPK	Mitogen-activated protein kinase
MCL	Mantle cell lymphoma
MEK	MAPK and ERK kinase
MHC	Major histocompatibility complex
MIF	Macrophage inhibitory factor
MM	Multiple myeloma
MMB	MiniMacs buffer
MSC	Microbiological Safety Cabinet
MSP	Macrophage-stimulating protein
MTOC	Microtubule-organising centre
mTOR	mammalian target of rapamycin
NAC	N-acetyl cysteine
NBR1	Neighbour of BRCA1 gene 1

NDP52	Nuclear dot protein 52 kDa
NEMO	NFκB essential modulator
NES	Nuclear export signal
NFKBIA	NFκB inhibitor α
NFKBIE	NFκB inhibitor ε
NFκB	Nuclear factor κ B
NGF	Nerve growth factor
NIK	NFκB-inducing kinase
NK	Natural Killer cell
NLPHL	Nodular lymphocyte predominant Hodgkin lymphoma
NLS	Nuclear localisation signal
NRf2	Nuclear factor erythroid-2-related factor 2
NSCLC	Non-small cell lung cancer
NUBL1	NEDD8 ultimate buster 1 long isoform
Oct-2	Octamer transcription factor 2
p62	p62/ Sequestosome 1 (SQSTM1)
PAGE	Polyacrylamide gel electrophoresis
PAS	Pre-autophagosomal structure
Pax5	Paired box 5
PB1	Phox and Bem1p domain
PBS	Phosphate buffered saline
PcG	Polycomb group
PDGFA	Platelet derived growth factor α chain
PDGFRA	Platelet derived growth factor α chain receptor
PDK	Phosphoinositide-dependent kinase
PE	Phosphatidylethanolamine
PI	Propidium iodide
PI3K	Phosphatidylinositol 3-kinase
PI3P	Phosphatidylinositol-3-phosphate
PIAS	Protein inhibitors of activated STATs
PKC	Protein kinase C
PLIC-1	Protein linking IAP with cytoskeleton 1
PML	Promyelocytic leukaemia protein

PolyQ	polyglutamate
PRC	polycomb repressive complex
PTP	Protein tyrosine phosphatase
Pu.1	Transcription factor binding to the PU-box
Rad23	Radiation sensitive 23
RANK	Receptor activator of NFκB
RANKL	Receptor activator of NFκB ligand
RASSF1A	Ras-associated domain family 1 isoform a
RIP	Receptor interacting protein
RIP1	Receptor-interactin serine-threonine kinase 1
RLU	Relative light units
RON	Receptor d'origine nantais
ROS	Reactive oxygen species
Rpn	Regulatory particle of non-ATPase subunit
Rpt	Regulatory particle of triple-ATPase subunit
RS	Reed-Sternberg cell
SASP	Senescence-associated secretory profile
SCID	Severe combined immune-deficient
SDS	Sodium dodecyl sulfate
SNARE	soluble N-ethylmaleimide-sensitive attachment protein receptor
SOCS	Suppressors of cytokine signalling
SOD	Superoxide dismutase
SOS	Son of sevenless
SQSTM1	Sequestosome 1 (p62)
STAT	Signal transducer and activator of transcription
SYK	Spleen tyrosine kinase
TAC1	Transmembrane activator and calcium-modulator and cytophilin ligand interactor
TARC	Thymus and activation regulated chemokine
TB	TRAF binding domain
TCR	T cell receptor
TGF	Transforming growth factor
T _h	Helper T lymphocyte

TKI	Tyrosine kinase inhibitor
TNF	Tumour necrosis factor
TNFAIP3	TNF- α -induced protein 3
TRAF	TNF receptor-associated factor
TRAIL	TNF-related apoptosis-inducing ligand
T _{reg}	Regulatory T lymphocyte
TRKA	Tyrosine receptor kinase A
Ub	Ubiquitin
UBA	Ubiquitin-associated domain
Ubl7	Ubiquitin-like 7
Uch37	Ubiquitin carboxy-terminal hydrolase 37
ULK1	Unc-51-like kinase
UPS	Ubiquitin-proteasome system
Usp14	Ubiquitin-specific peptidase 14
VAMP8	Vesicle-associated membrane protein 8
WFA	Withaferin A
ZZ	ZZ-type zinc finger domain
γ H2AX	Phosphorylated histone protein H2AX

Chapter 1. Introduction

1.1 The Cell Biology of Hodgkin lymphoma

1.1.1 Hodgkin Lymphoma

Hodgkin lymphoma (HL) is a lymphoid malignancy and one of the most frequent lymphomas in the Western World, with approximately 3 in 100,000 cases per year (Kuppers et al., 2012). In about 40% of cases Epstein-Barr virus (EBV) has been identified as an etiological agent (Kuppers, 2009). This association is much higher in the developing world. HL can be further classified into classical HL (approximately 95% of cases) and nodular lymphocyte-predominant HL (NLPHL) (approximately 5% of cases) (Kuppers, 2009). The focus of this thesis was on cell lines derived from patients with classical HL and for ease classical HL will simply be referred to as HL hereafter.

The malignant cells of HL are mononuclear Hodgkin (H) and bi-or multi-nucleate Reed-Sternberg (RS) cells, collectively HRS cells. Surprisingly, unlike many human cancers, the malignant HRS cells make up less than 1% of the tumour mass (ranging from 0.1-10%) with the rest made up of a vast mixed immune cellular infiltrate (Kuppers, 2009). HL can be further subdivided into nodular sclerosis, mixed cellularity, lymphocyte-rich and lymphocyte-depleted HL based on histological differences observed in the tumour microenvironment and the malignant cells (Kuppers et al., 2012).

1.1.2 Cellular origin of HL

Confusion over the cellular origin of HL originates from the diverse range of cellular markers expressed by HL cells. HRS cells have been found to co-express markers of several different cell lineages including B and T lymphocytes, dendritic cells, myeloid cells, cytotoxic cells and granulocytes (Schmitz et al., 2009b). HL cells are commonly identified by the expression of granulocyte-associated cluster of differentiation 15 (CD15) and the marker of activated T and

B lymphocytes CD30 as these tend to be consistently expressed (Schmitz et al., 2009b).

HL cells are generally thought to be of B cell origin due to rearrangements of their immunoglobulin (Ig) genes (Kuppers et al., 1994, Marafioti et al., 2000). A small proportion harbour rearrangements of their T cell receptor (TCR) suggesting a T cell origin in rare cases (Muschen et al., 2000, Seitz et al., 2000). During the course of normal B cell development a diverse antibody repertoire is generated through the rearrangement of Ig V, D and J gene segments resulting in numerous B cells with unique Ig light- and heavy-chain variable (V) regions (Li et al., 2004). This region houses the antigen-binding site of the antibody expressed on the surface of the B cell. Following antigen-binding and co-stimulation by T helper cells, the activated B cell migrates to the germinal centre (GC) of lymphoid organs and is termed a centroblast (Klein and Dalla-Favera, 2008). In the GC, further antibody diversification is achieved through somatic hypermutation of the V region. To allow somatic hypermutation, these cells specifically down-regulate their ability to detect and respond to DNA damage, as this process involves the generation of DNA strand breaks (Phan and Dalla-Favera, 2004). This may provide a window for transforming events. The centroblasts are highly proliferative resulting in the generation of large numbers of cells expressing different modified V regions over a relatively short period of time (Klein and Dalla-Favera, 2008). Cells expressing somatically hypermutated Ig on their cell surface are termed centrocytes at this stage. Those cells expressing high-affinity antigen binding V regions are selected for clonal expansion by interactions with follicular dendritic cells, which present the relevant antigen to B cells, and follicular T helper cells in the GC (Gatto and Brink, 2010). B cells which generate non-functional or poor-affinity antigen binding sites undergo apoptosis. HL cells have clonal somatically mutated V regions in both light- and heavy-chain Ig genes suggesting they are of a mature GC B cell origin (Brauninger et al., 2006). In approximately one quarter of cases loss of function mutations were detected in the V regions (Kuppers et al., 1994, Kanzler et al., 1996, Brauninger et al., 2003), which should result in apoptosis.

This would suggest that transforming events allowing cell survival and escape from apoptosis in HL may occur within the GC or at earlier stages of B cell development. In EBV⁺ cases, the virus may play a pivotal role in the transformation events as it has been found to selectively deregulate and even repress the DNA damage response (O'Nions et al., 2006). There have been reports of a putative cancer initiating cell (CIC) or cancer stem-like cell (CSC) in HL derived cell lines (Jones et al., 2009, Shafer et al., 2010, Nakashima et al., 2010, Ikeda et al., 2010, Ikeda et al., 2012). These cells are proposed to be responsible for maintaining HL-derived cell lines and, as with other malignancies, are thought to be responsible for therapy resistance and relapse. Therefore, there may be a scenario in which CIC/CSCs give rise to mononuclear Hodgkin cells, which in turn give rise to multi-nucleate RS cells. These putative CIC/CSCs will be discussed in detail in Chapter 6.

1.1.3 Transcriptional reprogramming

Although they appear to be of B cell origin, HL cells display a global down-regulation of B cell-associated genes (Hertel et al., 2002, Schwering et al., 2003). B cell specific transcription factors, such as Oct-2, B-cell oct binding protein 1 (Bob1), Pu.1 and early B cell factor 1 (EBF1), are commonly down-regulated (Stein et al., 2001, Torlakovic et al., 2001, Hertel et al., 2002). A number of B cell-related transcription factors are still expressed; however the activities of these proteins are impaired by the expression of non-B cell lineage proteins. For example, the products of the E2A gene, E12 and E47, important in B cell commitment, are expressed at low levels but are functionally impaired by the expression of autonomously replicating sequence binding factor 1 (ABF1) and Natural Killer (NK) cell-associated inhibitor of DNA binding 2 (ID2) (Mathas et al., 2006, Kuppers et al., 2003, Renne et al., 2006). HL cells also express B-cell commitment factor paired box 5 (Pax5) (Foss et al., 1999). The B cell-specific activity of this protein is likely impaired by binding to Notch1, a T cell-associated protein expressed in HL (Jundt et al., 2008). Additionally, Notch1 up-regulates E2A-inhibitor ABF1 and down-regulates E2A and EBF expression (Jundt

et al., 2008). Therefore the B cell transcriptional profile is repressed by the expression of transcription factors associated with other cell lineages. T cell-associated GATA-binding protein 3 (GATA3) is also expressed in HL, and has been found in HL-derived cell lines to influence cytokine expression (Stanelle et al., 2010). This may also be of relevance to the expression of signal transducer and activator of transcription 5 (STAT5) observed in HRS cells and its subsequent down-regulation of B cell-associated genes. When over-expressed in B cells, STAT5 caused immortalisation, a down-regulation of B cell-related genes, loss of the B cell phenotype and the formation of multinucleate cells reminiscent of RS cells (Scheeren et al., 2008). These changes could be partially prevented by over-expression of the E47 transcription factor, suggesting an important role for STAT5 and loss of B cell-related transcription factors in HL pathogenesis (Scheeren et al., 2008).

1.1.4 Epigenetic silencing

A number of genes are found to be down-regulated through epigenetic changes in HL cells. For example, the following genes were found to be repressed through DNA methylation: KLF4 (a B cell maturation transcription factor) (Guan et al., 2010); tumour suppressors CHEK2 (Kato et al., 2004), CDKN2C (Sanchez-Aguilera et al., 2004) and RASSF1A (Murray et al., 2004); and B cell-related genes BOB1, SYK and CD79B (Doerr et al., 2005, Ushmorov et al., 2006). Additionally, a comparison of HL-derived cell lines with B cell lines found that a number of B cell-related genes were hypoacetylated at histone H3 or had undergone H3 lysine 27 (H3K27) trimethylation in HL-derived cell lines (Seitz et al., 2011). Both of these are characteristic of epigenetic silencing. Such epigenetic modifications are likely due to the activities of Polycomb group (PcG) proteins. These function predominantly in establishing and maintaining repressive chromatin modifications (Kerppola, 2009). PcG proteins form two functionally distinct Polycomb repressive complexes (PRCs), PRC1 and PRC2. PRC2 represses transcriptional activity through histone H3K27 trimethylation, while PRC1 maintains this repressive modification (Kerppola, 2009). PcG proteins

are involved in normal GC B cell development, with the two repressive complexes expressed in a mutually exclusive pattern. The highly proliferative centroblasts express PRC2 and their non-proliferative derivatives, centrocytes, express PRC1 (Raaphorst et al., 2000). HRS cells co-express members of both repressive complexes which may result in unusual patterns of epigenetic silencing (Dukers et al., 2004, Raaphorst et al., 2000), although the extent to which PcG proteins are involved in epigenetic modifications in HL remains unclear.

1.1.5 Interactions with the immune system

The vast immune infiltrate attracted by HRS cells would suggest that interactions between these cells and the immune system are important in the pathology of the disease (Steidl et al., 2011a). Indeed, the few B cell lineage-associated genes that are maintained in HRS cells are largely related to their interaction with T cells (Kuppers, 2009). This is of significance as HRS cells are commonly observed to be rosetted by CD4⁺ T cells, predominantly helper (T_h) and regulatory (T_{reg}) T cells (Poppema et al., 1982, Poppema et al., 1996, Ma et al., 2008a). As mentioned previously HL is an unusual malignancy in that the vast majority of the tumour mass is composed of a mixed cellular immune infiltrate consisting of CD4⁺ T cells, CD8⁺ T cells, NK cells, B cells, macrophages, eosinophils, neutrophils, mast cells and fibroblasts. HRS cells appear to actively attract these cells through the secretion of various cytokines and chemokines (Figure 1-1). For example, the secretion of chemokine (C-C motif) ligand 5 (CCL5), thymus and activation regulated chemokine (TARC/CCL17) and CCL22 by HRS cells is involved in the recruitment of T_h and T_{reg} cells (Aldinucci et al., 2008, van den Berg et al., 1999, Hedvat et al., 2001). HRS cells are then bound by T_h cells through adhesion molecules (CD54-CD18/11a) and key-signalling molecules in B cell-T cell interaction (CD40-CD40L, CD80-CD28) (Gruss et al., 1996, Kuppers et al., 2012). These interactions likely lead to stimulation of both HRS and T cells, particularly as CD40-CD40L signalling results in pro-survival nuclear factor- κ B (NF κ B) activation (Steidl et al., 2011a). There may also be co-

stimulatory activity through major histocompatibility complex class II (MHC II)-TCR binding, however, MHC II is down regulated in a proportion of HL cases (Steidl et al., 2011b). The secretion of CCL5, CCL28, granulocyte-macrophage colony-stimulating factor (GM-CSF), interleukin 5 (IL-5), eotaxin, and IL-9 by HRS cells is thought to recruit eosinophils to the HL microenvironment (Skinnider and Mak, 2002, Teruya-Feldstein et al., 1999, Glimelius et al., 2006). Additionally, HRS cells secrete tumour necrosis factor α (TNF- α) and transforming growth factor β (TGF- β) to stimulate eotaxin and CCL5 production by fibroblasts to recruit eosinophils (Aldinucci et al., 2004, Jundt et al., 1999). CCL5 also attracts mast cells to the microenvironment (Fischer et al., 2003). Both eosinophils and mast cells are capable of stimulating pro-survival NF κ B signalling through binding of their CD30L to CD30 on HRS cells (von Wasielewski et al., 2000, Molin et al., 2001). Neutrophils are also attracted by the secretion of IL-8 (Skinnider and Mak, 2002). These activate pro-survival NF κ B signalling through the binding of a proliferation-inducing ligand (APRIL) to B-cell maturation antigen (BCMA) on HRS cells (Chiu et al., 2007, Schwaller et al., 2007) and can stimulate phosphatidylinositol 3-kinase (PI3K) /Akt and protein kinase C (PKC) signalling through the secretion of nerve growth factor (NGF) which binds to tyrosine receptor kinase A (TRKA) on HRS cells (Renne et al., 2008, Renne et al., 2005). HRS cells stimulate macrophages through macrophage migration inhibitory factor (MIF) and colony stimulating factor 1 (CSF-1) secretion (Leng et al., 2003, Ma et al., 2008b, Hsu et al., 1991). The exact role of macrophages in HL pathogenesis is unclear although they appear to be of prognostic significance as increased numbers of tumour-associated macrophages correlates with poor outcome (treatment failure, disease-progression, refractory disease, low survival rate) (Steidl et al., 2010a). Generally macrophages have been found to enhance tumour progression and suppress anti-tumour immune responses in many malignancies (Qian and Pollard, 2010). They may contribute to HL pathogenesis through secretion of MIF and its subsequent binding to CD74 on HRS cells (Hsu and Hsu, 1994, Stein et al., 2004, Leng et al., 2003). They also may recruit neutrophils through IL-8 secretion (Foss et al., 1996, Luciani et al., 1998).

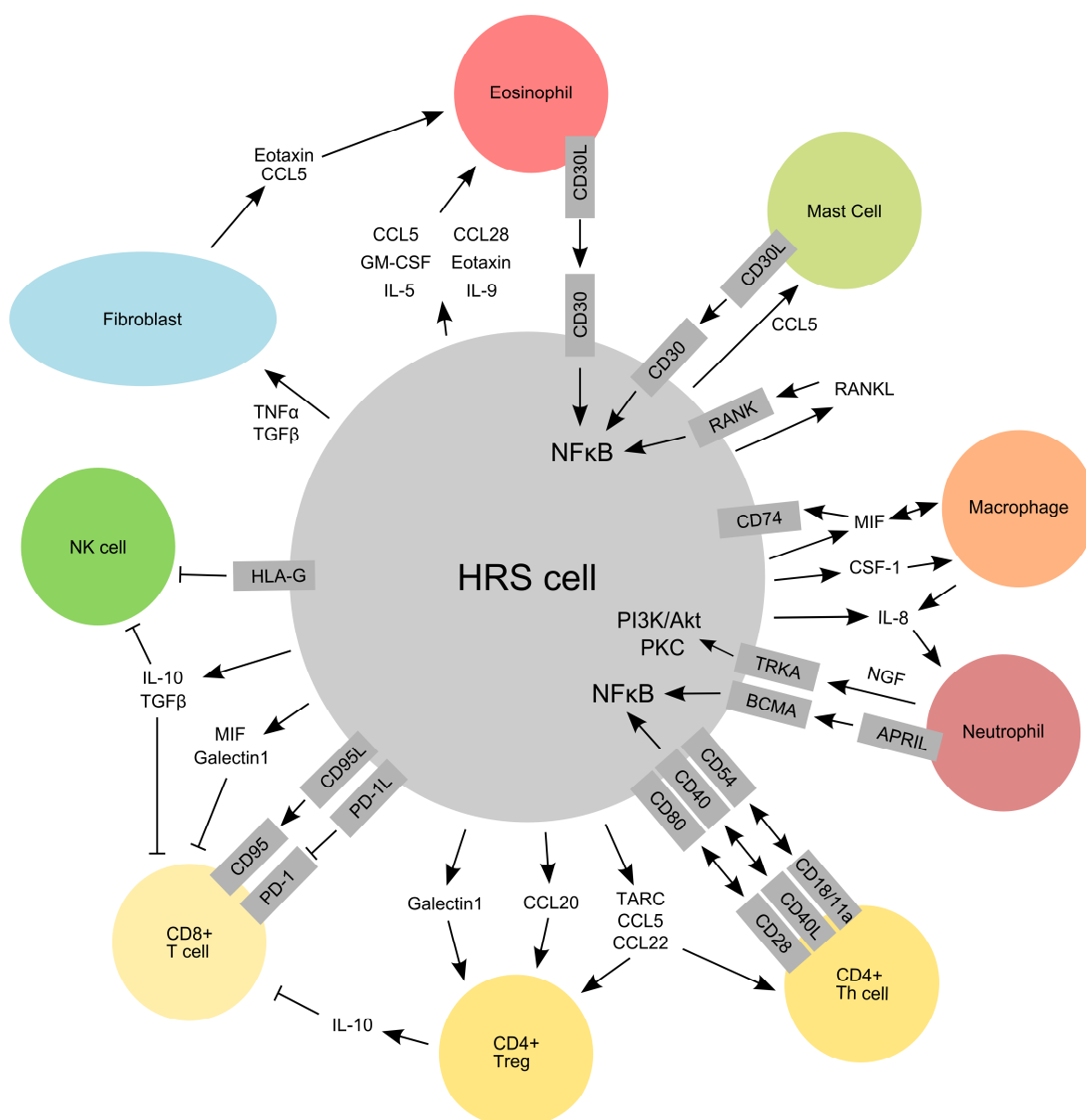


Figure 1-1 HRS cell interactions with the cellular microenvironment.

HRS cells secrete numerous cytokines and chemokines to recruit multiple cell types to their microenvironment and appear to rely on pro-survival signalling stimulated by receptor-ligand binding by these cells. Secretion of CCL5, CCL28, GM-CSF, Eotaxin, IL-5 and IL-9 recruits eosinophils; CCL5 secretion recruits mast cells; IL-8 recruits neutrophils; TARC, CCL5 and CCL22 recruit CD4⁺ T cells; MIF and CSF-1 recruit macrophages; and TNF-α and TGF-β secretion induce fibroblasts to produce eotaxin and CCL5 to further recruit immune cells. HRS cells also prevent their destruction by CD8⁺ T cells and NK cells by recruiting CD4⁺ T_{reg} cells which produce the inhibitory molecule IL-10. IL10 and TGF-β secretion by HRS cells, expression of non-classical MHC class I HLA-G, and CD95L (FASL) and PD-1L also inhibit these cytotoxic cells. Autocrine signalling through receptor activator of NFκB ligand (RANKL)-RANK may also stimulate NFκB activity. Adapted from (Kuppers et al., 2012, Steidl et al., 2011a).

HRS cells also evade the cytotoxic activities of the immune system by recruiting T_{reg} cell to the microenvironment by secretion of TARC (van den Berg et al., 1999), CCL5 (Aldinucci et al., 2008), CCL20 (Maggio et al., 2002) and CCL22 (Hedvat et al., 2001) and enhance their expansion through galectin 1 secretion (Juszczynski et al., 2007). These T_{reg} cells secrete IL-10 and inhibit the cytotoxic activity of T cells (Marshall et al., 2004, Skinnider and Mak, 2002). The cytotoxic function of these cells is further prevented by secretion of IL-10 (Skinnider and Mak, 2002, Herbst et al., 1996), TGF- β (Newcom and Gu, 1995), MIF (Ma et al., 2008b) and galectin 1 (Juszczynski et al., 2007) by HRS cells and by the binding of PD-1L and CD95L (FASL) on HRS cell surface with their respective receptors (PD-1 and CD95, respectively) on $CD8^+$ T cells (Yamamoto et al., 2008). HRS cells also inhibit the anti-tumour cytotoxic activity of NK cells by the expression of non-classical MHC class I HLA-G (Diepstra et al., 2008) and by secretion of IL-10 and TGF- β . NK activity may also be inhibited by T_{reg} cells through IL-10 secretion (Kuppers et al., 2012).

These interactions with the cellular microenvironment appear to be of critical importance in the survival of HRS cells, as they are rarely found in the peripheral blood, when found in non-lymphoid organs they are still in the presence of this microenvironment, and have proven extremely difficult to culture or to grow in immunodeficient mice (Kuppers, 2009, Vockerodt et al., 1998, Kapp et al., 1993). This would suggest that pro-survival NF κ B signalling through receptor-ligand binding is important in HL pathogenesis. The mixed immune infiltrate also produces its own cytokine and chemokine cocktail which would suggest that signalling pathways such as the Janus kinase (JAK) - Signal Transducer and Activator of Transcription (STAT) pathway may also be of significance.

1.1.6 Constitutively active signalling pathways

1.1.6.1 The NF κ B pathway in HL

There are two arms of the NF κ B pathway, the canonical (classic) and non-canonical (alternative) pathways (Figure 1-2) (Oeckinghaus and Ghosh, 2009, Chen, 2005). In the canonical pathway, inactive NF κ B is held in the cytoplasm by interaction with the inhibitor of NF κ B (I κ B) complex, which consists of I κ B α , I κ B β and I κ B ϵ . This pathway is initiated through stimulation of various receptors by their corresponding ligands. In HL, the relevant receptors are CD30, CD40, RANK and TNF receptor 1 and 2 (TNFR1/2) and their corresponding ligands CD30L, CD40L, RANKL, TNF α and lymphotaxin α (LT- α) (Molin et al., 2001, Pinto et al., 1996, Carbone et al., 1995, Fiumara et al., 2001, Kretschmer et al., 1990, Steidl et al., 2011a). Receptor stimulation results in the formation of a complex containing receptor interacting protein (RIP) and TNF receptor-associated factors (TRAFs) (Chen, 2005). These are activated by ubiquitination, facilitated by p62 (Sanz et al., 1999, Sanz et al., 2000), and activate the I κ B kinase (IKK) complex, consisting of IKK α , IKK β and IKK γ (NF κ B essential modulator, NEMO), through phosphorylation by atypical protein kinase Cs (aPKCs) amongst other kinases. The activating ubiquitinations can be inhibited by the de-ubiquitinating enzymes cylindromatosis (CYLD), which can be recruited by p62/Sequestosome 1 (SQSTM1), and A20 (Chen, 2005, Wooten et al., 2008). The active IKK complex phosphorylates the I κ B complex resulting in its further modification by ubiquitination and targeting for proteasomal degradation. This allows the nuclear translocation of the NF κ B transcription factors (p50-RELA) and subsequent pro-survival, inflammatory, proliferation and differentiation transcriptional activity. In the non-canonical pathway, the relevant receptors and their ligands are CD40-CD40L, transmembrane activator and calcium-modulator and cytophilin ligand interactor (TACI) - B-cell activating factor (BAFF) and BCMA-APRIL (Chiu et al., 2007, Steidl et al., 2011a). These receptor-ligand interactions activate an IKK complex consisting of only IKK α subunits through mitogen-activated protein kinase kinase kinase 14 (MAP3K14), also known as NF κ B-inducing kinase (NIK) (Chen, 2005). In this pathway there is no

I κ B complex, instead the NF κ B transcriptional activity is masked by the p100 subunit bound to the RELB subunit. IKK α phosphorylates the p100 subunit, resulting in its proteasomal processing into the active p52 subunit. Active p52-RELB can then translocate to the nucleus and engage in its transcriptional activity. NF κ B transcription factors have been found to be constitutively active in HRS cells, which led to investigations into genomic alterations affecting this pathway (Bargou et al., 1997). A number of mutations and amplifications are associated with elements of the canonical pathway in HL. Mutations affecting A20 (TNFAIP3) are present in approximately 40% of cases (Kato et al., 2009, Schmitz et al., 2009a), while those affecting CYLD are rare although have been detected (Schmidt et al., 2010). Mutations in genes involved in the I κ B complex, NFKBIA and NFKBIE, encoding I κ B α and I κ B ϵ , respectively, have been detected in 10-20% of cases tested (Emmerich et al., 1999, Emmerich et al., 2003, Jungnickel et al., 2000, Lake et al., 2009). Amplifications in the REL gene have been detected in approximately 30% of cases tested (Joos et al., 2002, Martin-Subero et al., 2002). In the non-canonical pathway gains of MAP3K14 have been detected in approximately 25% of cases tested (Otto et al., 2012, Steidl et al., 2010b). In the roughly 40% of cases where EBV is present in HRS cells, the viral latent membrane protein 1 (LMP1) protein can activate both arms of the NF κ B pathway (Kilger et al., 1998, Kuppers et al., 2012). Of note, EBV infection and A20 mutation tend to be mutually exclusive (Schmitz et al., 2009a). Taken together, the NF κ B stimulatory activity provoked by the immune infiltrate recruited by HRS cells and the number of genomic alterations preventing inhibition or enhancing activity of this pathway would suggest that the NF κ B signalling pathway is of great importance in the pathogenesis of HL.

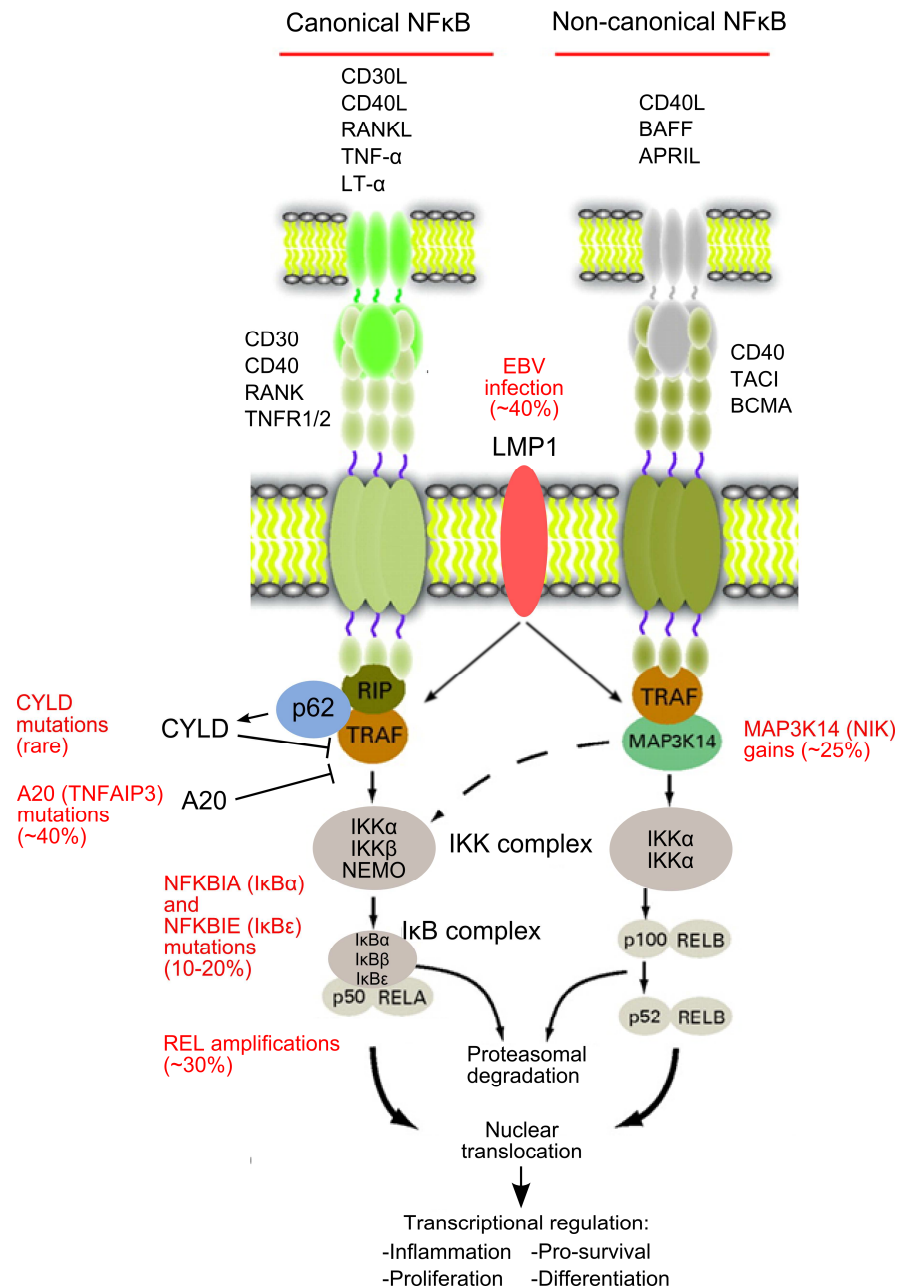


Figure 1-2 NFκB signalling pathway in HL.

Both arms of the NFκB pathway, the canonical and non-canonical, are activated by the binding of various ligands to their relevant receptors on the surface of HRS cells. The canonical pathway is activated by the binding of CD30L, CD40L, RANKL, TNF-α and LT-α to CD30, CD40, RANK and TNFR1/2, respectively. This results in the formation of a complex containing RIP and TRAF proteins. The complex is activated by ubiquitination, mediated by p62, and subsequently activates the IKK complex. The activating ubiquitination can be inhibited by CYLD, recruited by p62, and A20. IKK phosphorylates members of the IκB complex resulting in their proteasomal degradation. This frees NFκB subunits p50 and RELA to translocate to the nucleus and activate transcription related to inflammation, cell survival and proliferation. The non-canonical pathway can be activated by binding of CD40L, BAFF and APRIL to their corresponding receptors CD40, TACI, and BCMA,

respectively. This results in the TRAF-dependent activation of MAP3K14, which activates the IKK complex consisting of IKK α subunits only. Active IKK phosphorylates the p100 NF κ B subunit, resulting in its proteasome-dependent cleavage into the p52 active form. This molecule, in conjunction with RELB, can then translocate to the nucleus and initiate transcription. The EBV protein LMP1 is capable of activating both pathways. HL-associated mutations affecting each pathway are shown in red. Adapted from (Steidl et al., 2011a, Kuppers et al., 2012)

1.1.6.2 JAK/STAT signalling in HL

The JAK-STAT signalling pathway, the principle signalling pathway of cytokines and growth factors in mammalian cells, has also been found to be constitutively active in HRS cells. In particular STAT3, STAT5 and STAT6 activity have been reported in HL (Kube et al., 2001, Scheeren et al., 2008, Skinnider et al., 2002). This is likely due to both autocrine and paracrine signalling provided by numerous cytokines (Figure 1-3) (Steidl et al., 2011a). The JAK family of proteins consists of four members: JAK1, JAK2, JAK3 and Tyk2 (Rawlings et al., 2004). JAKs are often found in association with the cytoplasmic tail of various cytokine receptors. Ligand-mediated multimerisation of receptors brings JAKs together allowing trans-phosphorylation of the JAKs. The active kinases then phosphorylate the receptor and STATs, which are resident in the cytoplasm until activated. Phosphorylated STATs can then dimer- or oligomerise. These complexes are then imported into the nucleus where they function in activating transcription of genes associated with cell survival and proliferation amongst other things. There are three main classes of JAK-STAT inhibitors: suppressors of cytokine signalling (SOCS), protein inhibitors of activated STATs (PIAS) and protein tyrosine phosphatases (PTPs) (Rawlings et al., 2004). SOCS are part of a negative feedback loop and their transcription is initiated by STATs. SOCS inhibit JAK-STAT signalling by binding to JAKs to inhibit their kinase activity and to the receptors to prevent the recruitment of signal transducers, such as STATs, to the activated receptor. PTPs similarly interfere with JAK function by reversing the activating phosphorylation of JAKs and their receptors. PIAS bind to activated STAT dimers and prevent them from binding to DNA, thus inhibiting their transcriptional activity. In HL, amplifications of JAK2 have been detected in 20% of cases and translocation events, although rare, have also been found (Joos et

al., 2000, Van Roosbroeck et al., 2011). Additionally inactivating mutations of SOCS1 have been detected in approximately 40% of cases tested (Weniger et al., 2006). These would highlight the importance of this signalling pathway in HL.

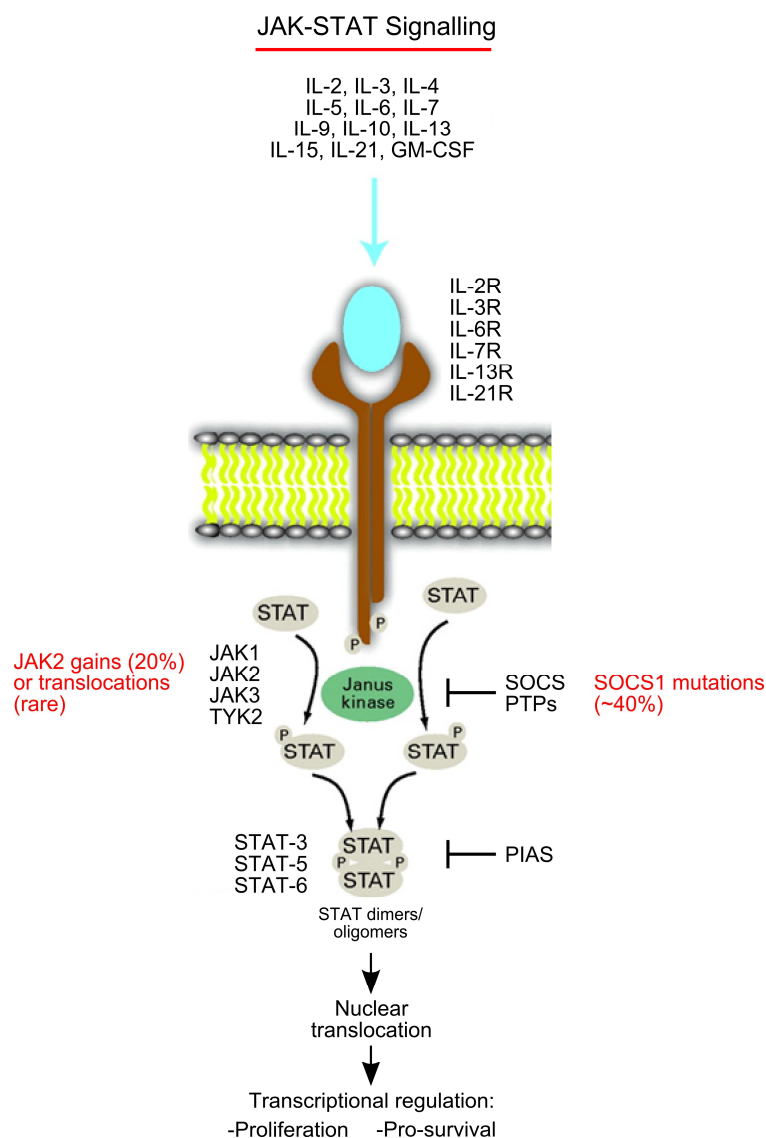


Figure 1-3 The JAK-STAT signalling pathway in HL.

The JAK-STAT pathway is constitutively active in HRS cells, likely due to the autocrine and paracrine secretion of numerous cytokines and growth factors. Stimulation by the relevant ligand results in receptor multimerisation and trans-phosphorylations of receptor-associated JAK. Active JAK phosphorylates STAT proteins, allowing their dimerisation or oligomerisation and subsequent nuclear translocation to regulate inflammation-, pro-survival- and proliferation-associated transcription. JAK activity can be inhibited by SOCS and PTPs, while STAT activity can be inhibited by PIAS. Cytokines and their receptors, JAKs and STATs expressed in HL are shown. HL-relevant mutations are shown in red. Adapted from (Steidl et al., 2011a, Kuppers et al., 2012)

1.1.6.3 ERK/MAPK and Akt signalling pathways

The extracellular signal-regulated kinase/ mitogen-activated protein kinase (ERK/ MAPK) and Akt signalling pathways are also constitutively active in HL (Zheng et al., 2003, Dutton et al., 2005). Both can be activated by CD30-CD30L, CD40-CD40L, RANK-RANKL interactions and through receptor tyrosine kinase signalling. A number of receptor tyrosine kinases have been found to be aberrantly expressed in HL, particularly in the nodular sclerosis subtype (Figure 1-4). These include c-MET, TRKA/B, discoidin domain receptor 2 (DDR2), platelet-derived growth factor α chain receptor (PDGFRA), ephrin receptor B1 (EPHB1), and receptor d'origine nantais (RON) (Pons et al., 1998, Teofili et al., 2001, Renne et al., 2008, Renne et al., 2005). They are likely activated by both autocrine and paracrine signalling through their corresponding ligands; hepatocyte growth factor (HGF), nerve growth factor (NGF), collagen type I, platelet-derived growth factor α chain (PDGFA), EphrinB1 and macrophage-stimulating protein (MSP), respectively (Renne et al., 2005, Steidl et al., 2011a). Upon binding to the relevant ligand, receptor tyrosine kinases dimerise resulting in trans-phosphorylation at the intracellular domain (Kolch, 2005). The activated receptor, through adaptor proteins such as growth factor receptor bound protein 2 (GRB2) and GRB2-associated binding protein 1 (GAB1), recruits guanine nucleotide exchange factors such as son of sevenless (SOS). This activates Ras guanosine triphosphatases (GTPases) through the conversion of guanosine diphosphate (GDP) to guanosine triphosphate (GTP) on the Ras protein. Active Ras recruits Raf kinases to the receptor where they are activated by phosphorylation. These, in turn, phosphorylate and activate MAPK and ERK kinase (MEK) which phosphorylates and activates ERK/ MAPKs. ERK/ MAPKs have numerous targets in both the cytoplasm and nucleus and can influence transcription through activation of transcription factors and by altering chromatin conformation. Three ERKs (ERK1, ERK2 and ERK5) have been found to be expressed in HL-derived cell lines and inhibition of this pathway led to loss of proliferative potential (Zheng et al., 2003, Nagel et al., 2007).

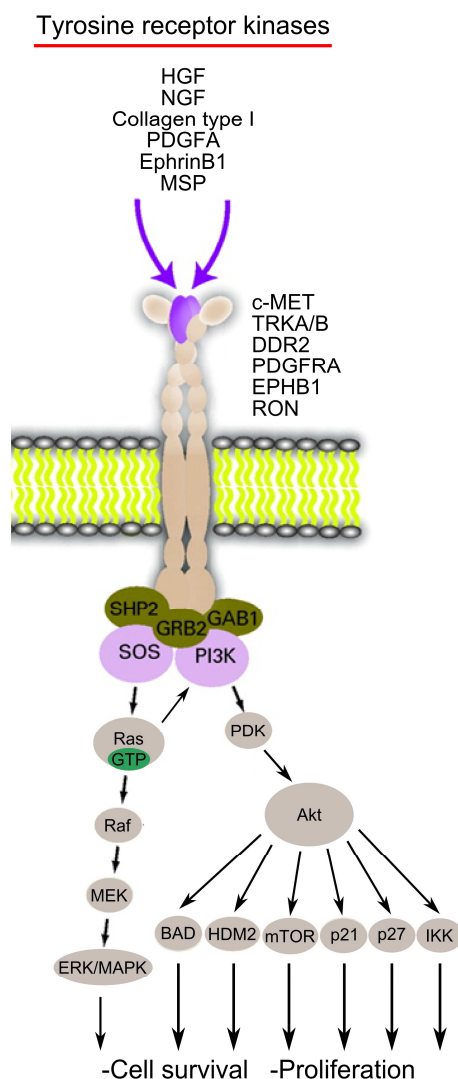


Figure 1-4 ERK/MAPK and AKT signalling through tyrosine receptor kinases.

A number of tyrosine receptor kinases are aberrantly expressed in HL: c-MET, TRKA/B, DDR2, PDGFRA, EPHB1 and RON. Their corresponding ligands (HGF, NGF, collagen type I, PDGFA, EphrinB1 and MSP, respectively) have also been detected in HL. On stimulation with the relevant ligand, receptor tyrosine kinases dimerise and undergo activating trans-phosphorylations. This results in the recruitment of a number of adaptor proteins (for example GRB2, GAB1, SHP2) which recruit guanine nucleotide exchange factors such as SOS. These activate Ras GTPases through the conversion of GDP to GTP. This results in the recruitment of Raf kinases and PI3K to the active receptor and the subsequent initiation of kinase cascades in the ERK/MAPK and Akt signalling pathways. These pathways function in enhancing cell survival and proliferation. Adapted from (Steidl et al., 2011a).

Active Ras can also recruit PI3K to the active receptor and induce signalling through the Akt pathway (Fresno Vara et al., 2004). This is also a kinase cascade

in which PI3K activates phosphoinositide-dependent kinase (PDK) by phosphorylation, which activates Akt also by phosphorylation. Akt, through further phosphorylation of its targets, can regulate a number of cellular processes involved in cell survival and proliferation. For example, Akt inactivates B-cell lymphoma 2 (Bcl-2)-associated agonist of cell death (BAD) preventing its pro-apoptotic activity (Datta et al., 1997). Akt-mediated phosphorylation of human double minute 2 homolog (HDM2) induces its nuclear localisation where it can inhibit p53 function, preventing cell cycle arrest and apoptosis (Mayo and Donner, 2001). Similarly, phosphorylation of cell cycle regulators p21 and p27 by Akt results in their cytoplasmic retention, preventing their anti-proliferative activities (Zhou et al., 2001, Liang et al., 2002). The IKK complex can also be activated by Akt resulting in pro-survival NF κ B activity (Bai et al., 2009). Akt activity also phosphorylates and activates mammalian target of rapamycin (mTOR), which has numerous cellular activities including regulation of cell survival, proliferation and metabolic activity (Laplane and Sabatini, 2009). Inhibition of Akt signalling in HL-derived cell lines results in cell death, suggesting an important role for this pathway in these cell lines (Dutton et al., 2005).

1.1.7 HL-derived cell lines and mouse models

1.1.7.1 HL-derived cell lines

As mentioned previously, HRS cells have proven difficult to culture likely due to their reliance on pro-survival signalling provided by interactions with their microenvironment. There are currently 9 HL-derived cell lines available from the Deutsche Sammlung von Mikroorganismen und Zellkulturen (DSMZ), all established from HL patients with advanced stage refractory disease (Table 1-1). Other attempts to establish cell lines from HL patients have resulted in out-growth of EBV infected B cells or in the discovery of misdiagnosis of primary material resulting in re-classification of the cell line (Drexler, 1993). The majority of the HL-derived cell lines were established many years ago, with the

exception of the U-H01 cell line (Mader et al., 2007), and there have been no recent published attempts to establish HL-derived cell lines from primary material. All HL-derived cell lines were established from pleural effusions, peripheral blood or bone marrow suggesting the cells had already adapted to conditions outside of their usual environment in lymphoid tissue (Kuppers and Re, 2007). This would suggest that they were no longer as reliant on interactions with their microenvironment for survival. These cell lines are recognised as HL-derived based on their morphology, expression of HL-associated markers and clonal rearrangements of the Ig or TCR gene loci (Kuppers and Re, 2007). HL-derived cell lines contain a mix of mononuclear Hodgkin-like and multinuclear Reed-Sternberg-like cells and express HL-associated CD30 and CD15, with the exceptions of SUP-HD1 (CD30⁻) and HD-MyZ (CD30⁻CD15⁻). They have been found to harbour clonal Ig gene rearrangements suggesting a B cell origin in all but L-540 and HDLM-2, in which rearrangements of the TCR would suggest a T cell origin (Drexler, 1993, Kuppers and Re, 2007). The SUP-HD1 line contains rearrangements of both Ig and TCR genes shedding some doubt on its origin, although the expression of the Ig κ light chain would suggest a B cell derivation. Of all the HL-derived cell lines only L-591 contains EBV. This combined with its expression of B cell-associated CD19 and CD20, rarely expressed in HL, has led to speculation that this is more likely to be an EBV immortalised lymphoblastoid cell line rather than a genuine HL-derived line (Drexler, 1993). Other than an ability to generate multinucleate RS-like cells, HD-MyZ is unlike the other HL-derived cell lines. This cell line is now thought to be of non-lymphoid origin due to the expression of the macrophage-associated CD68 and myeloid-associated CD13 antigens (Bargou et al., 1993, Kuppers and Re, 2007). Furthermore, each of the commonly used cell lines has a characteristic phenotype, making comparisons between them very difficult. Although the cell lines lack the multicellular microenvironment associated with HL, they generate a significant secretory profile of chemokines and cytokines reminiscent of HRS cells *in vivo*, making them a valid cellular model for studying HL.

Table 1-1 HL-derived cell lines

Cell line	HL Subtype	Source	Stage	CD30	CD15	Gene rearrangement		EBV	Year
						Ig	TCR		
KM-H2	MC → LD	PE	IV	+	+	IgH,L	-	-	1974
L-540	NS	BM	IVB	+	+	-	TCR α , β , δ	-	1978
L-428	NS	PE	IVB	+	+	IgH,L	-	-	1978
HDLM-2	NS	PE	IV	+	+	-	TCR α , β , δ	-	1982
L-591	NS	PE	IVB	+	+	IgH,L	-	+	1982
SUP-HD1	NS → LD	PE	IV	-	+	IgH,L	TCR β	-	1987
HD-MyZ	NS	PE	IIIB	-	-	-	-	-	1991
L-1236	MC	PB	IV	+	+	IgH,L	-	-	1994
U-H01	NS	PE	IIB	+	+	IgH	-	-	2005

MC- mixed cellularity, LD- lymphocyte depleted, NS – nodular sclerosis, PE – pleural effusion, BM – bone marrow, PB – peripheral blood, Ig – immunoglobulin, TCR – T cell receptor, EBV – Epstein-Barr Virus. Year refers to the year in which the cell line was established or first reported.

1.1.7.2 Animal models of HL

Animal models for HL are currently very limited. The immunodeficient background of mouse models has proven to be important in growth of tumours derived from HL-derived cell lines. Subcutaneous transplantation into athymic T cell-deficient nude mice did not result in tumour growth, however, subcutaneous or intraperitoneal inoculation of severe combined immune-deficient (SCID) mice with HL-derived cell lines did result in tumour outgrowth (Kapp et al., 1992). In this instance only L-540 displayed disseminated growth

involving lymphoid tissue. Similarly, only L-540 and a related cell line L540cy displayed HL-like growth in lymph nodes following intravenous inoculation in SCID mice (Kapp et al., 1994). Xenograft models similar to these have been used in the development of anti-CD30 antibodies and anti-CD30 antibody-drug conjugates, the most recent being brentuximab vedotin (Wahl et al., 2002, Senter and Sievers, 2012). Hodgkin-like lymphoma has been described in numerous species including dogs (Maeda et al., 1993), cats (Walton and Hendrick, 2001), rats (Majeed and Gopinath, 1985), skunks (Smith and Barker, 1983) and even in a killer whale (Yonezawa et al., 1989). To date none of these species appear to have been pursued as an animal model of HL. Hodgkin-like disease has also been described in domestic ferrets, with epidemiological data of this disease indicating an infectious aetiology (Ammersbach et al., 2008). Currently sequencing studies are underway with the goal of identifying a possible viral involvement.

1.1.8 Current treatments of HL

1.1.8.1 Treatment Options

In developed countries, there is a bimodal age incidence of HL, with a peak in 15-35 year olds and a second peak in the over 55 age group (Jarrett et al., 2003). Treatment of HL is generally very successful, achieving cure rates of 80-90%; consequently there is a heavy focus on reducing treatment toxicity to enhance quality of life post-therapy, particularly for younger patients (Eichenauer and Engert, 2012). HL therapy is based on the patient's clinical stage and largely consists of chemotherapy combined with radiotherapy. The clinical stage is determined by the number of lymph nodes and extranodal sites involved and is assessed based on the internationally-recognised Ann Arbor staging system (Table 1-2) (Lister et al., 1989).

Patients with stage IA or IIA are said to have early stage disease and are treated successfully with a combination of chemotherapy and involved-field radiotherapy

(Engert et al., 2010). The chemotherapy regimen used is called ABVD and consists of Adriamycin (Doxorubicin), Bleomycin, Vinblastine and Dacarbazine (Bonadonna et al., 1975). Patients presenting with B symptoms or stage III or IV disease are classified as having advanced stage disease. These patients are treated with ABVD chemotherapy only (Longo, 2013). The ABVD regimen is used in the United Kingdom, United States of America and commonly throughout the rest of the world. In Germany, a harsher regimen is used called BEACOPP (Eichenauer and Engert, 2011, Longo, 2013). This consists of Bleomycin, Etoposide, Adriamycin (Doxorubicin), Cyclophosphamide, Oncovin (Vincristine), Prednisone and Procarbazine. While the BEACOPP regimen is more successful at treating HL, it has been associated with infertility (Behringer et al., 2005) and increased risk of developing secondary malignancies such as acute myeloid leukaemia (AML) (Engert et al., 2009).

Table 1-2 Ann Arbor staging system for HL

Stage I	Single lymph node or localised extranodal site*
Stage II	Two or more lymph node regions and/or localised extranodal sites* on the same side of the diaphragm
Stage III	Lymph node regions and/or localised extranodal sites* on both sides of the diaphragm
Stage IV	Diffuse or disseminated involvement of one or more non-lymphatic organs with or without associated lymph node involvement

*Extranodal involvement is indicated by E, i.e. stage IE

The absence or presence of B symptoms are indicated by A or B, respectively (e.g. Stage IVB). These include night sweats, significant weight loss and unexplained fever and are associated with poor outcome. Adapted from (Lister et al., 1989)

Patients with refractory disease or who relapse are subject to salvage therapy consisting of high-dose multi-agent chemotherapy, often combined with autologous or allogeneic haematopoietic stem cell transplant (Eichenauer and Engert, 2012). There is no standard for this treatment and its constituents depend on patient health. Prognosis is poor for patients with primary refractory disease and for those who relapse within 12 months (Josting et al., 2000, Josting et al., 2002).

1.1.8.2 Side-effects

While ABVD therapy is generally accepted to be less toxic than BEACOPP there are a number of side-effects associated with both regimens. These include: endocrine dysfunction; immunosuppression; sterility; myocardial damage; fatigue; growth abnormalities; secondary malignancies; and cardiovascular disease. Secondary malignancies include: AML, non-Hodgkin lymphomas, lung cancer, colon cancer, breast cancer, and melanoma (Aleman et al., 2003). As primary therapy is largely successful in curing patients of HL, it is these secondary cancers and cardiovascular disease which are becoming bigger issues.

1.1.8.3 Novel agents against HL

Due to the success of current regimens of ABVD, BEACOPP and radiotherapy, novel therapeutics against HL are usually only trialled against patients with refractory or relapsed disease and generally have limited success. Previously there has been a focus on histone deacetylase inhibitors, with the idea being to undo epigenetic silencing of pro-apoptotic genes. These trials included vorinostat, mocetinostat and most recently panobinostat (Kirschbaum et al., 2012, Younes et al., 2011, Younes et al., 2012b). Although these agents showed some anti-tumour activity, it was in the form of partial responses and protracted stable disease rather than cure. There have also been trials of targeted therapeutics utilising the expression of cell surface receptors by HRS cells. For example, rituximab, an anti-CD20 molecule, has shown some efficacy in phase I and II trials against EBV⁺ HL (Kasamon et al., 2012, Younes et al., 2012a). Similarly, brentuximab vedotin, an anti-CD30 antibody conjugated to the anti-microtubule agent monomethyl auristatin E, has shown promise in phase I trials (Younes et al., 2010). Consequently it has been licensed for use against relapsed and refractory disease. This agent showed such promise that it is in numerous additional trials against refractory disease (Goyal and Bartlett, 2012) and in phase III trials as a component of primary HL therapy in combination with Bleomycin, Vinblastine and Dacarbazine (Group, 2013).

The current treatment regimens, ABVD and BEACOPP, focus heavily on DNA damage-inducing agents (the exceptions being anti-microtubule agents Vinblastine and Oncovin, and the immunosuppressant prednisone). Consequently the identification of new targets in order to reduce treatment toxicity is of increasing interest in this field. Protein degradation pathways may be relevant to HL as they are involved in the regulation of NF κ B activity by removing NF κ B inhibitors. Although controversial, it has also been suggested that aneuploid cells, such as RS cells, may be under protein handling stress as they have an abnormal number of copies of certain genes which may translate to the protein level (Gordon et al., 2012). This could result in enhanced activity of protein degradation pathways, the interference of which may be of therapeutic benefit.

1.2 Protein degradation pathways

There are two main pathways related to selective protein degradation in eukaryotic cells: the ubiquitin-proteasome system (UPS) and the autophagy pathway, which feeds into the lysosomal degradation pathway. Although aspects of autophagy were originally thought to be non-specific, a common feature of both pathways is the ability of the cell to target misfolded or redundant proteins for degradation by ubiquitin signalling (Clague and Urbe, 2010).

1.2.1 Ubiquitin

Ubiquitin signalling is an extremely diverse process and is involved in numerous cellular processes not least protein degradation (Welchman et al., 2005). Ubiquitination is a post-translational modification achieved by an enzyme cascade involving E1 ubiquitin-activating enzymes, E2 ubiquitin-conjugating enzymes and E3 ubiquitin ligase enzymes. While there are relatively few E1 and E2 enzymes encoded by the human genome, there are more than 500 E3 ubiquitin ligases which are responsible for substrate selection (Saeki and Tanaka, 2012). Ubiquitination occurs when an ubiquitin molecule is attached by its carboxyl terminus to an external lysine residue of a target protein. The addition

of ubiquitin to one or more lysine residue results in a mono- or multi-monoubiquitinated protein. The versatility of ubiquitin as a signalling molecule arises from its ability to form 8 functionally distinct polyubiquitin chains. This is achieved through by the formation of homotypic linkage-specific chains on one of 7 external lysine (K) residues (K6, K11, K27, K29, K33, K48, K63) or the amino-terminal Met1 (Komander and Rape, 2012).

The best characterised chains are those of K48- and K63-linked polyubiquitin. K48-linked polyubiquitin chains are the most abundant chain type in eukaryotic cells and are well established as markers for proteasomal degradation (Komander and Rape, 2012). K63-linked polyubiquitin chains are associated with microtubule transport, aggresome formation, degradation by the UPS and autophagy pathways, numerous cell signalling cascades and DNA damage-related pathways (Komander and Rape, 2012). K6-linked polyubiquitin chains have also been associated with the DNA damage response (Kulathu and Komander, 2012). K11-linked polyubiquitin chains are associated with proteasomal degradation, particularly of cell cycle related proteins, and with membrane trafficking and TNF α -signalling (Kulathu and Komander, 2012). K27-linked polyubiquitin chains are involved in mitochondrial degradation by mitophagy (selective degradation of mitochondria by the autophagy pathway) (Geisler et al., 2010). K29- and K33-linked polyubiquitin chains have been associated with a non-degradative inhibition of adenosine monophosphate (AMP)-activated protein kinase (AMPK) (Kulathu and Komander, 2012). K29- and K33-linked polyubiquitin have also been associated with proteasomal degradation and TCR signalling, respectively (Kulathu and Komander, 2012). Met1-linked polyubiquitin chains have been found to have an important role in the activation of NF κ B (Kulathu and Komander, 2012). Thus, although primarily associated with protein degradation, ubiquitin functions as a signalling molecule in numerous cellular processes.

1.2.2 The Proteasome

The ubiquitin-proteasome system is generally considered to be the main source of targeted proteolytic activity within the cell, operating in both the cytoplasm and the nucleus. In addition to being responsible for protein quality control through the removal of misfolded or damaged proteins, the proteasome is involved in almost all cellular processes including cell cycle regulation, signal transduction, cell death, antigen presentation, inflammation and transcriptional regulation (Finley, 2009). The 26S proteasome is a multi-subunit structure consisting of a 20S core particle and two 19S regulatory particles (Figure 1-5, Table 1-2) (Saeki and Tanaka, 2012). The 20S core particle consists of 4 heptameric rings, 2 α -rings and 2 β -rings, which form a barrel-shaped structure with the β -rings in the centre. The proteolytic activities of the proteasome are harboured in the β 1, β 2 and β 5 subunits which possess caspase-like, trypsin-like and chymotrypsin-like activities, respectively. These catalytic subunits have interferon inducible counterparts (β 1i, β 2i and β 5i) which result in the formation of the immunoproteasome (Groettrup et al., 2010). These subunits display altered caspase-like, trypsin-like and chymotrypsin-like activities and produce different cleavage products believed to enhance their presentation by MHC class I molecules. The immunoproteasome has also been found to be more active than the regular proteasome (Seifert et al., 2010). Since it is induced in an inflammatory environment, often accompanied by protein-damaging oxidative stress which would increase the burden on the UPS, it has been suggested that the immunoproteasome can be expressed in order to increase basal proteasome activity and prevent the accumulation of toxic protein aggregates (Seifert et al., 2010, van Deventer and Neefjes, 2010). An additional subunit is present exclusively in cortical thymic epithelial cells, the β 5t subunit (Murata et al., 2008). This is found in conjunction with the β 1i and β 2i subunits in these cells and displays lesser chymotrypsin-like activity than β 5 or β 5i. This results in altered cleavage products for MHC presentation and is important for T cell development.

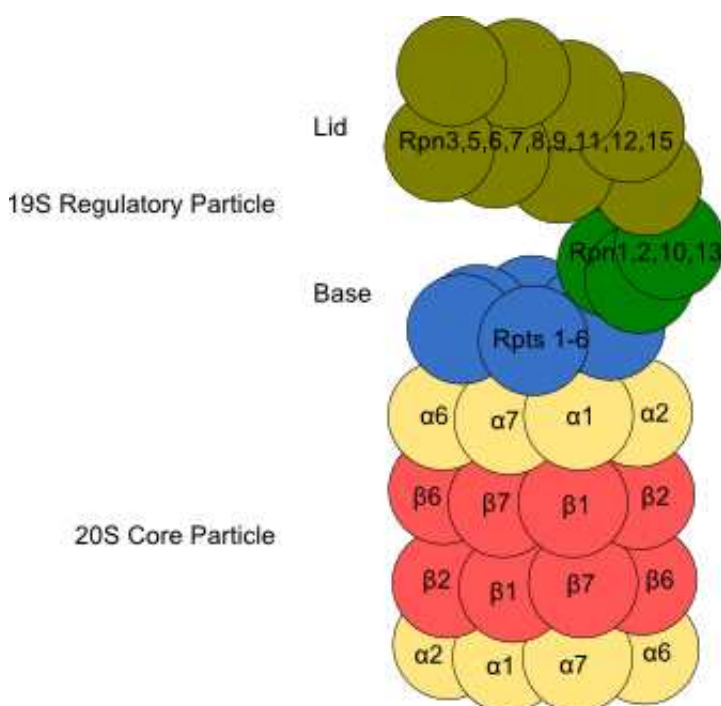


Figure 1-5 Components of the 26S Proteasome.

The 26S proteasome is made up of a 20S core particle and two 19S regulatory particles. Here only one 19S regulatory particle is shown. A second 19S regulatory particle can bind to the free alpha ring at the opposing end of the core particle. The 20S core particle is a barrel-like structure consisting of 2 heptameric α -rings and 2 heptameric β -rings, with the β -rings in the centre harbouring the proteolytic sites. The 19S regulatory particle is responsible for the recognition of ubiquitinated substrates and their subsequent de-ubiquitination and unfolding for proteolytic cleavage. This particle consists of a base containing the ATPases Rpt1-6 critical for proteasome function, and Rpn1,2,10 and 13 which act as scaffolds for proteasome interacting proteins (Rpn1/2) and as ubiquitin receptors (Rpn10/13).

Alone, the 20S core particle is inactive as the conformation of the alpha rings block entry to the catalytic chamber formed by the β -rings (Finley, 2009). The 19S regulatory particle binds to the α -ring on one or both ends of the proteasome forming a substrate translocation channel into the enzymatic central chamber. The 19S complex is also responsible for the recognition of ubiquitinated substrates and their subsequent de-ubiquitination and unfolding for proteolytic cleavage within the core particle, although the exact sequence of events during processing is unknown (Finley, 2009).

The 19S regulatory particle consists of 2 sub-structures, a 10 subunit base and a 9 subunit lid, which act in tandem to regulate entry and processing of ubiquitinated substrates (Finley, 2009). The base contains a hexameric ring of adenosine triphosphatases (ATPases) (Rpt1-6) which are crucial for the processing (de-ubiquitination and unfolding) of target proteins (Rubin et al., 1998, Liu et al., 2006). Recognition of ubiquitinated proteins is attributed to components of the base structure. Rpn10 (Deveraux et al., 1994) and Rpn13 (Husnjak et al., 2008) act as intrinsic ubiquitin receptors and a host of other ubiquitin-binding proteins interact with base structure proteins Rpn1 and Rpn2 to deliver ubiquitinated substrates to the proteasome (Finley, 2009). Among these are Rad23, Dsk2, Ddi1, PLIC-1, AIRAPL, NUBL1, Ubl7 and p62/SQSTM1. Rpn1 and 2 also act as scaffolds for the interaction of deubiquitinating enzymes (DUBs) Uch37 and Usp14 (Hamazaki et al., 2006, Leggett et al., 2002). The lid structure of the 19S regulatory particle also harbours de-ubiquitinating activity through the Rpn11 subunit (Yao and Cohen, 2002). This subunit is the only component of the lid structure with a known function and its activity is adenosine triphosphate (ATP)-dependent, thus requires the activity of the Rpt1-6 ATPases in the base. A number of ubiquitin ligases also associate with the proteasome. It is thought that they function to elongate ubiquitin chains, as longer ubiquitin chains have been found to associate more tightly with the proteasome, thus enhancing degradation of mono- or short chain polyubiquitinated substrates (Crosas et al., 2006, Thrower et al., 2000).

Table 1-2 Components of the 26S proteasome and their known functions

Proteasome Structure	Sub-structure	Nomenclature	Function
20S Core Particle	α -ring	α 1	Structure
		α 2	Structure
		α 3	Structure
		α 4	Structure
		α 5	Structure
		α 6	Structure
		α 7	Structure
	β -ring	β 1/ β 1i	Caspase-like activity
		β 2/ β 2i	Trypsin-like activity
		β 3	Structure
		β 4	Structure
		β 5/ β 5i/ β 5t	Chymotrypsin-like activity
		β 6	Structure
		β 7	Structure
19S Regulatory Particle	Base	Rpt1	ATPase
		Rpt2	ATPase
		Rpt3	ATPase
		Rpt4	ATPase
		Rpt5	ATPase
		Rpt6	ATPase
		Rpn1	Scaffold/PIP receptor
		Rpn2	Scaffold/PIP receptor
		Rpn10	Ub receptor
		Rpn13	Ub receptor
	Lid	Rpn3	Scaffold?
		Rpn5	Scaffold?
		Rpn6	Scaffold?
		Rpn7	Scaffold?
		Rpn8	Scaffold?
Rpn9	Scaffold?		
Rpn11	DUB		
Rpn12	Scaffold?		
Rpn15	Scaffold?		

Rpt- regulatory particle of triple-ATPase subunit, ATPase- adenosine triphosphatase, Rpn- regulatory particle of non-ATPase subunit, PIP- proteasome interacting protein, Ub- ubiquitin, DUB- deubiquitinating enzyme, ?- suspected function, exact function unknown. Adapted from (Saeki and Tanaka, 2012).

Due to its role in regulation of numerous cellular processes, including pro-survival NF κ B signalling and cell cycle progression, the proteasome has become a promising target for therapeutic intervention. One drug in particular,

Bortezomib (Velcade) is used to treat refractory multiple myeloma and mantle cell lymphoma and has been trialled in combination with other agents against numerous other malignancies such as non-Hodgkin lymphoma, Hodgkin lymphoma, metastatic pancreatic cancer, T cell prolymphocytic leukaemia and non-small cell lung cancer (Richardson et al., 2006). This drug primarily targets the chymotrypsin-like activity of the B5 subunit, displays limited activity against the caspase-like B1 subunit and at high doses can also inhibit the trypsin-like activity of the B2 subunit. Next generation proteasome inhibitors, carfizomib and salinosporamide A, have also become available and are undergoing clinical trials against refractory multiple myeloma (Lawasut et al., 2012).

1.2.3 Protein aggregation and aggresome formation

When proteasome function becomes impaired or the UPS becomes overwhelmed by the volume of protein requiring degradation, ubiquitinated proteins form cytoplasmic aggregates. These aggregates often also contain molecular chaperones such as p62 and neighbour of BRCA1 (breast cancer 1, early onset) gene 1 protein (NBR1) (Zatloukal et al., 2002, Komatsu et al., 2007, Kirkin et al., 2009). Two functional domains in p62 and NBR1 allow them to regulate aggregate formation: the ubiquitin-associated (UBA) domain and the Phox1 and Bem1p (PB1) domain (Lamark et al., 2009). The UBA domain allows binding to ubiquitinated target proteins and the PB1 domain is a protein-protein interaction domain allowing the homo- or hetero-oligomerisation of PB1 domain containing proteins. Protein aggregates are targeted for immediate degradation by autophagy (see Section 1.2.4) or, under conditions of limiting protein degradation, are funnelled to the microtubule-organising centre (MTOC) to form an aggresome (Tyedmers et al., 2010). The aggresome is a cytoprotective aggregate that assimilates protein aggregates into a large insoluble structure, effectively separating potentially cytotoxic aggregates from the rest of the cell. The function of E3 ubiquitin ligases is important in aggregate clearance/aggresome formation as specific ubiquitin linkages are required. For example, under normal conditions, misfolded Parkinson's disease-associated protein DJ-1

is targeted for proteasomal degradation by the addition of K48-linked polyubiquitin chains (Olzmann et al., 2007). When proteasome function is impaired, the E3 ligase Parkin promotes the addition of K63-linked polyubiquitin chains to misfolded DJ-1, targeting it to the aggresome (Olzmann et al., 2007). Histone deacetylase 6 (HDAC6) is a key player in the cellular strategy for dealing with aggregates (Tyedmers et al., 2010). Through binding to K63-linked polyubiquitin chains and association with dynein motors, HDAC6 facilitates the trafficking of protein aggregates along microtubules to the perinuclear MTOC (Kawaguchi et al., 2003). This is the site of aggresome formation, where protein aggregates are caged by the intermediate filament vimentin. Ultimately aggresomes are removed by the autophagy pathway (Ravikumar et al., 2004, Webb et al., 2003, Fortun et al., 2003). There is evidence that aggresome removal by autophagy is not a universal phenomenon; however an alternative mechanism of aggresome degradation has yet to be discovered (Wong et al., 2008).

1.2.4 Autophagy

The autophagy pathway is a multifaceted degradation pathway designed for the bulk delivery of proteins, protein aggregates and organelles to lysosomes for degradation. Autophagy literally means “self-eating” and was first associated with nutrient starvation, as the degradation of proteins and organelles by this pathway results in the recycling of their constituents (Lum et al., 2005). There are three types of autophagy: microautophagy, chaperone mediated autophagy (CMA) and macroautophagy (Figure 1-6). In microautophagy, a portion of the cytoplasm containing proteins or whole organelles is directly engulfed by the invagination or protrusion of arm-like structures of the lysosomal membrane (Li et al., 2012). CMA is a very selective form of autophagy that targets only soluble proteins. Proteins containing the pentapeptide motif KFERQ are recognised by heat shock cognate protein 70 (Hsc70) and delivered directly to the lysosome through interaction with the lysosome-associated membrane protein type 2a (LAMP-2A) on the lysosomal membrane (Dice, 2007). The main form of autophagy

is macroautophagy, which involves the sequestration of proteins, protein aggregates and organelles into a double-membraned vesicle called the autophagosome (Boya et al., 2013). This is then transported in a dynein-dependent manner along microtubules to fuse with a lysosome. This structure is known as the autolysosome (also called the autophagolysosome) and its contents are degraded by the lysosomal enzymes. The resulting degradation products can be released into the cytoplasm and recycled by the cell, presented to the immune system by MHC molecules or ejected into the extracellular environment (Johansen and Lamark, 2011). Although generally thought to be non-specific, there are a number of specific forms of autophagy including the selective degradation of large protein aggregates (aggrephagy), damaged mitochondria (mitophagy), peroxisomes (pexophagy), ribosomes (ribophagy), endoplasmic reticulum (ER) (reticulophagy), and bacteria and viruses (xenophagy) (Boya et al., 2013). The main function of basal autophagy is for protein quality control, and involves the targeted degradation of misfolded protein aggregates and damaged organelles.

Autophagy has been best studied in yeast, in which a number of autophagy related (ATG) genes have been identified (Mizushima et al., 2011). The 18 core Atg proteins (Atg1-10, 12-14, 16-18, 29, and 31) are mostly conserved in humans and when visualised by fluorescence microscopy are seen to accumulate as a single punctate structure next to the vacuole in yeast and as multiple punctate accumulations close to the ER in mammalian cells (Suzuki et al., 2001, Itakura and Mizushima, 2010). These Atg protein accumulations are believed to be the sites of autophagosome formation and are termed the pre-autophagosomal structure (PAS). Through the action of Atg protein complexes and lipid recruitment the autophagosomal precursor is generated.

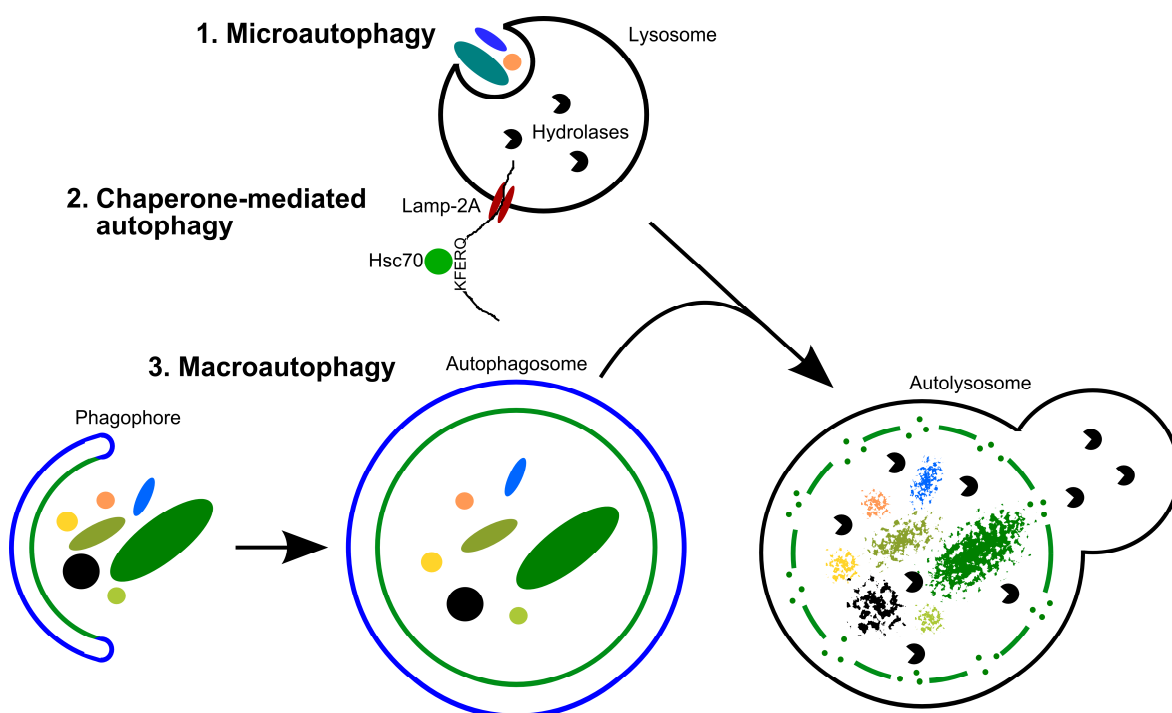


Figure 1-6 The three forms of autophagy.

There are three forms of autophagy: microautophagy, chaperone-mediated autophagy (CMA) and macroautophagy. 1. Microautophagy is the process in which a portion of the cytoplasm containing proteins or organelles (e.g. mitochondria) is directly engulfed by a lysosome. 2. Chaperone-mediated autophagy is the selective degradation of proteins containing a KFERQ motif. This motif is recognised by molecular chaperone Hsc70, which delivers the protein directly to the lysosome via interaction with Lamp-2A in the lysosomal membrane. 3. Macroautophagy is the main form of autophagy and involves the sequestration of protein aggregates and organelles into a double membraned vesicle known as the autophagosome. The process begins by the formation of the phagophore or isolation membrane, which closes to mature into the autophagosome. This then fuses with a lysosome to form an autolysosome, in which the contents of the autophagosome are degraded by lysosomal hydrolases. Adapted from (Mizushima et al., 2008)

The exact mechanism behind the formation of the autophagosome precursor, known as the phagophore or isolation membrane, is not fully understood but is known to involve a number of protein complexes, including the Atg1/unc-51-like kinase (ULK1) complex and the Atg6 (Beclin-1)/class III PI3K complex, and vesicles containing the transmembrane protein Atg9 (Figure 1-7). In yeast a dimer complex of Atg1-13-17-31-29 is thought to regulate the fusion of Atg9 positive vesicles resulting in nucleation of the autophagosomal membrane (Hamasaki et al., 2013). In mammalian cells the Atg1 homologue ULK1 forms a complex with Atg13, Atg101 and Atg17 homologue FIP200 (Choi et al., 2013).

This is believed to play a similar role to the Atg1 complex in yeast. When active, the kinase activity of ULK1 phosphorylates and activates components of the mammalian Atg6 homologue Beclin-1/ PI3K complex, most importantly Beclin-1 (Kroemer et al., 2010, Russell et al., 2013). The Beclin-1/ PI3K complex consists of Beclin-1, p150, Atg14L, and the PI3K Vps34 (Choi et al., 2013). The phosphatidylinositol-3-phosphate (PI3P) generating activity of Vps34 is regulated by phosphorylated Beclin-1 in conjunction with other components of this complex and is crucial for autophagosome membrane formation (Kroemer et al., 2010). The exact source of the membrane is a subject of much debate as it has been reported to originate from the ER, the Golgi, mitochondria and the plasma membrane (Hamasaki et al., 2013). It is possible that all of these can act as a lipid source simultaneously or individually depending on the requirements of the autophagy-inducing stress.

The elongation of the autophagosomal membrane and formation of the complete autophagosome is dependent on two ubiquitin-like protein conjugation systems, the Atg5-Atg12 conjugation system and the microtubule associated light chain 3 (LC3), the mammalian homologue of Atg8, conjugation system (Glick et al., 2010). In the Atg5-Atg12 system, Atg12 is conjugated to Atg5 by the actions of Atg7 and Atg10, which act in a manner similar to an E1 ubiquitin-activating enzyme and an E2 ubiquitin-conjugating enzyme, respectively. The Atg5-Atg12 conjugate forms a complex with Atg16L1 and is associated with the growing phagophore but is not present on the surface of the complete autophagosome. The LC3 conjugation system involves the conjugation of LC3I to a lipid molecule, phosphatidylethanolamine (PE). This is achieved by the E1- and E2-like actions of Atg7 and Atg3, respectively, to form LC3II present in the membrane of the growing phagophore and the complete autophagosome. The site of LC3 lipidation is dependent on the membrane location of the Atg5-Atg12-Atg16L1 complex as Atg3-dependent conjugation of LC3 to PE is mediated by an interaction between Atg12 and Atg3 (Fujita et al., 2008). The presence of LC3II in the outer membrane of the autophagosome allows its association with dynein motors on microtubules and subsequent transport to the MTOC, where lysosomes tend to

cluster (Kimura et al., 2008). LC3 also functions as a receptor for interaction with molecular chaperones such as p62, NBR1 and nuclear dot protein 52 kDa (NDP52), thus allowing the selective degradation of ubiquitinated substrates (Johansen and Lamark, 2011).

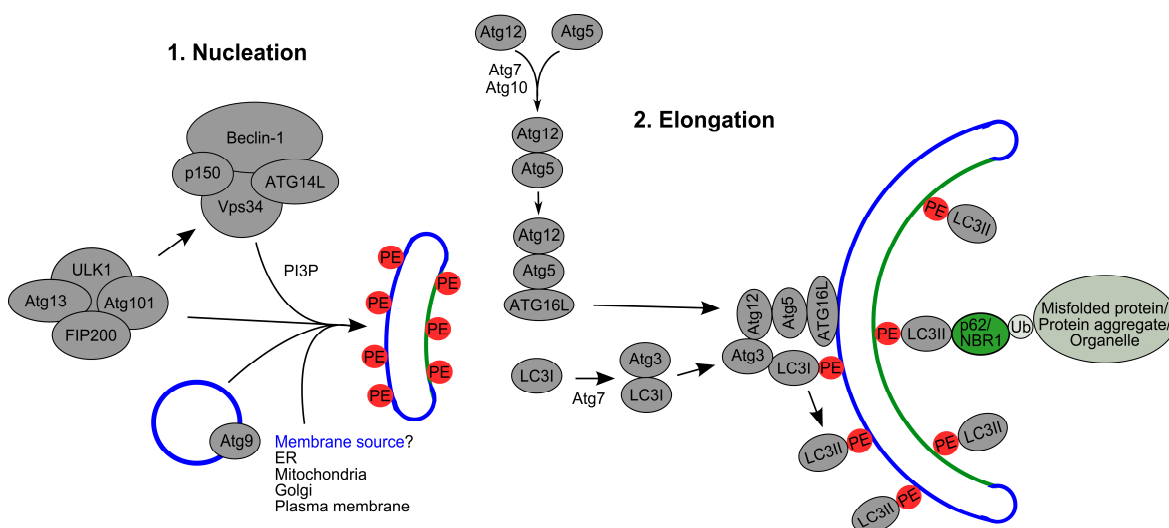


Figure 1-7 Autophagosome biogenesis.

The formation of the autophagosomal precursor is not fully understood but involves 2 main protein complexes and two ubiquitin-like protein conjugation systems. **1. Nucleation.** The process begins by the nucleation of a double-membraned structure. This is achieved through the actions of the ULK1 complex (ULK1, Atg13, Atg101, FIP200), which is believed to recruit Atg9 containing vesicles and the Beclin-1 complex (Beclin-1, p150, ATG14L, Vps34), which is activated by the kinase activity of ULK1. The active Beclin-1 complex relies on the phosphatidylinositol-3-phosphate (PI3P) generating activity of Vps34 to form the lipid membrane. The exact source of the membrane components is unclear although the ER, mitochondria, Golgi and plasma membrane have all been identified as sources. **2. Elongation.** The elongation of the membrane involves the activity of two ubiquitin-like conjugation systems. In the first, an Atg12-Atg5 conjugate is generated by the actions of Atg7 and Atg10. This then forms a complex with ATG16L which can associate with the lipid membrane. This is the site of the second conjugation reaction in which LC3I associates with Atg3 in an Atg7-dependent manner. The LC3I-Atg3 conjugate binds the Atg12-Atg5-ATG16L complex on the membrane through interactions between Atg3 and Atg12. This facilitates the conjugation of LC3I to phosphatidylethanolamine (PE) forming LC3II on the surface of the phagophore/autophagosomal membrane. LC3II interacts with microtubule-associated dynein motors to allow autophagosomal trafficking and also acts as a receptor for ubiquitin (Ub)-binding chaperones such as p62 and NBR1.

The fusion of the autophagosome with a lysosome requires the HDAC6-dependent deacetylation and recruitment of cortactin, a component of the f-actin polymerisation machinery (Lee et al., 2010). This results in the remodelling of the f-actin network to facilitate autolysosome formation. Of note, this is specific to basal or quality control autophagy, as no such HDAC6-dependent mechanism for fusion is required for autophagosome-lysosome fusion during starvation induced autophagy (Lee et al., 2010). Furthermore, a number of Rab GTPases involved in intracellular vesicle transport have been implicated in autophagosome-lysosome fusion (Gutierrez et al., 2004, Jager et al., 2004, Fader et al., 2008). It has also been found that SNARE proteins (soluble N-ethylmaleimide-sensitive attachment protein receptors) are required for fusion of autophagosomes with lysosomes in starvation-induced autophagy and xenophagy of bacteria (Furuta et al., 2010). In these instances, Vti1b on the autophagosomal surface interacted with VAMP8 (vesicle-associated membrane protein 8) to facilitate fusion. Due to the differences between starvation-induced autophagy and xenophagy (autophagosome size, morphology and conditions of initiation) it is likely that the involvement of SNAREs in autolysosome formation is a general feature of all forms of autophagy (Furuta and Amano, 2010).

1.2.5 p62/ Sequestosome 1 (SQSTM1)

p62/ Sequestosome 1 (SQSTM1), hereafter referred to as p62, is a multi-functioning signalling adapter involved in a diverse range of cellular processes including pro-survival signalling, cell death, the oxidative stress response, the inflammatory response, and protein degradation (Moscat and Diaz-Meco, 2012). p62 expresses a number of functional domains which allow it to act in multiple pathways (Figure 1-8). At the N-terminus there is a PB1 domain which is a protein-protein interaction domain and allows dimer- and oligomerisation of p62 along with its interaction with multiple protein kinases and other PB1 domain containing proteins such as autophagy-related protein NBR1 (Nezis and Stenmark, 2012). Different motifs within this domain allow p62 to bind to

multiple partners simultaneously making this domain central to p62's role as a signalling scaffold (Seibenhener et al., 2007). This is followed by two domains associated with the role of p62 in NF κ B signalling; a ZZ-type zinc finger domain (ZZ) and a TRAF6 binding domain (TB) allow the binding of RIP1 (receptor-interacting serine-threonine kinase 1) and TRAF6 (TNF receptor-associated factor 6), respectively (Nezis and Stenmark, 2012). There are also 2 nuclear localisation signals (NLS) and a nuclear export signal (NES) allowing this protein to shuttle between cytoplasm and nucleus (Pankiv et al., 2010). Following these there is a LC3 interaction region (LIR) linking p62 to the autophagy pathway (Pankiv et al., 2007) and a kelch-like ECH-associated protein 1 (KEAP1) interacting region (KIR) which links p62 to the oxidative stress response (Jain et al., 2010). At the c-terminus there is an ubiquitin-associated (UBA) domain which allows p62 to bind to mono and polyubiquitin chains (Seibenhener et al., 2004).

p62 plays an important role in protein degradation through its ability to recognise ubiquitinated substrates via the UBA domain. This domain recognises both K48- and K63-linked polyubiquitin chains, with a higher affinity for the latter (Seibenhener et al., 2004). The PB1 domain allows the interaction of p62 with other PB1 containing proteins and also with the Rpt1 subunit of the 19S regulatory particle of the 26S proteasome (Seibenhener et al., 2004). Thus p62 can act as a molecular chaperone to deliver ubiquitinated substrates, such as tau and TrkA, to the proteasome for degradation (Babu et al., 2005, Geetha et al., 2008).

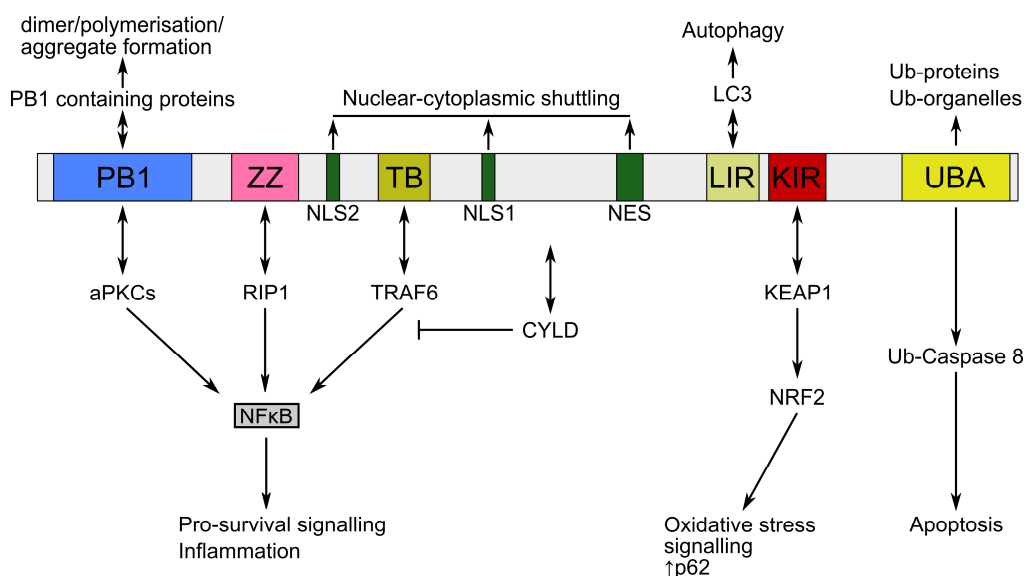


Figure 1-8 Representation of organisation of the functional domains of p62.

The functional domains of p62 allow it to interact with numerous proteins and regulate a number of cellular processes. The N-terminal PB1 domain allows the interaction of p62 with protein kinases involved in cellular signalling processes, particularly with atypical protein kinase Cs (aPKCs) important in NFκB signalling. This domain also allows p62 to form homodimers and to polymerise with itself and other PB1 containing proteins to facilitate aggregate formation. This is followed by a ZZ-type zinc finger domain (ZZ), the binding site of RIP1, and a TRAF6 binding domain (TB). Both proteins are also involved in NFκB signalling. Flanking the TB domain are two nuclear localisation signals (NLS) followed by a nuclear export signal (NES). These are followed by a LC3 interacting region (LIR), important for the role of p62 in autophagy, and a KEAP1 interacting region (KIR), linking p62 to the oxidative stress response. At the C-terminus, there is an ubiquitin-associated domain (UBA) which allows p62 to bind to both mono- and poly-ubiquitinated proteins and organelles, facilitating their degradation or involvement in signalling pathways. Adapted from (Nezis and Stenmark, 2012).

p62 also functions in the aggregation of misfolded proteins and their subsequent degradation by autophagy. Once bound to an ubiquitinated substrate, p62 can oligomerise with other substrate-bound p62 molecules through its PB1 domain, or with other PB1 domain containing proteins, such as NBR1 (Nezis and Stenmark, 2012). NBR1 functions in a similar manner to p62 in terms of protein aggregations and targeting for autophagy. Both p62 and NBR1 contain a LC3-interaction region (LIR) allowing them to act as chaperones for ubiquitinated proteins and deliver them to LC3II on autophagosomal membranes (Lamark et al., 2009). The delivery of p62/NBR1-containing protein aggregates to autophagosomes relies on HDAC6-dependent transport along microtubules

(Johansen and Lamark, 2011). Once bound to LC3II, p62 and NBR1 do not release their ubiquitinated cargo and escape the autophagosome but are degraded following autophagosome-lysosome fusion. Consequently, the accumulation of p62 has been associated with impaired autophagy (Klionsky et al., 2012). Additionally, p62 is involved in the degradation of mitochondria by mitophagy. Damaged mitochondria become depolarised and are ubiquitinated by Parkin (Matsuda et al., 2010). Parkin has been found to add both K63-linked and K27-linked polyubiquitin chains to proteins in the mitochondrial outer membrane resulting in the recruitment of p62 and HDAC6 and ultimately the delivery of damaged mitochondria to autophagosomes (Narendra et al., 2010, Geisler et al., 2010).

A number of other processes relevant to HL are regulated by p62. For example, when seen as small cytoplasmic speckles p62 is believed to be acting as a signalling hub in pro-survival NF κ B signalling pathways or in cell death pathways (Sanz et al., 2000, Jin et al., 2009, Moscat and Diaz-Meco, 2009a). When in an inactive state NF κ B is bound by I κ B in the cytoplasm. Activation of NF κ B involves the phosphorylation of I κ B by its kinase (IKK) which results in its polyubiquitination and subsequent proteasomal degradation. This frees the active NF κ B form to enter the nucleus and regulate pro-survival signalling and inflammatory responses amongst other things. The interactions of p62 with RIP1 and TRAF6 in response to TNF α , IL-1 β , NGF and RANK signalling result in activation of aPKCs, the degradation of I κ B and the release and activation of NF κ B (Sanz et al., 1999, Sanz et al., 2000, Wooten et al., 2005, Duran et al., 2004). p62 can also negatively regulate NF κ B activity by facilitating the recruitment of the deubiquitinating enzyme CYLD to TRAF6, thus preventing its ubiquitination and the subsequent downstream events resulting in NF κ B activation (Wooten et al., 2008). In response to TRAIL (TNF-related apoptosis-inducing ligand), p62 speckles are associated with promoting the apoptotic activities of caspase 8 (Jin et al., 2009). Following binding of TRAIL to death receptors DR4/5, caspase 8 is ubiquitinated in a Cullin 3-dependent manner at the DISC (death inducing signalling complex) allowing it to self-cleave into its

active form. The addition of the polyubiquitin chain to caspase 8 allows its recognition by p62, which subsequently stabilises the caspase as a dimer in cytosolic aggregates and enhances its half-life and activity as an initiator caspase of the extrinsic apoptotic pathway.

The oxidative stress response also relies on p62 activity (Nezis and Stenmark, 2012). Nuclear factor erythroid-2-related factor 2 (NRF2) is a transcription factor that induces the expression of cytoprotective genes such as those involved in the reduction of reactive oxygen species (ROS), members of the glutathione S-transferase gene family involved in detoxification, and members of the multi-drug resistance protein gene family (Taguchi et al., 2011). NRF2 levels are kept in check under normal conditions by KEAP1. KEAP1 binds to NRF2 and facilitates its Cullin 3-dependent ubiquitination and subsequent proteasomal degradation (Kobayashi et al., 2004). Under oxidising conditions the interaction between KEAP1 and Cullin 3 is disrupted, freeing NRF2 (Itoh et al., 2004). p62 lends an additional level of regulation to this process by binding to KEAP1 at the NRF2 binding site, resulting in the recruitment of the p62-KEAP1 complex to autophagosomes and allowing NRF2 to induce antioxidant gene expression (Komatsu et al., 2010). NRF2 also induces the expression of p62, creating a positive feedback loop (Jain et al., 2010).

The inflammatory response is both positively and negatively regulated by p62. The receptor/ligand based p62-dependent activation of NF κ B mentioned above links this protein to the inflammatory response. p62 has also been found to activate the p38/MAPK pathway in response to inflammatory cytokines such as IL-1 β (Kawai et al., 2008). This p62-dependent activation resulted in the stabilisation of the mRNA of other inflammatory cytokines, specifically IL-8. p62 has also been found to prevent excessive cytokine production following macrophage activation by interacting with transcription factors such as IRF8 (IFN regulatory factor 8) and Ro52 (Kim and Ozato, 2009). This regulation of inflammatory and pro-survival signalling is particularly relevant to HL due to the

large number of cells recruited by HRS cells and the high degree of pro-survival cross-talk between the immune infiltrate and the malignant cells.

1.2.6 Autophagy and disease

Autophagy is accepted to be a tumour suppressive mechanism as it removes toxic protein aggregates and organelles, such as damaged, ROS-producing mitochondria (White, 2012). Autophagy activity has also been found to be required for initiation and maintenance of tumour suppressive cellular senescence following oncogene expression (Young et al., 2009). Additionally, the regulation of p62 expression by autophagy has emerged as an important tumour suppressive mechanism. Accumulation of p62 due to defective autophagy has been reported to increase NRF2 activity and NF κ B signalling, thus promoting inappropriate cell survival (Inami et al., 2011, Mathew et al., 2009). Tumourigenic chronic inflammation has also been associated with defective autophagy in liver cancer and Crohn's disease (Mathew et al., 2009, Cadwell et al., 2008).

Conversely, autophagy has also been reported to support tumour growth, as cells in the middle of a tumour mass will be subject to nutrient deprivation and hypoxia, both of which are countered by autophagy activity (Degenhardt et al., 2006). Furthermore, the role of autophagy in protein turnover is important in the regulation of metabolic stress experienced by highly proliferative cells, such as tumour cells (White, 2012). Autophagy has also been implicated in metastasis, as an up-regulation of autophagy has been associated with escape from anoikis following matrix detachment (Fung et al., 2008). As mentioned above, the initiation and maintenance of the senescent state requires autophagy activity and its inhibition results in the cytoplasmic accumulation of cytokines and chemokines associated with the senescence-associated secretory profile (SASP) (Young et al., 2009). Although, cellular senescence is a mechanism of tumour suppression, it may be of relevance to HL. RS cells have been demonstrated to be non-replicative (Hsu et al., 1988, Newcom et al., 1988) and during my MRes

project (Nuclear stress responses in Hodgkin's Lymphoma, 2009) a small population of RS cells in HL-derived cell lines stained positively for senescence-associated β -galactosidase, a commonly used marker of cellular senescence (Dimri et al., 1995). Although the secretory profile of HRS cells does not exactly match the SASP, they appear to serve a similar function in attracting the immune system (Steidl et al., 2011a, Coppe et al., 2010). It is likely that its generation also requires autophagy activity, as autophagy has been demonstrated to regulate the secretion of various cytokines both positively and negatively (Harris, 2011).

Resistance to chemotherapy has been associated with an up-regulation of autophagy following treatment in a number of human malignancies (Sui et al., 2013). Consequently autophagy inhibitors have been used in conjunction with conventional therapies in several tumour models including chronic myeloid leukemia (CML), glioma, multiple myeloma, breast, colon, pancreatic, and prostate cancer (Sui et al., 2013). One of the best examples of the success of a combination of autophagy inhibition with current therapy was in CML. Here autophagy was found to be induced and promote cell survival following treatment with tyrosine kinase inhibitor (TKI) imatinib (Ertmer et al., 2007). Autophagy inhibition using hydroxychloroquine (HCQ) was shown to enhance cell death induced by imatinib in CML cell lines and in primary cells (Bellodi et al., 2009). Furthermore, TKI-resistant CML stem cells were found to be almost completely eliminated following treatment with a combination of TKIs with HCQ (Bellodi et al., 2009).

Pharmacological strategies employed to inhibit autophagy include the use of 3-methyladenine (3-MA), bafilomycin A1, and chloroquine (CQ) and its derivative HCQ. 3-MA inhibits PI3K activity of Vps34, preventing autophagosome biogenesis (Blommaert et al., 1997). Bafilomycin A1 inhibits vacuolar H^+ -ATPases and prevents acidification of the lysosome (Yamamoto et al., 1998). CQ and HCQ are weak bases and accumulate in lysosomes preventing their acidification (Rote and Rechsteiner, 1983, Poole and Ohkuma, 1981). So far only CQ and HCQ have been

approved for clinical use (Sui et al., 2013). There are currently a large number of clinical trials exploring the use of autophagy inhibition, mostly in conjunction with conventional chemotherapy, against a large number of human malignancies. These include breast cancer, CML, colorectal cancer, glioblastoma, melanoma, multiple myeloma, non-small-cell lung cancer (NSCLC), ovarian cancer, prostate cancer, pancreatic cancer, and renal cell carcinoma (Sui et al., 2013). This highlights the important role that the autophagy pathway plays in human disease and establishes it as a promising therapeutic target.

1.3 Summary

The cell biology of Hodgkin lymphoma reveals an overreliance on hyperactive pro-survival signalling pathways achieved through transformation events and through an extensive interaction with the immune system. Although believed to be of B cell origin, HRS cells display a global down-regulation of B cell related genes and express markers, both cell-surface and transcriptional, of numerous cell lineages. The generation of numerous cytokines and chemokines, combined with the aneuploid nature of HRS cells, may put these cells under a protein handling stress. To date, previous studies of HL have not addressed the activity of protein degradation pathways, largely due to the limited numbers of malignant cells in primary material and also due to technological limitations. The degradation pathways represented by the UPS and autophagy pathway are involved in numerous cellular processes relevant to HL and are targetable by pharmacological agents, a number of which are approved for clinical therapy.

1.4 Aims

The primary aims of this project were to characterise the activities of protein degradation pathways in HL-derived cell lines, which represent a model of advanced-stage metastatic HL cells, and to determine the sensitivity of the cell lines to inhibition of these pathways by clinically available drugs. It was hypothesised that HL cells may be under protein handling stress given their aneuploid status and the vast secretory profile they generate to manipulate their microenvironment, and consequently that they would be sensitive to inhibition of protein handling pathways such as the proteasome, autophagy pathway and HDAC6-mediated transport. It was hypothesised that p62, which has a diverse role in protein handling pathways, may serve as a tool to inform on the status of these pathways and serve as a biomarker of susceptibility to therapeutic interference of these pathways to mediate cell death.

In Chapter 3, the expression of the multi-functional signalling adapter p62 in HL-derived cell lines is examined. The expression of p62 in the tumour cells of HL biopsy material is also examined to establish the relevance of p62 expression in HL-derived cell lines to primary patient material.

In Chapter 4, the activities of protein degradation pathways in HL-derived cell lines are measured and the sensitivities to inhibition of these pathways are determined in an effort to derive correlates for pathway activity and sensitivity to inhibition.

In Chapter 5, the phenotypic differences of HD-MyZ compared to other HL-derived cell lines are further explored and exploited in an effort to enhance cell killing with alternative therapeutic agents.

In Chapter 6, the presence of putative cancer stem-like cells (CSCs) is examined in a selection of HL-derived cell lines.

Chapter 2. Materials and Methods

2.1 Suppliers and Manufacturers

The materials used are described in the relevant methods sections. The Suppliers and their addresses are listed in Table 2-1. Unless stated otherwise, all chemicals were purchased from Sigma-Aldrich.

Table 2-1 Suppliers and Manufacturers

Supplier	Address
Abcam	330 Cambridge Science Park, Cambridge, CB4 0FL, UK
Becton Dickinson (BD) Biosciences/ Transduction Laboratories	Edmund Halley Road, Oxford Science Park, Oxford, OX4 4DQ, UK
Beckman Coulter	Oakley Court, Kingsmead Business Park, London Road, High Wycombe, HP11 1JU, UK
BioRad	Bio-Rad Laboratories Ltd., Bio-Rad House, Maxted Road, Hemel Hempstead, Hertfordshire, HP2 7DX, UK
Cell Signaling Technology (affiliated with New England Biolabs)	Cell Signaling Technology, Inc., 3 Trask Lane, Danvers, MA 01923, USA
DAKO	Dako UK Ltd, Cambridge House, St Thomas Place, Ely Cambridgeshire, CB7 4EX, UK
DJB Labcare Ltd	DJB Labcare Ltd, 20 Howard Way, Interchange Business Park, Newport Pagnell, Buckinghamshire, MK16 9QS, UK
Enzo Life Sciences	Enzo Life Sciences (UK) LTD., Palatine House, Matford Court, Exeter, EX2 8NL, UK
Eppendorf	102 Motor Parkway, Hauppauge, NY 11788, USA
Fisher Scientific	Fisher Scientific UK Ltd, Bishop Meadow Road, Loughborough, LE11 5RG, UK

IBM	IBM United Kingdom Limited, PO Box 41, North Harbour, Portsmouth, Hampshire, PO6 3AU, UK
LC Laboratories	165 New Boston Street, Woburn, MA 01801, USA
Leica Microsystems	Leica Microsystems (UK) Ltd., Davy Avenue Knowlhill, Milton Keynes, MK5 8LB, UK
Life Technologies	3 Fountain Drive, Inchinnan Business Park, Paisley, UK
MBL International	15A Constitution Way, Woburn, MA 01801, USA
Mettler-Toledo	Mettler-Toledo Ltd., 64 Boston Road, Beaumont Leys, Leicester, LE4 1AW
Millipore	Merck Millipore, 290 Concord Road, Billerica, MA 01821, USA
National Diagnostics	Unit 4, Fleet Business Park, Itlings Lane, Hessle Hull, HU13 9LX, UK
New England Biolabs	New England Biolabs (UK) Ltd., 75-77 Knowl Piece, Wilbury Way, Hitchin, Hertfordshire, SG4 0TY, UK
Olympus	Olympus Europa Holding GmbH, Wendenstraße 14-18, 20097 Hamburg, Germany
Promega	Promega UK, Delta House, Southampton Science Park, Southampton, SO16 7NS, UK
Roche	Roche Diagnostics Corporation, Roche Applied Science, 9115 Hague Road, P.O. Box 50414, Indianapolis, IN 46250-0414, USA
R&D Systems	R&D Systems Europe Ltd., 19 Barton Lane, Abingdon Science Park, Abingdon, OX14 3NB, UK
Santa Cruz Biotechnology	Santa Cruz Biotechnology, Inc., Bergheimer Str. 89-2, 69115 Heidelberg, Germany
Sigma-Aldrich	Sigma-Aldrich Company Ltd., Dorset, UK

Stem Cell Technologies	STEMCELL Technologies SARL, 40 Rues des Berges, Miniparc Polytec, Bâtiment Sirocco, 38000 Grenoble, France
Thermo Scientific	Thermo Fisher Scientific Inc., 81 Wyman Street. Waltham, MA 02454, USA

2.2 Consumables

All tissue culture flasks (25 cm² 10-126-28, 75cm² 10-126-37), 6-well (08-772-1B) and 96-well (08-772-3) tissue culture plates, pipettes (5 ml 13-676-10H, 10 ml 13-676-10J), cryovials (12567501), cell scrapers (07-200-365), cytofunnels (59910390) and fluorescence-activated cell sorting (FACS) tubes (14-959-11A) were purchased from Fisher Scientific. Pipette tips (p20 GP-20F, p200, GP-200F, p1000 GP-1000F) were purchased from Mettler-Toledo.

2.3 Equipment

Large items of equipment used for this project are listed in Table 2-2.

Table 2-2 Equipment and suppliers

Item	Supplier
Haraeus Multifuge 3SR Plus	DJB Labcare Ltd
Shandon Cytospin 2	Thermo Scientific
Microcentrifuge 5415R	Eppendorf
iBlot® Gel Transfer Device	Life Technologies
Luminoskan Ascent Microplate Luminometer	Thermo Scientific
Beckman Coulter Cytomics FC 500	Beckman Coulter
BD FACSAria™ Cell Sorter	BD Biosciences

2.4 Cell Culture

Hodgkin lymphoma-derived cell lines L-540, KM-H2, HDLM-2, L-1236, L-428 and HD-MyZ and EBV immortalised lymphoblastoid cell line IM-9 were purchased from the Deutsche Sammlung von Mikroorganismen und Zellkulturen (DSMZ). KM-H2, L-1236, L-428 and HD-MyZ cells were maintained in complete medium (RPMI 1640 supplemented with foetal bovine serum (FBS) to a final concentration of 10% and Penicillin-Streptomycin (Life Technologies, 15070-063) to a final concentration of 50 U/ml and 50 µg/ml, respectively) at 37°C in a humidified incubator gassed to 5% CO₂. Cell lines were maintained from original aliquots. L-540 and HDLM-2 cells were maintained from in complete medium containing 20% FBS. Cells were grown in 25 cm² or 75 cm² tissue culture flasks with a ventilated cap (Fisher Scientific, 10-126-28 and 10-126-37, respectively) and split twice a week to

prevent cell density exceeding 1×10^7 cells/ml. All cell lines were suspension cells with the exception of HD-MyZ, which contained only adherent cells, and L-1236, which contained a mixture of both adherent and suspension cells. Adherent cells were detached using a cell scraper (Fisher Scientific, 07-200-365). During splitting, cells were washed in PBS and resuspended in complete media.

Commonly used media and buffers for cell preparation are listed in Table 2-3

Table 2-3 Commonly used media and buffers

Buffer	Components
Complete medium	RPMI 1460 10% v/v foetal bovine serum (FBS) Penicillin (50 U/ml) - Streptomycin (50 µg/ml)
Freezing mix	10% v/v dimethylsulphoxide (DMSO) 90% v/v FBS
MiniMacs buffer (MMB)	0.5% w/v bovine serum albumin (BSA) 0.02 M ethylenediaminetetraacetic acid (EDTA) in PBS

RPMI 1640 (Life Technologies, 61870-044), FBS (Life Technologies, 10082-147), Penicillin-Streptomycin (Life Technologies, 15070-063)

All cell culture and experiments involving live cell preparation for staining procedures were performed in a Class II Microbiological Safety Cabinet (MSC).

2.5 Cell counts with Trypan Blue dye exclusion

Cells were counted using the Trypan Blue exclusion method, in which a 1:1 mixture of cell suspension and 0.4% Trypan Blue (Sigma-Aldrich, T8154-100ML) was applied to a haemocytometer and both the live (unstained) and dead cells (stained) were counted in the 25 central squares. This number was multiplied by the dilution factor of cells and Trypan Blue and multiplied by 10^4 to give the number of cells per ml of cell suspension.

2.6 Cryopreservation of Cells

Cells were centrifuged (using a Heraeus Multifuge 3SR Plus, DJB Labcare Ltd, 75004371) for 5 minutes at $300 \times g$ and the pellet was re-suspended in 1 ml of freezing mix (10% v/v dimethylsulphoxide (DMSO), 90% v/v FBS) and transferred to 1.8 ml cryovials (Fisher Scientific). Cryovials were stored overnight at -80°C and then transferred to liquid nitrogen for long-term storage.

2.7 Immunocytochemistry

2.7.1 Solutions

Solutions used for immunocytochemistry are listed in Table 2-4

Table 2-4 Buffers used for immunocytochemistry

Buffer	Components
Fixatives	4% v/v paraformaldehyde/ PBS Methanol (chilled to -20°C)
Permeabilisation buffer	0.25% Triton X-100/ PBS
Wash Solution	0.2% Tween-20/ PBS
Blocking Buffer	10% powdered milk w/v in PBS/ 0.1% Tween 20
Staining Buffer	5% powdered milk w/v in PBS/ 0.1% Tween 20

2.7.2 Procedure

Cytospins were prepared using a Shandon Cytospin 2 (Thermo Scientific) onto a glass slide at 400 x g for 10 minutes. A wax ring was then drawn around each cell spot on the slide using a Dako Pen (Dako, S2002) and the cells were fixed for 5 minutes using 4% v/v paraformaldehyde/ PBS. Alternatively, to preserve microtubule networks for visualisation of α -tubulin, cells were fixed at -20°C with pre-chilled methanol for 3 minutes and immediately washed in wash solution. When 4% v/v paraformaldehyde/ PBS was used cells were treated with permeabilisation buffer for 5 minutes. Cells were then incubated in blocking buffer for 1 hour at room temperature, washed in wash solution and stained with the appropriate antibody diluted to the relevant concentration (Table 2-5) in staining buffer overnight at 4°C. This was followed by 3 x 5 minute washes in

wash solution at room temperature. Reactivity with primary antibodies was detected by incubation with the appropriate alexa fluor conjugated secondary antibody diluted 1: 1000 in staining buffer. Secondary antibody incubations were carried out at room temperature for 1 hour. The cells were then washed for 3 x 5 minutes in wash solution at room temperature. Cytospins were treated with mounting medium containing DAPI (ProLong® Gold antifade reagent, Life Technologies, P-36931) overnight protected from light and coverslips were sealed using clear nail varnish. Stained cells were visualized on a Leica DM IRB microscope equipped with a HCX PL FLUOTAR 63x/ 1.25 oil objective lens; images were captured using a Leica DFC420 camera.

Table 2-5 Antibodies used for immunocytochemistry

Antibody	Species of origin	Supplier (Catalogue number)	Dilution
Anti-acetylated-tubulin	Mouse monoclonal	Abcam (ab24610)	1: 1000
Anti-alpha-tubulin	Rabbit polyclonal	Abcam (ab18251)	1: 1000
Anti-cathepsin B	Rabbit polyclonal	Abcam (ab33538)	1: 250
Anti-CENPF	Rabbit polyclonal	Abcam (ab5)	
Anti-phospho-histone H2AX (Ser-139)	Mouse monoclonal	Millipore (05-636)	1:250
Anti-gamma-tubulin	Mouse monoclonal	Abcam (ab11316)	1: 200
Anti-LAMP2	Mouse monoclonal	Abcam (ab25631)	1: 100
Anti-LC3B	Rabbit polyclonal	Cell Signalling Technology (#2775)	1: 250
Anti-p62 ^{Ick ligand}	Mouse monoclonal	BD Transduction Laboratories (610832)	1: 500
Anti-p62/SQSTM1	Rabbit polyclonal	MBL International (PM045)	1: 500
Anti-Parkin (PRK8)	Mouse monoclonal	Abcam (ab77924)	1: 250
Anti-Parkin	Rabbit polyclonal	Abcam (15954)	1: 250
Anti-PML (N-19)	Goat polyclonal	Santa Cruz Biotechnology (sc-9862)	1: 1000
Anti-TARC	Goat polyclonal	R&D Systems (AF364)	1:200
Anti-tom20 (FL-145)	Rabbit polyclonal	Santa Cruz Biotechnology (sc-11415)	1: 200

Anti-TPX2 (18D5-1)	Mouse monoclonal	Abcam (ab32795)	1:200
Anti-vimentin-Cy3	Mouse monoclonal	Sigma-Aldrich (C9080)	1: 200
Alexa Fluor 488 Anti-Goat IgG	Donkey	Life Technologies (A11055)	1:1000
Alexa Fluor 488 Anti-Mouse IgG	Chicken	Life Technologies (A21200)	1:1000
Alexa Fluor 488 Anti-Mouse IgG	Donkey	Life Technologies (A21202)	1:1000
Alexa Fluor 488 Anti-Mouse IgG	Goat	Life Technologies (A11001)	1:1000
Alexa Fluor 488 Anti-Rabbit IgG	Chicken	Life Technologies (A21441)	1:1000
Alexa Fluor 488 Anti-Rabbit IgG	Goat	Life Technologies (A11008)	1:1000
Alexa Fluor 555 Anti-Mouse IgG	Goat	Life Technologies (A21426)	1:1000
Alexa Fluor 555 Anti-Mouse IgG	Rabbit	Life Technologies (A31570)	1:1000
Alexa Fluor 555 Anti-Rabbit IgG	Donkey	Life Technologies (A31572)	1:1000

2.8 Immunohistochemistry (IHC)

All immunohistochemistry was performed by the Veterinary Diagnostic Services at the University of Glasgow Veterinary School. A dilution series using human tonsil sections was performed to establish the optimal concentration of antibody. For immunohistochemistry, paraffin-embedded tissue sections were deparaffinised and rehydrated using a graded alcohol series. Antigen retrieval was performed by incubating slides in sodium citrate buffer (pH 6.0) and endogenous peroxidase activity was blocked using DAKO Real TM Peroxidase blocking solution (DAKO, K5007). Tissue sections were incubated with anti-p62 antibody (MBL International, PM045, 1: 8,000) with signal detection using EnVision (DAKO, K5007). Stained sections were visualized using an Olympus BX51

microscope (Olympus, Tokyo, Japan) fitted with an Olympus DP-71 camera. Patient biopsy material was obtained under the following ethics application, “Investigation of the cause of Hodgkin lymphoma” REC number: 06/MRE00/83. All patients gave written informed consent. Immunohistochemistry was performed using freshly cut sections stained synchronously using a DAKO Autostainer.

2.9 SDS-PAGE and Western blot

2.9.1 Solutions

The buffers and gel recipes used for SDS-PAGE and western blotting are listed in Table 2-6. Unless stated otherwise, chemicals were purchased from Sigma-Aldrich.

Table 2-6 Buffers and gel recipes used for SDS-PAGE and western blotting

Buffer	Components
RIPA lysis Buffer	25 mM Tris-HCl pH 7.6 150 mM NaCl 1 mM EDTA 1% Triton X-100 1% sodium deoxycholate 0.1% sodium dodecyl sulfate (SDS) Pierce® Protease Inhibitor Tablet (Thermo Scientific, 88660) in distilled H ₂ O (dH ₂ O)

15% running gel	<p>5 ml 30% acrylamide, 0.8% bis-acrylamide stock solution (National Diagnostics, EC-890)</p> <p>2.5 ml 1.5 M Tris pH 8.8 (BioRad, 161-0798)</p> <p>0.1 ml 10% SDS</p> <p>100 μl 10% ammonium persulphate (APS)</p> <p>10 μl tetramethylethylenediamine (TEMED)</p> <p>2.29 ml H₂O (to a final volume of 10 ml)</p>
10% running gel	<p>3.3 ml 30% acrylamide, 0.8% bis-acrylamide stock solution (National Diagnostics, EC-890)</p> <p>2.5 ml 1.5 M Tris pH 8.8 (BioRad, 161-0798)</p> <p>0.1 ml 10% SDS</p> <p>100 μl 10% ammonium persulphate (APS)</p> <p>10 μl tetramethylethylenediamine (TEMED)</p> <p>3.99 ml H₂O (to a final volume of 10 ml)</p>
5% stacking gel	<p>0.83 ml 30% acrylamide, 0.8% bis-acrylamide stock solution (National Diagnostics, EC-890)</p> <p>1.26 ml 0.5 M Tris pH 6.8 (BioRad, 161-0799)</p> <p>0.05 ml 10% SDS</p> <p>100 μl 10% ammonium persulphate (APS)</p> <p>10 μl tetramethylethylenediamine (TEMED)</p> <p>2.75 ml H₂O (to a final volume of 10 ml)</p>
Running buffer	<p>25 mM Tris base</p> <p>193 mM Glycine</p> <p>0.1% SDS</p> <p>in dH₂O</p>
Sample loading buffer	50 μ l β -mercaptoethanol (BioRad, 161-0710)

	950 μ l of Laemmli Sample Buffer (BioRad, 161-0737)
Blocking buffer	10% powdered milk w/v in PBS/0.1% Tween 20
Washing solution	PBS/0.2% Tween 20
Staining buffer	5% powdered milk w/v in PBS/0.1% Tween 20
Stripping buffer	100 mM β -mercaptoethanol 2% SDS 62.4 mM Tris-HCl pH 6.0 in dH ₂ O
Quick stripping buffer	0.2 M NaOH

2.9.2 Cell lysis

Samples were prepared for lysis by washing in PBS to remove culture medium. Cells were lysed with RIPA buffer for 30 minutes on ice. In the case of lysis for subsequent detection of p62 and vimentin, and for LC3B analysis RIPA buffer was supplemented with SDS to a final concentration of 1%, incubated on ice for 30 minutes and then boiled for 5 minutes to aid solubilisation of protein (Klionsky et al., 2012). The lysate was centrifuged (using a Microcentrifuge 5415R, Eppendorf, 022621408) at 16,100 x g at 4°C for 15 minutes and the supernatant was aspirated and stored at -80°C. Protein concentrations were measured using the BCA protein assay kit (Sigma-Aldrich, BCA-1) using BSA as standard.

2.9.3 Protein separation

Samples, including a pre-stained protein marker (Precision Plus Protein™ Dual Colour Standards, BioRad, 161-0374), were diluted 1:1 in loading buffer and incubated at 95°C for 5 minutes to denature the protein. 20 μ g protein from each sample was loaded onto SDS-PAGE gels submerged in running buffer. The majority of gels were 10% acrylamide gels, 15% acrylamide gels were used for examining LC3B levels during analysis of autophagy flux (section 2.12). A

stacking gel was used in each case. Proteins were separated at 100 V for approximately 1.5 hours, and subsequently transferred to a nitrocellulose membrane using the iBlot system (Life Technologies) for subsequent western blot analysis.

2.9.4 Western blotting

Membranes were immersed in blocking buffer for 1 hour, followed by a 5 minute wash in washing solution. Blocking and washing steps were performed at room temperature with gentle agitation. Membranes were then incubated with the appropriate antibody diluted in staining buffer to the appropriate dilutions (Table 2-7) overnight at 4°C with gentle agitation. This was followed by 3 x 5 minute washes in washing solution at room temperature. The membranes were then incubated with the appropriate HRP-conjugated secondary antibody diluted 1: 1000 in staining buffer for 1 hour at room temperature with gentle agitation. This was followed by 3 x 5 minute washes in washing solution at room temperature. HRP conjugates were detected using the Millipore Immobilon Western Chemiluminescent HRP substrate kit as instructed by the manufacturer.

2.9.5 Membrane stripping and re-probing for loading controls

Following HRP detection, membranes were re-immersed in washing solution. In the case of using α -tubulin as a loading control for western blots measuring the expression of p62, Parkin, and Vimentin, membranes were stripped using stripping buffer. Membranes were incubated in stripping buffer for 30 minutes in a 50°C water-bath in a fume hood. For all other stripping purposes, membranes were incubated in quick stripping buffer for 10 minutes at room temperature with gentle agitation. For both stripping methods, following incubation in stripping buffer, membranes were subject to 3 x 5 minutes washes in washing solution. Membranes were then immersed in blocking buffer for 1 hour and subject to usual western blotting procedures using the relevant loading control antibodies: α -tubulin or glyceraldehyde 3-phosphate dehydrogenase (GAPDH).

Table 2-7 Antibodies used for western blotting

Antibody	Animal of origin	Supplier (catalogue number)	Dilution
Anti-acetylated-tubulin	Mouse monoclonal	Abcam (ab24610)	1: 1000
Anti-alpha-tubulin	Rabbit polyclonal	Abcam (ab18251)	1: 100,000
Anti-cleaved caspase 3 (Asp175)	Rabbit polyclonal	Cell Signalling Technology (#9661)	1: 1000
Anti-cathepsin B	Rabbit polyclonal	Abcam (ab33538)	1: 250
Anti-LC3B	Rabbit polyclonal	Cell Signalling Technology (#2775)	1: 250
Anti-GAPDH	Rabbit monoclonal	Cell Signalling Technology (#2118)	1: 10,000
Anti-histone H3 (Acetyl K9)	Rabbit polyclonal	Abcam (ab10812)	1: 5000
Anti-K48-linkage specific polyubiquitin	Rabbit polyclonal	Cell Signalling Technology (#4289)	1: 1000
anti-K63-linkage specific polyubiquitin	Rabbit monoclonal	Cell Signalling Technology (#5621)	1: 500
Anti-p62 ^{lck ligand}	Mouse monoclonal	BD Transduction Laboratories (610832)	1: 2000
Anti-p62/SQSTM1	Rabbit polyclonal	MBL International (PM045)	1: 2000
Anti-Parkin (PRK8)	Mouse monoclonal	Abcam (ab77924)	1: 250
Anti-Parkin	Rabbit polyclonal	Abcam (15954)	1: 250
Anti-mouse immunoglobulins HRP conjugate	Goat polyclonal	Dako (P0447)	1: 1000
Anti-rabbit immunoglobulins HRP conjugate	Goat polyclonal	Dako (P0448)	1: 1000

2.10 Drug Treatments for ICH/western blotting

Unless stated otherwise, cells at a density of 5×10^5 cells/ml were incubated in 6-well cell culture plates (Fisher Scientific, FDR-063-400T) with the relevant drugs for 16 hours at 37°C before cells were lysed or cytopins prepared as required. All cell lines were treated simultaneously. The concentrations used are

described in the text. Drug concentrations and incubation times were based on relevant publications: proteasome inhibition (Kashkar et al., 2007), autophagy inhibition (Mizushima and Yoshimori, 2007, Klionsky et al., 2012), HDAC6 inhibition (Kozikowski et al., 2008). All experiments included untreated controls and were repeated at least 3 times. Histone deacetylase-6 inhibitor BML-281 (BLM-GR361), cathepsin B inhibitor Ca074Me (PI-126-0001) and cysteine protease inhibitor E-64 (ALX-260-007) were purchased from Enzo Life Sciences. The inhibitor of chymotrypsin-like proteasome activity Bortezomib (Velcade) (B-1408), inhibitor of CRM-dependent nuclear export Leptomycin B (L-6100) and microtubule-stabilising mitotic inhibitor Paclitaxel (P-9600) were purchased from LC Laboratories. The autophagy inhibitors Bafilomycin A1 (B1793) and Hydroxychloroquine (HCQ) (H0915), microtubule polymerisation inhibitor Nocodazole (M1404), mitochondrial depolarising agent cyanide 3-chlorophenylhydrazine (CCCP) (C2759) and vimentin-targeting multifunctional inhibitor Withaferin A (W4394) were purchased from Sigma-Aldrich.

2.11 Chymotrypsin-like Proteasome activity

Chymotrypsin-like proteasome activity was measured using the Proteasome-Glo™ Chymotrypsin-like Cell-based assay (Promega, G8660) according to the manufacturer's instructions. The Proteasome-Glo™ Chymotrypsin-like Cell-based Reagent contains a peptide sequence specifically targeted by the chymotrypsin-like proteolytic activity of the proteasome conjugated to aminoluciferin (Suc-LLVY-aminoluciferin). It also contains luciferase (Ultra-Glo™ Recombinant Luciferase). Following cleavage of Suc-LLVY-aminoluciferin by the proteasome, the luciferase substrate aminoluciferin is freed and becomes available for the light producing luciferase reaction.

Cells were grown under normal culture conditions or with the addition of any drug (5 nM Bortezomib or 10 nM Bafilomycin A1) overnight at 37°C prior to preparation for this assay. In triplicate, 15,000 cells were plated in 100 µl of fresh culture media, containing inhibitors where relevant, in a Costar 96-well

white solid flat- bottomed plate (Fisher Scientific, 07-200-589). Cells were allowed to equilibrate to plate culture conditions for 2.5 hours at 37 °C and were then cooled to room temperature for 30 minutes. 100 µl of Proteasome-Glo™ Reagent was added to each well and mixed by pipetting. The plate was then incubated at room temperature for 10 minutes with gentle agitation to further mix the contents of each well. Luminescence was read using a Luminoskan Ascent Microplate Luminometer (Thermo Scientific). Values were normalized for background luminescence with relative light units (RLU) for no-treatments controls designated 100% or basal activity. Inclusion of Bortezomib was used to indicate chymotrypsin-like proteasome activity that could not be inhibited using this proteasome inhibitor i.e. non-proteasomal chymotrypsin-like activity.

2.12 Autophagy activity

Autophagy activity was measured by LC3B flux as recommended (Mizushima and Yoshimori, 2007, Klionsky et al., 2012). During the process of autophagy, the cytoplasmic light chain 3-I protein (LC3BI) is converted to the autophagosomal membrane bound LC3BII by phosphatidylethanolamine conjugation. The addition of this group increases the hydrophobicity of the protein allowing LC3BII to be easily separated from LC3BI by SDS-PAGE. Following autolysosome formation by autophagosome-lysosome fusion, LC3BII is degraded along with the contents of the autophagosome. By preventing the acidification of autophagolysosomes (with hydroxychloroquine (HCQ)) it is possible to preserve LC3BII. Changes in LC3BII concentration can therefore be used as a dynamic measure of material entering the autophagy pathway. An increased signal for LC3BII in the presence of HCQ indicates active autophagy and therefore positive flux.

Cell lines at a density of 5×10^5 cells/ml were incubated in complete medium with or without 20 µM hydroxychloroquine (HCQ) for 4 hours at 37 °C. For "low serum" conditions, cells were grown in RPMI 1640 containing 1% FBS overnight. To determine whether autophagy was induced following proteasome inhibition, cells were incubated in complete medium with 5 nM Bortezomib for 12 hours

prior to the addition of HCQ for 4 hours. Cells were washed in PBS and pelleted for lysate preparation. LC3 is inefficiently solubilised by detergents such as Triton X-100, instead it requires heating in the presence of 1% SDS (Klionsky et al., 2012). Consequently cell lysates were prepared using RIPA buffer containing 1% SDS and were heated at 95°C for 5 minutes (Section 2.9.2). Western blotting was performed as described (Section 2.9.4). For analysis, LC3B-II was normalised to the relevant loading control and compared between HCQ-treated and untreated lanes as recommended (Mizushima and Yoshimori, 2007). Densitometry was performed using ImageJ software.

2.13 Viability assay

Cell viability was assessed by MTS assay (CellTiter 96® AQueous Cell Proliferation Assay (MTS), Promega, G3580 (Fitchburg, WI, USA)), according to the manufacturer's instructions. In 96-well plate format, 5×10^4 cells in 100 μ l were incubated with the relevant drugs for 24 hours. After 20 hours, 20 μ l of MTS assay reagent was added to each well and the absorbance at 492 nm was measured following completion of the 24 hour incubation period. Viability data represent the mean of 3 separate experiments, each performed in triplicate, expressed as the percentage of a DMSO control.

2.14 Mitochondrial permeability

Cells were incubated with 200 nM MitoTracker™ Red CMXRos (Life Technologies, M-7512) in complete medium. Following washing in PBS, cytopins were prepared for paraformaldehyde fixation and permeabilisation with Triton x-100. As a positive control for de-polarised mitochondria, cells were incubated with the depolarising agent CCCP for 16 hours at 37°C before incubation with MitoTracker™ dye and slide preparation as above.

2.15 Statistical analysis

All statistical analyses were performed using SPSS Statistics version 9 (IBM, New York, USA). Data normality was assessed using the Kolmogorov-Smirnov statistic. Treatment groups were compared using the (non-parametric) Mann-Whitney U Test and probability (p) values were determined.

2.16 Cell cycle analysis using propidium iodide (PI)

Cells at a concentration of 1×10^6 cells/ml were washed three times by centrifugation at $300 \times g$ for 5 minutes at 4°C in ice-cold PBS containing 1 mg/ml glucose. Following the final wash, the supernatant was aspirated and discarded. The pellet was resuspended in the residual buffer by vortexing and fixed by the drop-wise addition of ice-cold 70% ethanol with constant agitation of the cell pellet. After fixation was for 18 hours at 4°C , cells were pelleted by centrifugation at $1875 \times g$ for 5 minutes at 4°C . The pellet was resuspended in PI staining solution (50 $\mu\text{g}/\text{ml}$ propidium iodide, 100 U/ml RNase, 4 mM EDTA, 1mg/ml glucose, in PBS) and incubated at room temperature for 60 minutes with gentle agitation protected from light. Cells were vortexed gently and passed through a 50 μm filter to remove cell clumps prior to analysis on a Beckman Coulter Cytomics FC 500 Series flow cytometer.

2.17 Detection of CD30, CD20 and CD27 by flow cytometry

Cells at a concentration of 1×10^6 cells/ml were distributed into 5 ml FACS tubes in 1ml MiniMacs Buffer (MMB) (0.5% w/v BSA, 0.02 M EDTA, in PBS) added prior to centrifugation at $300 \times g$ for 5 minutes. The supernatant was aspirated, cells resuspended and 20 μl of antibody were added and tubes incubated for 20 minutes at 4°C . One ml of MMB was then added and cells centrifuged as before. The resultant cell pellet was re-suspended in 0.5 ml of MMB and kept covered in

the dark until analysis was performed using the Beckman Coulter FC 500 Series flow cytometer. An unstained tube of cells in MMB containing 2 µg/ml propidium iodide was included to detect apoptotic cells. This was used to set up a gate to exclude apoptotic cells prior to the analysis of antibody stained samples. Antibodies used were CD30PE (IM2033U), CD20PE (IM1451) and CD27PE (IM2578) from Beckman Coulter and CD30FITC (F0849 clone Ber-H2) from Dako.

2.18 Side population analysis by Hoechst 33342 dye exclusion

Cells at a density of 1×10^6 cells/ml were incubated with 5 µg/ml Hoechst 33342 in 1 ml pre-warmed RPMI 1640 containing 2% v/v FBS and 10 mM HEPES for 105 minutes at 37°C with or without 50 µM Verapamil (Sigma-Aldrich, V4629) in 5 ml FACS tubes. Cells were then washed with ice cold 2% RPMI/ 10 mM HEPES, resuspended in 1 ml 2% RPMI/ 10 mM HEPES containing 2 µg/ml PI and kept on ice prior to analysis on a BD FACSAria™ cell sorter. Hoechst 33342 was excited at 350 nm and blue and red emissions were collected at 450 nm and 675 nm, respectively.

2.19 Side population analysis by Vybrant® DyeCycle Violet

Cells at a density of 1×10^6 cells/ml were incubated with 5 µM Vybrant® DyeCycle Violet stain in complete media for 30 minutes at 37°C, with protection from light, and with or without 50 µM Verapamil (Sigma-Aldrich, V4629) in 5 ml FACS tubes. Cells were analysed on a BD FACSAria™ cell sorter as for Hoechst 33342 side population cells, without washing out the dye.

2.20 ALDEFLUOR™ assay

Aldehyde dehydrogenase activity was measured using the ALDEFLUOR™ kit (Stem Cell Technologies, 01700). Cells at a density of 1×10^6 cells/ml were resuspended in 1 ml ALDEFLUOR™ assay buffer in 5 ml FACS tubes. 5 μ l of ALDEFLUOR™ substrate were added, mixed and immediately half of the mixture was transferred to a separate tube containing 5 μ l 1.5 mM DEAB (to make a final concentration of 15 μ M). Each tube was incubated at 37°C for 30 minutes. Cells were then washed twice in ice-cold ALDEFLUOR™ assay buffer and resuspended in ice-cold ALDEFLUOR™ assay buffer. Cells were kept on ice until analysis on a Beckman Coulter Cytomics FC 500 Series flow cytometer. For analysis, 100,000 events were collected.

2.21 Measurement of reactive oxygen species (ROS)

Cells at a density of 1×10^6 cells/ml were incubated with 10 μ M CM-H₂DCFDA or 5 μ M CellROX® Deep Red reagent (Life Technologies C6827 and C10422, respectively) for 20 minutes at 37°C in 5 ml FACS tubes. Cells were then washed 3 times with PBS, resuspended in MiniMacs buffer (MMB) and analysed immediately on a Beckman Coulter Cytomics FC 500 Series flow cytometer. CM-H₂DCFDA treated cells were excited at 490 nm and emission was recorded at 525 nm. CellROX® Deep Red reagent treated cells were excited at 635 nm and emission was recorded at 650 nm. For analysis, 100,000 events were collected and ROS^{low} and ROS^{hi} cells were determined as the cells exhibiting the lowest and highest 10% ROS expressing cells of the total cell population, respectively.

2.22 Fluorescence-activated cell sorting

All fluorescence-activated cell sorting (FACS) was performed on a BD FACSAria™ Cell Sorter (BD Biosciences).

2.22.1 FACS of Hoechst 33342 stained SP cells

FACS was performed on KM-H2 cells following side population (SP) analysis with Hoechst 33342 (Section 2.18). Briefly, the population to be sorted as the side population was selected based on loss of staining following incubation with 50 μM Verapamil. Once the gate for these cells was set up, KM-H2 cells were incubated with 5 $\mu\text{g}/\text{ml}$ Hoechst 33342 in the absence of Verapamil as before (Section 2.18). In 2 batches, 10,000 SP cells were sorted into a 5 ml FACS tube and transferred to a 96-well tissue culture plate. These cells were cultured in pre-conditioned media from the total cell population. This pre-conditioned media was obtained simply by centrifuging KM-H2 cells at 300 x g for 5 minutes following growth in normal culture conditions. The media was then aspirated and used for culturing SP cells.

2.22.2 FACS of Vybrant® DyeCycle Violet stained SP cells

FACS was performed on KM-H2 cells following side population (SP) analysis with Vybrant® DyeCycle violet (Section 2.19). Briefly, the population to be sorted as the side population was selected based on loss of staining following incubation with 50 μM Verapamil. Once the gate for these cells was set up, KM-H2 cells were incubated with 5 μM Vybrant® DyeCycle Violet stain in the absence of Verapamil as before (Section 2.19). 10,000 SP cells were sorted into a 5 ml FACS tube and transferred to a 96-well tissue culture plate. These cells were cultured in RPMI 1640 containing 20% v/v FBS and 2 μM β -mercaptoethanol for 2 weeks prior to preparation of cytopins for analysis of p62, PML, γH2AX , Vimentin and Tom20 expression by immunocytochemistry (Section 2.7).

2.22.3 FACS of ROS^{low} and ROS^{hi} cells

FACS of ROS^{low} and ROS^{hi} L-428 and L-1236 cells was performed using the CM-H₂DCFDA dye. Cells were incubated with 10 μM CM-H₂DCFDA as before (Section 2.21). ROS^{low} and ROS^{hi} cells were selected as the cells exhibiting the lowest and

highest 10% ROS expression of the total cell population, respectively. Each population was sorted into a 5 ml FACS tube, transferred to a 96-well tissue culture plate and cultured in complete medium.

Chapter 3. p62 expression in HL-
derived cell lines and in patient
sections

3.1 Summary

This chapter examined the expression of the multi-functional signalling adapter p62 in Hodgkin lymphoma (HL)-derived cell lines and tissue sections. This protein was initially chosen due to its involvement in pro-survival and cell death signalling and for its involvement in the regulation of inflammatory responses, all of which are highly relevant to HL. p62 distributions in HL derived cell lines were found to be heterogeneous with some cell lines displaying high levels of cytoplasmic material, some displaying lower levels and one cell line expressing nuclear p62. These scenarios were also evident in the tumour cells of biopsy material, with nuclear p62 often present in immune system cells also. On examination of nuclear p62, by inhibiting nuclear export, p62 was trapped in the nucleus of all cell lines indicating a high degree of nuclear-cytoplasmic traffic. When trapped in the nucleus p62 associated with PML bodies, known sites of nuclear proteasomes. This suggested that another of p62's functions, its involvement in protein degradation, may be of interest in HL. Indeed by inhibiting proteasome function using Bortezomib, p62 was found to accumulate in all HL-derived cell lines except HD-MyZ. This led to the investigation into protein handling pathways in HL-derived cell lines as described in the following chapter.

3.2 Introduction

The malignant cells of Hodgkin lymphoma (HL), Hodgkin and Reed-Sternberg (HRS) cells, have characteristically hyperactive pro-survival signalling (Kuppers et al., 2012). This has been found to also be the case in HL-derived cell lines (Bargou et al., 1997, Mathas et al., 2003). As in many cancer cells, the combination of pro-survival signalling and failed cell death responses allows the development and continued survival of the malignant cells. In HL, a significant proportion of pro-survival signalling is provided by the immune infiltrate attracted by the inflammatory environment promoted by HRS cells (Section 1.1.5). We were therefore interested in examining a protein involved in all of these pathways with the potential to indicate the activity of each. The multi-functional signalling adaptor p62/sequestosome-1 (hereafter referred to as p62) fits this profile.

p62 was of interest as it is involved in multiple pathways relevant to tumour progression including, NF κ B signalling, caspase-8 activation, the oxidative stress response, the inflammatory response, and in protein degradation pathways (Section 1.2.5). Its distribution in cytoplasmic speckles generally indicates its function in these signalling pathways (Sanz et al., 2000, Jin et al., 2009), while the formation of larger aggregates has been associated with impaired protein degradation (Moscat and Diaz-Meco, 2009b). Increased p62 expression has been associated with both increased and impaired autophagy function; therefore p62 expression must be interpreted carefully (Klionsky et al., 2012). p62 has not previously been examined in HL, and due to the scarcity of patient material, it was of interest initially to determine whether there was evidence of p62 speckling or aggregation in HL-derived cell lines. To this end its expression and distribution in HL-derived cell lines was examined by immunocytochemistry and western blotting. Following this, p62 expression was examined in paraffin-embedded biopsy samples from HL patients to determine whether p62 distributions observed in HL-derived cell lines were comparable.

Following examination, p62 protein was found to be present at heterogeneous levels and displayed a number of different staining patterns in HL-derived cell lines which appeared to be representative of the patterns seen in patient material. p62 was observed to traffic constantly between cytoplasm and nucleus and to interact with promyelocytic leukaemia (PML) bodies, known sites of nuclear proteasome activity. Additionally, following proteasome inhibition p62 was seen to rapidly aggregate in the majority of HL-derived cell lines suggesting that the role of p62 in protein degradation pathways may be of interest in HL. Previous unpublished data from Dr. T. Rich has also indicated that PML knockdown could augment the expression of p62, possibly indicating compensatory activity.

3.3 Results

3.3.1 Basal p62 expression in HL-derived cell lines

The analyses of HRS cells from patient samples is limited by the scarcity of malignant cells, therefore this project focused on 6 EBV-negative HL-derived cell lines (L-540, KM-H2, HDLM-2, L-1236, L-428 and HD-MyZ). HD-MyZ was included to determine whether its questionable status as an HL-derived cell line (due to a lack of CD30, CD15 and immunoglobulin or T cell receptor gene rearrangements (Bargou et al., 1993, Kuppers and Re, 2007)) would be evidenced by significant differences from the other HL-derived cell lines. Initially, basal p62 expression was examined in HL-derived cell lines by immunocytochemistry and western blotting using the well characterised anti-p62^{lck ligand} antibody (BD Transduction Laboratories). In the majority of cell lines, p62 displayed a diffuse expression pattern in the cytoplasm with KM-H2 and HDLM-2 showing more intense staining than the other lines (Figure 3-1). A number of small cytoplasmic p62 puncta were also evident in L-540, KM-H2, HDLM-2 and HD-MyZ. In L-428, which appeared to express the least p62, the protein appeared as a number of small perinuclear puncta. The exception to this staining pattern was L-1236, in which p62 was present in both the cytoplasm and the nucleus, with the majority appearing in the latter compartment. Analysis by western blot revealed no differences in molecular weight in p62 derived from L-1236 lysates compared to those from the other cell lines. Initially high levels of p62 were detected in KM-H2 and HDLM-2 compared with intermediate levels in L-540 and HD-MyZ and low levels detected in L-1236 (Figure 3-2). No p62 was detected in L-428 by this method. Since only puncta of p62 were seen in this cell line, rather than the mix of diffuse and punctate p62 seen in the other cell lines, and aggregated proteins are often insoluble in regular lysis buffers (Klionsky et al., 2012), these expression levels were hypothesised to represent the soluble fraction of p62. By increasing the percentage of SDS in standard RIPA lysis buffer (from 0.1 to 1%), p62 was detected in L-428 and higher levels were detected in the other cell lines.

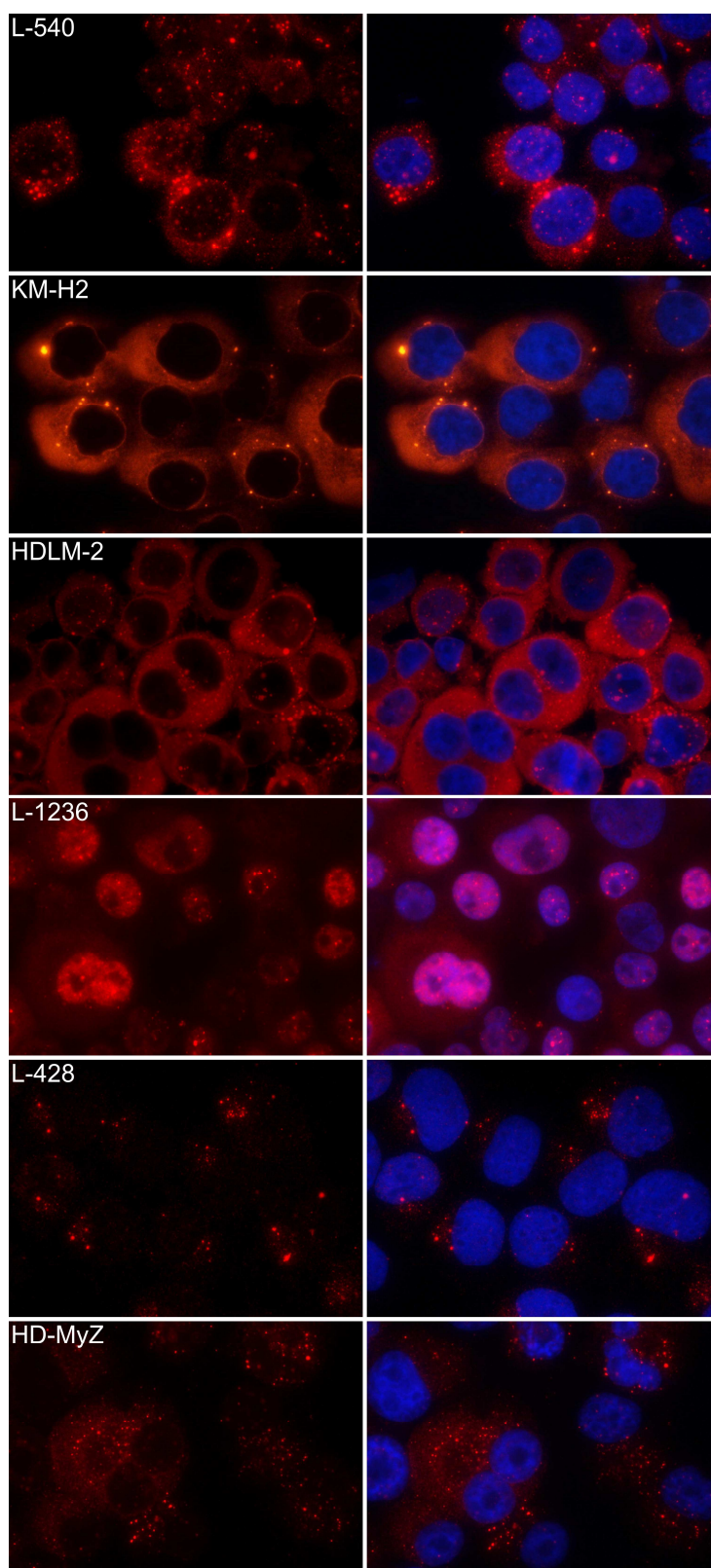


Figure 3-1 p62 expression in HL-derived cell lines as measured by immunocytochemistry.

Immunocytochemistry of p62 in HL-derived cell lines. Left panels show p62 (red). Right panels show the merged micrographs with a DAPI co-stain to identify the nuclei (blue). Imaging was with a 63x oil objective lens.

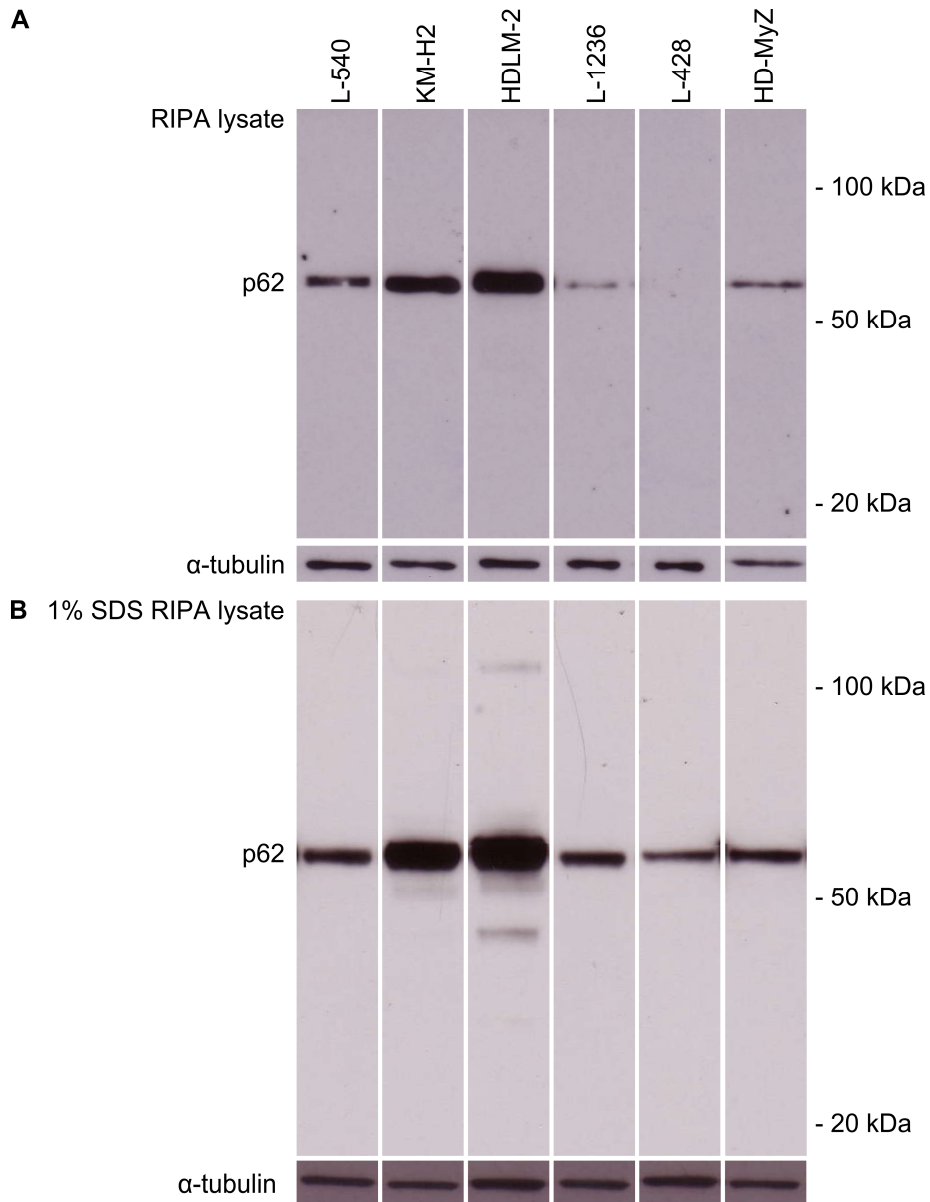


Figure 3-2 p62 expression in HL-derived cell lines as measured by western blotting.

Western blot analysis of p62 expression in HL-derived cell lines. **(A)** p62 western blot generated using standard RIPA lysates. **(B)** p62 western blot generated using a more stringent lysis process involving a RIPA lysate containing 1% SDS (rather than 0.1%) and heating at 95°C for 5 minutes (see Chapter 2 Materials and Methods). An α -tubulin loading control is included for each blot.

3.3.2 p62 staining in patient sections

To determine whether the p62 distributions seen in HL-derived cell lines were of relevance to HL patients, p62 staining patterns were examined by immunohistochemistry in paraffin-embedded HL biopsy samples (Figure 3-3). p62 expression in bi- or multi-nucleate RS cells was focused on as these cells are clinically diagnostic of HL and are considerably easier to identify than mononuclear Hodgkin cells due to their nuclear morphology. As with the cell lines heterogeneous staining patterns were observed in RS cells. Of 47 cases examined, 27 displayed exclusively cytoplasmic staining of varying intensities, 8 displayed nuclear staining of varying intensities and 3 displayed both nuclear and cytoplasmic staining of various intensities. In 9 cases p62 was not detected in RS cells. Cytoplasmic and nuclear staining was also observed in a number of non-RS cells.

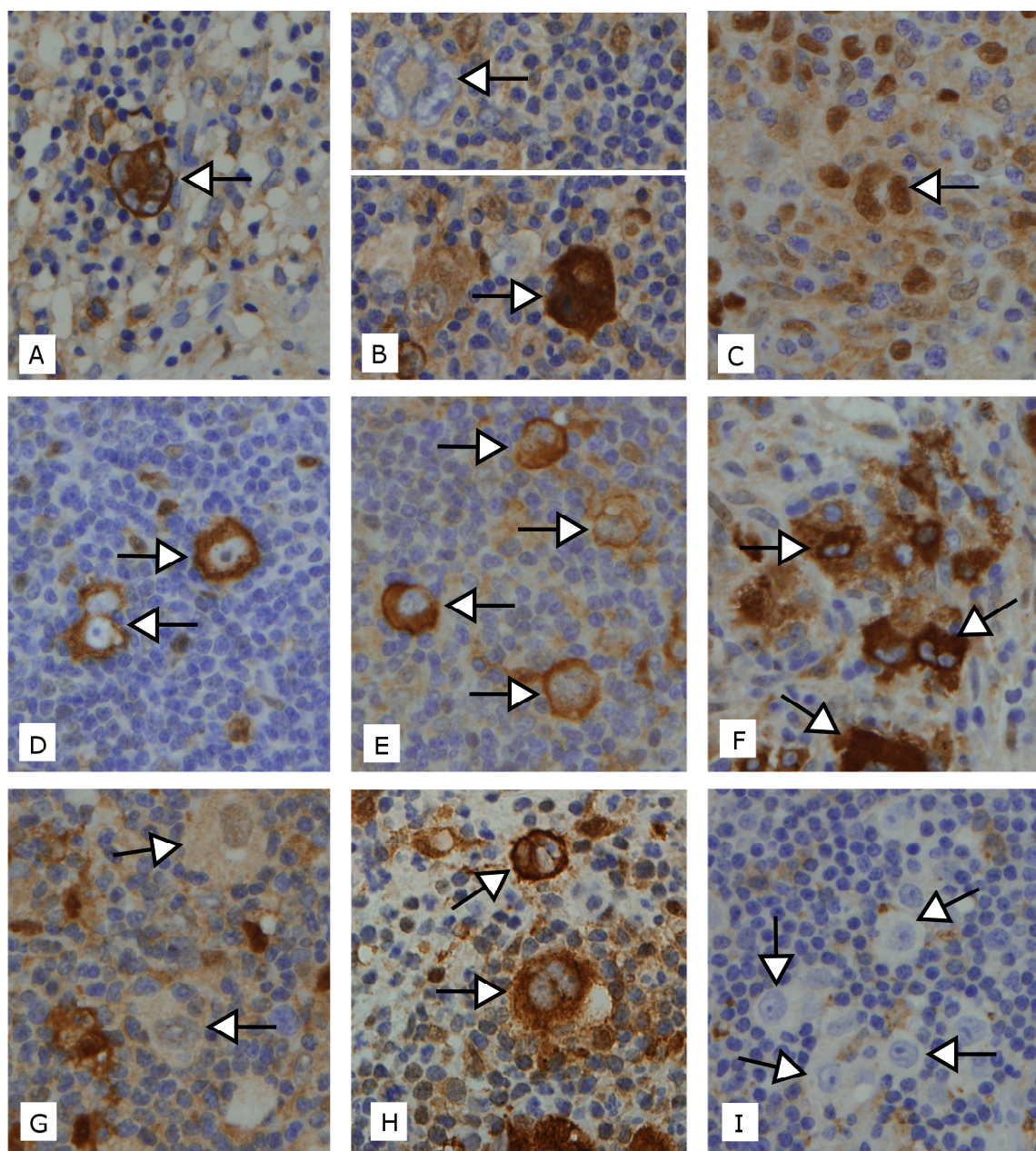


Figure 3-3 p62 staining patterns in HL patient biopsy material.

p62 staining (brown) revealed by EnVision+ System-HRP (Dako) in paraffin embedded tissue sections from HL patients. Strong cytoplasmic staining is evident in (A), (D), (E), (F) and (H). Strong cytoplasmic and nuclear expression of p62 is seen in the lower panel of (B). The top panel of (B) shows the multilobed nucleus of a p62^{ve} RS cell from the same biopsy as the bottom panel, indicating heterogeneity of staining within the same patient sample. Nuclear staining of a multinucleate RS cell in the centre of the panel can be seen in (C). Nuclear staining is also evident in a number of mononuclear cells in this panel. Weak cytoplasmic and nuclear staining is evident in (G). Smaller cells display stronger staining in this panel compared to RS cells. p62^{ve} RS cells are seen in (I). Note the pale areas (lacuna) around these nuclei which is a fixation artefact caused by formalin-induced cytoplasmic shrinkage. Prominent nucleoli which typify transformed H/RS cells can be seen in this panel as well as in (D). Key features are indicated by arrows.

3.3.3 Nucleo-cytoplasmic shuttling of p62

The presence of nuclear p62 in HL-derived cell lines and RS cells in patient material was intriguing as it is generally thought to be a cytoplasmic protein. Constitutive nuclear expression of p62 has only been previously reported in prostate cancer (Pankiv et al., 2010). p62 has also been demonstrated to shuttle continuously between cytoplasm and nucleus and to deliver ubiquitinated substrates to PML bodies in the nucleus when this shuttling process was impaired (Pankiv et al., 2010). To test whether a similar scenario existed in HL-derived cell lines, they were incubated with the nuclear export inhibitor Leptomycin B (LMB) and p62 localisation was examined by immunocytochemistry. Following this treatment p62 displayed a dramatic change in distribution from cytoplasm to nucleus with nuclear aggregates apparent in all lines; particularly in KM-H2 and HDLM-2, in which these aggregates were substantial (Figure 3-4). The almost complete loss of cytoplasmic staining and trapping of p62 in the nucleus suggested a constant traffic between these two cellular compartments. The nuclear p62 puncta resembled PML nuclear bodies which act as hubs of proteasome activity in the nucleus (Rockel et al., 2005). Indeed, the p62 puncta commonly co-localised with PML nuclear bodies (Figure 3-4, inset panels), suggesting that this nuclear p62 may be involved in the disposal of ubiquitinated substrates. Interestingly, these aggregates were excluded from the nucleolus, which has been suggested as a repository for ubiquitinated nuclear proteins (Latonen et al., 2011, Latonen, 2011). In KM-H2 the pattern of PML protein expression showed co-localisation of PML nuclear bodies with similar sized and considerably larger puncta of p62 (Figure 3-5, upper and middle panels). In the case of larger p62 aggregates, PML bodies were often seen to be cupping the aggregate rather than appearing as puncta (lower panel). This pattern of expression mimics that seen when PML bodies are sequestered by aggregates of pathogenic proteins expressing expanded tracts of polyglutamine (polyQ proteins) (Takahashi et al., 2003, Janer et al., 2006). In this scenario the PML body initially assimilates the excess protein until it fills and ruptures.

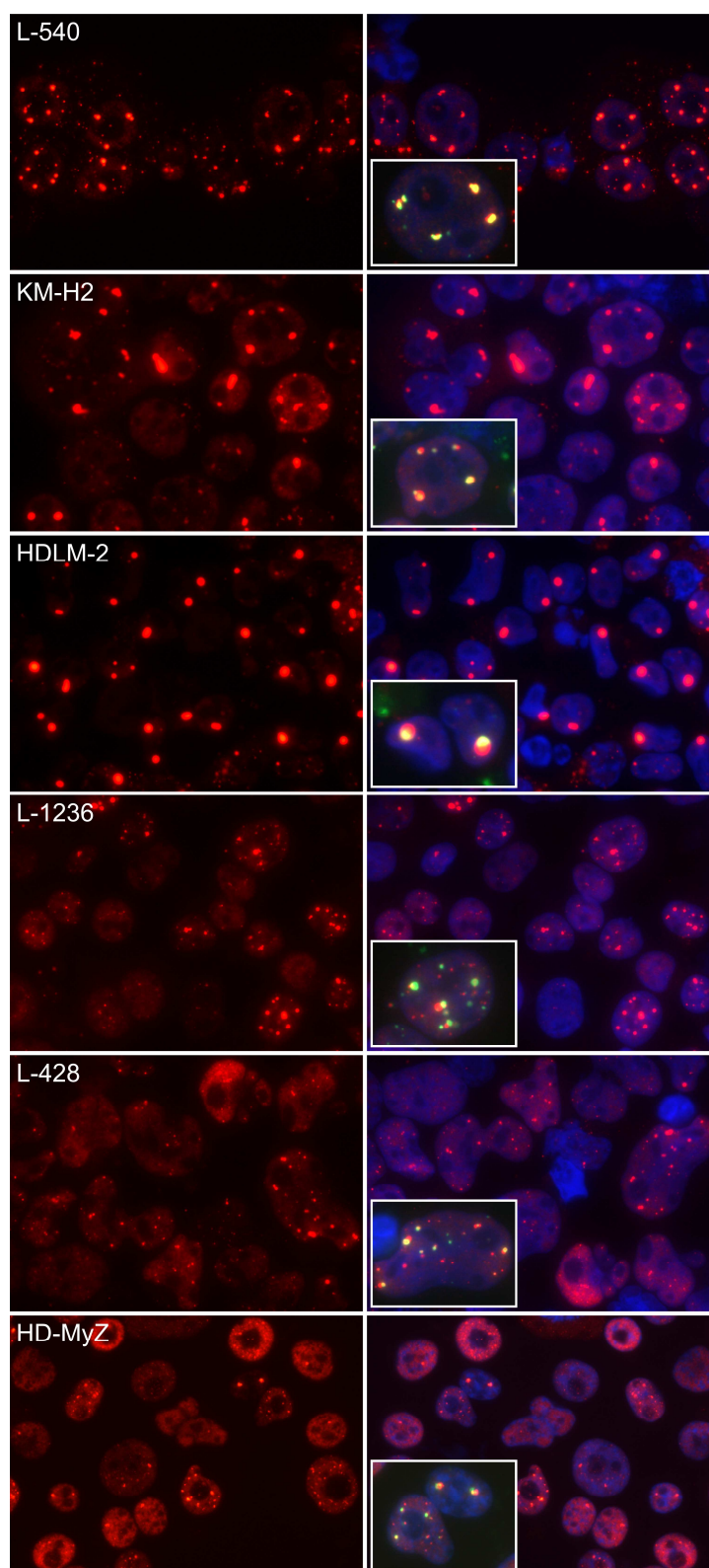


Figure 3-4 p62 is trapped in the nucleus following Leptomycin B treatment.

Immunocytochemistry of p62 following incubation for 16 hours with 2 nM Leptomycin B. Left panels show p62 (red). Right panels show the left panel merged with a DAPI stain to identify the nuclei in blue). Inset panels show co-localisation of p62 (red) with PML (green) in the nucleus of a representative cell from each cell line. Imaging was with a 63x oil objective lens.

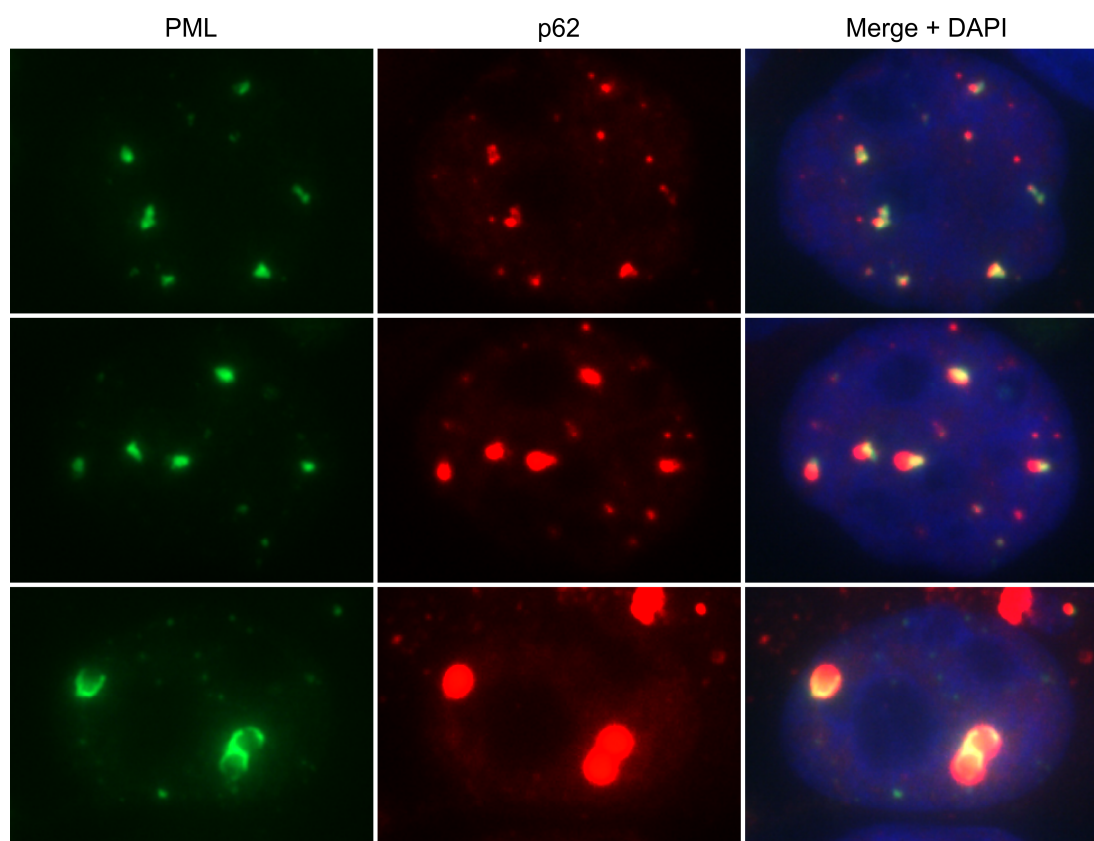


Figure 3-5 Examples of p62 localisation with PML bodies in Leptomycin B treated KM-H2 cells.

Immunocytochemistry of p62 and PML in individual KM-H2 cells following incubation for 16 hours with 2 nM Leptomycin B. Left panels show PML (green). Middle panels show p62 (red). Right panels show the merged micrographs with a DAPI co-stain to identify the nuclei (blue).

3.3.4 Proteasome inhibition in HL-derived cell lines

The high degree of association between p62 and PML following inhibition of nuclear export would suggest an important role for p62 in protein handling in these cells. A role in proteasomal degradation, in particular, is hinted at by these data as nuclear proteasomes also associate with PML bodies to deal with ubiquitinated waste protein in the nucleus (Rockel et al., 2005). To determine whether p62 distribution would reflect induced protein handling stress by proteasome inhibition, HL-derived cell lines were treated overnight with 5 nM Bortezomib. A low concentration was selected, sufficient to cause a protein handling stress through proteasome inhibition, yet not too toxic to avoid significant cell death. p62 displayed a dramatic redistribution in the majority of cell lines, with the exception of HD-MyZ (Figure 3-6). In KM-H2 and HDLM-2, an

increase in cytoplasmic staining was observed accompanied by the formation of multiple large aggregates, which were larger and more irregular in shape in HDLM-2. In L-428, p62 staining was enhanced and larger aggregates were formed in the perinuclear region where p62 was previously detected. In L-1236, p62 redistributed from the nucleus to the cytoplasm, although some nuclear p62 remained. A dramatic loss of diffuse cytoplasmic p62 in favour of one or two large aggregates was observed in L-540.

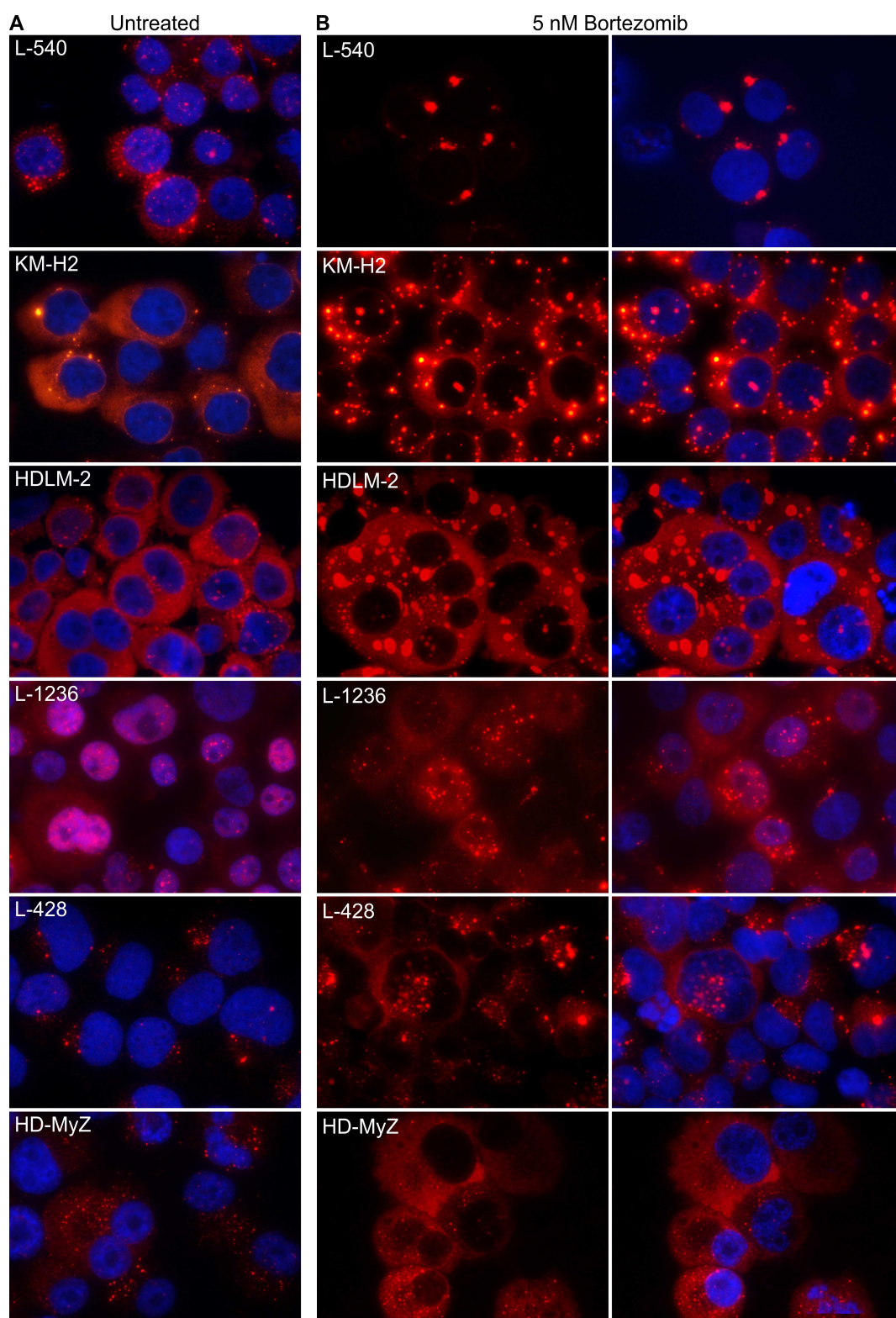


Figure 3-6 p62 distribution following proteasome inhibition.

Immunocytochemistry of p62 following incubation for 16 hours with 5 nM Bortezomib. **(A)** Untreated cells from Figure 3-1. **(B)** Bortezomib treated cells. Left panels show p62 (red). Right panels show the left panel merged with a DAPI stain to identify the nuclei (blue). Imaging was with a 63x oil objective lens.

To ensure proteasome activity was inhibited, chymotrypsin-like activity was measured following 3 hours incubation with inhibitor (5 nM Bortezomib), as per assay instructions. This revealed residual chymotrypsin-like activity, which varied from approximately 10-20% of baseline activity depending on the cell line (Figure 3-7A). A separate experiment using only some of the cell lines (L-540, KM-H2, HD-MyZ and L-428) revealed a greater level of inhibition of this activity following 24 hours of treatment with Bortezomib (Figure 3-7B). Levels of K48-linked polyubiquitin were also assessed following Bortezomib treatment and found to increase in all cell lines, confirming proteasome inhibition (Figure 3-7C).

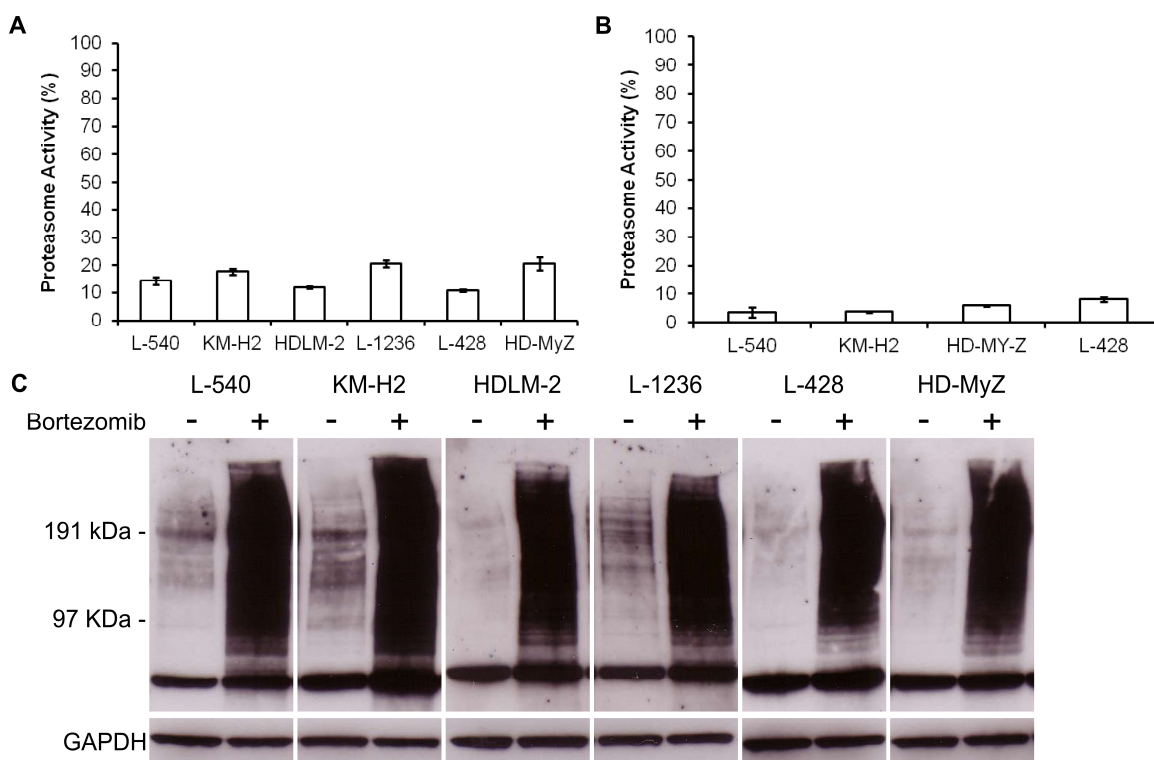


Figure 3-7 Effect of Bortezomib on proteasome activity.

Chymotrypsin-like proteasome activity as measured by Proteasome-Glo™ assay following incubation with 5 nM Bortezomib for 3 hours (**A**) and 24 hours (**B**). Values represent the mean of triplicates and are expressed as the percentage of a DMSO control. Error bars represent standard deviation of the mean. (**C**) Expression of K48-linked polyubiquitin following incubation for 24 hours with 5 nM Bortezomib. Lanes with + above were treated with Bortezomib, while lanes with – were treated with DMSO. GAPDH was included as a loading control.

3.4 Discussion

Here the expression of the multi-functional signalling adaptor p62 was examined in HL-derived cell lines. The distribution of this protein when present as cytoplasmic speckles is thought to indicate its role as a signalling hub in both pro-survival and cell death pathways (Sanz et al., 2000, Jin et al., 2009). Although speckles were detected in all of the HL-derived cell lines to some extent, a number of distinct p62 distributions were observed. In L-540, KM-H2, HDLM-2 and HD-MyZ p62 appeared in a diffuse cytoplasmic distribution. This was particularly apparent in KM-H2 and HDLM-2 in which a small number of larger aggregates were also present. In L-428 rather than being distributed throughout the cytoplasm, p62 appeared as a number of puncta focused in the same perinuclear region. Finally, in L-1236, p62 displayed a predominantly nuclear distribution in both diffuse and punctate forms. Although HL-derived cell lines are reported to have constitutively active NF κ B (Bargou et al., 1997, Mathas et al., 2003), it seemed highly unlikely that these different distributions could be related to the same signalling function.

That higher levels of p62 were detected by western blotting following lysis with a more stringent lysis buffer suggested that p62 was present as insoluble aggregates in these cell lines. Such larger insoluble aggregates may be related to its role in the ubiquitin proteasome system, as the PB1 and UBA domains of p62 allow it to polymerise and aid in the organisation of ubiquitinated proteins into insoluble protein aggregates, an extreme example of this being aggresomes (Tyedmers et al., 2010). When in its monomeric form p62 has been associated with the traffic of ubiquitinated proteins to the proteasome for degradation. This may account for the diffuse fraction of p62 observed in the HL-derived cell lines. This role in proteasomal degradation would be further supported by the association of p62 with PML bodies following inhibition of nuclear export with LMB. PML bodies are known sites of nuclear proteasomes and are involved in the ubiquitin-dependent degradation of a number of nuclear proteins such as CBP (St-Germain et al., 2008).

The 26S proteasome is a barrel structure made up of a 20S core flanked by two 19S complexes that regulate substrate specificity (Section 1.2.2). The 20S core is made up of a number of different subunits that are subject to change. It is made up of 4 α - and β -rings that form a barrel shaped structure. A central chamber is created by the two inner β -rings which harbour the catalytic activities of the proteasome; the chymotrypsin-like, trypsin-like and caspase-like activities. Proteins are targeted for proteasomal degradation by the addition of polyubiquitin chains, with K48-linked polyubiquitin the most common degradation signal (Komander and Rape, 2012). Ubiquitinated substrates are recognised by the 19S complexes of the proteasome and channelled into the central chamber of the barrel structure for degradation. There is evidence that nuclear proteasomes may have a different composition from their cytoplasmic counterparts. So called immunoproteasomes are often found in association with PML bodies in the nucleus (Fabunmi et al., 2001). Immunoproteasomes are present in cells of the immune system (IS) and are inducible by TNF and interferon γ (IFN γ). In place of the enzymatically active β 1, β 2 and β 5 subunits, these contain β 1i, β 2i and β 5i which confer different catalytic activities and thus different peptide products following substrate degradation (Groettrup et al., 2010). These immunoproteasomes have also been found to be more active than standard proteasomes and, as they are inducible by the inflammatory cytokines, which can also produce oxidative stress and an accumulation of ROS-damaged proteins, it has been suggested that they are expressed to enhance basal proteasome activity in order to deal with increased traffic through the ubiquitin proteasome system (UPS) and prevent the formation of toxic protein aggregates (Seifert et al., 2010, van Deventer and Neefjes, 2010). This is of relevance to HL, as these cells are believed to be of immune cell (B-cell) origin (Section 1.1.2) and exist within a complex inflammatory microenvironment (Section 1.1.5), both of which would predispose these cells to immunoproteasome expression. This may explain the lack of p62 aggregation observed in HD-MyZ following proteasome inhibition. Adenocarcinoma cell lines with induced resistance to Bortezomib have been found to increase expression of immunoproteasome subunits β 5i and β 2i (Suzuki et al., 2011). While Bortezomib inhibits the chymotrypsin-like activity of the proteasome and the

immunoproteasome, the immunoproteasome was observed to be more resistant to Bortezomib in primary Waldenström macroglobulinemia cells (Roccaro et al., 2010). Therefore, if HD-MyZ cells express high levels of immunoproteasome subunits they may be more resistant to Bortezomib. This may also explain the uninspiring results of clinical trials involving Bortezomib as a single agent therapy against refractory HL (Younes et al., 2006, Strauss et al., 2006, Blum et al., 2007). The development of selective immunoproteasome inhibitors capable of overcoming Bortezomib resistance in multiple myeloma cells would suggest that further studies of the proteasome composition in HL would be of value in the future (Kuhn et al., 2009, Kuhn and Orłowski, 2012).

The role of p62 in the degradation of ubiquitinated proteins in the nucleus has been previously reported (Pankiv et al., 2010), although not in HL. It was found to shuttle between the cytoplasm and nucleus to facilitate the accumulation of ubiquitinated proteins in PML bodies. p62 was also found to be involved in the formation of proteasome-containing aggregates in response to the formation of polyQ aggregates (ataxin1Q84) and therefore contributed to the degradation of this protein in the nucleus. It would appear, given the frequency and size of PML-associated p62 aggregates formed following inhibition of nuclear export, that p62 may be playing a similar role in PML/proteasome-mediated nuclear protein degradation in HL-derived cell lines. Alternatively, p62 may itself be a substrate for such degradation at this site.

The PB1 domain of p62 allows it to interact with Rpt1, a subunit of the 26S proteasome (Geetha et al., 2008). Thus through binding of ubiquitinated proteins with its UBA domain, p62 can act as a chaperone for proteins marked for degradation by the proteasome. Following proteasome inhibition, p62 formed numerous larger aggregates, reminiscent of ALISs (aggresome-like induced structures), aggregates of ubiquitinated proteins formed following proteasome inhibition, oxidative stress or starvation (Szeto et al., 2006). This would suggest that proteasomal degradation is a highly active process in HL-derived cell lines and may warrant further investigation as it poses an attractive therapeutic

target. Indeed other protein degradation pathways may also be of interest, as p62 also plays an important role in autophagy. Through its interaction with LC3 by its LIR domain, p62 delivers ubiquitinated proteins/protein aggregates and damaged organelles to autophagosomes (Pankiv et al., 2007). These double-membraned structures ultimately fuse with lysosomes resulting in the degradation of their contents. As p62 is also a substrate of autophagy, its accumulation has been used to indicate impairment/inhibition of autophagy (Klionsky et al., 2012). The high levels of p62 present in some of the HL-derived cell lines (particularly KM-H2 and HDLM-2) may therefore indicate a problem with this pathway. That the heterogeneous p62 distributions observed in the cell lines was recapitulated in HL tissue sections suggested a similar situation may exist in HRS cells *in vivo* and that protein handling pathways may be of therapeutic relevance to HL. The activities of these protein handling pathways are investigated in the following chapter.

Chapter 4. Protein handling pathways in HL-derived cell lines

4.1 Summary

In this chapter the activities of the proteasome and autophagy pathways were examined in HL-derived cell lines. The responses to inhibition of each pathway, by Bortezomib and Bafilomycin A1, respectively, were assessed, using the multi-functional signalling adaptor p62 to monitor protein aggregation. Cell viability was also monitored in response to inhibition of these pathways. Evidence for polarisation of protein degradation was observed and, as this process requires HDAC6-mediated transport, the effect of HDAC6 inhibition by the HDAC6-specific inhibitor BML-281 was examined in terms of p62 distribution and cell viability. Surprisingly, this inhibitor caused DNA damage in mitotic cells and proved most effective against L-1236, the only cell line expressing nuclear p62. p62 was observed to co-localise with DNA damage-associated protein γ H2AX in both the nucleus and cytoplasm in KM-H2 and L-1236, suggesting an involvement in the degradation of repair proteins. Since no single pathway inhibition proved successful against all cell lines, dual pathway inhibition was examined with proteasome and HDAC6 inhibition (by Bortezomib and BML-281, respectively) proving more potent than proteasome and autophagy inhibition (by Bortezomib and Hydroxychloroquine, respectively).

4.2 Introduction

Conventional therapy for HL is generally successful in terms of complete remission / freedom from treatment failure (FFTF), but there is still a significant risk of serious post-therapy disease and premature death for patients that are refractile to therapy or that relapse after autologous hematopoietic stem cell transplant. Current therapies, ABVD (Adriamycin, Bleomycin, Vinblastine and Dacarbazine) and BEACOPP (Bleomycin, Etoposide, Adriamycin, Cyclophosphamide, Oncovin, Procarbazine and Prednisone), largely focus on DNA-damage inducing agents (Section 1.1.8.1). The exceptions are Vinblastine, Oncovin and Prednisone, with Vinblastine and Oncovin acting against microtubules and Prednisone against the immune system. New therapeutic targets are always of great interest in this field, to alleviate toxicity of the current regimens and to treat patients who fail to respond.

In Chapter 3, heterogeneous levels of p62 expression were identified in HL-derived cell lines, with some cell lines displaying a higher level than others. p62 was found to associate with PML bodies in the nucleus, known sites of proteasome activity, and accumulated in cytoplasmic aggregates following proteasome inhibition. This suggested an important role for proteasomal degradation in HL-derived cell lines. High levels of p62 have also been shown to indicate inhibition of another protein degradation pathway: autophagy. Impairment of either pathway can result in build up of toxic protein aggregates, which could be responsible for genotoxic stress, such as that reported in HL. These protein degradation pathways are interlinked and capable of compensating for one another so if there was found to be a failure in either pathway, the other would present an attractive target for therapeutic intervention.

The two main protein degradation pathways focused on in this study were the proteasome and autophagy pathways. The proteasome is a barrel shaped structure made up of numerous subunits and possessing three main proteolytic

activities: chymotrypsin-like, trypsin-like and caspase-like (Finley, 2009). Substrates are targeted for proteasomal degradation through the addition of K48-linked polyubiquitin chains (Komander and Rape, 2012). Substrates can also be targeted for degradation by the autophagy pathway, although this is generally achieved through K63-linked polyubiquitin (Tan et al., 2008). Briefly, the autophagy pathway involves the sequestration of substrates into a double-membraned vesicle termed the autophagosome. This then fuses with a lysosome to form an autolysosome in which its contents are degraded and can be recycled in the cell or expelled into the extra cellular environment.

Proteasome inhibitors (PIs) are under intense scrutiny as chemo-sensitizers. The best studied proteasome inhibitor is Bortezomib (VELCADE/PS-341) which is licensed for multiple myeloma (MM) and mantle cell lymphoma (MCL) (Richardson et al., 2006). This molecule acts by binding to the $\beta 5$ -subunits of the proteasome inhibiting their chymotrypsin-like activity. While the other activities of the proteasome (trypsin-like and caspase-like) are not directly targeted by Bortezomib, they have been found to be impaired in a concentration dependent manner. Responses to Bortezomib in HL have been disappointingly poor (Younes et al., 2006, Strauss et al., 2006, Blum et al., 2007); however it has proved more successful against other malignancies when coupled with additional agents such as histone deacetylase (HDAC) inhibitors (McConkey, 2010). Mechanistic studies of Bortezomib in HL have tended not to focus on its effects on the activities of protein handling pathways (Zheng et al., 2004, Kashkar et al., 2007). Consequently there are no data linking protein metabolism to sensitivity to this agent in HL.

Autophagy inhibitors are less common in therapeutic settings, although molecules such as Hydroxychloroquine (HCQ) are in use or in trial against numerous malignancies (Sui et al., 2013). This alkaline agent acts by accumulating in acidic vesicles, preventing the pH-dependent degradation process (Rote and Rechsteiner, 1983, Poole and Ohkuma, 1981). In this chapter another autophagy inhibitor, Bafilomycin A1, was also used. This molecule acts

in a similar way to HCQ in that it impairs acidification of vesicles. However, it does this through inhibition of V-ATPase, on the vesicle surface (Yamamoto et al., 1998). This action prevents the fusion of autophagosomes with lysosomes.

Another commonly used cytoprotective mechanism is to polarize protein degradation to one part of the cell, the microtubule organizing centre (MTOC) (Tyedmers et al., 2010). Navigation to the MTOC is achieved by the back-tracking of waste protein (retrograde transport) along microtubules. Histone deacetylase-6 (HDAC6) deacetylates tubulin, and associates with dynein, in order to transport protein to the MTOC (Kawaguchi et al., 2003). Ultimately, aggregated protein deposited at the MTOC is thought to be cleared by autophagy. Although there are to date no HDAC6-specific inhibitors approved for clinical use, non-specific HDAC inhibitors are available such as Vorinostat (SAHA). Although this agent's activity is in no way limited to HDAC6, it has proved successful in combination with Bortezomib against multiple myeloma (Mazumder et al., 2010, McConkey, 2010). In this chapter a more specific HDAC6-inhibitor was used, BML-281, which has displayed HDAC6 inhibition in the nanomolar range and toxicity against pancreatic cancer cell lines (Kozikowski et al., 2008).

In order to monitor accumulation of waste protein, p62 distribution in response to inhibition of individual protein handling pathways was examined. This was due to a need for a marker that can be used for immunohistochemistry, as this is the main method used by pathologists to stratify patients. p62 is a scaffold/adaptor protein involved in the disposal of toxic protein by delivering ubiquitinated protein to proteasomes, autophagosomes and aggresomes (Section 1.2.5). p62 is itself a substrate for autophagic degradation and its accumulation can indicate an impairment in autophagy function, although its aggregation (at the expense of speckled or diffusely expressed cytoplasmic fractions) has also been reported to indicate autophagy induction (Klionsky et al., 2012). Radial expression of p62 at the MTOC is also indicative of its activity in delivering protein waste for aggresome formation and autophagy clearance.

4.3 Results

4.3.1 Basal proteasome and autophagy activity in HL-derived cell lines

In order to gauge the baseline activity of proteasome and autophagy pathways they were initially examined in unstressed cells. To assess the activity of the proteasome pathway the chymotrypsin-like activity was measured as this is the principle target of therapeutic proteasome inhibition. Chymotrypsin-like activity was measured using the luminescent Proteasome-Glo™ Chymotrypsin-like cell-based assay (Section 2.11). All of the cell lines displayed evidence of chymotrypsin-like proteasome activity, although each assay differed in terms of absolute levels. A trend emerged in which KM-H2 and HDLM-2 consistently displayed lower activity than L-428 and HD-MyZ (Figure 4-1A). These activities were reflected in levels of K48-linked polyubiquitin, with L-540, KM-H2 and HDLM-2 expressing higher levels of this proteasome substrate than L-428 and HD-MyZ (Figure 4-1B). The exception was L-1236, which expressed equivalent levels of this substrate to the cell lines with lower proteasome activity.

The activity of the autophagy pathway was measured by assessing LC3B flux (Section 2.12). During autophagy, the cytoplasmic light chain 3-I protein (LC3-I) is converted to a membrane bound form (LC3-II) by phosphatidylethanolamine conjugation. The addition of this group increases the hydrophobicity of the protein allowing LC3-II to be easily separated from LC3-I by SDS-PAGE. The accumulation of LC3-II is transient as this molecule is then degraded within the autophagolysosome. By preventing the acidification of autophagolysosomes (in this case with hydroxychloroquine (HCQ)) it is possible to preserve LC3-II. Changes in LC3-II concentration can therefore be used as a dynamic measure of material entering the autophagy pathway. An increased signal for LC3-II in the presence of HCQ indicates active autophagy and therefore positive flux. LC3 is inefficiently solubilised by detergents such as Triton X-100, instead it requires heating in the presence of 1% SDS (Klionsky et al., 2012). Consequently cell lysates were prepared using RIPA buffer containing 1% SDS and were heated at

95 °C (Section 2.9.2). With the exception of HD-MyZ, all cell lines tested positive for LC3B flux in the presence of HCQ (Figure 4-1C). Serum starvation is frequently used to induce autophagy, which occurs as part of a cytoprotective response to reclaim nutrients and biosynthetic precursors, consequently HL-derived cell lines were subject to serum starvation overnight prior to LC3B flux measurements. In half the cell lines examined (L-540, KM-H2 and L-1236), starvation in culture media containing 1% FBS resulted in a drop in the LC3BII ratio suggesting reduced autophagy activity. Culture in these conditions also resulted in phenotypic changes in the cell lines. With the exception of HD-MyZ, the cell lines are suspension cells, however culture in low serum conditions resulted in the cells adhering to the bottom of the tissue culture flask and poor viability. Long term culture in low serum resulted in death for the majority of cell lines, particularly KM-H2 and L-540. HD-MyZ appeared largely unaffected by low serum conditions. Therefore, these cells were unable to protect themselves against starvation conditions using autophagy, suggesting that the detected autophagy activity may be serving a different function, such as protein quality control.

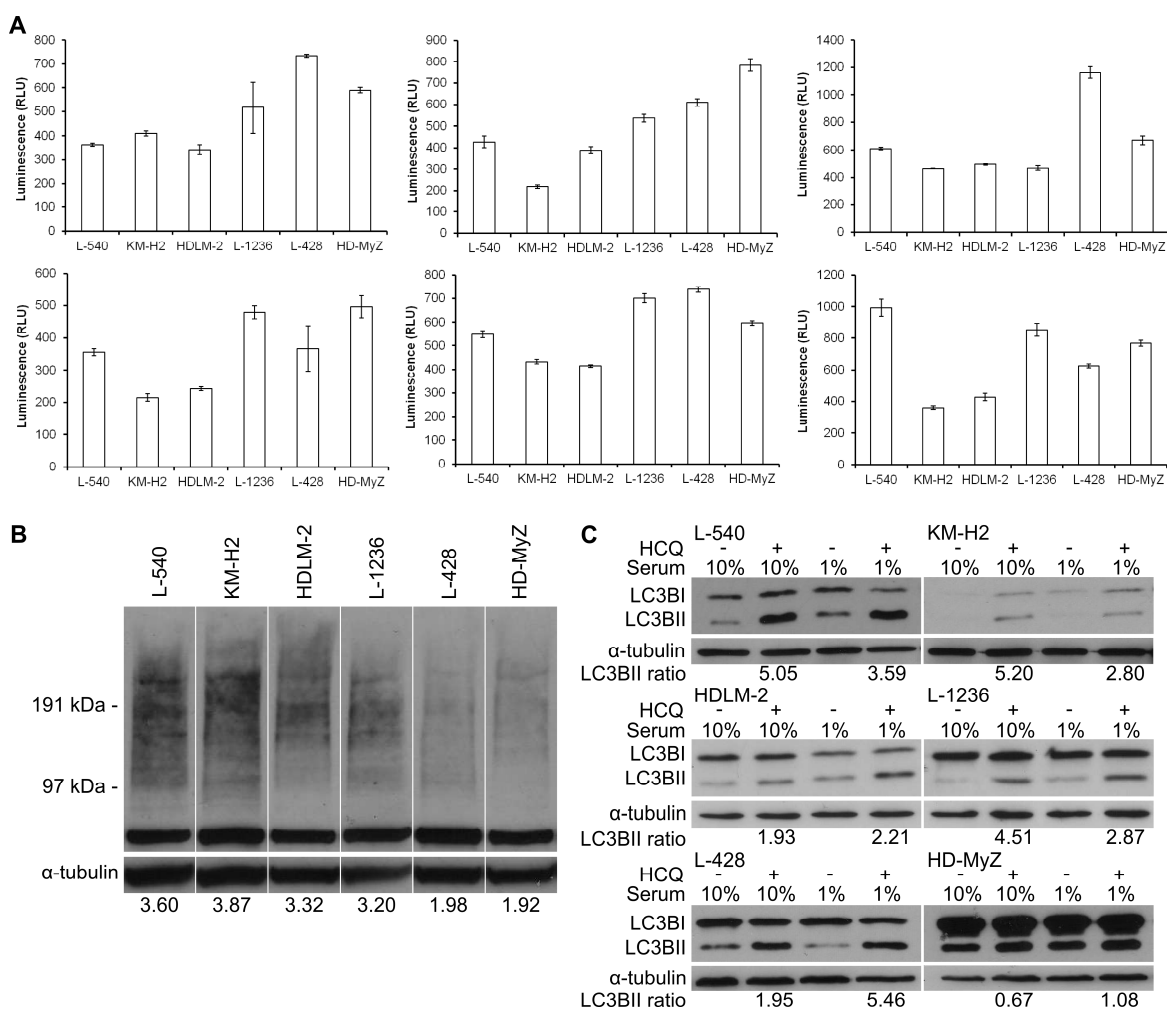


Figure 4-1 Basal proteasome and autophagy activity in HL-derived cell lines.

(A) Chymotrypsin-like proteasome activity as measured by Proteasome-Glo assay. 6 separate experiments are presented. Values represent the mean of triplicates and are expressed as luminescence in relative light units (RLU). Error bars represent standard deviation of the mean. (B) Western blot analysis of K48-linked polyubiquitin. α -tubulin was included as a loading control. Values under each lane represent ImageJ densitometry analyses normalising each K48-linked polyubiquitin lane to its loading control. (C) Autophagy activity as measured by LC3BII flux under basal (10% serum) or starvation (1% serum) conditions as indicated. +/- indicates inclusion of the drug hydroxychloroquine (HCQ). α -tubulin was used as a loading control. The positions of the LC3BI and II proteins are shown to the left. Values beneath each blot represent levels of flux induction in the presence of HCQ as determined by ImageJ densitometry analysis. These values were obtained by comparing the intensity of the LC3BII bands with and without HCQ, normalized to the loading controls.

4.3.2 Evidence of mitophagy in HL-derived cell lines

Examination of p62 expression in Section 3.3.1 revealed that the occasional KM-H2 cell displayed a large perinuclear “fleck” of p62 (Figure 4-2A). The numbers of cells expressing such an accumulation could be enhanced by culturing the cells in unfavourable conditions, i.e. at high density for an extended length of time without replenishing the media (Figure 4-2B). The spatially constrained distribution of p62 was of interest as it suggested a localised degradation process. It was hypothesised that this accumulation represented an autophagic response to growth conditions, although this was not detected by LC3B flux in the previous starvation conditions (Figure 4-1C). The selective degradation of mitochondria by the autophagy pathway, known as mitophagy, is used by cells to remove damaged mitochondria to prevent both reactive oxygen species (ROS) generation and the spread of damaged mitochondrial DNA throughout the mitochondrial population of the cell (Boya et al., 2013). Mitochondria are targeted for mitophagy by the ubiquitination of one or more surface proteins by the E3 ubiquitin ligase Parkin results in their recognition by p62 and subsequent association with the autophagy machinery (Geisler et al., 2010, Narendra et al., 2010). In the “fleck” scenario it was believed mitophagy was induced to remove mitochondria damaged by starvation-induced ROS.

On examination by confocal microscopy, large p62 accumulations in KM-H2 were seen to localise with a small population of mitochondria, identified by immunostaining with an antibody specific for the mitochondrial pore protein Tom20 (Figure 4-3A). Mitochondria were generally observed to circle the nucleus in these cells, although often a small population appeared to form a ring in a perinuclear area (Figure 4-3B). To determine whether this was the case in another HL cell line, mitochondrial distribution was also examined in L-428 cells. Here the mitochondria were found polarised in one area of the cell and clearly ringed a portion of the cytoplasm (Figure 4-3B). Following autophagy inhibition by HCQ, p62 expression within this mitochondrial ring was accentuated, suggesting a role in mitophagy (Figure 4-3C). Dual staining is not an unequivocal method to establish a role in mitophagy and alternative methods such as

immunoprecipitation with p62 followed by probing for Tom20, VDAC1 or Mitofusin 1/2 would be required to further implicate a role in mitophagy. Mitochondria clustered at the MTOC are ordinarily damaged and therefore depolarised. To determine whether this was the case, KM-H2 and L-428 cells were incubated with the cell permeable MitoTracker™ dye (Section 2.14), which accumulates in healthy mitochondria but is not retained by damaged depolarised mitochondria. Staining intensity between cells was heterogeneous in both cell lines, with some cells staining strongly for MitoTracker™ dye and some staining poorly (Figure 4-4A). In either case the polarised distribution was the same. As a positive control for the staining procedure KM-H2 cells were treated with the mitochondrial depolarising agent carbonyl cyanide 3-chlorophenylhydrazone (CCCP). This resulted in loss of MitoTracker™ staining in the majority of cells (Figure 4-4B).

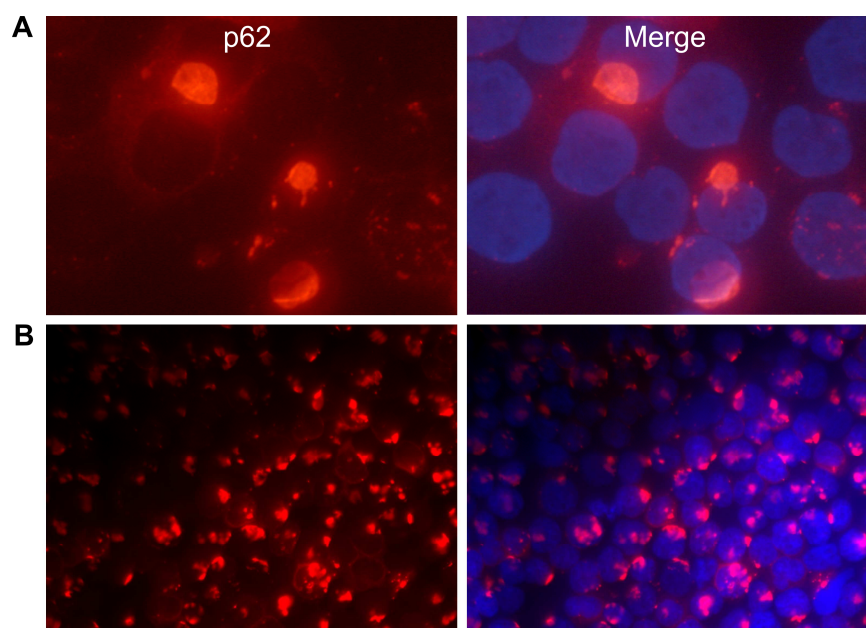


Figure 4-2 p62 “fleck” in KM-H2 cells.

Immunocytochemistry of p62 accumulations in KM-H2 cells under normal conditions (**A**) and following 7 days of growth at high density (**B**). In both (**A**) and (**B**), the left panels show p62 (red) and the right panels show the left panel merge with a DAPI stain to identify the nuclei in blue. Imaging was performed using a 63x (**A**) or 40x (**B**) oil objective lens.

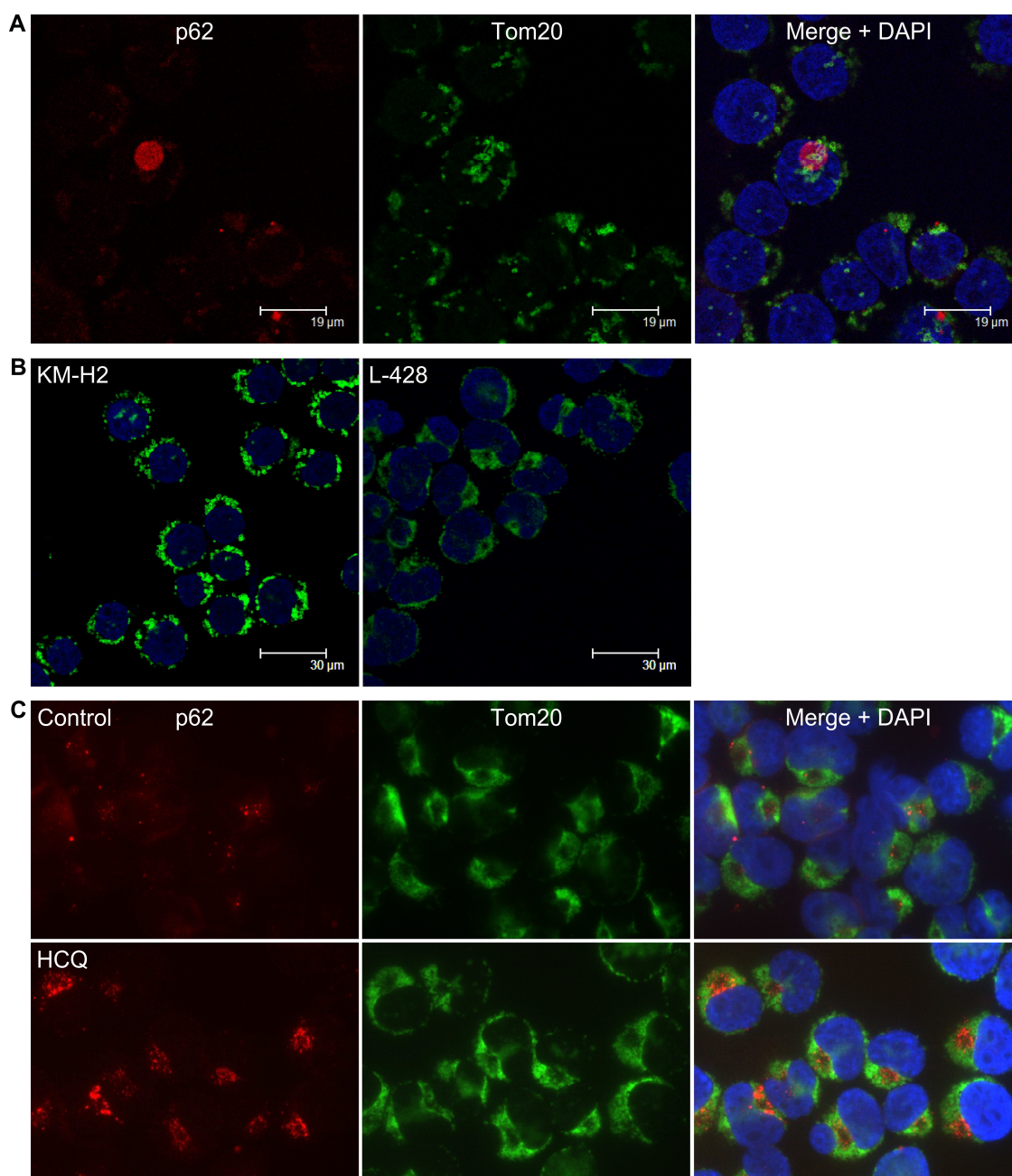


Figure 4-3 Distribution of mitochondria in KM-H2 and L-428 cells.

(A) Confocal microscopy of p62 and mitochondria (Tom20) expression in KM-H2 cells. Left panel shows p62 (red), middle panel shows Tom20 (green) right panel shows left and middle panels merged with a DAPI stain to identify the nuclei in blue. (B) Confocal microscopy of mitochondria distribution (identified by Tom20 staining, green) in relation to the nuclei (blue) in KM-H2 and L-428 cells. (C) Immunocytochemistry of p62 (red) expression in L-428 cells in relation to mitochondrial distribution (Tom20, green) following treatment with 20 μ M HCQ or water as a vehicle control. Nuclei were stained blue with DAPI.

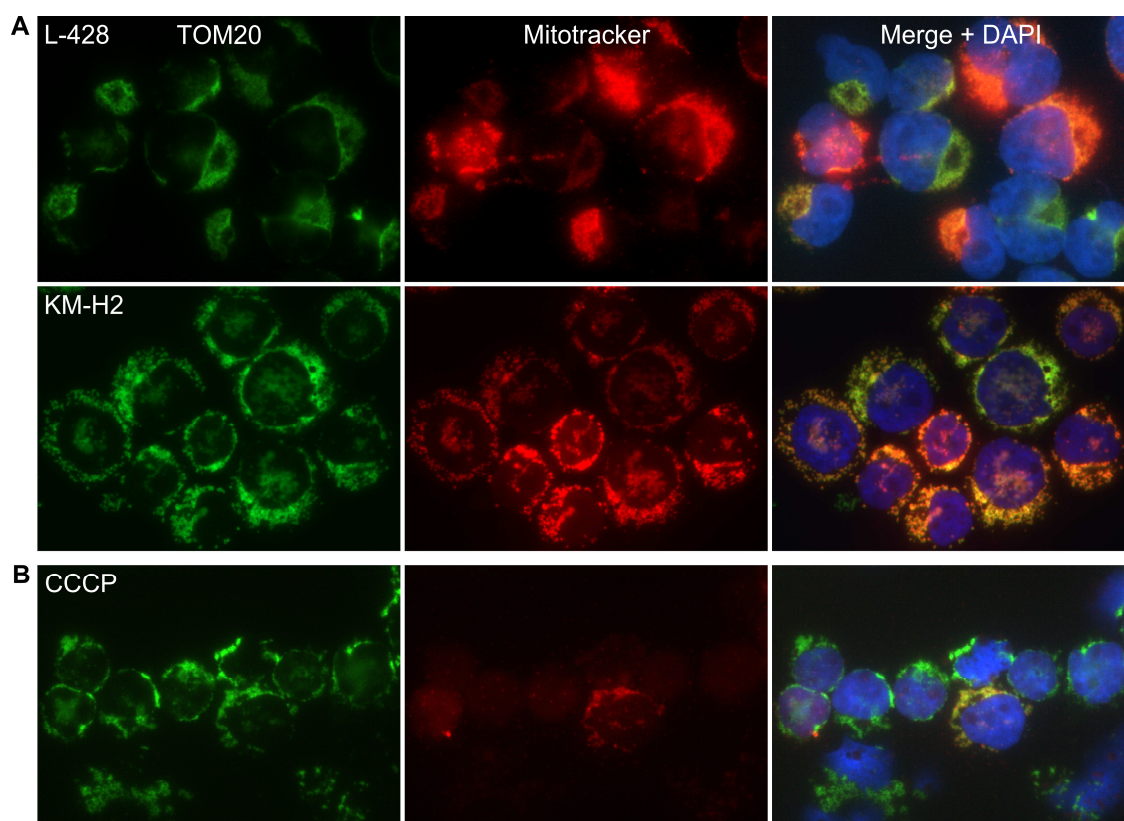


Figure 4-4 MitoTracker™-retaining mitochondria can accumulate in an MTOC-like distribution(A) Immunocytochemistry of Tom20 and MitoTracker™ dye in KM-H2 and L-428 cells. Left panels show Tom20 (green), middle panels show MitoTracker™ staining (red) and right panels show left and middle panels merged with DAPI stain to identify nuclei in blue. (B) Immunocytochemistry of KM-H2 cells treated with 20 μ M CCCP for 16 hours. Left panels shows Tom20 (green), middle panel shows MitoTracker™ staining (red) and right panel shows left and middle panel merged with DAPI stain to identify nuclei in blue.

Ubiquitination of mitochondrial surface proteins by E3 ubiquitin ligase Parkin is responsible for p62-mediated mitochondrial clustering (Geisler et al., 2010, Narendra et al., 2010). To determine whether there was any evidence of this, the association between Parkin and mitochondria was examined by immunocytochemistry. Parkin distribution (detected using anti-Parkin clone PRK8) differed greatly between KM-H2 and L-428. In L-428, Parkin appeared as small puncta distributed within the mitochondrial population but not limited to an MTOC-like distribution as might be expected if these mitochondria were truly

marked for degradation (Figure 4-5A). In KM-H2, on the other hand, a number of small puncta also appeared to co-localise with mitochondria; however one larger puncta appeared in the small mitochondrial ring seen in these cells (Figure 4-5B). To confirm these Parkin distributions, a polyclonal anti-Parkin antibody (ab15954) was used. In L-428 cells, the distribution suggested that Parkin was predominantly present on mitotic spindle, while in KM-H2 the distribution observed was similar to that seen with the original anti-Parkin antibody, clone PRK8 (Figure 4-5C).

Western blot analysis of Parkin expression was performed on all HL-derived cell lines. Using the anti-Parkin clone PRK8 antibody, Parkin was detected in the HD-MyZ cell line only, whereas the polyclonal antibody (ab15954) detected Parkin in all the cell lines at comparable levels (Figure 4-5D). The discrepancies between Parkin detection using these antibodies may be due to recognition of different Parkin species, i.e. different isoforms or posttranslational modifications, or non-specific binding to non-Parkin peptides. To confirm the specificity of the antibodies, knockdown experiments of Parkin would be required. Perinuclear accumulations of Parkin, as seen with both anti-Parkin reagents in KM-H2 cells, have been associated with limiting proteasome activity and an adoption of polarised protein degradation to the MTOC which results in bystander deposition of Parkin at this site (Zhao et al., 2003, Muqit et al., 2004, Junn et al., 2002).

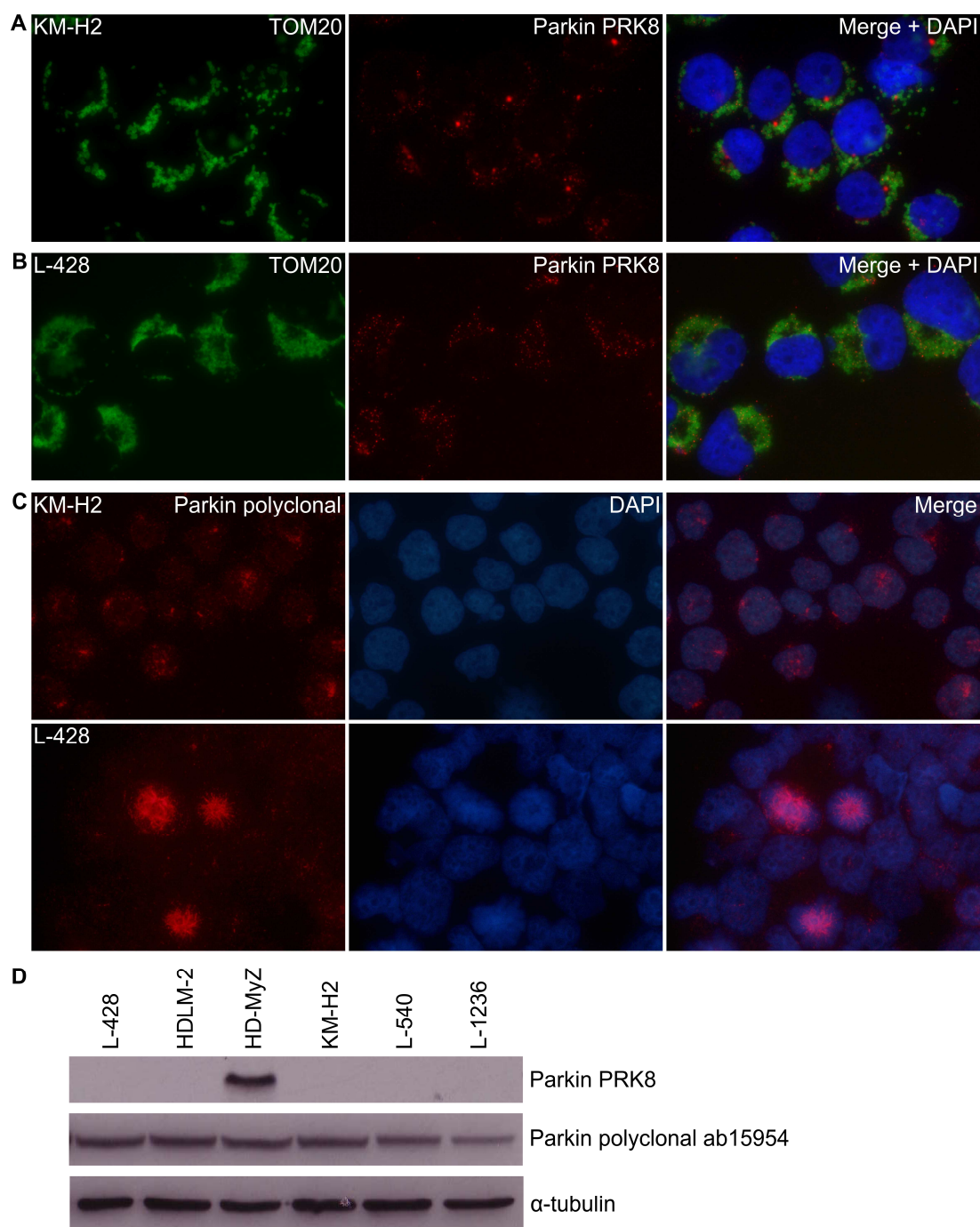


Figure 4-5 Parkin expression in KM-H2 and L-428.

Immunocytochemistry of Tom20 and Parkin in **(A)** KM-H2 and **(B)** L-428. Left panels show Tom20 (green), middle panels show Parkin identified by anti-Parkin clone PRK8 antibody (red) and right panels show left and middle panels merged with DAPI to identify nuclei (blue). **(C)** Immunocytochemistry of Parkin in KM-H2 and L-428 using polyclonal anti-Parkin antibody ab15954. Left panels show Parkin (red), middle panel show DAPI stain of nuclei (DAPI), right panel shows left and middle panels merged. **(D)** Western blot analysis of Parkin expression using anti-Parkin clone PRK8 and anti-Parkin polyclonal ab15954 antibodies. α -tubulin was included as a loading control.

4.3.3 Evidence of polarised protein degradation in HL-derived cell lines

The clustered mitochondria observed in L-428 cells could not be definitively attributed to mitophagy; therefore another explanation for this phenomenon was sought. p62 continued to display a perinuclear distribution in L-428 cells regardless of the induced protein handling stress. Following autophagy inhibition by 20 μ M HCQ, p62 expression was enhanced in this region (Figure 4-3C). Proteasome inhibition by 10 nM Bortezomib also resulted in p62 accumulation at this site; however, instead of appearing as multiple small puncta, one larger p62 aggregate appeared (Figure 4-6A). This suggested a polarisation of protein degradation. Consistent with this, p62 and lysosome-associated membrane protein LAMP2 were found to co-localise at this site in L-428 cells (Figure 4-6B). Such polarisation is thought to be a mechanism to enhance the efficiency of protein clearance by concentrating the degradation apparatus at one site (Nawrocki et al., 2006). This process requires retrograde transport along microtubules to the microtubule organising centre (MTOC), a bystander effect of which is the accumulation of organelles and cytoskeletal elements at this site (Trinczek et al., 1999). The microtubule network can be disrupted using Nocodazole. This agent binds to and prevents tubulin polymerisation and has been found to cause depolymerisation of microtubules at higher doses (Samson et al., 1979). It was found that by disrupting the microtubule network using Nocodazole, mitochondrial polarisation was lost in L-428 (Figure 4-6C). To firmly establish a polarisation of degradation at this site, an examination of p62 and LAMP2 co-localisation following Nocodazole treatment would be required. A loss of co-localisation would further indicate polarised degradation.

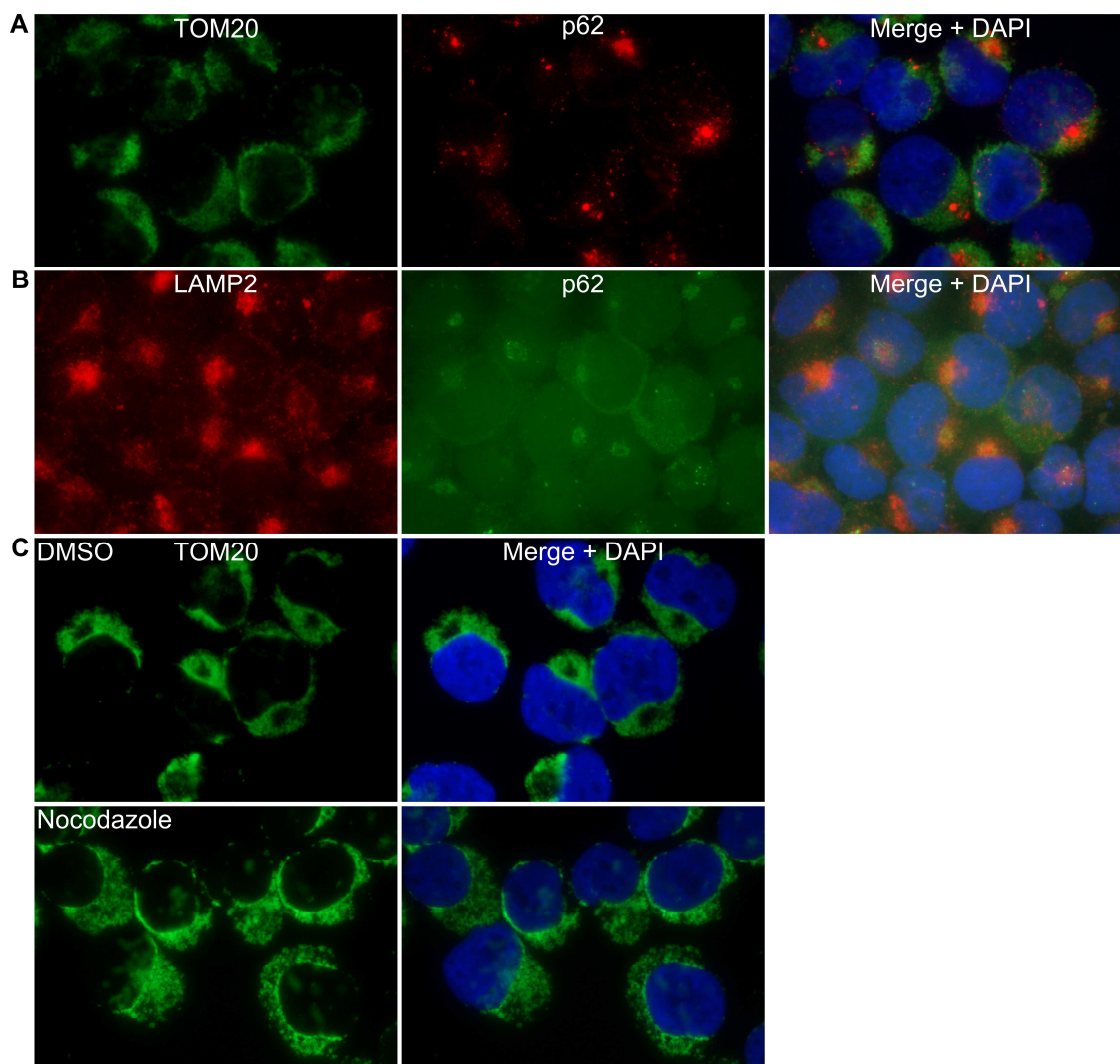


Figure 4-6 Distribution of mitochondria, p62 and LAMP2 in L-428.

Immunocytochemistry of (A) Tom20 (green) and p62 (red) following incubation with 10 nM Bortezomib for 16 hrs and (B) LAMP2 (red) and p62 (green). Nuclei are stained with DAPI (blue). (C) Effect of 200 nM Nocodazole on distribution of mitochondria identified by Tom20 (green). Nuclei were stained with DAPI (blue).

To determine if there was any evidence of similar polarisation in the other HL-derived cell lines, the distribution of mitochondria, indicated by Tom20 staining, and intermediate filament vimentin were examined with respect to the MTOC, indicated by puncta of γ -tubulin. The majority of cell lines displayed some degree of co-clustering of vimentin and Tom20, with the exception of L-540, in which they were expressed in a mutually exclusive pattern (Figure 4-7). Co-staining of Tom20 with γ -tubulin revealed that, to some extent the mitochondria were clustered around the MTOC in all of the cell lines (Figure 4-8). This was most evident in the L-428 cell line. To determine if there was a similar polarisation of degradative machinery, principally lysosomes, the distribution of LAMP2 was examined. In all of the cell lines there was evidence of polarisation of LAMP2, which had a similar distribution to Tom20 (Figure 4-9A). Again, this phenotype was most pronounced in L-428 cells. A similar degree of polarisation has been described during the formation of immune synapses in activated B cells, in which the lysosomal compartments are recruited to the MTOC for their directional secretion to facilitate antigen processing (Yuseff et al., 2011). Cytokine and chemokine secretion play an important role in the recruitment of the immune infiltrate in HL; a portion of the T cell recruitment has been attributed to TARC/CCL17 secretion by HL cells (van den Berg et al., 1999). Therefore the distribution of this chemokine was examined in HL-derived cell lines to determine if there was any evidence of polarised secretion of this chemokine. TARC expression was also of interest as nuclear p62 has been reported to modulate cytokine signalling (Kawai et al., 2008, Kim and Ozato, 2009) so any differences between L-1236 and the other cell lines would be of note. TARC was detected in HDLM-2 and L-428 cells only, with no evidence of TARC expression detected in the other cell lines. In HDLM-2 and L-428, TARC appeared clustered in an MTOC-like distribution (Figure 4-9B).

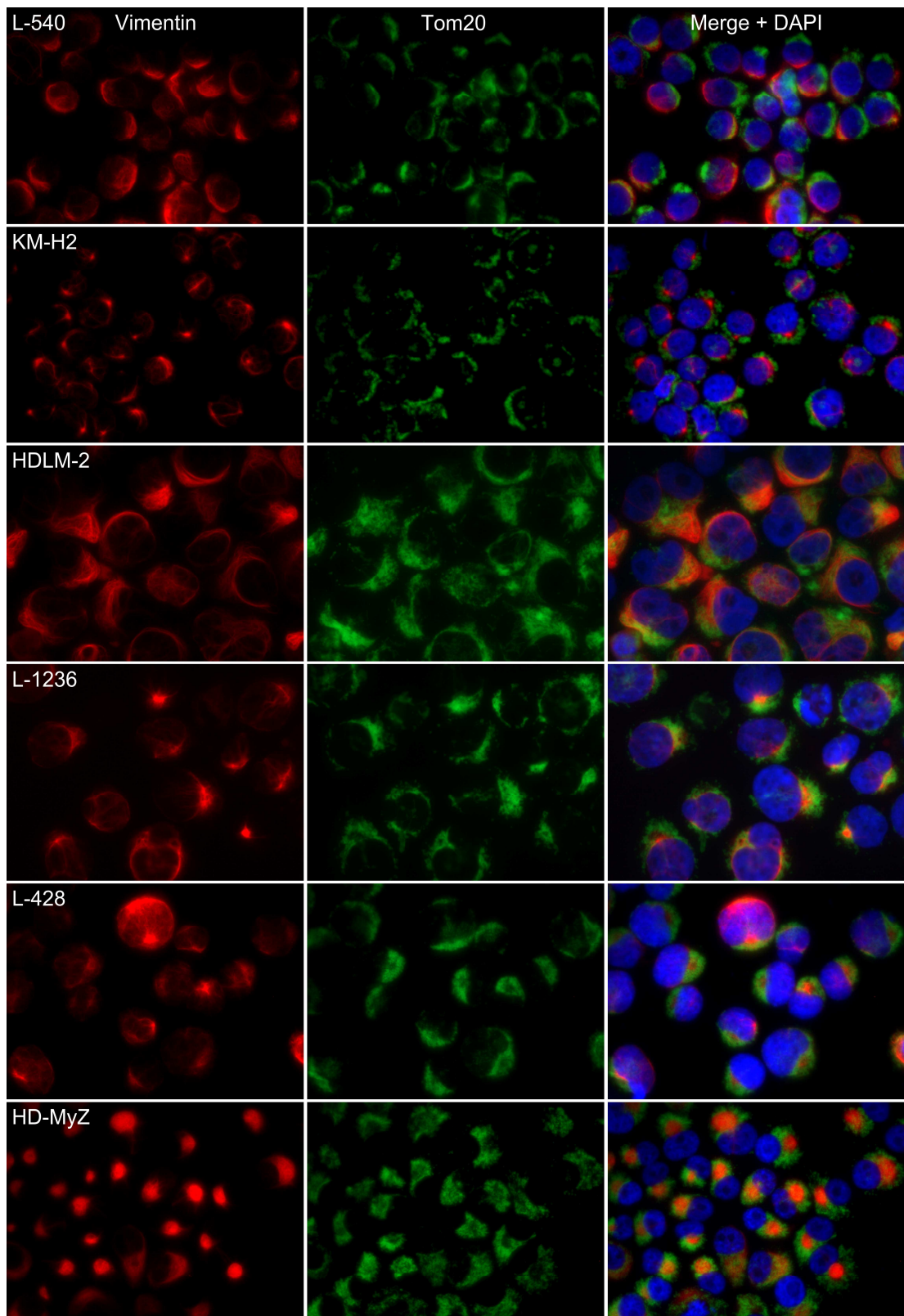


Figure 4-7 Vimentin and Tom20 distribution in HL-derived cell lines.

Immunocytochemistry of Vimentin (red, left panel) and Tom20 (green, middle panel). Nuclei were stained with DAPI (blue, right panel).

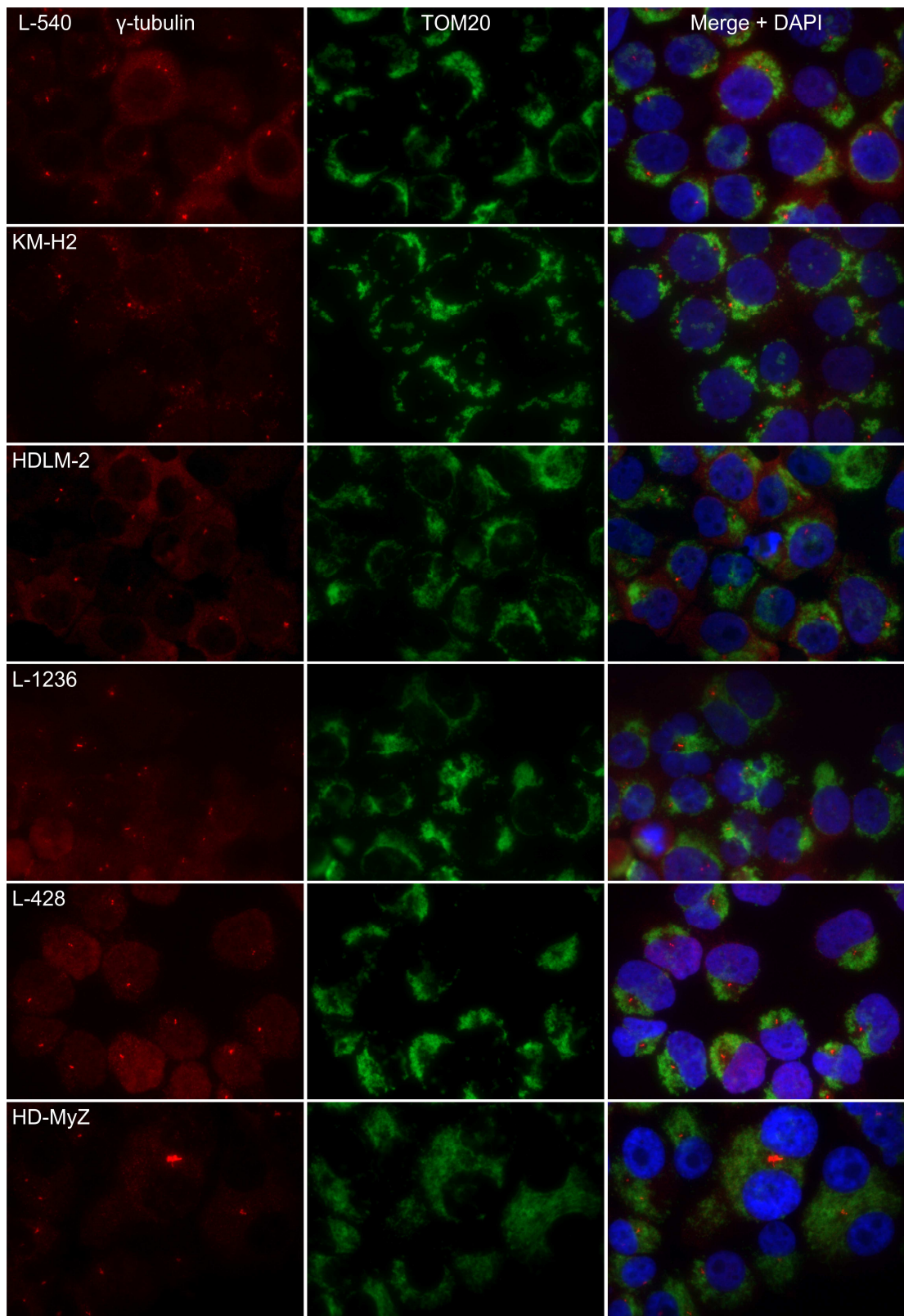


Figure 4-8 γ -tubulin and Tom20 distribution in HL-derived cell lines.

Immunocytochemistry of γ -tubulin (red, left panel) and Tom20 (green, middle panel). Nuclei were stained with DAPI (blue, right panel).

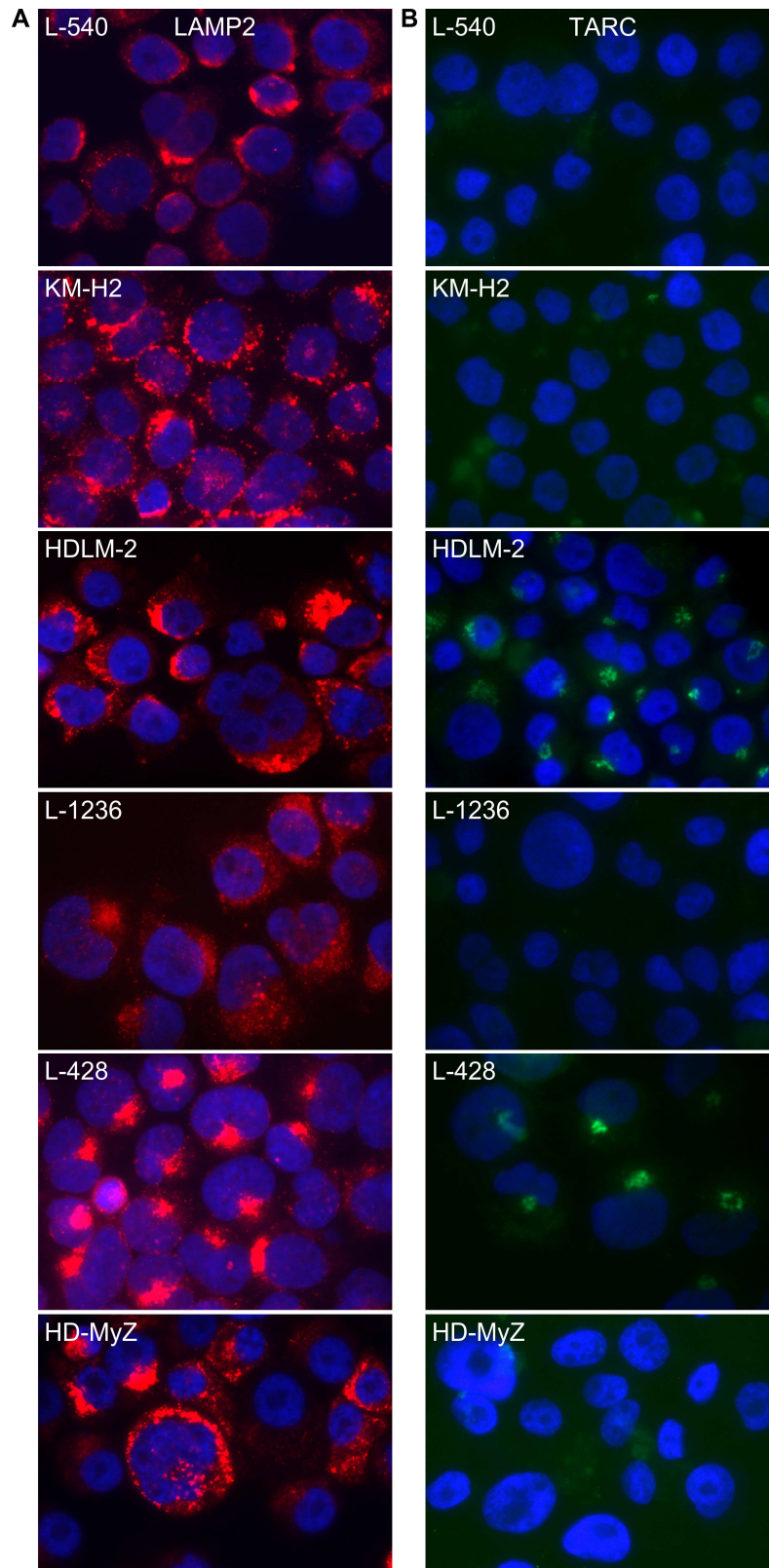


Figure 4-9 LAMP2 and TARC distribution in HL-derived cell lines.

Immunocytochemistry of (A) LAMP2 (red) and (B) TARC (green). In both cases the images are merged with a DAPI stain to identify nuclei (blue).

4.3.4 Proteasome inhibition in HL-derived cell lines

As described in section 3.3.4, proteasomal inhibition resulted in a dramatic change in p62 distribution with the formation of large aggregates in the majority of cell lines (Chapter 3, Figure 3-6). In L-540 cells, proteasome inhibition was accompanied by a loss of diffuse p62 staining (Chapter 3, Figure 3-6) and an increase in fractured nuclei following preparation of cytospins, suggesting poor cell viability. The effect of proteasome inhibition on cell viability was therefore measured by MTS assay (Figure 4-10A). L-540 and HDLM-2 were most susceptible to Bortezomib treatment, particularly at concentrations over 5 nM, while L-1236 and L-428 displayed less dramatic concentration-dependent drops in viability. In KM-H2, an initial increase in MTS assay was observed followed by a concentration dependent decrease in viability. HD-MyZ remained largely unaffected by Bortezomib treatment.

A compensatory mechanism is reported to exist between protein handling pathways (Pandey et al., 2007, Iwata et al., 2005). For example, under conditions of proteasome impairment, the proteasome-specific K48-linked polyubiquitin chains on proteins marked for degradation have been found to be changed in a Parkin-dependent manner to K63-linked chains, allowing transport to the MTOC for aggresome formation and ultimately degradation by the autophagy pathway (Olzmann et al., 2007). Consequently, the activity of the autophagy pathway was examined after proteasome inhibition. LC3B flux was measured following 5 nM Bortezomib treatment for 16 hours (section 2.12). An increase in LC3B flux was detected in L-540, L-428 and KM-H2; the increase was most pronounced in KM-H2 cells (Figure 4-10B). In HDLM-2 and L-1236 a decrease in flux was measured despite an apparent increase in LC3BII levels in Bortezomib treated but HCQ untreated cells. Very little difference was seen between treated and untreated HD-MyZ cells indicating a very low level of flux.

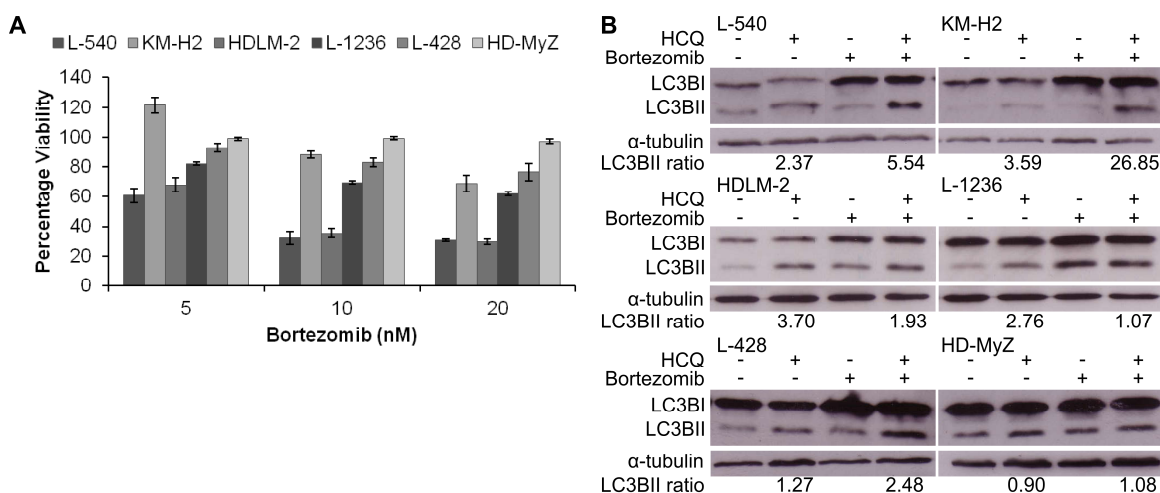


Figure 4-10 Effect of Bortezomib on cell viability and autophagy activity.

(A) Cell viability as measured by MTS assay following incubation for 24 hours with increasing concentrations of Bortezomib. Values represent the mean of 3 separate experiments and are expressed as percentage viability of a DMSO control. Error bars represent standard error. (B) Autophagy activity following incubation for 16 hours with 5 nM Bortezomib as measured by LC3BII flux. +/- indicates inclusion of the drug hydroxychloroquine (HCQ) and Bortezomib. α -tubulin was used as a loading control. The positions of the LC3BI and II proteins are shown to the left. Values beneath each blot represent levels of flux in the presence of HCQ as determined by ImageJ densitometry analysis, normalized to the loading controls.

The apparent increase in cell viability observed by MTS assay in KM-H2 cells following 5 nM Bortezomib treatment was thought to represent a G2/M arrest. Such an arrest has been reported following Bortezomib treatment as cell cycle progression is to a large extent controlled by the ubiquitin proteasome system (Bassermann et al., 2013). The MTS assay measures the reducing power of a cell; large cells enriched for by G2/M arrest contain more mitochondria than their early stage counterparts and consequently possess greater reducing power (James and Bohman, 1981). To determine whether there was an increase in the number of cells in later stages of cell cycle, the expression of cell cycle marker Tpx2, expressed in the S and G2/M phases of cell cycle (Heidebrecht et al., 1997), was assessed before and after incubation with 5 nM Bortezomib. Following drug treatment, the number of cells expressing Tpx2 was found to be greatly enhanced (Figure 4-11A). Double staining with Tpx2 and CENPF, a cell

cycle marker highly expressed at G2/M, verified a significant increase in the percentage of cells at G2/M suggesting cell cycle arrest at this stage (Figure 4-11B).

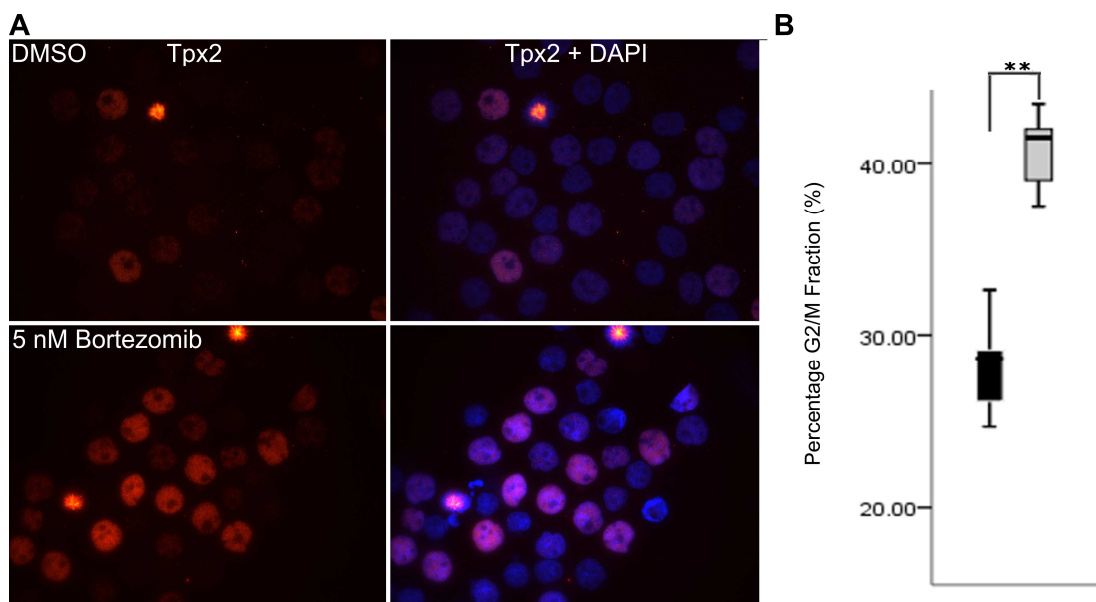


Figure 4-11 Proteasome inhibition results in G2/M arrest in KM-H2 cells.

(A) Immunocytochemistry of Tpx2 in KM-H2 cells following incubation for 16 hours with 5 nM Bortezomib. Left panels show Tpx2 (red). Right panels show left panel merged with DAPI stain to identify the nuclei (blue). (B) Increase in the post-replicative fraction of KM-H2 cells following incubation with 5 nM Bortezomib for 16 hours as assessed by Tpx2 and CENPF expression. The black and grey box whisker plots indicate control and Bortezomib treated cells, respectively. Asterisks indicate $P \leq 0.01$.

4.3.5 Autophagy inhibition in HL-derived cell lines

So far, HL-derived cell lines had displayed very different protein handling phenotypes in terms of pathway activity, sensitivity to Bortezomib, and the apparent degree of polarisation of protein degradation. Furthermore, proteasome activity and the accumulation of K48-linked polyubiquitin did not always result in p62 aggregation, as in the case of HD-MyZ. To determine whether similar differences would be observed following inhibition of autophagy,

HL-derived cell lines were treated with Bafilomycin A1. This resulted in the redistribution of p62 in all of the cell lines (Figure 4-12). Multiple small aggregates of p62 were formed in all cell lines, including HD-MyZ, to the detriment of diffuse staining. In L-428 cells these puncta were in the perinuclear area. Larger puncta were also formed in the KM-H2 and in HDLM-2 cell lines, although they were much more prominent in the latter. In L-1236, p62 redistributed from the nucleus to the cytoplasm as with Bortezomib treatment. Although this redistribution was generally more pronounced than that following proteasome inhibition, Bafilomycin A1 treatment did not greatly affect cell viability as measured by MTS assay (Figure 4-13A). L-1236 and, to a lesser extent, HDLM-2 displayed concentration-dependent reductions in viability.

Unlike the situation with proteasome inhibition, a reciprocal increase in chymotrypsin-like proteasome activity was not observed following autophagy. In fact, proteasome activity appeared largely unaffected by Bafilomycin A1 treatment in the cell lines, with only KM-H2 and HDLM-2 displaying a drop in chymotrypsin-like activity was measured (Figure 4-13B).

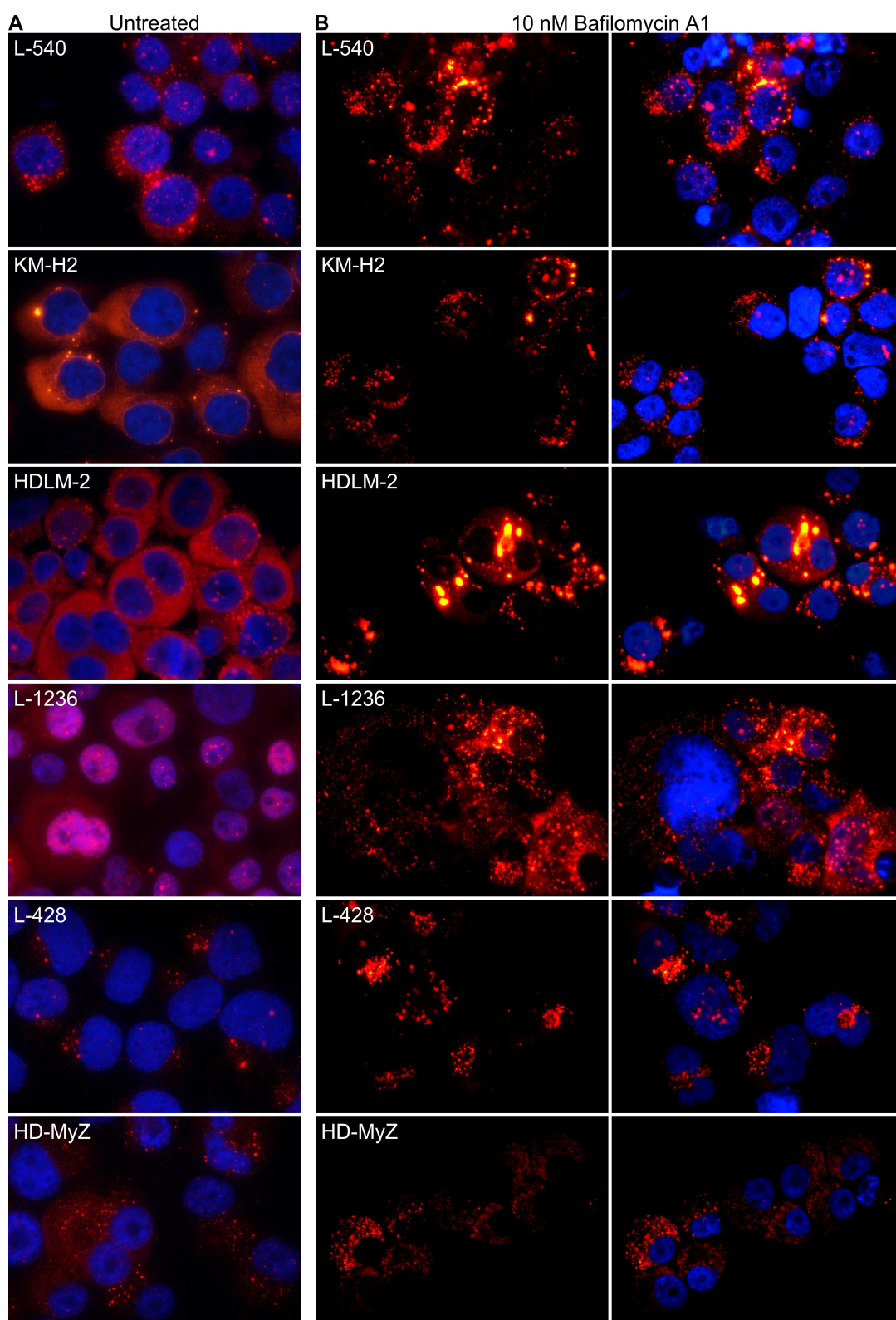


Figure 4-12 p62 distribution following autophagy inhibition.

Immunocytochemistry of p62 following incubation for 16 hours with 10 nM Bafilomycin A1. **(A)** Untreated cells from Figure 3-1. **(B)** Bafilomycin A1 treated cells. Left panels show p62 (red). Right panels show the left panel merged with a DAPI stain to identify the nuclei (blue).

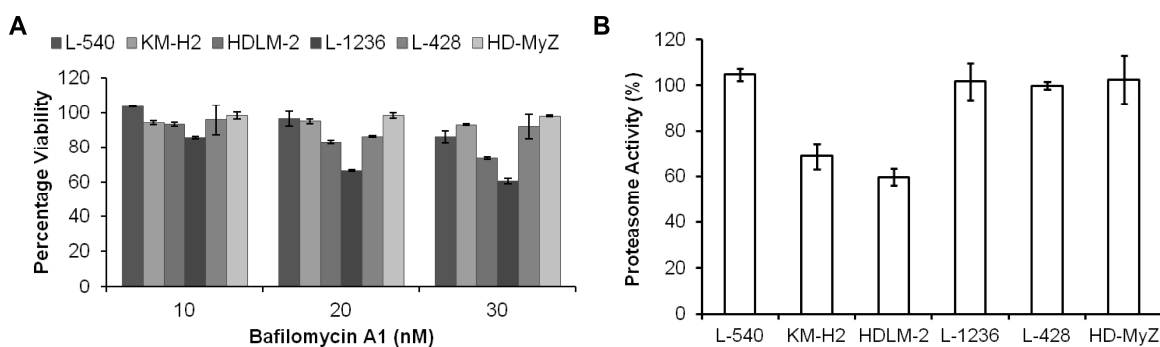


Figure 4-13 Effect of Bafilomycin A1 on cell viability and proteasome activity.

(A) Cell viability as measured by MTS assay following incubation for 24 hours with increasing concentrations of Bafilomycin A1. Values represent the mean of 3 separate experiments and are expressed as percentage viability of a DMSO control. Error bars represent standard error. (B) Chymotrypsin-like proteasome activity as measured by Proteasome-Glo assay following incubation for 24 hours with 10 nM Bafilomycin A1. Values represent the mean of triplicates and are expressed as percentage activity of a DMSO control. Error bars represent standard deviation of the mean.

4.3.6 HDAC6 inhibition in HL-derived cell lines

As described in section 4.3.3, MTOC clustering of organelles and cytoskeletal elements is a bystander effect of retrograde transport along microtubules (Trinczek et al., 1999). This transport allows polarisation of degradative machinery and directional secretion and is controlled in part by HDAC6 (Nawrocki et al., 2006, Yuseff et al., 2011). Since all the cell lines displayed some degree of polarisation, it was proposed that they would be sensitive to interference with HDAC6-mediated transport. Consequently, HL-derived cell lines were incubated with the HDAC6-specific inhibitor BML-281 and p62 distribution and cell viability were assessed. While p62 distribution was not greatly affected by HDAC6 inhibition (Figure 4-14), there appeared to be an enrichment of mitotic prophase-like cells, most notable in KM-H2, HDLM-2 and L-428. Cell viability as measured by MTS assay revealed that HDLM-2 and, in particular, L-1236 proved highly sensitive to HDAC6 inhibition (Figure 4-15). The remaining cell lines displayed concentration-dependent decreases in viability.

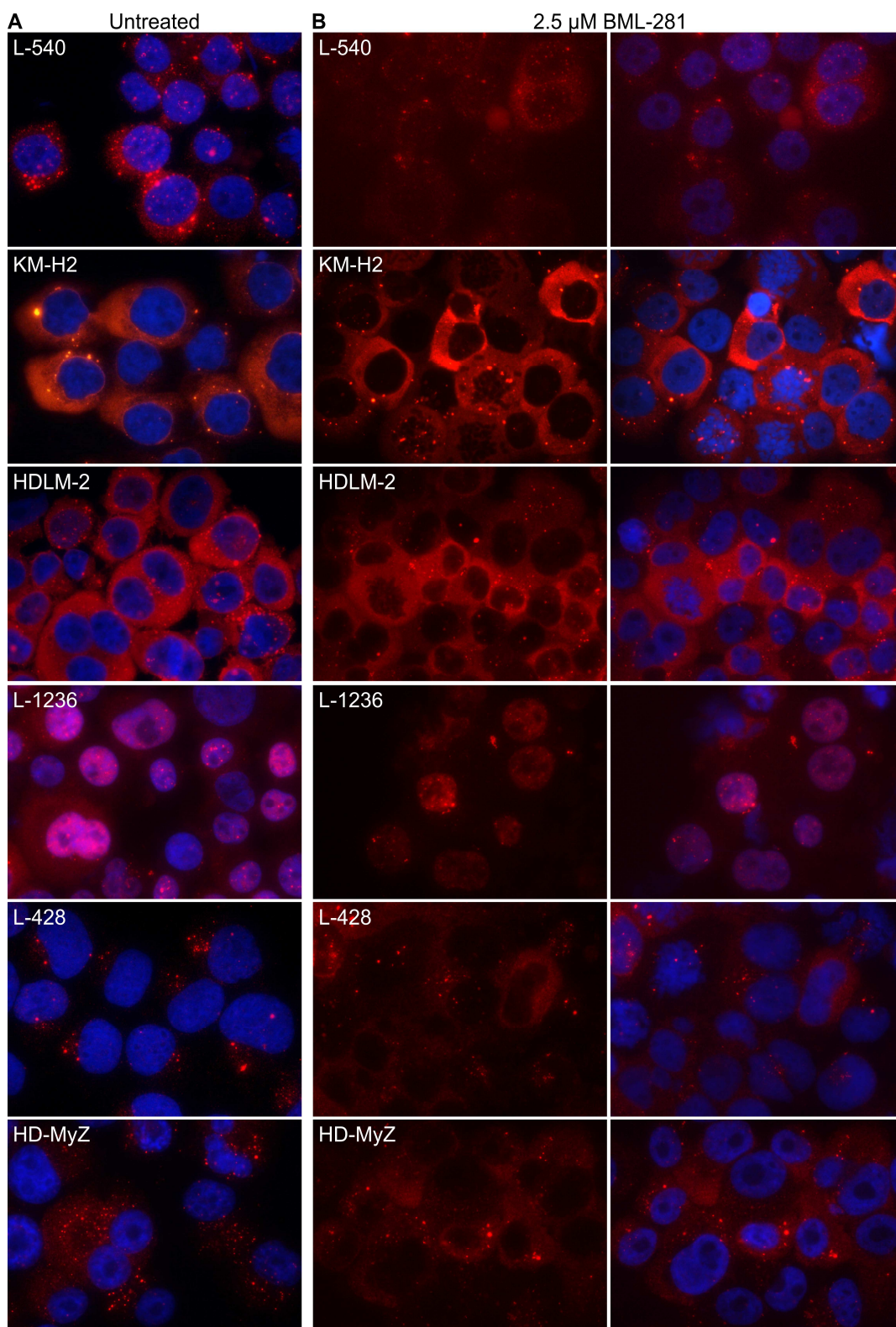


Figure 4-14 p62 distribution following HDAC6 inhibition.

Immunocytochemistry of p62 following incubation for 16 hours with 2.5 μ M BML-281. (A) Untreated cells from Figure 3-1. (B) BML-281 treated cells. Left panels show p62 (red). Right panels show left panel merged with DAPI stain to identify nuclei (blue).

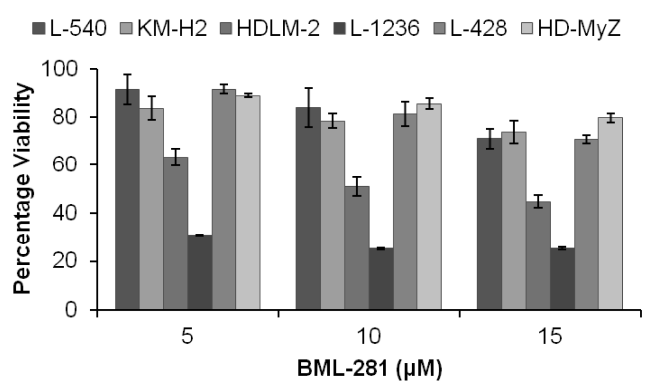


Figure 4-15 Effect of HDAC6 inhibition on cell viability.

MTS assay following incubation for 24 hours with increasing concentrations of BML-281. Values represent 3 separate experiments and are expressed as the percentage of a DMSO control. Error bars represent standard error.

To ensure BML-281 inhibition affected HDAC6 activity the levels of its main substrate acetylated- α -tubulin were assessed following overnight treatment with 5 μ M BML-281. Levels of acetylated- α -tubulin greatly increased following drug treatment (Figure 4-16A). An increase in acetylated-tubulin following BML-281 treatment was also confirmed in KM-H2 by immunocytochemistry (Figure 4-16B). While this inhibitor displays an IC₅₀ of 0.002 nM against HDAC6 in isolated enzyme assays, it also displays some inhibitory activity against other HDACs at nanomolar concentrations (IC₅₀s of 271, 252, 0.42, 6851 and 90.7 nM for HDACs 1,2,3,8 and 10 respectively) (Kozikowski et al., 2008). Consequently levels of acetylated-histone H3 were measured following 5 μ M BML-281 treatment to determine whether the nuclear HDACs were also affected. Levels of acetylated-histone H3 increased (Figure 4-16C), suggesting that at this concentration the activity of BML-281 was not restricted to HDAC6 inhibition.

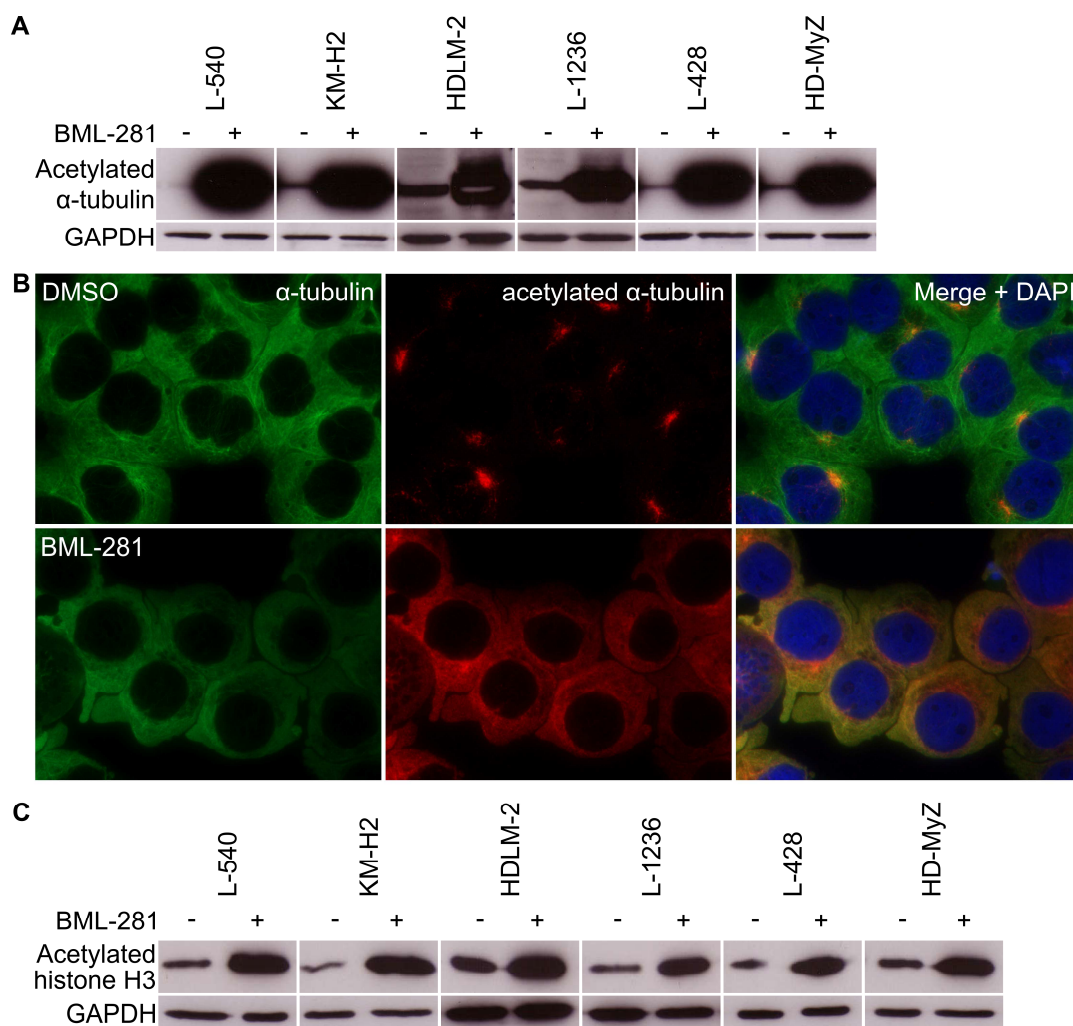


Figure 4-16 Effects of BML-281 on acetylated tubulin and histone H3.

(A) Western blot analysis of acetylated α -tubulin expression following incubation for 16 hours with 5 μ M BML-281. (+) indicates presence of BML-281, (-) indicates presence of DMSO as vehicle control. GAPDH was included as a loading control. (B) Immunocytochemistry of acetylated tubulin expression in KM-H2 following incubation for 16 hours with 5 μ M BML-281. Left panels show α -tubulin (green), middle panels show acetylated tubulin (red) and right panels show left and middle panels merged with DAPI stain to identify nuclei (blue). (C) Western blot analysis of acetylated histone H3 expression following incubation for 16 hours with 5 μ M BML-281. (+) indicates presence of BML-281, (-) indicates presence of DMSO as vehicle control. GAPDH was included as a loading control.

4.3.7 Nuclear targets of p62

The lack of p62 redistribution, increased acetylation of nuclear histone H3, and poor viability of the one cell line expressing constitutively nuclear p62 (L-1236) following incubation with BML-281 suggested that the principle targets of this agent affecting cell viability may reside in the nucleus. The localisation of p62 within specific cellular compartments generally reflects the distribution of its ubiquitinated substrates and the constant traffic of p62 between the cytoplasm and nucleus identified in section 3.3.3 suggested that many p62 target proteins may reside within the nucleus. Indeed, on examining K48-linked polyubiquitin expression patterns in HL-derived cell lines, these proteins displayed a predominantly nuclear expression pattern, although there was also evidence of cytoplasmic expression (Figure 4-17A). For example, in L-428 K48-linked polyubiquitin was also identified surrounding the MTOC in a pattern that was becoming characteristic of this cell line. As a link between p62 and genotoxic stress has been reported (White, 2012) and HL-derived cell lines are known to harbour high levels of DNA damage (Knecht et al., 2009), it was hypothesised that p62 may be involved in the turnover of ubiquitinated proteins involved in the DNA damage response. Consistent with the literature, high levels of DNA damage were identified by the expression of multiple phosphorylated-histone protein H2AX (γ H2AX) puncta, indicative of numerous double strand breaks (DSBs) (Bonner et al., 2008), in the majority of HL-derived cell lines (Figure 4-17B). KM-H2 appeared to have lower levels of expression of this protein compared to the other cell lines with the exception of mitotic cells; in which strong diffuse γ H2AX was evident throughout the chromatin.

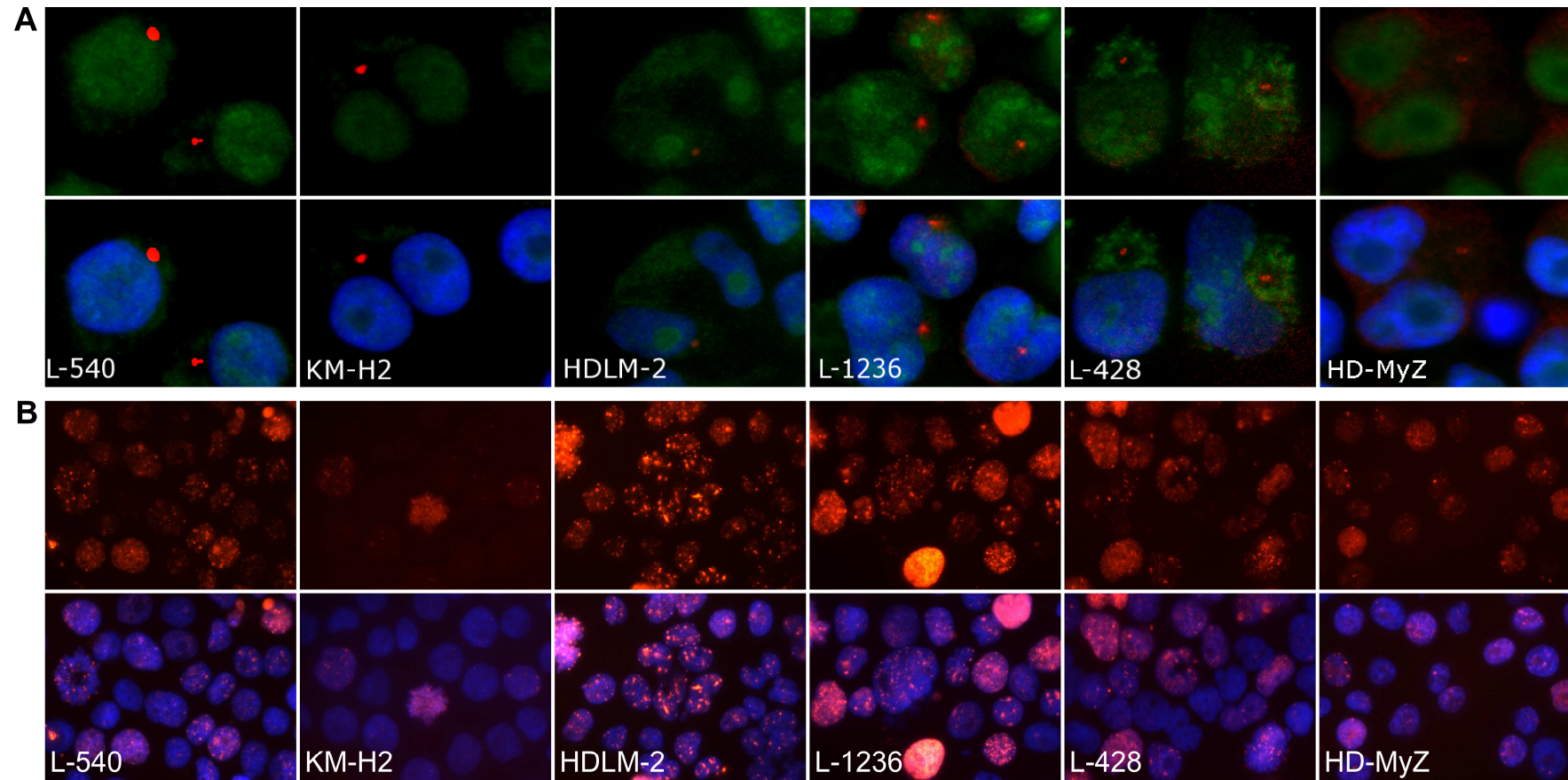


Figure 4-17 K48-linked polyubiquitinated proteins are found mostly in the nuclei of HL-derived cell lines, which also contain high levels of DNA damage. Immunocytochemistry of (A) K48-linked polyubiquitin (green) and γ -tubulin (red) and (B) DNA damage indicated by γ H2AX puncta (red). In both (A) and (B) lower panels indicate images merged with a DAPI counter stain to identify nuclei (blue).

To further explore the link between p62 and DNA damage, immunocytochemistry for p62 and γ H2AX expression were performed on L-1236 and KM-H2 as these cell lines expressed high and low levels of DNA damage, respectively (Figure 4-17B). There was evidence of both co-localisation and juxtaposition of p62 and γ H2AX puncta in L-1236 nuclei (Figure 4-18A), and to a lesser extent in KM-H2 where this was most evident in occasional enlarged nuclei (Figure 4-18B). As in section 3.3.1, p62 expression was predominantly cytoplasmic in the KM-H2 cell line and in the case where cytoplasmic aggregates were identified they co-localised perfectly with γ H2AX puncta (Figure 4-18C). These cytoplasmic aggregates did not co-stain with DAPI, suggesting they were protein aggregates and not microbodies or micronuclei. Of particular interest, in KM-H2 cells where the p62 “fleck” was observed, which had previously been attributed to a mitophagy response in section 4.3.2, this was also found to co-localise with γ H2AX (Figure 4-18D). This suggested that p62 was involved in a robust clearance of DNA damage-related proteins and that the “fleck” observed in previous cell populations may have indicated injury clearance.

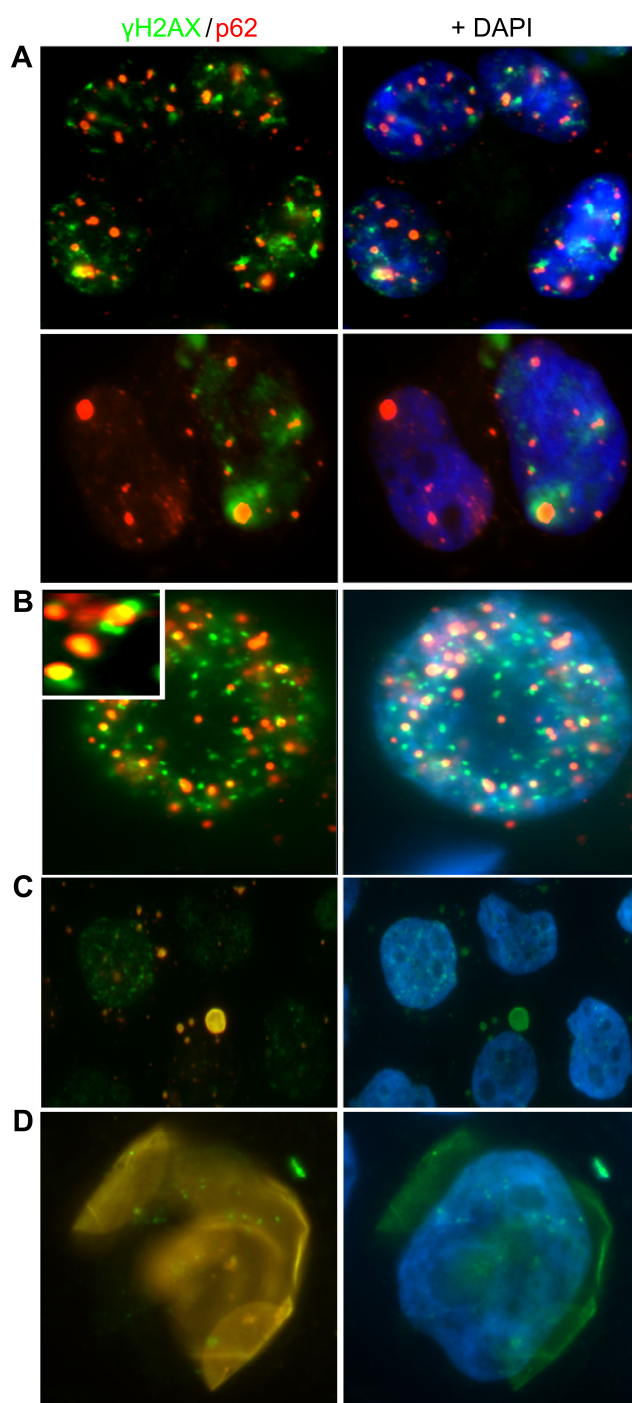


Figure 4-18 p62 juxtaposes and co-localises with γ H2AX puncta in KM-H2 and L-1236.

Immunocytochemistry showing juxtaposition and co-localisation of p62 (red) with γ H2AX (green) in nuclei of (A) L1236 and (B) KM-H2 cells. Inset panel of (B) shows enhanced image of p62 and γ H2AX co-localisation. (C) and (D) show co-localisation of p62 in the cytoplasm of KM-H2 cells as a large aggregate (C) or as the p62 “fleck” (D) previously associated with mitophagy. Left hand panels in (A), (B), (C) and (D) show p62 and γ H2AX. Right hand panels in (A) and (B) show left hand panel merged with a DAPI stain to identify nuclei (blue). Right hand panels in (C) and (D) show γ H2AX stain merged with DAPI stain.

4.3.8 BML-281 causes DSBs in prophase-like cells

Recent reports of a protective role for HDAC6 following genotoxic stress (Wang et al., 2012) led us to examine γ H2AX expression in KM-H2 and L-1236 following incubation with 2.5 μ M BML-281. In KM-H2, DNA damage was most evident in mitotic rather than interphase cells. As in section 4.3.6, enrichment for prophase-like cells was observed in this cell line. Upon closer examination, the nuclei of these cells were unusual as the chromosomes appeared round and enlarged as if the chromatin was incompletely condensed (Figure 4-19A). In contrast to the diffuse staining pattern observed in control mitotic cells, these prophase-like nuclei also contained large puncta of γ H2AX, indicative of DSBs. L-1236 was highly sensitive to BML-281, as before, and the predominant phenotype was DAPI-bright apoptotic bodies. There was some evidence of similar DNA damage in mitotic cells in this line, however these were rarely observed amongst the cell debris. The mitotic arrest in KM-H2, indicated by the enrichment of prophase-like nuclei, was confirmed by increased numbers of post-replicative cells following incubation with BML-281 (Figure 4-19B). A similar increase was not observed in L-1236, supporting the notion that, unlike KM-H2, this cell line underwent apoptosis rather than cell cycle arrest in response to this drug.

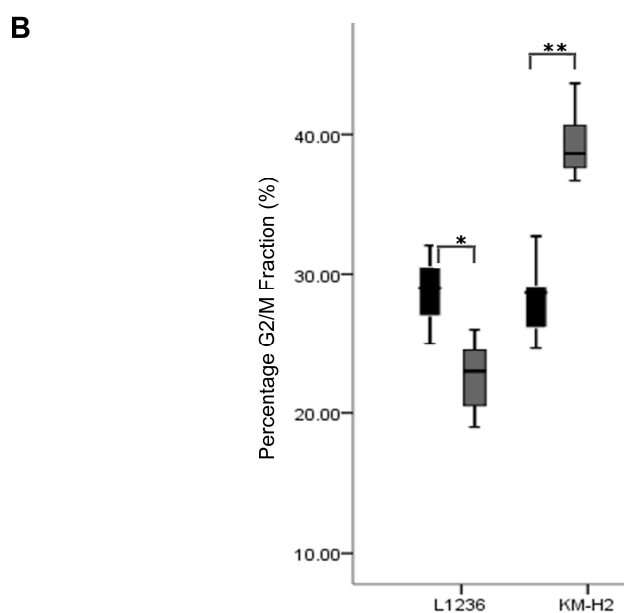
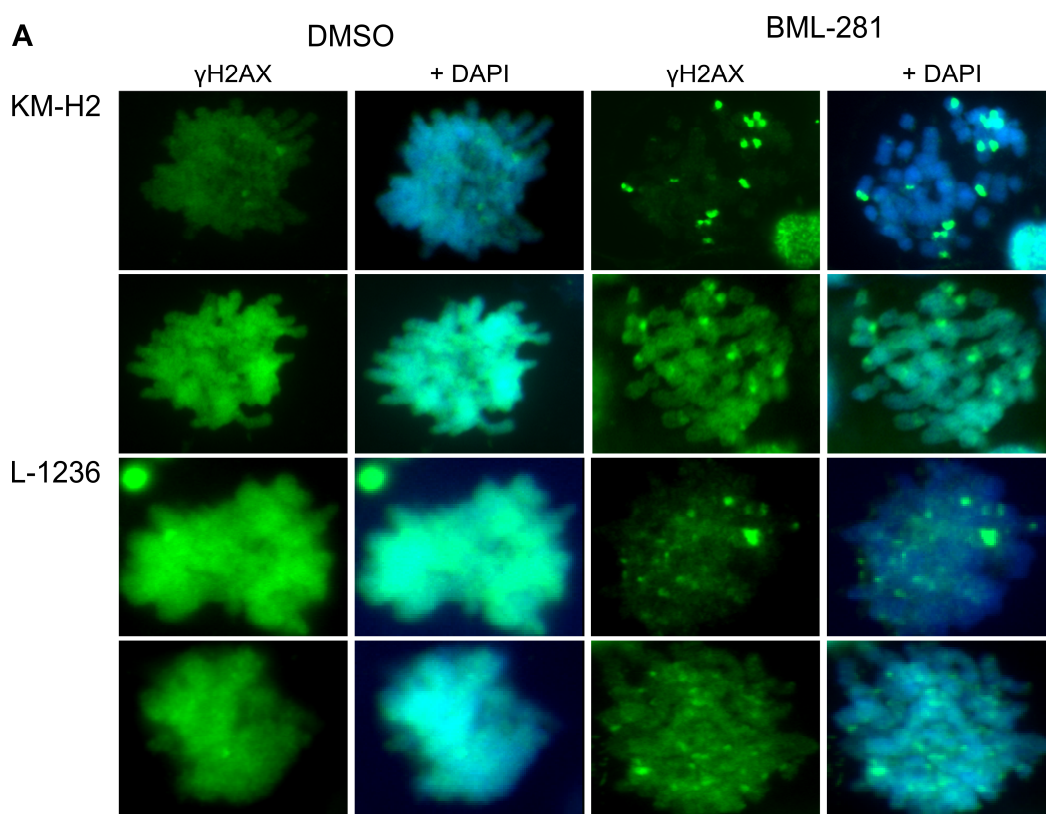


Figure 4-19 BML-281 causes DSBs in mitotic cells.

(A) Immunocytochemistry of γ H2AX (green) in KM-H2 and L-1236 cells treated with DMSO (left hand panels) or 2.5 μ M BML-281 (right hand panels). A DAPI stain was included for each cell to identify nuclei (blue). (B) Incubation with 2.5 μ M BML-281 for 24 hours causes an increase in the post replicative fraction in KM-H2 but not L-1236 cells. The G2/M fraction was assessed by TPX2 and CENPF immunocytochemistry. Black box-whisker plots indicate DMSO treated control cells; light grey box-whisker plots indicate BML-281 treated cells. Asterisks indicate $P \leq 0.05$ (*) and $P \leq 0.001$ (**).

4.3.9 Dual protein-handling pathway inhibition

As no single pathway inhibitor had proved effective against all the cell lines, dual inhibition of proteasome and autophagy was tested against those lines which displayed an increase in autophagy activity following proteasome inhibition (L-540, KM-H2 and L-428, Figure 4-10B). HCQ was used for autophagy inhibition as it is clinically available and less toxic than Bafilomycin A1 (Furst, 1996). In KM-H2 and L-428 the addition of increasing concentrations of HCQ to Bortezomib treatment resulted in a slight concentration-dependent decrease in viability in both cell lines, down to approximately 75% viability in KM-H2 at higher HCQ concentrations, but did not greatly affect them (Figure 4-20A). L-540 showed an initial drop in viability from treatment with Bortezomib alone but there was no additional loss of viability gained from increasing HCQ concentration.

Combination inhibition of the proteasome and HDAC6-mediated transport, to create a protein handling stress and then remove the compensatory mechanism of protein transport, was then tested (Figure 4-20B). Although L-540 and HDLM-2 were already susceptible to Bortezomib, the addition of HDAC6 inhibition exacerbated their drop in viability as measured by MTS assay. It also resulted in reduced viability in KM-H2 and L-428 to a greater extent than combined proteasome and autophagy inhibition. Of note, although the addition of BML-281 reduced the viability of L-1236 compared to Bortezomib alone, combined proteasome and HDAC6 inhibition appeared to have a protective effect against HDAC6 inhibition alone. HD-MyZ remained relatively resistant to the combined inhibition and its viability did not drop below 80%.

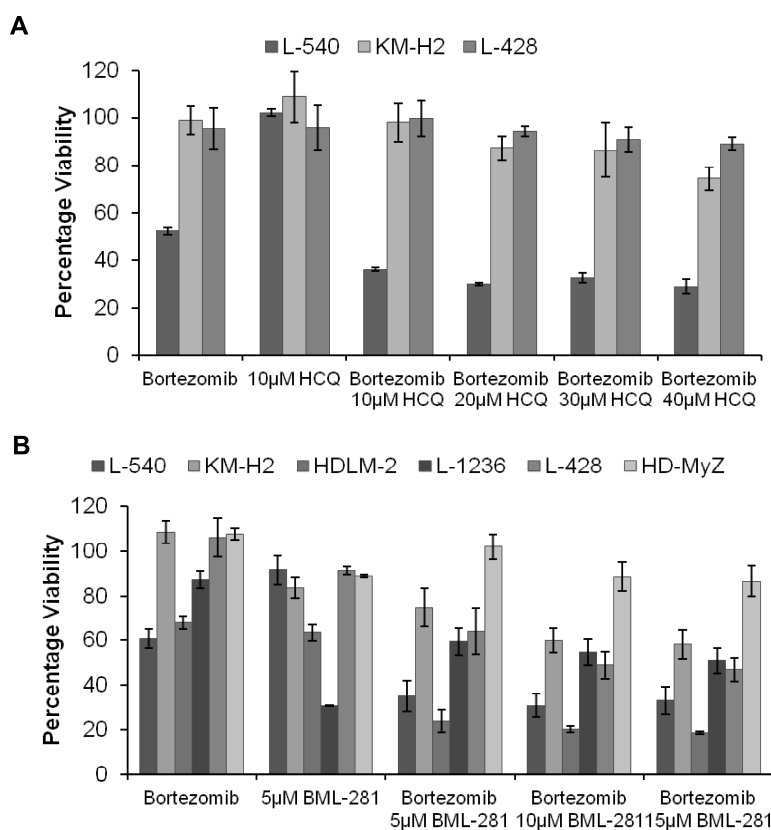


Figure 4-20 Effect of dual proteasome and autophagy or HDAC6 inhibition on cell viability. MTS assay following incubation for 24 hours with 5 nM Bortezomib and increasing concentrations of HCQ (**A**) or BML-281 (**B**). Values represent 3 separate experiments and are expressed as the percentage of a DMSO control. Error bars represent standard error.

4.3.10 Mechanism of cell death following proteasome- and HDAC6-inhibition

Inhibition of protein degradation results in the accumulation of misfolded proteins that can induce potentially toxic reactive oxygen species (ROS) (Tabner et al., 2005). Consequently ROS levels were assessed following treatment with 5 nM Bortezomib and 5 μM BML-281. ROS levels were found to increase in all cell lines tested (L-540, KM-H2, HD-MyZ and L-428) to varying degrees (Figure 4-21A). To confirm that the decreased MTS reading (Figure 4-20B) correlated with cell death a number of the cell lines were incubated with Bortezomib and BML-281 overnight, stained with PI and analysed by flow cytometry. An increase in PI

positive cells was observed in L-540, KM-H2 and L-428, while the percentage of PI positive cells in HD-MyZ remained roughly the same following drug treatment (Figure 4-21B). The death inducing effect of the double treatment was also confirmed by analysing cleavage of caspase-3. Following incubation with 5 nM Bortezomib and 5 μ M BML-281, all cell lines, excluding HD-MyZ, displayed an increase in the 17 and 19 kDa subunits of cleaved caspase 3 (Figure 4-21C), indicating activation of this executioner caspase. As reported previously, only low levels of caspase-3 were detected in KM-H2 (Izban et al., 1999). In untreated L-540 cells, a 19 kDa caspase-3 subunit was detected. The proteasome has been reported to regulate caspase-3 function by degrading the active subunits, particularly the smaller 17 kDa form; this prevents cell death in the presence of constitutively expressed subunits (Chen et al., 2003). When the proteasome was inhibited this subunit was stabilised, accelerating the process of cell death. This may explain the susceptibility of L-540 to proteasome inhibition by Bortezomib (Figure 4-10A). As caspase-3 appeared to be constitutively cleaved, stabilisation of the 17 kDa subunit by proteasome inhibition would result in enhanced cell death.

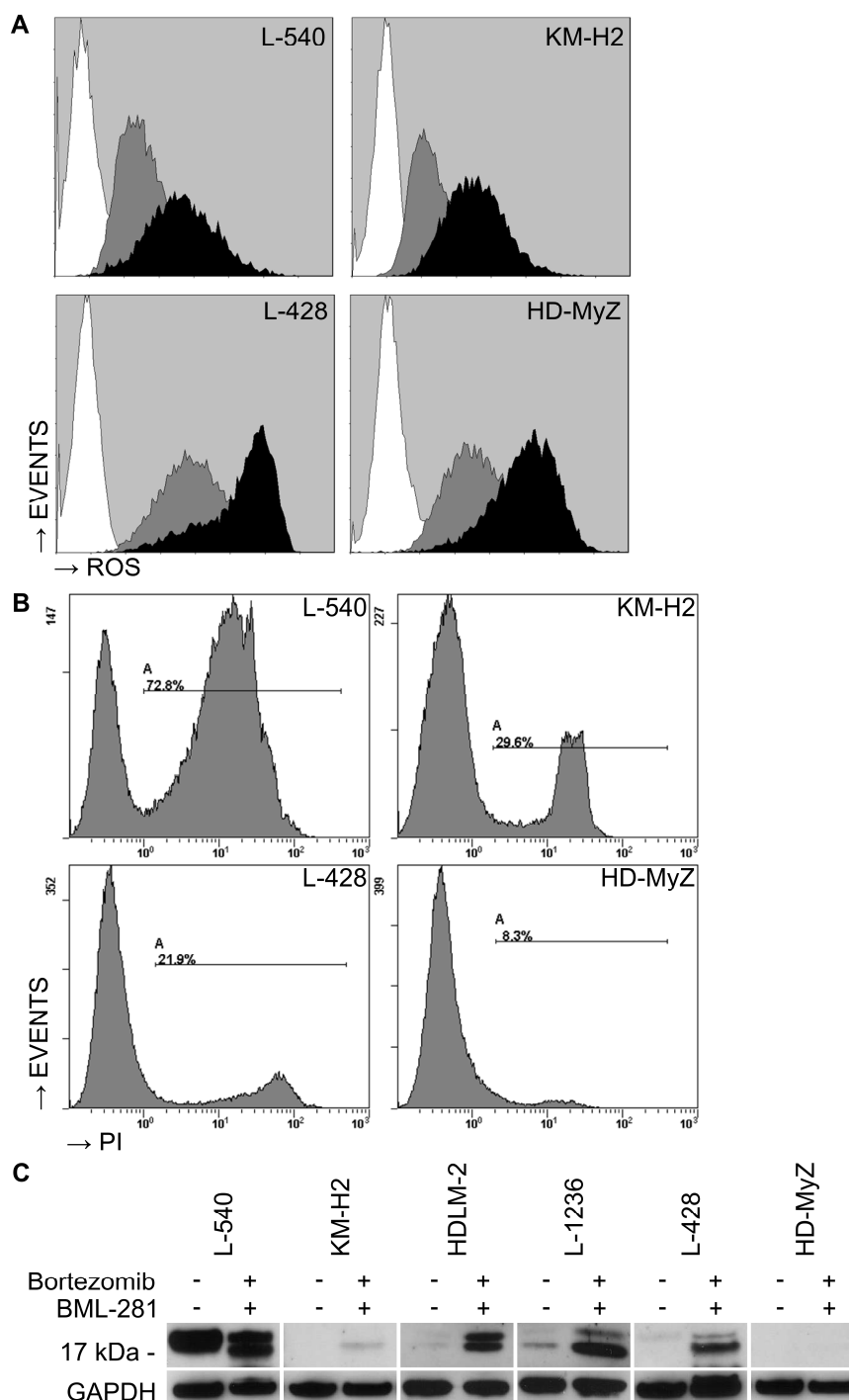


Figure 4-21 Confirmation of cell death following proteasome and HDAC6 inhibition.

(A) ROS levels detected by flow cytometry using 10 μ M CM-H₂DCFDA ROS dye following incubation for 16 hours with 5 nM Bortezomib and 5 μ M BML-281. White histograms represent unstained cells, grey histograms represent DMSO and ROS dye treated cells, black histograms represent cells treated with 5 nM Bortezomib, 5 μ M BML-281 and ROS dye. (B) Percentage of PI positive cells detected by flow cytometry following incubation for 16 hours with 5 nM Bortezomib and 5 μ M BML-281. (C) Western blot analysis of caspase-3 cleavage following incubation for 16 hours with 5 nM Bortezomib and 5 μ M BML-281. GAPDH was included as a loading control.

4.4 Discussion

A number of studies have examined proteasome and HDAC inhibitors in HL-derived cell lines in the context of NF κ B regulation and cell death (Zheng et al., 2004, Buglio et al., 2010); however, to date none of these studies have focused on the effects on protein handling pathways. This chapter used p62 to monitor protein accumulation in response to inhibition of protein degradation pathways. The activities of protein degradation pathways and the sensitivities of HL-derived cell lines to individual protein degradation pathway inhibition and combination inhibition of proteasome and autophagy or HDAC6 are reported.

4.4.1 Proteasome activity does not directly correlate with sensitivity to proteasome inhibition

Considering each pathway in turn, the chymotrypsin-like proteasome activity was heterogeneous in the HL cell lines. L-540, KM-H2 and HDLM-2 consistently displayed lower proteasome activity than L-1236, L-428 and HD-MyZ (Figure 4-1A). These activities did not transfer to sensitivity, however, as L-540 and HDLM-2 were highly sensitive to Bortezomib treatment (Figure 4-10A) despite having lower pathway activity. This would suggest that the conventional wisdom that high pathway activity indicates an over-reliance and therefore, sensitivity to inhibition, may not always be the case. The data showing lower pathway activity was supported by the higher levels of K48-linked polyubiquitin found in the cell lines with lower proteasome activities (Figure 4-1B), suggesting that the proteasome may not deal with its load as well as those cell lines with higher proteasome activity, although L-1236 also expressed higher levels of K48-linked polyubiquitin.

4.4.2 Sequestration of p62 into aggregates correlates with cell death in the L-540 cell line

In L-540 the loss of diffuse p62 following Bortezomib treatment was striking (Chapter 3, Figure 3-6). The role of this diffuse fraction was originally thought to

correlate to proteasome activity and this may be true in L-540. However, in KM-H2 and HDLM-2 proteasome inhibition did not result in a loss of diffuse p62 staining, if anything it was enhanced. A plausible explanation would be that diffuse cytoplasmic p62 can also function as a signalling adapter in pro-survival pathways. We could speculate that in L-540, the loss of diffuse p62 indicated its diversion into protein aggregates or autophagosomes, as suggested by the increase in autophagy activity (Figure 4-10B). This hypothesis would also be supported by recent data showing partitioning of p62 between soluble and aggregated fractions in order to regulate cAMP signalling (Houslay and Christian, 2010). The loss of a protective p62 fraction may have been responsible for the dramatic reduction in viability following proteasome inhibition in this cell line.

4.4.3 Cytoplasmic aggregates of p62 were found to increase under conditions of increased and stalled autophagic flux

In order to explain the sensitivity of HDLM-2 to proteasome inhibition the autophagy pathway must be examined. All the cell lines, excluding HD-MyZ, displayed autophagy activity in the form of LC3B flux (Figure 4-1C). The greatest difference was the response of this pathway to proteasome inhibition. L-540, KM-H2 and L-428 all increased their LC3B flux, KM-H2 to a much greater extent than the others (Figure 4-10B). However, although convention dictates the correct way to interpret LC3B flux blots is to determine the ratio between LC3II in cells treated with an autophagy inhibitor versus untreated cells (Klionsky et al., 2012), a clear increase in LC3BI levels was observed in all HL-derived cell lines, excluding HD-MyZ, following Bortezomib treatment (Figure 4-10B). A similar increase in LC3BI has been reported in response to nutrient deprivation and was attributed to an unregulated autophagy response caused by p53 deficiency (Scherz-Shouval et al., 2010). In that scenario this uncontrolled autophagy led to cell death, however this was not the case in HL-derived cell lines and the increase was seen in all cell lines, both p53-positive (KM-H2 and L-540) and negative (HDLM-2, L-1236, L-428 and HD-MyZ) (Janz et al., 2007, Drexler, 1993). It is possible that this increase in LC3BI represented an attempt by all the cell lines to up-regulate components of the autophagy machinery in

response to proteasome inhibition, although it may not translate into an increase in end-stage pathway activity as measured by the LC3BII flux method. Similarly, in Bortezomib treated HDLM-2 and L-1236, an increase in LC3BII was observed compared to untreated cells (Figure 4-10B). Despite this, a decrease in LC3B flux was measured. However, as these two cell lines proved most sensitive to autophagy inhibition by Bafilomycin A1 (Figure 4-13A), this apparent increase in LC3BII may represent an insupportable increase of material into the autophagy pathway to the extent that it became over-loaded and stalled. This would be supported by the redistribution of p62 seen in HDLM-2 cells following proteasome inhibition (Chapter 3, Figure 3-6). Compared to KM-H2, which displayed a dramatic increase in autophagy activity following proteasome inhibition, p62 aggregates formed in HDLM-2 were much larger and less regular in shape. Therefore it would appear that in response to proteasome inhibition, HDLM-2 attempted to compensate using the autophagy pathway but was unable to do so, resulting in cell death. Therefore, p62 aggregation may arise from increased as well as stalled autophagy.

4.4.4 Non-reciprocal compensation of pathway activity

It is interesting to note that while the cell lines appeared to attempt to compensate for proteasome inhibition through increased autophagy, no such reciprocal increase was seen in proteasome activity following autophagy inhibition (Figure 4-13B). In fact in KM-H2 and HDLM-2 quite the reverse was seen, with Bafilomycin A1 treatment resulting in decreased chymotrypsin-like activity. It has been reported that p62 accumulation following autophagy inhibition can impair proteasome function, as the aggregates appear to slow substrate navigation to the proteasome (Korolchuk et al., 2009). While all cell lines formed multiple p62 aggregates following Bafilomycin A1 treatment (Figure 4-12), in HDLM-2 large irregular aggregates were again formed, which could easily be imagined to impair proteasome function. In KM-H2 cells, some cells also formed larger p62 aggregates, although not to the same extent as in HDLM-2.

4.4.5 A unique constitutively nuclear fraction of p62 was identified in L-1236 cells

The majority of HL-derived cell lines expressed p62 in the cytoplasm under non-stressed conditions (Chapter 3, Figure 3-1). L-1236 was an exception; although there was some cytoplasmic p62, the majority appeared in the nucleus. p62 is known to shuttle continuously between the nucleus and cytoplasm to deal with protein waste (Pankiv et al., 2010), however treatment with nuclear export inhibitor Leptomycin B resulted in an almost complete redistribution of p62 into the nucleus in all of the HL cell lines (Chapter 3, Figure 3-5). To our knowledge this is the first demonstration of this in Hodgkin lymphoma. Nuclear p62 formed small or large aggregates once redistributed to the nucleus depending on the cell line. Interestingly these aggregates rarely appeared to associate with nucleoli, as is often the case with nuclear protein waste (Latonen, 2011), rather they associated with PML bodies, which are known sites of nuclear proteasomes (Rockel et al., 2005). The predominantly nuclear expression pattern of K48-linked polyubiquitin (Figure 4-17A) would suggest a requirement for degradation-associated proteins in the nuclear compartment and may also highlight the importance of proteasomal degradation in these cells, as the presence of nuclear proteasomes is well known. Nuclear autophagy, on the other hand, has yet to be demonstrated, although the autophagosome-associated protein LC3 has been detected in the nucleus (Drake et al., 2010). The association of nuclear p62 with γ H2AX in KM-H2 and L-1236 (Figure 4-18AB) would suggest a role for p62 in the clearance of DNA damage-related proteins or damage-associated chromatin. The presence of cytoplasmic aggregates containing both p62 and γ H2AX in KM-H2 supported this notion and suggested a robust clearance of this marker of damage in these cells. These data would suggest that p62 is involved in the transport of nuclear proteins for degradation in the cytoplasm, where autophagy would be available to supplement proteasomal degradation. This hypothesis would be supported by the formation of larger nuclear aggregates of p62 following LMB treatment in the 3 cell lines possessing low proteasome activity and higher levels of K48-linked polyubiquitin (L-540, KM-H2 and HDLM-2) compared to the other cell lines (Chapter 3, Figure 3-5).

4.4.6 Spatial restriction of p62 expression in L-428 cells was not due to its role in mitophagy

The large accumulations of p62 in KM-H2 that appeared to co-localise with mitochondria (Figure 4-3A), though these large aggregates were later found to co-localise with the marker of DSBs γ H2AX (Figure 4-18CD), and the distribution of mitochondria, with some or all clustering around a distinct area of the cytoplasm in KM-H2 and L-428, respectively, (Figure 4-3B) led us to examine the possibility of mitophagy, the degradation of mitochondria by autophagy. At the time the increased expression of p62 within the mitochondrial ring in L-428 cells following autophagy inhibition (Figure 4-3C) was thought to demonstrate its role in mitophagy. However, it is likely that it appeared at this site because the protein degradation machinery was localised here due to the high degree of polarisation in this cell line as evidenced by the accumulation of p62 at this site following proteasome inhibition (4-6A) and the co-localisation of p62 and lysosomal protein LAMP2 at this site (Figure 4-6B). In both KM-H2 and L-428, most mitochondria appeared polarised and healthy as indicated by retention of MitoTracker™ dye (Figure 4-4A) and there was no overwhelming evidence of mitophagy from localisation of the mitophagy adaptor Parkin. Two different populations of Parkin were detected using separate antibodies (Figure 4-5), with the polyclonal Parkin antibody ab15954 appearing to favour mitotic spindle-associated Parkin in L-428. Sadly, we lacked the time and resources to investigate this fully and the MTOC-like Parkin expression in KM-H2, indicative of proteasome impairment and polarisation of protein degradation to the MTOC (Junn et al., 2002, Muqit et al., 2004, Zhao et al., 2003), led us to investigate polarisation of protein degradation in the cell lines.

4.4.7 Evidence of polarisation of protein handling in L-428 cells

Polarization of organelles, vimentin and lysosomes to the MTOC, while apparent in all the HL-derived cell lines, was most evident in L-428. L-428 was also the only cell line in which there was clear co-localisation between MTOC-localized lysosomes and p62 (Figure 4-6B). This cell line also exhibited evidence of HDAC6-

mediated polarisation of secretory pathways with an MTOC-like TARC distribution (Figure 4-9B). HDLM-2 also expressed MTOC-localised TARC, which also may partly explain the increased sensitivity of this cell line to HDAC6 inhibition, despite appearing no more polarised than the other lines in other respects. The mutually exclusive expression patterns of MTOC-localised mitochondria and vimentin in L-540 were provocative (Figure 4-7) but, as yet, we have no explanation for this finding. The association of mitochondria with vimentin is reported to be protective against ROS-induced damage and subsequent cell death (Matveeva et al., 2010). Perhaps the lack of such an association in L-540 may play a part in its sensitivity to proteasome inhibition, as this inhibition would likely generate ROS. In addition to being a bystander effect of high retrograde transport, MTOC-localised mitochondria may indicate increased demand for ATP to fuel metabolic functions at this region (Skulachev, 2001, Yu et al., 2010). With such a degree of HDAC6-mediated retrograde microtubule transport apparent in HL-derived cell lines, this could partially explain the success of the microtubule targeting agent Vinblastine in HL therapy, despite the reported slow rate of cell cycle in RS cells. The unusual expression pattern of vimentin as a large cytoplasmic ball in HD-MyZ will be discussed further in the next chapter.

There appeared to be a high degree of retrograde transport in all of the cell lines as indicated by MTOC-localised mitochondria, vimentin and lysosomes, although the extent of this differed in each cell line (Figures 4-7, 4-8, 4-9A). As such transport is largely mediated by HDAC6 it was surprising that more cell lines were not susceptible to HDAC6 inhibition (Figure 4-15), with L-1236 and HDLM-2 most sensitive to this inhibition. HDAC6 is required for the remodelling of the f-actin network to facilitate the fusion of autophagosomes with lysosomes (Lee et al., 2010). L-1236 and HDLM-2 already appeared susceptible to autophagy inhibition with Bafilomycin A1 (Figure 4-13A) and appeared to suffer some impairment of autophagy activity when protein handling stress was induced with Bortezomib (Figure 4-10B). It is possible; therefore, that the role of HDAC6 in

the maturation of the autophagosome may contribute to the heightened sensitivity of these cell lines to HDAC6 inhibition.

4.4.8 HDAC6 inhibition provoked a mitotic phenotype associated with DNA damage

Given that there was evidence of polarised protein handling in all the HL-derived cell lines it was surprising that HDAC6 inhibition had such little effect. This may be due to the focus of the initial experiments on cytoplasmic phenotypes in interphase cells while the major phenotype observed was at mitosis. The finding that BML-281 caused an enrichment of prophase-like cells containing double strand breaks (DSBs) was unexpected and is, to the best of our knowledge, the first report of this phenotype (Figure 4-19A). HDAC6 has previously been reported to exert a protective effect in response to genotoxic stress (Wang et al., 2012); however its exact mechanism of action is yet to be identified. It has also been implicated in the regulation of chromatin condensation (Verdel et al., 2003). Diffuse γ H2AX expression at mitosis, such as that seen in KM-H2, has been reported to maintain genome integrity through the regulation of its epigenetic status (Ichijima et al., 2005). Therefore the reorganisation γ H2AX into large puncta following BML-281 treatment may alter the compaction and chromatin chemistry, rendering it more susceptible to DNA damage. These DSBs, marked by γ H2AX puncta, may have been a result of a non-specific activity of BML-281 or genotoxic stress caused by an inability to deacetylate microtubules for their breakdown and conversion to mitotic spindle. This lack of spindle may also account for the unusual appearance of the prophase-like nuclei. There was little evidence of prophase arrested cells in L-1236 following incubation with BML-281 (Figure 4-19B), instead the majority of cells appeared as apoptotic bodies. In contrast in KM-H2, cell cycle arrest was observed and prophase-like cells were preserved. This can be explained as the DNA damage response is temporarily suspended during the early stages of mitosis but fully operational following completion of mitosis (Zhang et al., 2011). Thus cells harbouring DSBs which appear to arrest at prophase, such as KM-H2, are protected from damage-induced cell death (at least temporarily) but cells such as L-1236, which do not

arrest and progress through mitosis, are subject to the full DNA damage response and its associated cell fate outcomes, in this case cell death. This would be supported by the observation of an increase in viability as measured by MTS assay in L-1236 cells following incubation with Bortezomib and BML-281 versus BML-281 alone (Figure 4-20B, Figure 4-15). Bortezomib is known to cause cell cycle arrest at G2/M (Bassermann et al., 2013), therefore it could be hypothesized that, in combination with BML-281, cell cycle arrest caused by Bortezomib had a temporary protective effect in L-1236 cells over the BML-281-induced DNA damage by preventing cell cycle progression through mitosis and thus the fatal recognition of DNA damage.

4.4.9 Combined proteasome and HDAC6 inhibition was the most effective cytotoxic drug combination

With no single agent proving successful against all HL cell lines, combination treatments were explored. The cell lines resistant to Bortezomib, which showed a compensatory increase in autophagy, L-540, KM-H2 and L-428, were challenged with dual pathway inhibition. Surprisingly, using the clinically available HCQ in place of Bafilomycin A1, little additive effect was seen by combining proteasome and autophagy inhibition in KM-H2 and L-428 (Figure 4-20A). It is possible that by extending the assay time, this combination would have seen more success. In contrast, combining proteasome inhibition with HDAC6 inhibition resulted in viability drops in the cell lines previously resistant to proteasome inhibition alone (Figure 4-20B). HD-MyZ was an exception and remained largely resistant to these treatments. The success of this dual inhibition is likely down to the creation of an additional protein handling stress by inhibiting the proteasome and then removing the preferred method of dealing with such stress by interfering with HDAC6-mediated polarised protein degradation. HDAC6 inhibition may also have the additional effect of inhibiting autophagy, as mentioned previously, given its role in the fusion of autophagosomes with lysosomes (Lee et al., 2010), thus preventing a benefit from a compensatory switch to this pathway.

In conclusion, although p62 was originally intended as a biomarker to inform on pathway activity and sensitivity to therapeutic intervention, its expression pattern was too complex in HL-derived cell lines and did not reliably correlate with pathway activity or sensitivity to inhibition. Throughout this chapter, HD-MyZ displayed numerous differences from the other HL-derived cell lines. It appeared to possess greater proteasome activity than a number of the other cell lines, however was insensitive to proteasome inhibition and unlike in the other cell lines p62 did not appear to aggregate in response to this stress (Chapter 3, Figure 3-6). HD-MyZ was also unresponsive to autophagy inhibition, although in this instance p62 did aggregate as in the other cell lines despite HD-MyZ displaying negligible autophagy activity as measured by LC3B flux. HD-MyZ was also the most resistant cell line to BML-281 and when challenged with proteasome and HDAC inhibition remained largely insensitive at the concentrations tested, while the other cell lines displayed drops in viability. Perhaps the most obvious phenotype of this cell line was its vimentin distribution. Unlike the other HL-derived cell lines, in which vimentin appeared as a perinuclear network, in HD-MyZ it was present as a large perinuclear ball. The status of this cell lines as representative of HL is questionable as it does not express CD30 or CD15, two diagnostic markers of HL, nor does it possess immunoglobulin or T cell receptor gene rearrangements suggesting that it may not be of lymphoid origin (Bargou et al., 1993, Kuppers and Re, 2007). In general this cell line differed from the other HL-derived cell lines and will be further examined in Chapter 5.

Chapter 5. Further examination of the HD-MyZ cell line

5.1 Summary

In this chapter the unusual expression pattern of the intermediate filament vimentin in HD-MyZ was examined in further detail and alternative therapies to those that proved unsuccessful against this cell line in the previous chapter are sought. The apparent co-localisation of Parkin with microtubules led us to test the sensitivity of this line to the anti-microtubule agent Paclitaxel, however it was again found to be more resistant than the other HL-derived cell lines tested. A nuclear expression pattern for lysosomal protease cathepsin B was identified in HL-derived cell lines, which was not seen in an EBV-immortalised lymphoblastoid cell line. It was proposed this enzyme could be released from the lysosomal compartment to deal with protein handling stress, however, no changes were seen in the expression of this protein following treatment with Bortezomib and BML-281. A second proteasome inhibitor, Withaferin A (WFA), was tested that preferentially targeted vimentin and its effects on vimentin, p62 and K48-linked polyubiquitin expression were examined. Despite apparently cleaving vimentin in a caspase-dependent manner in HD-MyZ but not in other HL-derived cell lines, this agent displayed limited death-inducing activity against HD-MyZ compared to the other cell lines. It also appeared to act in a specific way against this cell line as p62 was seen to aggregate at 5 μ M WFA in HD-MyZ but no increase in K48-linked polyubiquitin expression was seen. This was in contrast to L-540, KM-H2 and L-428 in which p62 aggregated at low WFA concentrations and K48-linked polyubiquitin expression increased following 5 μ M WFA treatment. Ultimately HD-MyZ remained resistant to all treatments tested and its phenotypic differences from HL-derived cell lines were further highlighted.

5.2 Introduction

Although listed as an HL-derived cell line on the Deutsche Sammlung von Mikroorganismen und Zellkulturen (DSMZ) website, HD-MyZ is not thought to be derived from HRS cells. The cell line was established from a patient with HL, however while the HRS cells from this patient were CD30⁺CD15⁺ the opposite is the case for HD-MyZ (Bargou et al., 1993). Additionally, the expression of the macrophage-associated CD68 and myeloid-associated CD13 antigens and the lack of T cell receptor or immunoglobulin gene rearrangements would suggest that this cell line is of non-lymphoid origin (Bargou et al., 1993, Kuppers and Re, 2007).

Throughout Chapter 4, in contrast to HL-derived cells lines, the HD-MyZ cell line remained largely resistant to drug inhibition of protein handling pathways. With the exception of autophagy, in which there was no apparent LC3B flux yet a dramatic aggregation of p62 following Bafilomycin A1 treatment, this cell line did not appear to differ greatly from the other cell lines in terms of pathway activity or polarisation of organelles, intermediate filament and lysosomes to the MTOC. Despite displaying similar levels of proteasome inhibition to the other cell lines, p62 was not seen to aggregate in this cell line following Bortezomib treatment. It was proposed, given the large vimentin aggregate seen in HD-MyZ, that it may have problems with its cytoskeletal network. Consequently this was investigated in further detail along with alternative therapeutic agents to those tested in the previous chapter.

The cytoskeleton forms a rigid framework providing structure and shape for the cell while also acting as a dynamic network allowing the movement of proteins, organelles and the cell itself (Fletcher and Mullins, 2010). The cytoskeleton consists of three filamentous networks: actin filaments (microfilaments), intermediate filaments and microtubules. Actin filaments are largely involved in dictating cell shape and are highly active in processes such as endocytosis and cell movement which require structural changes at the cell surface (Chhabra and

Higgs, 2007). Consequently actin filaments are generally found in close association with the plasma membrane. Intermediate filaments, such as vimentin, are responsible for providing structural support for the cell and are present throughout the nucleus and cytoplasm (Herrmann et al., 2007). The microtubule network is also spread throughout the cytoplasm yet comes to a focus at the perinuclear microtubule-organising centre (MTOC) (Fletcher and Mullins, 2010, Luders and Stearns, 2007). This network provides a structural framework on which a number of motor proteins operate, allowing the movement of proteins and organelles throughout the cytoplasm (Schliwa and Woehlke, 2003). In addition to facilitating movement of organelles and proteins throughout the cell, an intact microtubule network is also required for the assembly and maintenance of intermediate filament networks and for actin-mediated plasma-membrane remodelling (Schliwa and Woehlke, 2003). Therefore, the maintenance of a microtubule network is important not just for its own function but for the function of other components of the cytoskeleton.

Parkin, an ubiquitin E3 ligase implicated in the pathogenesis of Parkinson's disease, binds to microtubules and also to free heterodimers of α - and β -tubulin, the components of microtubules (Ren et al., 2003). This binding to the free components results in their ubiquitination and subsequent proteasomal degradation. Parkin may therefore play a key role in the degradation of tubulin heterodimers during microtubule depolymerisation. When bound to polymerised tubulin heterodimers in the form of microtubules, Parkin has a protective effect against microtubule depolymerising agents such as colchicines (Yang et al., 2005). This binding to and stabilisation of microtubules is not dependent on the E3 ligase activity of Parkin but relies instead on three separate functional domains. These were identified as really interesting new gene (RING) domains, RING0/ unique Parkin domain (UPD), RING1 and RING2. RING domains are associated with protein-protein interactions and are commonly found in proteins involved in the ubiquitin proteasome system (Deshaies and Joazeiro, 2009). The E3 ligase can therefore anchor to microtubules and retain its functional activity. This is likely important in terms of dealing with protein folding stress.

The unusual expression pattern of vimentin in HD-MyZ led us to further examine this intermediate filament protein and to examine microtubules and the microtubule-binding protein, Parkin, in this cell line.

5.3 Results

5.3.1 Parkin appears to localise with microtubules

Parkin is commonly studied in terms of its role in marking damaged mitochondria for degradation by the autophagy pathway, a process known as mitophagy (Geisler et al., 2010, Narendra et al., 2010). Subsequently Parkin expression in relation to mitochondria was examined in HD-MyZ. Parkin was seen to be expressed at relatively high levels by immunocytochemistry, as predicted by western blotting (Figure 4-5D), and appeared as multiple puncta (using the PRK8 monoclonal antibody) interspersed with the mitochondrial population (Figure 5-1A). As in KM-H2 and L-428, mitochondria in HD-MyZ retained MitoTracker™ dye suggesting that they were polarised and healthy (Figure 5-1B). In mitotic cells, using the anti-Parkin clone PRK8 antibody, Parkin was detected on the mitotic spindle in HD-MyZ (Figure 5-1C). Parkin had only previously been detected in this distribution using the polyclonal antibody ab15954 in the other HL-derived cell lines. Using this polyclonal Parkin antibody in HD-MyZ, Parkin was again predominantly detected on mitotic spindle with little or no evidence of the multiple puncta detected in other cell lines (Figure 5-1D, upper panels). Therefore, it would appear that this antibody selectively detected spindle-associated Parkin in HD-MyZ. Immunostains using ab15954 also detected strong Parkin expression at the spindle apparatus at late telophase / cytokinesis (Figure 5-1D, lower panels). The central 'dark-zone' of the polar microtubules that constitutes the mitotic spindle at these phases indicates the region of the midbody where antibody is typically excluded because of epitope alteration or masking through high protein and microtubule concentrations (Hu et al., 2012).

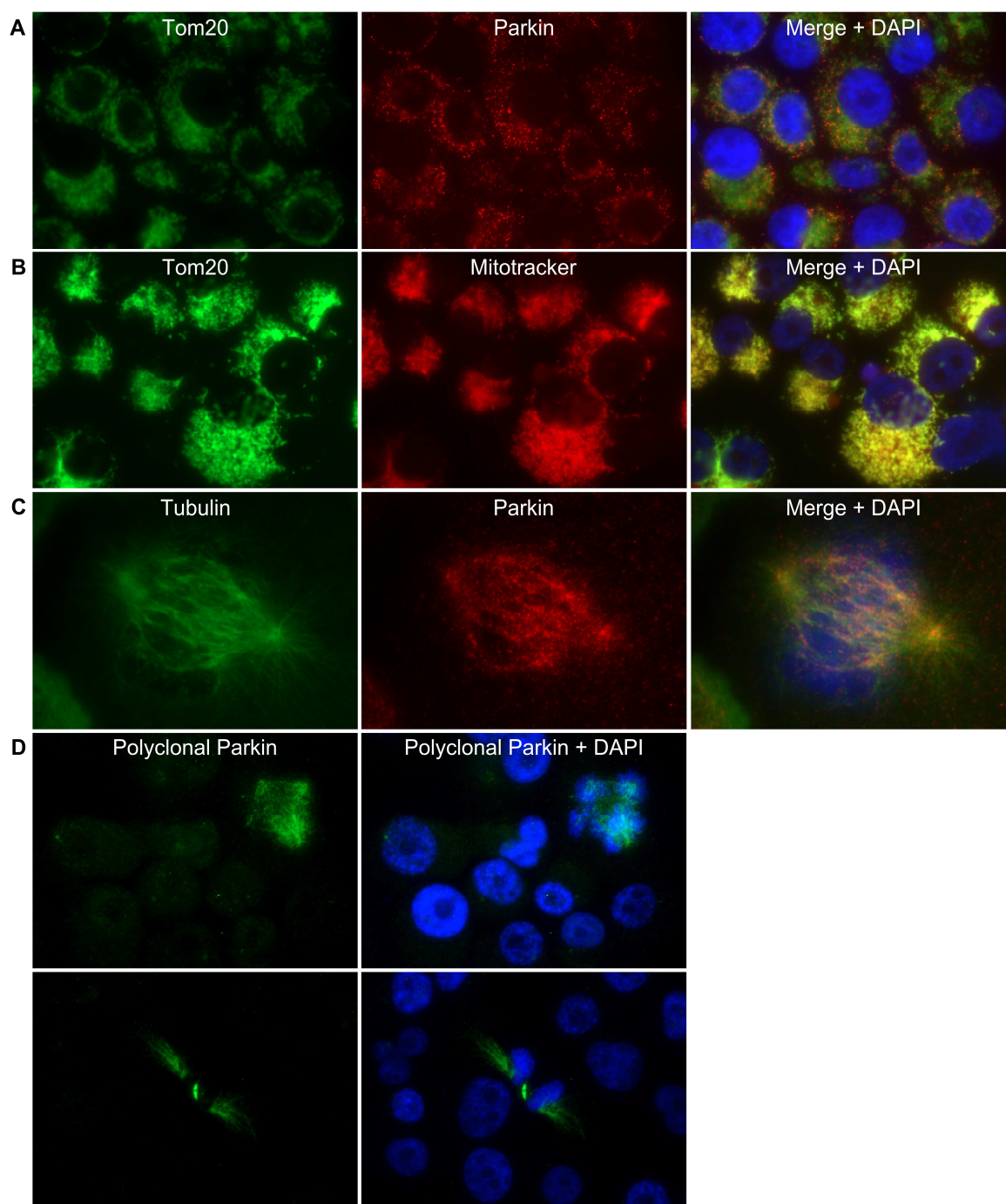


Figure 5-1 Parkin expression in HD-MyZ.

Immunocytochemistry of (A) Tom20 (green) and Parkin (red), (B) Tom20 (green) and MitoTracker (red) and (C) α -tubulin (green) and Parkin (red). In each the right panel represents the left and middle panels merged with a DAPI stain to identify nuclei (blue). In (A) and (C) the monoclonal Parkin antibody clone PRK8 was used. (D) Immunocytochemistry of Parkin (green) using polyclonal Parkin antibody (ab15954). Right panel represents left panel merged with a DAPI stain to identify nuclei (blue).

Given the unusual pattern of vimentin expression seen in this cell line it was proposed that this cell line may express an aberrant distribution of other cytoskeletal elements. On examination, HD-MyZ expressed a large filamentous microtubule network, consistent with a normal microtubule distribution, with the large bundle of vimentin occupying a perinuclear position within the network (Figure 5-2AB). As has been previously reported, Parkin puncta appeared to track along microtubules (Figure 5-2CD) (Ren et al., 2003). In addition to binding to and stabilising microtubules, Parkin has also been found to enhance the binding activity of Paclitaxel (Wang et al., 2009). This chemotherapeutic drug used against breast cancer, binds to microtubules and prevents their depolymerisation for the formation of mitotic spindle (Horwitz, 1994). It was therefore proposed that given its higher expression levels of Parkin and apparent microtubule localisation, HD-MyZ would be more sensitive to Paclitaxel than other HL cell lines. Analysis by MTS assay indicated that this was not the case as HD-MyZ displayed a similar slight decrease in viability as L-540, KM-H2 and L-428 following 24hrs incubation (Figure 5-3). In future, Paclitaxel treatment should be extended to 72hrs where it has been shown to have a significant action to conclusively determine its effect on these cell lines.

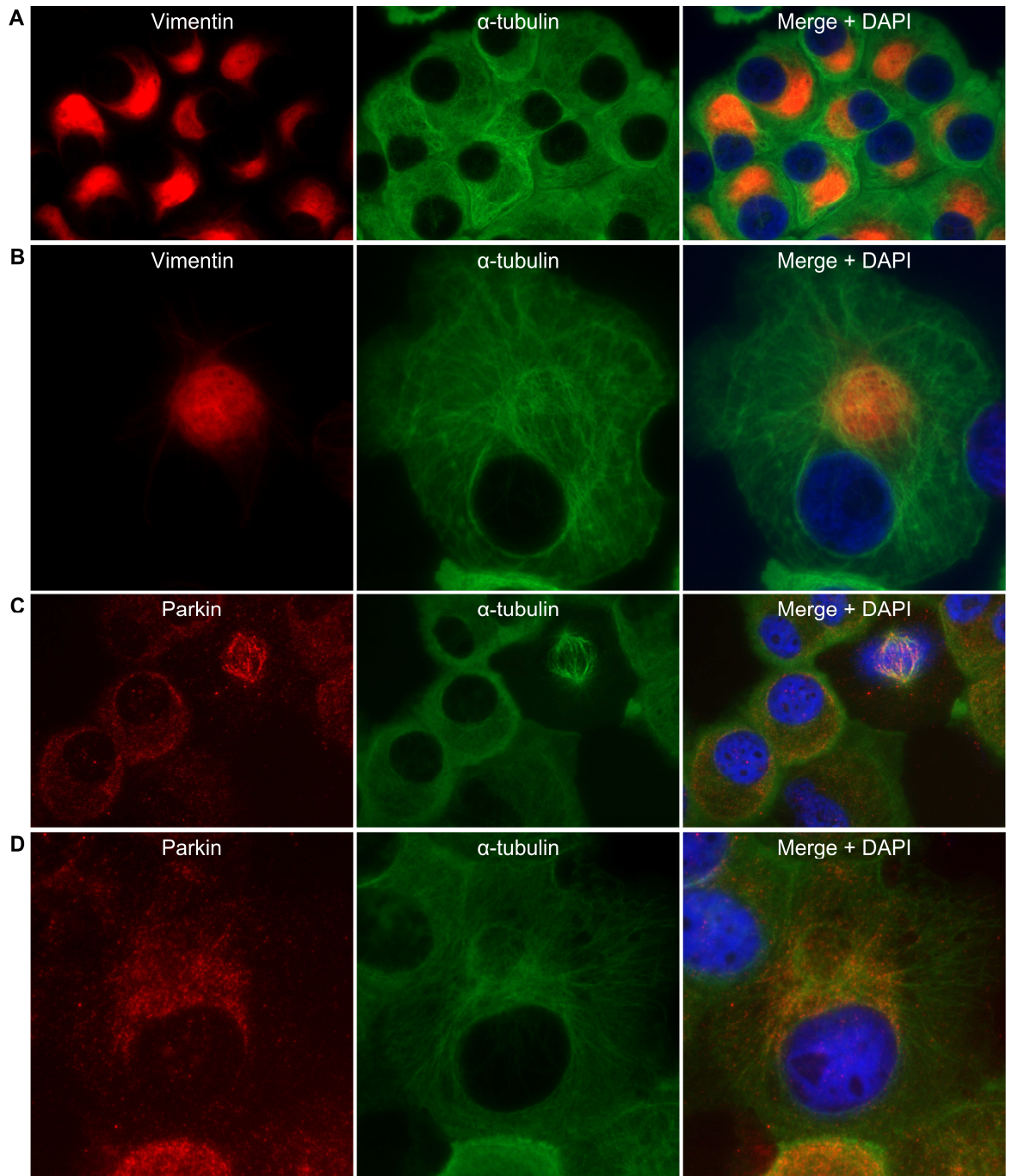


Figure 5-2 Distribution of vimentin and microtubules in HD-MyZ.

Immunocytochemistry of (A) and (B) vimentin (red) and α -tubulin (green) and (C) and (D) Parkin identified by the anti-Parkin clone PRK8 antibody (red) and α -tubulin (green) in HD-MyZ. Right panels represent left and middle panels merged with a DAPI stain to indicate nuclei (blue).

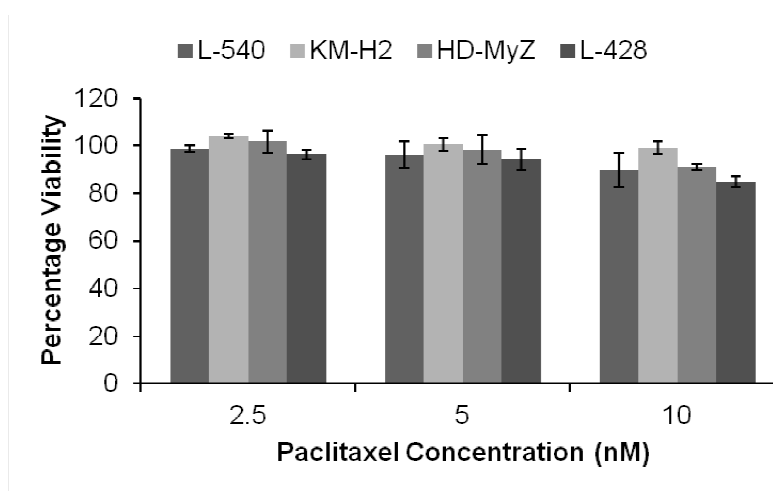


Figure 5-3 HD-MyZ is no more susceptible to Paclitaxel than other HL-derived cell lines.

Cell viability as measured by MTS assay following 24 hr incubation with increasing concentrations of Paclitaxel. Values represent the mean of triplicates and are expressed as the percentage of a DMSO control. Error bars represent standard deviation of the mean.

As noted previously, in HD-MyZ the intermediate filament vimentin displayed a very different expression pattern to the other HL-derived cell lines. The staining intensity was very high; often making it hard to fully distinguish the balled structure it formed using a normal fluorescent microscope. Using confocal microscopy, the large ball of vimentin seen in HD-MyZ cells was revealed to be a tight bundle of filaments rather than merely a large aggregate (Figure 5-4A). On examination by Western blot, there were a number of smaller bands of vimentin in the HD-MyZ cell line, which were not present in any of the other cell lines (Figure 5-4B).

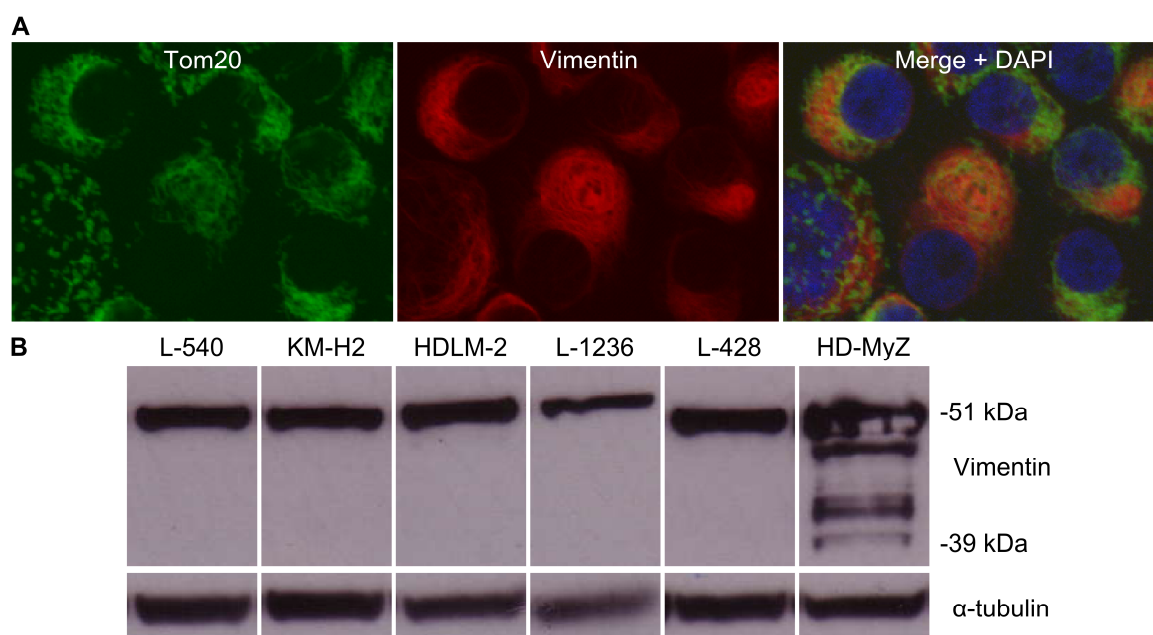


Figure 5-4 Vimentin expression in HD-MyZ.

(A) Confocal micrograph showing immunocytochemistry of Tom20 (green) and vimentin (red). Right panel represents left and middle panels merged with DAPI stain to identify nuclei (blue). (B) Expression of vimentin assessed by western blotting. α -tubulin was included as a loading control.

Vimentin is cleaved at multiple sites by caspases at an early stage of apoptosis (Byun et al., 2001). It was thought that the vimentin cleavage products in Figure 5-4B may indicate the initiation of this process. The HD-MyZ cell line commonly displayed an unusual nuclear morphology in which the chromatin appeared partially condensed (Figure 5-5), in keeping with the early stages of programmed cell death (Rao et al., 1996), although there was no evidence of constitutive caspase-3 cleavage (Figure 4-21C). Another mechanism of cell death has been reported in mammary tissue in which lysosomal enzymes, such as cathepsin B, are released from lysosomes in a STAT3-dependent manner to facilitate cell death (Kreuzaler et al., 2011). It was therefore hypothesised that HD-MyZ maybe initiating cell death pathways yet escaping the end result, perhaps through enhanced prosurvival signalling. Nuclear expression of a number of cathepsins has been reported including cathepsin B (Goulet et al., 2004, Bestvater et al., 2005, Tedelind et al., 2010). Examination by immunocytochemistry, revealed an

exclusively nuclear localisation of cathepsin B in HD-MyZ but also in KM-H2, L-1236 and L-428 (Figure 5-6). As a control, cathepsin B distribution was examined in the EBV-immortalised lymphoblastoid cell line IM-9, in which cathepsin B was stained poorly but in the cytoplasm rather than the nucleus. It was hypothesised that the lysosome membrane permeabilisation method of cell death could also be used to combat proteotoxic stress by allowing proteolytic lysosomal enzymes, such as cathepsins, to freely degrade proteins in the cytoplasm. However, on examination, cathepsin B localisation did not change when HD-MyZ was challenged with proteasome and HDAC6 inhibition to generate a protein handling stress in the cytoplasm (Figure 5-7A). Analysis of cathepsin B expression by western blot revealed the active subunits were only present in HD-MyZ and L-1236, while the pro-form of the enzyme was present in KM-H2 and no forms were detected in L-540 or L-428 (Figure 5-7B). There was no change in cathepsin B expression as detected by western blot following combined proteasome and HDAC6 inhibition in any of the HL-derived cell lines.

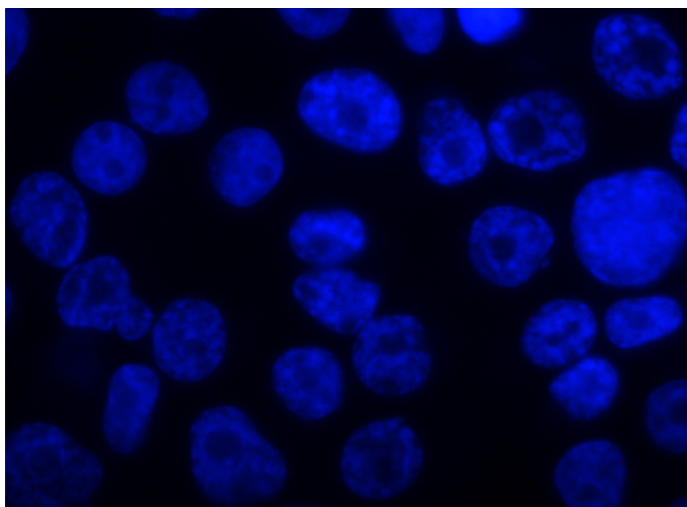


Figure 5-5 Partially condensed chromatin in HD-MyZ.

Fluorescent micrograph of HD-MyZ cells stained with DAPI (blue).

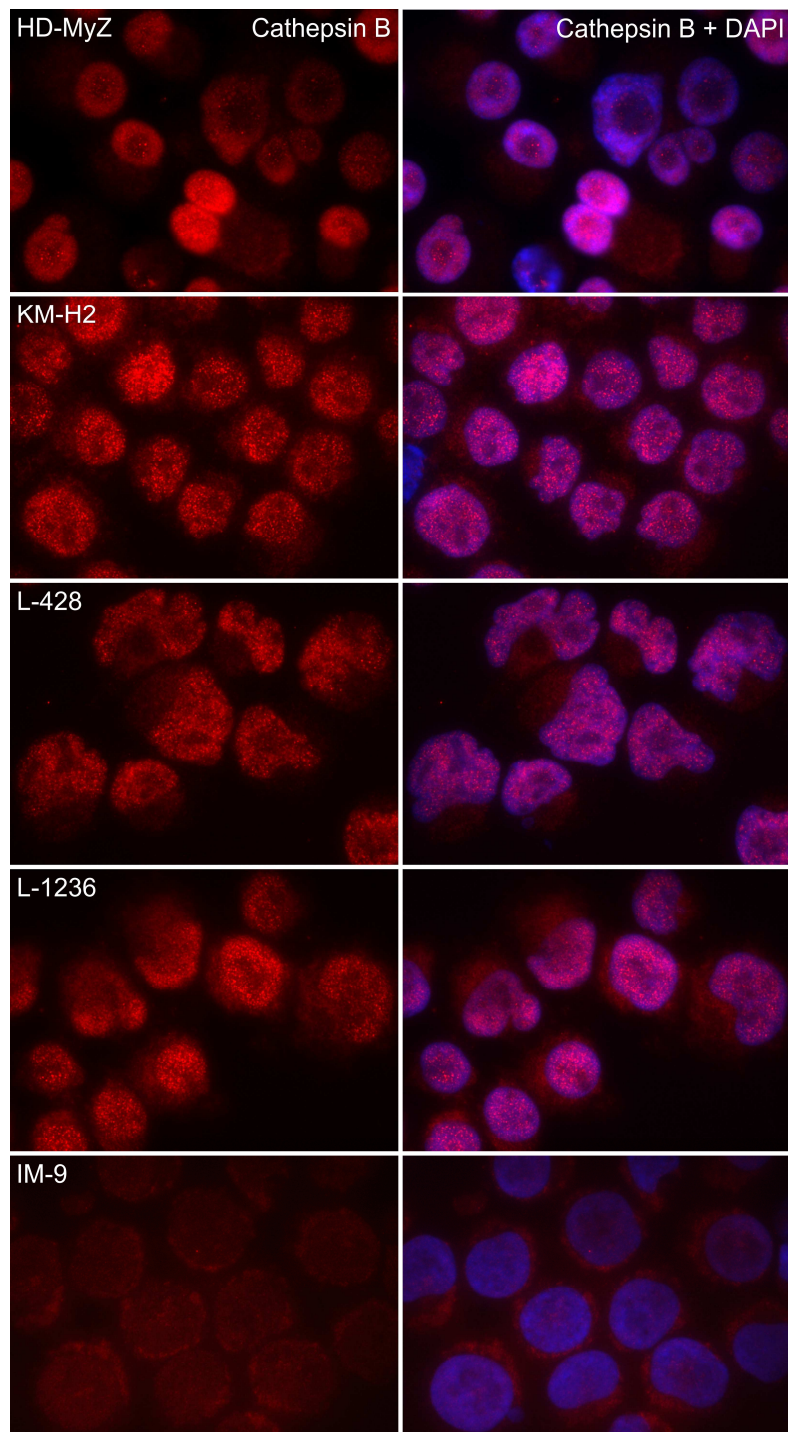


Figure 5-6 Cathepsin B expression in HL-derived cell lines.

Immunocytochemistry of cathepsin B (red) in HL-derived cell lines. Right panel represents left panel merged with DAPI stain to identify nuclei (blue).

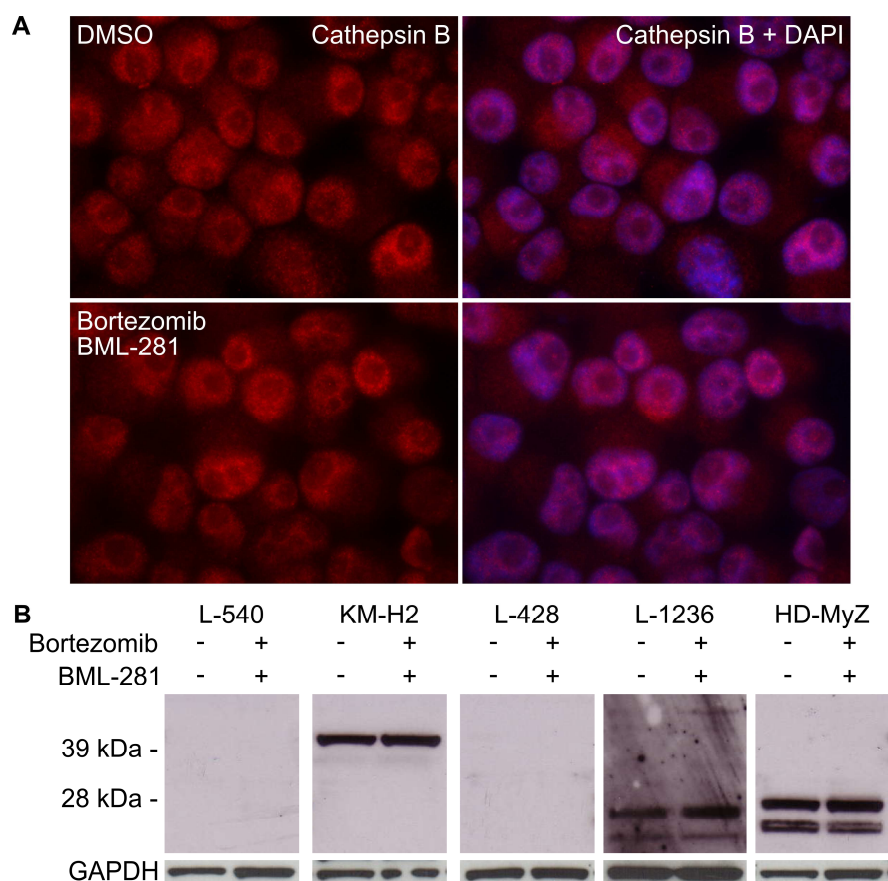


Figure 5-7 Cathepsin B does not change after interference with protein handling pathways.

Expression of cathepsin B as assessed by **(A)** immunocytochemistry in HD-MyZ and **(B)** by western blotting in a selection of HL-derived cell lines. **(A)** Left panel shows cathepsin B (red) expression, right panel represents left panel merged with DAPI stain to identify nuclei (blue). **(B)** + or – indicates the presence or absence of the named drugs. Pro-cathepsin B is detected at approximately 40 kDa and the mature forms of cathepsin B are detected at approximately 25 and 30 kDa. GAPDH was included as a loading control.

To address whether vimentin was a target of cathepsin B activity, we treated HD-MyZ cells with a specific cathepsin B inhibitor (Ca-074Me) and a general cysteine protease inhibitor (E-64); these experiments did not result in a loss of the lower vimentin bands seen by western blot, rather the number of these bands appeared to increase from previous experiments (Figure 5-8A). This led us to question the lysis buffer. At the outset of these experiments regarding vimentin expression, a new batch of protease inhibitors (cOmplete ULTRA

tablets, Roche, 05892791001) had been purchased to replace old stock (Pierce Protease inhibitor tablets, Thermo Scientific, 88660). While these went into solution at room temperature they appeared to precipitate at low temperatures (i.e. when lysis buffer was kept on ice or in the fridge at 4°C). Originally this precipitate had been attributed to the additional SDS added to the standard RIPA lysate to aid in the solubilisation of the large vimentin ball observed in HD-MyZ. However, when a fresh lysate was prepared using the Pierce protease inhibitors, the lower band of vimentin observed in HD-MyZ was no longer present; despite the presence of SDS (Figure 5-8B). In retrospect, the different cleavage patterns observed in lysates prepared using the new protease inhibitors should have indicated a problem in lysate preparation, however, originally it was naively attributed to inconsistencies in gel migration and membrane transfer.

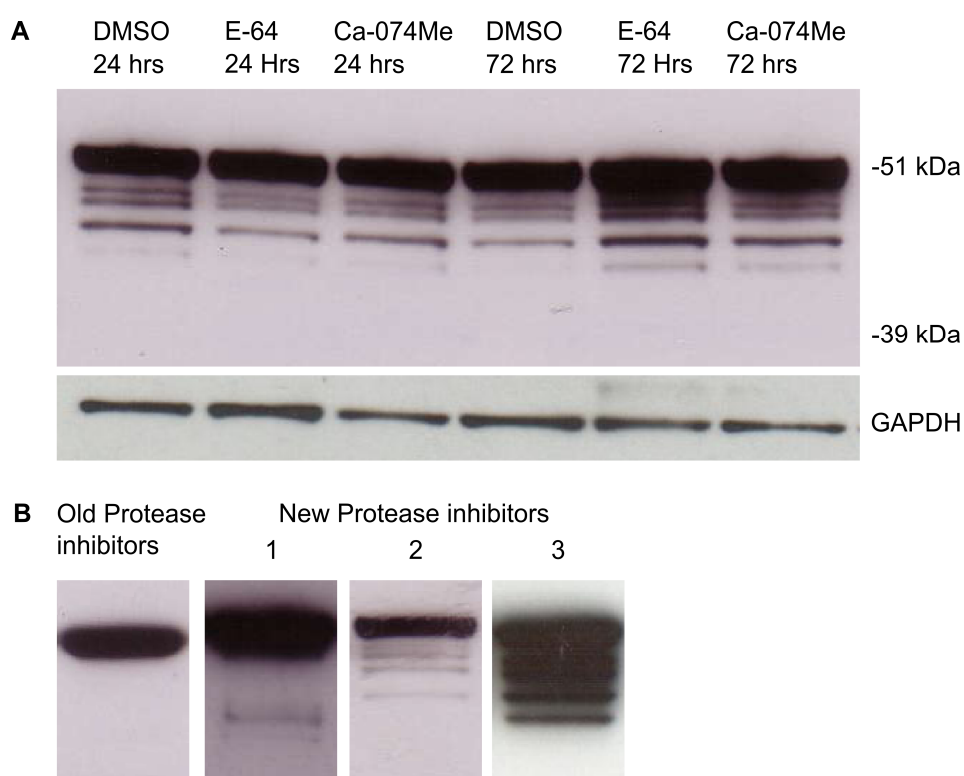


Figure 5-8 Discrepancies in vimentin cleavage products.

Western blot analysis of vimentin expression. **(A)** HD-MyZ cells were treated with E-64 or Ca-074Me for 24 or 72 hrs. GAPDH was included as a loading control. **(B)** Comparison of vimentin expression in HD-MyZ from lysates generated with old and new protease inhibitors.

5.3.2 Withaferin A treatment

The HD-MyZ cell line had so far remained resistant to every drug treatment tested. With this in mind an alternative drug was sought. Withaferin A (WFA) posed an attractive candidate as, although it acts as a proteasome inhibitor in a manner similar to Bortezomib (i.e. specifically targets the chymotrypsin-like activity of the proteasome), it also possesses other cellular targets such as the Akt and NF- κ -B pro-survival signalling pathways (Vanden Berghe et al., 2012). Another target is vimentin; WFA has been found to induce cell death through vimentin cleavage in a caspase-dependent manner (Lahat et al., 2010). Abrogation of this anti-vimentin activity alleviated the effects of WFA on its other targets, suggesting a pivotal role for vimentin cleavage in its mode of action (Lahat et al., 2010, Bargagna-Mohan et al., 2007, Bargagna-Mohan et al., 2010).

It was proposed that HD-MyZ, which expressed high levels of vimentin, may be susceptible to WFA treatment. This did not prove to be the case. The other HL-derived cell lines tested (L-540, KM-H2 and L-428) displayed concentration-dependent decreases in viability following 24 hr WFA treatment as measured by MTS assay, with L-540 highly sensitive (Figure 5-9A). HD-MyZ, however, remained resistant to this treatment. Although, initially the decrease in viability observed was thought to be greater than that achieved by Bortezomib treatment, on incubating these cell lines with an equivalent concentration of Bortezomib (5 μ M, previously used Bortezomib concentrations had been nM), similar effects were seen (Figure 5-9B). An increase in MTS read-out was observed in KM-H2 cells in response to low concentrations of WFA, similar to that observed following 5nM Bortezomib treatment. As mentioned previously this was believed to represent G2/M cell cycle arrest. To confirm this KM-H2 and HD-MyZ cells were subject to cell cycle analysis by DNA content (as determined by PI staining) following incubation with various concentrations of WFA for 24 hrs. Both cell lines displayed an increased percentage of cells in the S phase of cell cycle and an increase in G2/M cells was observed in KM-H2 following treatment with 1 μ M

WFA (Figure 5-9C). Following incubation with 5 μM WFA, an increase in the number of cells in G1 was observed in HD-MyZ but not KM-H2 cells.

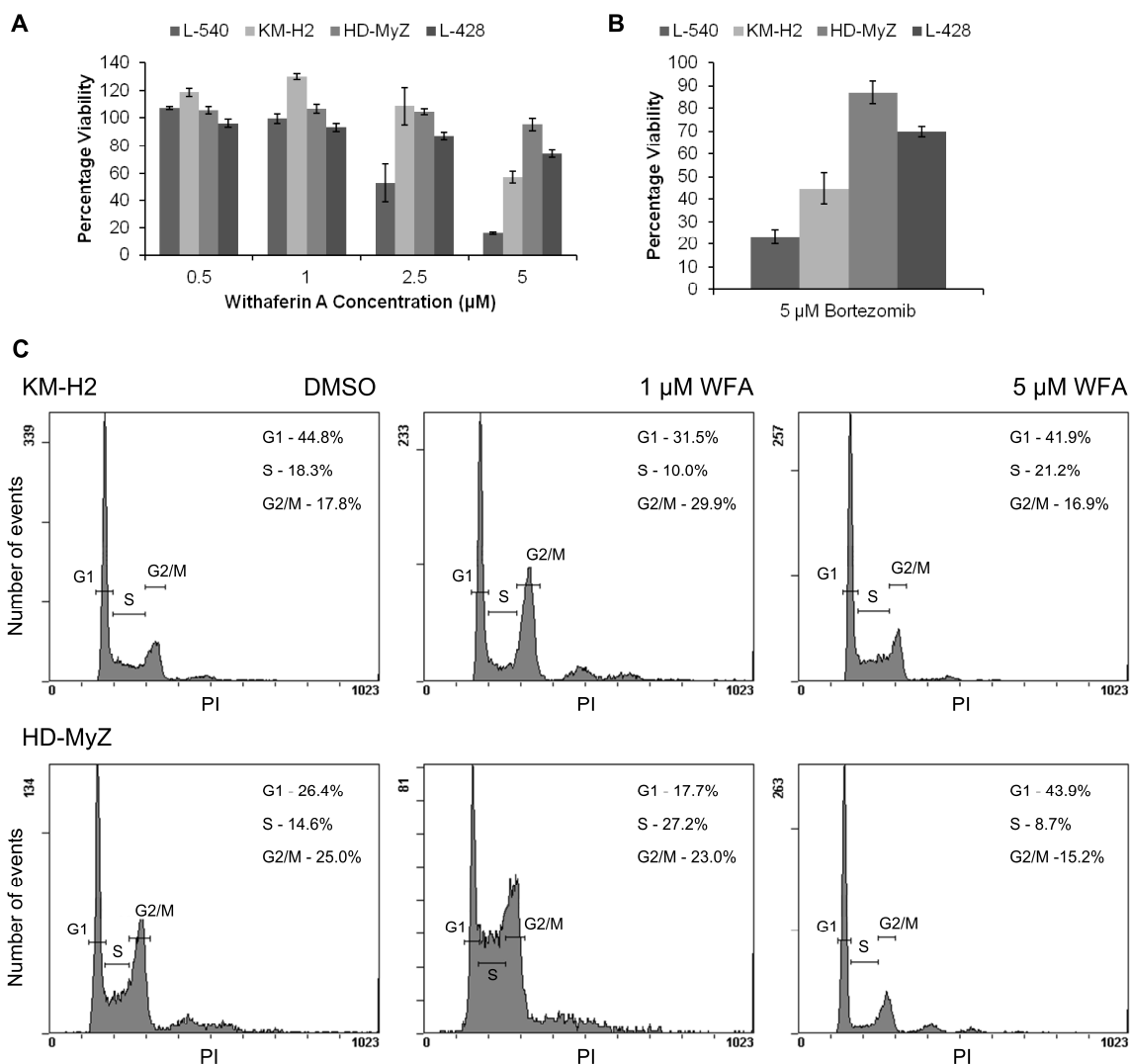


Figure 5-9 Effects of WFA on cell viability and cell cycle status.

Cell viability as measured by MTS assay following 24 hr incubation with (A) increasing concentrations of Withaferin A and (B) 5 μM Bortezomib. Values represent the mean of 3 separate experiments. Error bars represent standard error. (C) Cell cycle analysis by DNA content (propidium iodide staining) following 24 hr incubation with 1 or 5 μM WFA.

5.3.3 The effect of WFA on vimentin

The fact that HD-MyZ was resistant to WFA despite possessing high levels of its principle target was vexing. To determine whether WFA treatment was affecting vimentin, its expression was examined by western blot. Surprisingly, while the cell lines that were sensitive to WFA treatment displayed no changes in vimentin expression, HD-MyZ displayed vimentin cleavage at the highest concentration of 5 μM WFA (Figure 5-10A). This was reproducible using fresh lysates with no evidence of protease inhibitor precipitation. As the action of WFA against vimentin is caspase-dependent (Lahat et al., 2010), HD-MyZ was treated with 5 μM WFA alone and in combination with 20 μM Pan-Caspase inhibitor. This resulted in the loss of the prominent cleavage products detected between the 39 and 51 kDa size markers (Figure 5-10B). Instead a larger cleavage product just below the original vimentin band was observed, suggesting an initial caspase-independent cleavage event.

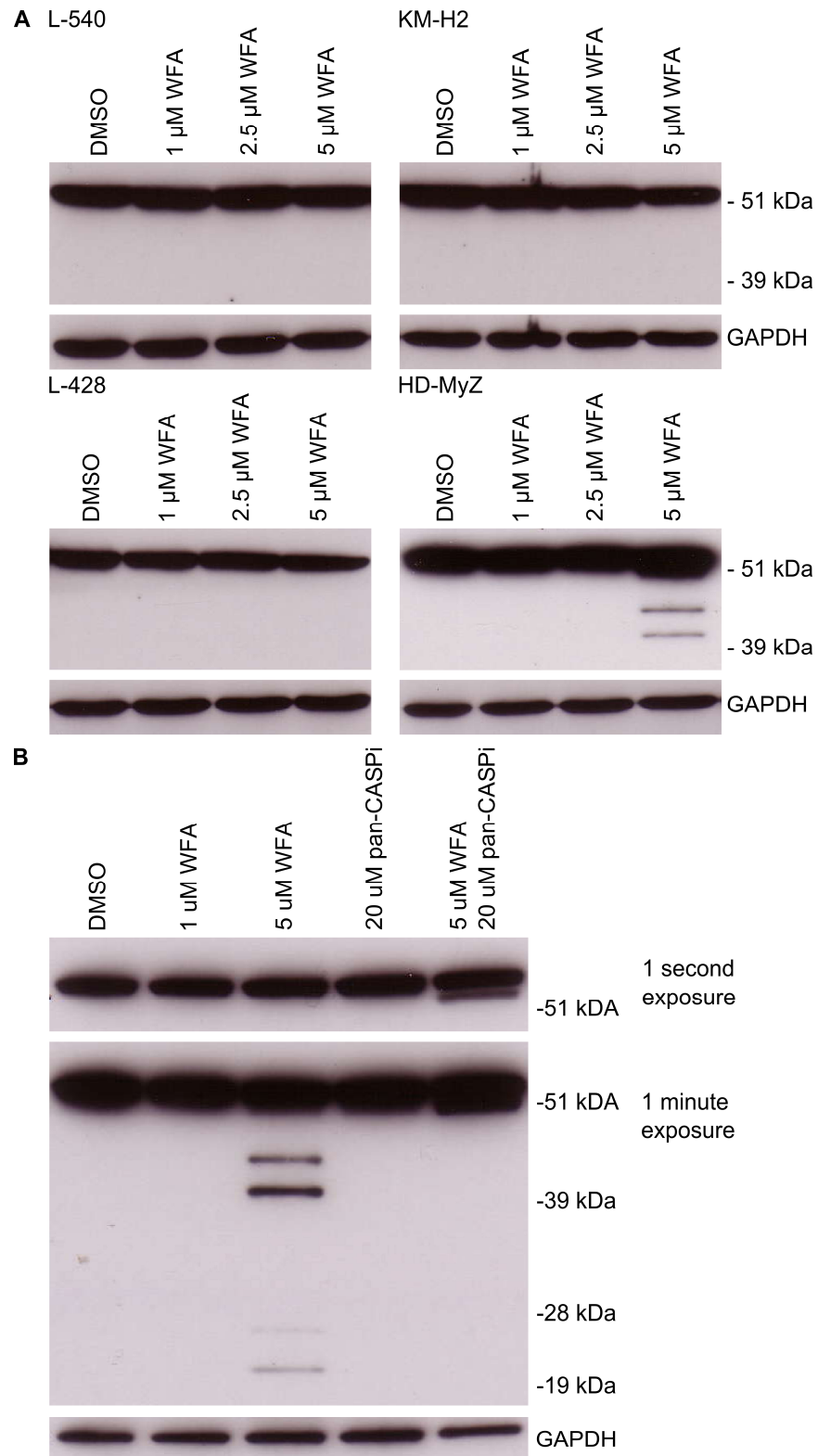


Figure 5-10 WFA targets vimentin in HD-MyZ but not other HL-derived cell lines.

(A) HL-derived cell lines were treated with increasing concentrations of WFA for 16 hours and vimentin expression was examined by western blotting. (B) HD-MyZ was treated with WFA alone and in combination with a pan-caspase inhibitor (R&D Systems, FMK001) and vimentin expression assessed by western blotting. In both (A) and (B) GAPDH was included as a loading control.

When examined by immunocytochemistry, the most dramatic changes in vimentin distribution were observed in HD-MyZ. Following treatment with 1 or 2.5 μM WFA an enrichment of mitotic cells was observed and in these cells the vimentin bundle had been broken up to form multiple large irregular-shaped aggregates (Figure 5-11). These were less apparent in HD-MyZ cells treated with 5 μM WFA, although the occasional interphase cell displayed multiple small vimentin aggregates (Figure 5-11, lower panels). Generally, interphase cells displayed no change from the bundle distribution of vimentin regardless of the WFA concentration. L-540, KM-H2 and L-428 were sensitive to WFA treatment, as suggested by MTS assay (Figure 5-9A). Consequently, incubation with 5 μM WFA resulted in unusable cytopins. No changes were observed in vimentin distribution in L-540 following 1 or 2.5 μM WFA (Figure 5-12). In KM-H2 there was an enrichment of mitotic cells at 1 μM WFA and, despite many fractured nuclei at 2.5 μM WFA, the vimentin distribution generally retained its polarised network appearance (Figure 5-12). In L-428, an enrichment of mitotic cells was also observed at 1 μM WFA, although interphase cells retained an MTOC-polarised vimentin distribution (Figure 5-13). This distribution was also retained following 2.5 μM WFA, however, there were many fractured nuclei and the occasional cell displayed a disruption of the vimentin network in favour of multiple small vimentin puncta (Figure 5-13, lower panels).

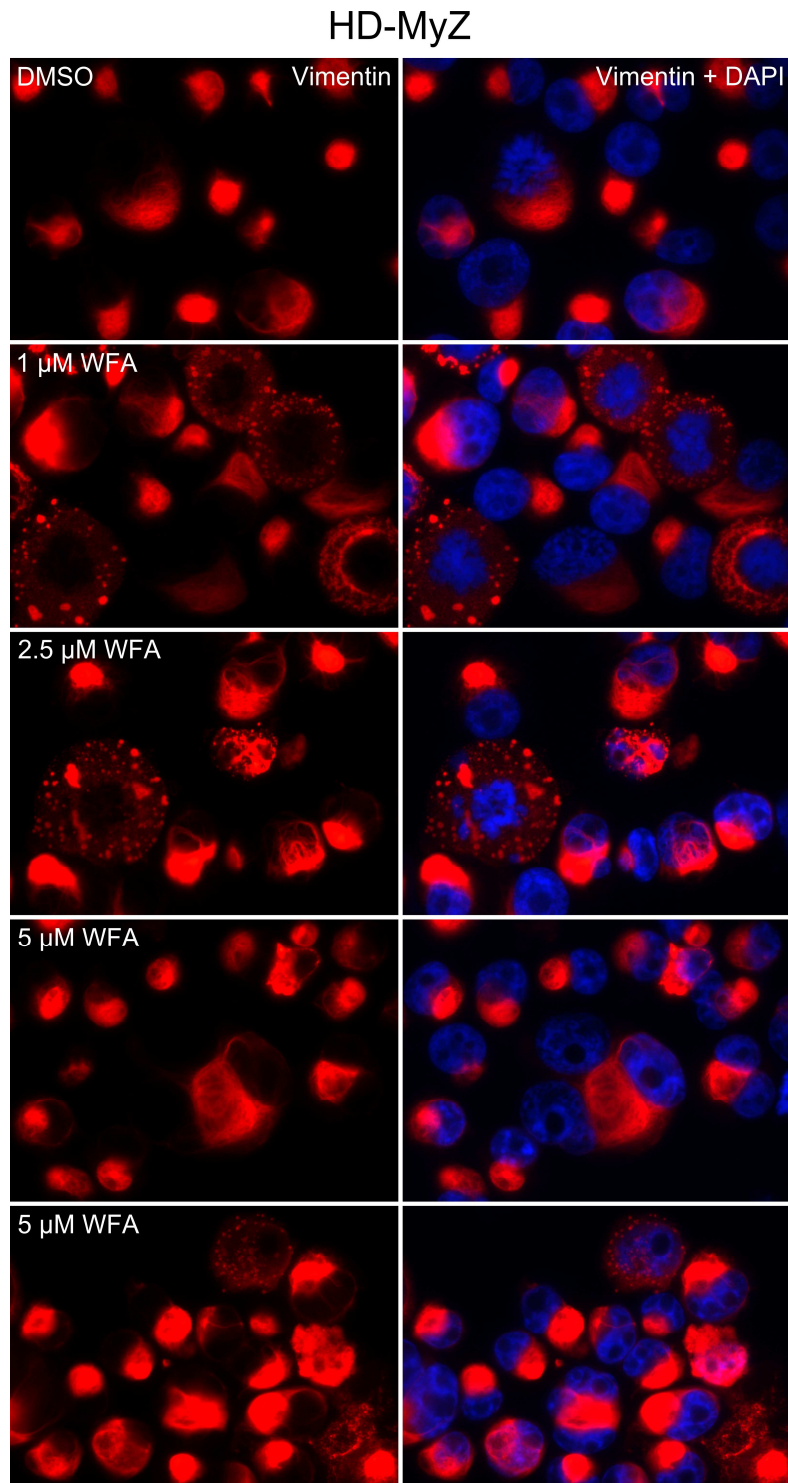


Figure 5-11 Effect of WFA on vimentin expression in HD-MyZ.

Immunocytochemistry of vimentin (red) in HD-MyZ following incubation for 16 hours with increasing concentrations of WFA. Right panel represents left panel merged with DAPI stain to identify nuclei (blue).

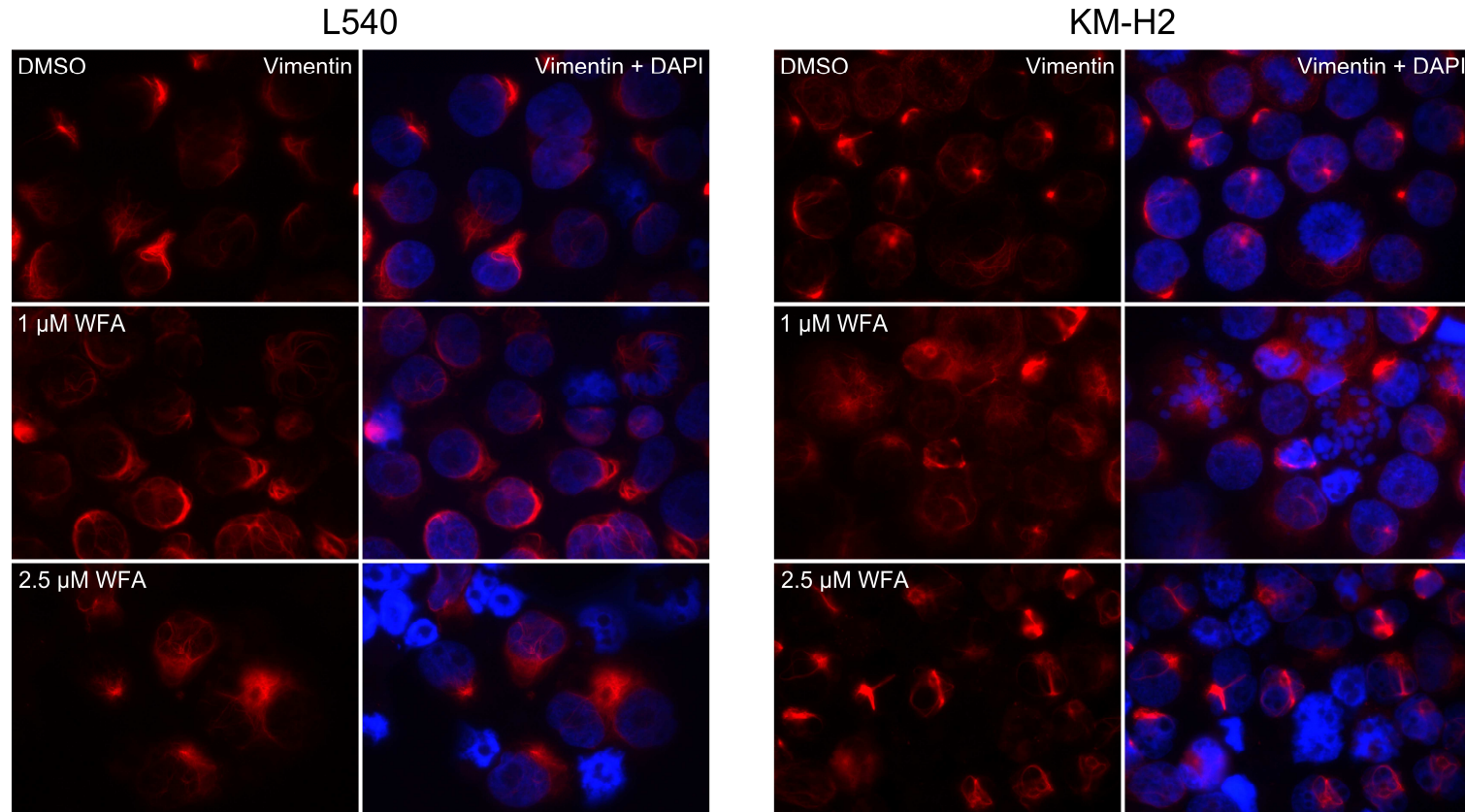


Figure 5-12 Effect of WFA on vimentin expression in L-540 and KM-H2.

Immunocytochemistry of vimentin (red) in L-540 and KM-H2 following incubation for 16 hours with increasing concentrations of WFA. Cells were also treated with 5 μM WFA, however poor cell viability prevented examination of these cells. Right panels represent left panels merged with a DAPI stain to identify nuclei (blue).

L-428

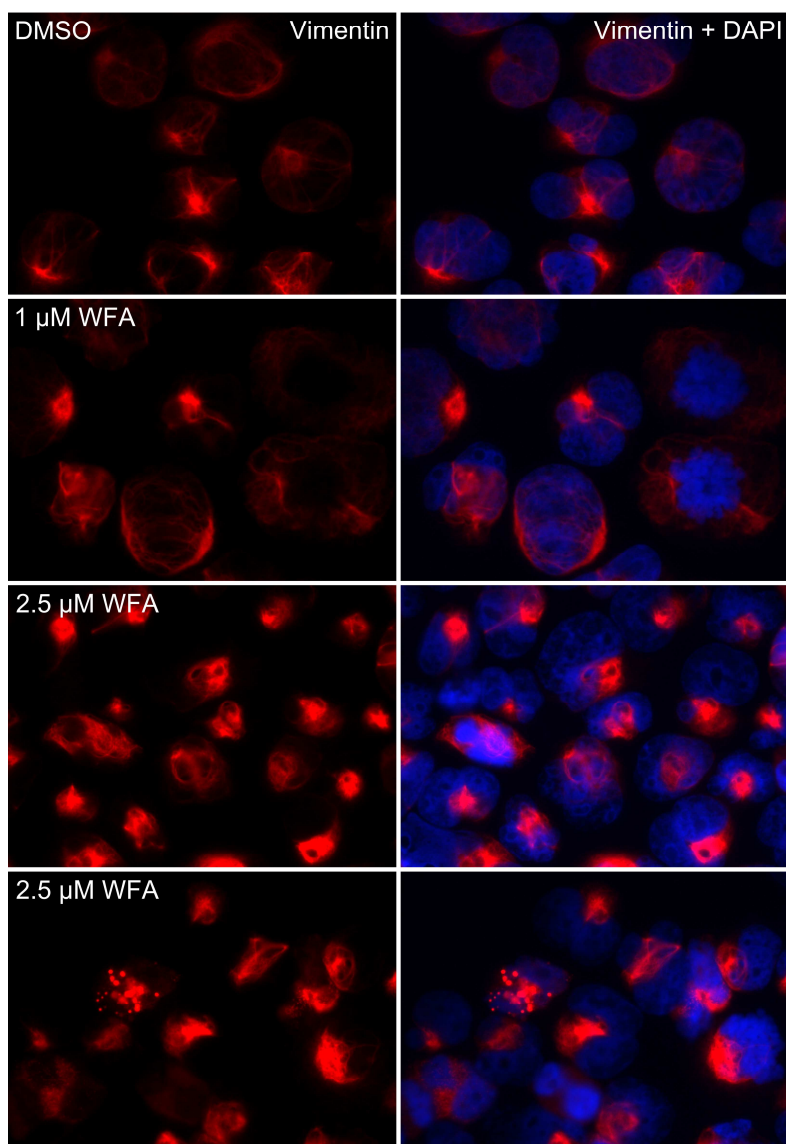


Figure 5-13 Effect of WFA on vimentin expression in L-428.

Immunocytochemistry of vimentin (red) in L-428 following incubation for 16 hours with increasing concentrations of WFA. Cells were also treated with 5 μM WFA, however poor cell viability prevented examination of these cells. Right panels represent left panels merged with a DAPI stain to identify nuclei (blue).

5.3.4 The effect of WFA on p62 distribution

Despite causing loss of viability, WFA treatment did not appear to greatly affect vimentin in L-540, KM-H2 or L-428. Another WFA target of interest to us was the proteasome (Yang et al., 2007); therefore the effect of WFA treatment on protein build up was examined, as in the previous chapters, using p62 to monitor protein accumulation and K48-linked polyubiquitin to assess proteasome activity. Similar to Bortezomib, WFA treatment at 1 or 2.5 μM resulted in formation of multiple aggregates of p62 in L-540, KM-H2 and L-428, to a lesser extent, but not in HD-MyZ (Figure 5-14, 5-15). Unlike Bortezomib, WFA treatment did not result in a loss of diffuse p62 staining in favour of large aggregates, but multiple p62 aggregates were formed while diffuse staining was maintained in L-540, KM-H2 and L-428. Treatment of HD-MyZ with 5 μM WFA also resulted in p62 aggregation (Figure 5-16A, upper panels). While this was not seen in Chapter 4 following proteasome inhibition of HD-MyZ with 5 nM Bortezomib, treatment with 5 μM Bortezomib resulted in a similar accumulation of p62 (Figure 5-16A, lower panels). In both scenarios the p62 accumulation co-localised with the large vimentin bundle. To confirm proteasome inhibition by WFA, K48-linked polyubiquitin expression was examined following treatment with increasing concentrations of WFA (Figure 5-16B). Levels of K48-linked polyubiquitin increased in L-540, KM-H2 and L-428 following incubation with 5 μM WFA, and at 2.5 μM WFA in L-540. No increase was observed at lower concentrations in KM-H2 or L-428 and no increase was observed in HD-MyZ at any concentration, despite apparent p62 accumulation at 5 μM WFA. This would suggest that the method of action of WFA against HD-MyZ differs from that against the other cell lines.

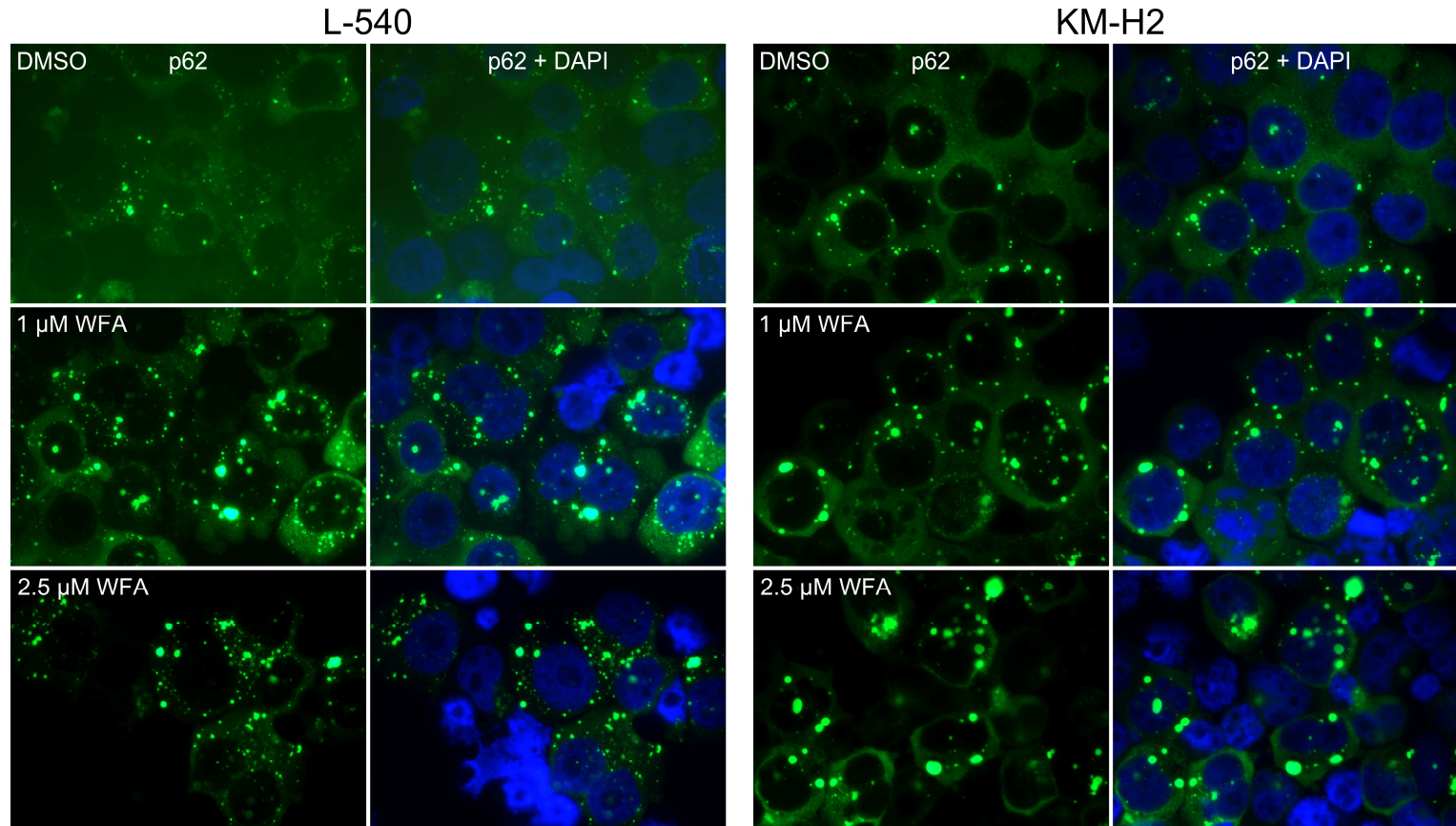


Figure 5-14 Effect of WFA on p62 expression in L-540 and KM-H2.

Immunocytochemistry of p62 (green) in L-540 and KM-H2 following incubation for 16 hours with increasing concentrations of WFA. Cells were also treated with 5 μM WFA, however poor cell viability prevented examination of these cells. Right panels represent left panels merged with a DAPI stain to identify nuclei (blue).

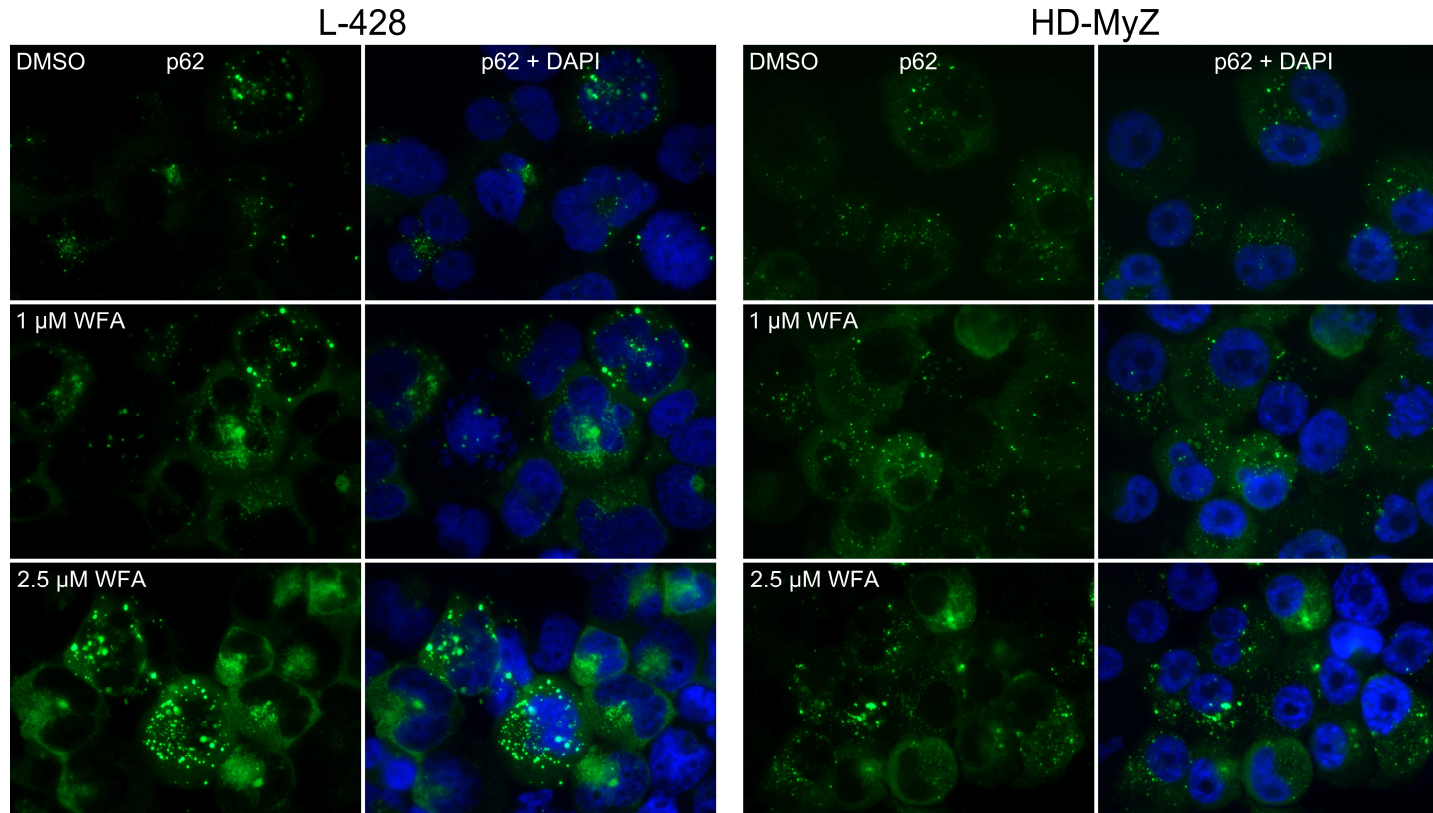


Figure 5-15 Effect of WFA on p62 expression in L-428 and HD-MyZ.

Immunocytochemistry of p62 (green) in L-428 and HD-MyZ following incubation for 16 hours with increasing concentrations of WFA. Cells were also treated with 5 μM WFA, however poor cell viability in prevented examination of these cells in L-428. The HD-MyZ cells are further examined in the following figure. Right panels represent left panels merged with a DAPI stain to identify nuclei (blue).

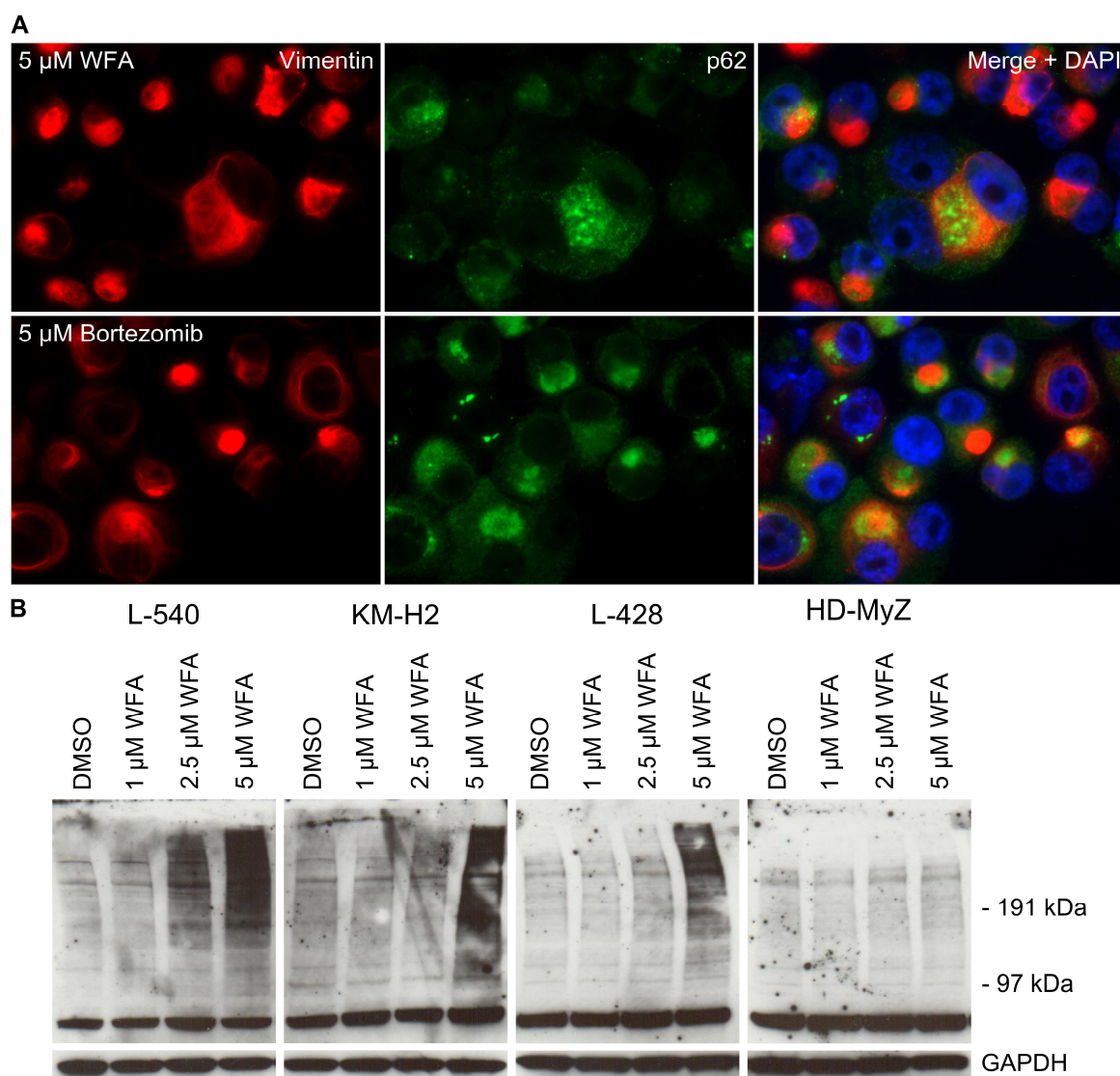


Figure 5-16 Effect of WFA on p62 in HD-MyZ and on K48-linked polyubiquitin levels.

(A) Immunocytochemistry of vimentin (red) and p62 (green) in HD-MyZ following incubation with 5 μ M WFA or 5 μ M Bortezomib for 16 hours. Right panels represent left and middle panels merged with a DAPI stain to identify nuclei (blue). (B) Expression of K48-linked polyubiquitin as assessed by western blotting following 16 hr incubation with increasing concentrations of WFA. GAPDH was included as a loading control.

5.4 Discussion

The HD-MyZ cell line is thought to have a non-lymphoid origin, in contrast to the other HL-derived cell lines, as it lacks HL-associated CD30 and CD15 antigens, immunoglobulin and T cell receptor gene rearrangements and expresses the macrophage-associated CD68 and myeloid-associated CD13 antigens (Bargou et al., 1993, Kuppers and Re, 2007). Despite attempts to target specific phenotypic differences of this cell lines, the microtubule-localised Parkin and high levels of vimentin expression, HD-MyZ remained resistant to all therapies tested and again displayed different responses to HL-derived cell lines L-540, KM-H2 and L-428 when challenged with the vimentin targeting inhibitor Withaferin A.

Parkin initially appeared to co-localise with the mitochondrial population, however, as with KM-H2 (section 4.3.2, Figure 4-4) the mitochondria all retained MitoTracker™ dye and were therefore considered to be viable. Subsequently Parkin was observed on the mitotic spindle and found to form multiple puncta along microtubules as has been previously reported (Ren et al., 2003). This may reflect a role for Parkin in the misfolded protein response/ ubiquitin proteasome system (UPS). Microtubules are important in stabilising and maintaining the morphology of the endoplasmic reticulum (ER) and are found in close association with this organelle (Cole and Lippincott-Schwartz, 1995). Microtubule-associated Parkin would be ideally placed to deal with misfolded proteins as they leave the ER (Yang et al., 2005). These ubiquitinated proteins would then be degraded by the proteasome. In the event that the ubiquitin proteasome system were to become saturated, misfolded proteins would be transported to the MTOC where they would form an aggresome and ultimately be degraded by the autophagy pathway. This transport is a microtubule-dependent process, so the stabilising effects of Parkin on microtubules may be beneficial to this process. Parkin also has a role in aggresome formation as an ubiquitin E3 ligase and as a bystander effect of impaired proteasome function can be deposited at the MTOC as part of the aggresome (Zhao et al., 2003). It is involved in the targeting of DJ-1 to the aggresome in an HDAC6-dependent manner (Olzmann et al., 2007). The addition

of K63-linked polyubiquitin chains to the misfolded DJ-1 protein allows its interaction with HDAC6 and subsequent dynein-mediated transport to the MTOC for aggresome formation.

Parkin was also observed to stain a bridge structure between two nuclei in the end stages of mitosis. This structure was consistent with the location of polar microtubules; staining was absent from the midbody possibly because of antibody exclusion at this site due to protein density (Hu et al., 2012). As Parkin appeared to be binding to mitotic spindle it may be transiently trafficking to this site as the spindle differentiated into the midbody-associated polar microtubules or it may be actively involved in this process. Parkin has previously been associated with mitotic progression as it negatively regulates the expression of a kinesin family motor protein, Eg5, crucial for spindle assembly (Liu et al., 2008). Loss of Parkin also resulted in spindle misorientation and multipolarity and an increased number of multinucleate cells in a model of pancreatic cancer (Sun et al., 2013). The ubiquitin proteasome system and autophagy pathway are both involved at various stages during cell division so it is also possible Parkin appeared at this site in its role as an E3 ubiquitin ligase involved in turnover of cell cycle related proteins. Furthermore, the expression of Parkin on the mitotic spindle places it in a perfect position to deal with protein turnover associated with mitotic exit. Waste protein is thought to be deposited at the midbody and can then be pinched off and ejected into the extracellular environment as the cells divide or be degraded by autophagy (Dubreuil et al., 2007, Pohl and Jentsch, 2009).

The distribution of vimentin was of particular interest in HD-MyZ as it appeared clustered in a large perinuclear filamentous bundle. This has been observed before in several scenarios in which abnormal interactions between microtubules and intermediate filaments arise. These include cells derived from skin biopsies of patients suffering from the neurodegenerative disorder giant axonal neuropathy (GAN), which is due to mutation in gigaxonin, an E3 ubiquitin ligase adaptor protein (Cleveland et al., 2009, Bomont and Koenig, 2003). Gigaxonin is

thought to link vimentin, microtubules and vesicles and is responsible for the organisation of the vimentin network. In GAN cells the expression of phenotypically similar bundles of vimentin at or next to the MTOC was thought to be due to a failure of vimentin to interact appropriately with the microtubule network. Comparable perinuclear balls of vimentin have also been detected in some virally transformed cells and in a subtype of acute myeloid leukaemia (Ball and Singer, 1981, Dellagi et al., 1985). In both cases aberrant microtubule-vimentin interactions were proposed to be responsible. Given that intermediate filaments such as vimentin play a role in protein metabolism via ubiquitin organization and autophagosome trafficking (Mayer et al., 1989), the aberrant vimentin organization detected in HD-MyZ cells may impact their use of autophagy as seen in sections 4.3.1 and 4.3.4. Expression levels of vimentin are also predictive of differentiation phenotypes, as more differentiated myeloid cells express greater levels of vimentin (Dellagi et al., 1985). More differentiated forms of mantle cell lymphoma have been found to be more resistant to proteasome inhibition (Perez-Galan et al., 2011). Given the high levels of vimentin expression in HD-MyZ and its resistance to Bortezomib, this may be of relevance to HL. Heterogeneous levels of vimentin positivity in HL biopsy material have been reported, with up to 40% of samples being described as vimentin positive (Angel et al., 1992). Although, as a single agent, Bortezomib showed poor activity against HL (Younes et al., 2006, Strauss et al., 2006, Blum et al., 2007), these vimentin-positive cases may be particularly resistant to this drug.

The apparent nuclear localisation of cathepsin B identified by immunofluorescence in HL-derived cell lines was an intriguing finding. There have been a number of reports of nuclear cathepsin B (Bestvater et al., 2005, Tedelind et al., 2010), which have been attributed to an N-terminal truncate of the enzyme that appears to have lost its ER-sorting signal. Although by western blot the antibody used (anti-cathepsin B, Abcam, ab33538) appeared to detect the pro-form and active forms of the enzyme but not the reported truncate, as

it was a polyclonal antibody it would appear it may favour this shortened nuclear form when used for immunocytochemistry.

Cathepsin B is a diverse proteolytic enzyme, which aside from its obvious role in lysosomal protein degradation, can also be secreted to degrade components of the extracellular matrix and promote tumour invasiveness and progression (Tu et al., 2008, Gocheva et al., 2006). There have been a number of reports of nuclear expression of cathepsins, including cathepsin B in thyroid carcinoma cells (Tedelind et al., 2010). Here a proteolytically active, N-terminal truncate of cathepsin B was found localised to the nucleus. Instead of displaying a general protease activity when purified with nuclear extracts, cathepsin B selectively cleaved histone H1 while other nuclear proteins remained undegraded. This would suggest a targeted activity for cathepsin B in the nucleus, perhaps in the relaxation of chromatin to allow access of transcription factors to DNA. Another cathepsin, cathepsin L, has been implicated in similar epigenetic modifications. During the differentiation of embryonic stem cells, cathepsin L was found to cleave histone H3, changing the epigenetic signature of the differentiated cells (Duncan et al., 2008). Thus nuclear cathepsins may act as transcriptional regulators by modifying the histone architecture. A further role for cathepsin L has been identified in cell cycle progression. During the G1-S transition, cathepsin L localised to the nucleus where it was responsible for the proteolytic processing of the CCAAT-displacement protein/Cut homeobox (CDP/Cux) transcription factor (Goulet et al., 2004). This resulted in an N-terminal truncated form of the transcription factor that had different DNA binding and transcriptional activities. It is likely that this form of transcriptional regulation is not unique to cathepsin L but may be a general feature of this family of cysteine proteases. The nuclear fraction of cathepsin B observed in HL-derived cell lines may therefore be active in transcriptional regulation.

The abundance of vimentin in HD-MyZ led us to test effects of the vimentin-targeting compound Withaferin A (WFA) against this cell line and against L-540, KM-H2 and L-428. While WFA caused a drop in viability for HL-derived cell lines,

L-540, KM-H2 and L-428, HD-MyZ proved resistant to this compound. L-540 was particularly sensitive to WFA, seemingly more so than to Bortezomib. Bortezomib experiments in the previous chapters had been performed at nanomolar concentrations so were not directly comparable to WFA concentrations. Incubation with 5 μM Bortezomib resulted in a similar decrease in viability in L-540, while KM-H2 and L-428 displayed decreased viability compared to 5 μM WFA. Low concentrations of WFA resulted in increased read-out of MTS assay compared to a DMSO control in KM-H2 cells. Similar to Bortezomib treatment this was hypothesised to be due to G2/M arrest caused by the anti-proteasome activity of WFA (Yang et al., 2007). This was confirmed by cell cycle analysis by DNA content as an increase in cells in G2/M stages of cell cycle were observed following incubation with 1 μM but not 5 μM WFA. A similar increase was observed in HD-MyZ cells at 1 μM WFA, however an increase in the number of cells in S phase was also observed. This may suggest a general increase in cycling cells rather than a G2/M arrest as MTS assay read-outs did not increase in this cell line. The increase in cells at G2/M in KM-H2 cells was confirmed by an enrichment of mitotic cells when examined by immunofluorescence, although this was also apparent in L-428 and HD-MyZ cells. This enrichment of mitotic cells in KM-H2 and L-428 may be due to proteasome inhibition while in HD-MyZ it may be due to the disruption of the vimentin network (both discussed in the following paragraph), which has been implicated in chromosome arrangement during mitosis.

WFA appeared to act in very different ways in HL-derived cell lines L-540, KM-H2 and L-428 compared to HD-MyZ. In the three afore mentioned HL-derived cell lines WFA resulted in decreased viability, but did not induce vimentin cleavage and appeared to have no effect on vimentin distribution. While there was some evidence of vimentin cleavage in L-428 at 2.5 μM concentrations it was very rare. This was believed to be associated with apoptosis and was consistent with the increased number of shattered nuclei (Byun et al., 2001). Instead, incubation with WFA resulted in p62 aggregation and increased levels of K48-linked polyubiquitin at higher concentrations of WFA (5 μM). These data were

consistent with proteasome inhibition as observed following incubation with Bortezomib in Chapters 3 and 4. The decreased viability observed in L-540, KM-H2 and L-428 may not be exclusively related to proteasome inhibition as WFA also acts against NF κ B signalling. By binding to the regulatory IKK γ subunit it obstructs its association with IKK β (Kaileh et al., 2007, Grover et al., 2010). This inhibits the phosphorylation and degradation of the inhibitor of NF κ B, I κ B, and prevents the release of NF κ B (Kaileh et al., 2007). This may be of more relevance to the L-540, KM-H2 and L-428 cell lines as they exhibit higher levels of NF κ B activity than the HD-MyZ cell line.

In contrast, HD-MyZ did not display reduced viability or an accumulation of K48-linked polyubiquitin and, although there did appear to be a concentration-dependent increase in p62 aggregates, p62 accumulation was not as marked as in the other cell lines. These data would suggest limited WFA activity against the proteasome in HD-MyZ. Following incubation with 5 μ M WFA multiple cleavage products of vimentin were observed. These cleavage products were lost following treatment with a pan-caspase inhibitor. The cleavage products were therefore consistent with those created during caspase-mediated induction of apoptosis (Lahat et al., 2010). The prominent cleavage product observed just below the uncleaved vimentin band that was not lost following incubation with the pan-caspase inhibitor is likely an artefact of incomplete caspase inhibition. In HeLa cells, staurosporine-induced apoptosis resulted in caspase-dependent cleavage of vimentin (Byun et al., 2001). This resulted in multiple cleavage products of varying molecular weights as observed in WFA treated HD-MyZ cells. The loss of caspase-mediated cleavage products was seen to be a concentration dependent effect of the pan-caspase inhibitor. Low doses (10 μ M and 50 μ M) comparable with the concentration used here (20 μ M) were sufficient to prevent lower molecular weight cleavage products. A higher concentration (250 μ M) was found to be required to prevent the formation of the higher molecular weight cleavage products yet even then they are not completely absent. As western blots of vimentin examining vimentin cleavage are often over-exposed to detect faint cleavage products, the uncleaved form of vimentin is often saturated. This

makes comparison with the cleavage product observed here problematic as this product appears to be larger than those observed in other studies (Byun et al., 2001, Lahat et al., 2010). This does not mean it is not present in other studies, merely that it is not observed due to the prominent uncleaved form of vimentin masking the band. Although caspase-cleavage is the most likely explanation for this product, a caspase-independent cleavage event cannot be ruled out without removing caspases from the equation, by siRNA knockdown or using significantly higher concentrations of caspase inhibitor. An explanation for the different activity of WFA in HD-MyZ compared to the other cell lines may be that the high level of vimentin expression saturates WFA preventing it from acting on its other targets.

In conclusion, the questionable HL-derived cell line HD-MyZ displayed further phenotypic differences to accepted HL-derived cell lines L-540, KM-H2 and L-428. This line expressed higher levels of Parkin, detected by the Parkin clone PRK8 antibody by western blot (in the previous chapter) and by immunofluorescence. This protein was observed to associate with mitotic spindle and also with microtubules in interphase cells. This association did not increase the sensitivity of HD-MyZ to the microtubule-targeting agent Paclitaxel compared to other HL-derived cell lines. Similarly the high expression level of vimentin in HD-MyZ was targeted with WFA. As with the inhibitors of protein degradation tested in Chapter 4, this cell line was more resistant than the other HL-derived cell lines. WFA treatment caused p62 and K48-linked polyubiquitinated protein accumulation and decreased viability in HL-derived cell lines L-540, KM-H2 and L-428. In contrast HD-MyZ did not accumulate p62 to the same extent as the other HL-derived cell lines or K48-linked polyubiquitin at all. Instead its large vimentin bundle was dissociated into multiple large irregular aggregates and multiple cleavage products were detected by western blotting, a markedly different response from the HL-derived cell lines. As mentioned repeatedly, despite its derivation from a HL patient, HD-MyZ is not thought to be a genuine HL-derived cell line (Kuppers and Re, 2007). The lack of HL-associated CD30 and CD15 expression, T cell receptor or immunoglobulin

gene rearrangements and the expression of macrophage-associated antigen CD68 and myeloid-associated CD13 support the notion that this cell line is not of lymphoid origin (Bargou et al., 1993). Additionally, the vimentin expression reported here was more in keeping with myeloid leukaemia cells than a cell of lymphoid origin (Dellagi et al., 1985). This cell line consistently displayed different sensitivities and reactions to inhibition of protein handling pathways compared to HL-derived cell lines L-540, KM-H2, HDLM-2, L-1236 and L-428, further suggesting a different cellular origin.

Chapter 6. Putative cancer stem cells in HL-derived cell lines

6.1 Summary

The aims of this chapter were to identify and characterise cancer initiating cells (CICs) or cancer stem cells (CSC) in HL-derived cell lines and to purify them for functional studies. Previous studies have identified putative CICs/CSCs in these cell lines using a number of different strategies. In this investigation, the results of previous studies were replicated, in terms of identifying stem cell-like populations in HL-derived cell lines, and where possible expanded upon in terms of comparing the detected stem cell-like populations. Using 2 different dyes, Hoechst 33342 and Vybrant® DyeCycle Violet, a small population of cells were identified in the KM-H2 and L-428 cells lines, which exhibited the highly active efflux commonly associated with stem cells. A small population was also identified in the L-428 and L-1236 cell lines, which possessed slightly higher aldehyde dehydrogenase (ALDH) activity than the main population, another characteristic of cancer stem cells. These cells were heterogeneous in size, although CICs/stem cells are generally thought to be small cells. Levels of reactive oxygen species were also examined in these two cell lines and found to be heterogeneous. ROS^{low} cells were deemed a good candidate for CICs as they were also small in size while ROS^{hi} cells were intermingled with the main cell population. Using a red fluorescent ROS dye (CellROX® Deep Red Reagent, Life Technologies) in conjunction with the green fluorescent ALDEFLUOR™ kit to measure ALDH activity, a comparison of the ALDH^{hi} population with the ROS^{low} population was possible. This revealed that there was little overlap between these two populations. Attempts were made to purify SP cells from KM-H2 and ROS^{low} cells from L-1236 and L-428 for functional studies using the protein degradation inhibitors investigated in Chapters 3 and 4, however we were unable to retain cell viability during or after cell sorting and further experiments were not possible.

6.2 Introduction

A number of tumours are now known to have a population of cancer-initiating cells (CICs) that often share characteristics with stem cells and have thus been termed cancer stem cells (CSCs) (Ghiaur et al., 2012). This would suggest that many diagnostic tumour cells represent a differentiated form of the cancer. Indeed in Hodgkin lymphoma, the mononuclear Hodgkin cells have been found to give rise to multi-nucleate Reed-Sternberg (RS) cells when the two populations are separated in cell culture (Newcom et al., 1988). Additionally, the numbers of RS cells have been enhanced in cell culture by TPA-induced differentiation (Hsu and Hsu, 1986, Hsu et al., 1988). Furthermore, RS cells have been found to incorporate BrdU poorly or not at all, suggesting their replicative cycle is very slow or that they are not actively cycling (Hsu et al., 1988). During my MRes project (Nuclear stress responses in Hodgkin's Lymphoma, 2009), a small proportion of RS cells in HL cell lines were found to stain positively for senescence associated β -galactosidase suggesting that these cells had entered a damage-induced replicative senescence and perhaps represented an end-stage in the cellular differentiation of this cancer. Taken together, these data would suggest that there is some form of cellular progression resulting in the generation of a population of non-replicative RS cells, yet HL-derived cell lines are considered to be immortalised. Therefore there is likely to be a pool of cells maintaining the cell lines, which may also be relevant for HL patients.

CSCs have been implicated in resistance to therapy and relapse in many cancers (Abdullah and Chow, 2013). Their resistance has been attributed to a number of factors: CSCs are often slow growing or quiescent and therefore resistant to many agents that target cycling cells; they also express high levels of membrane transporter activity leading to enhanced drug efflux capabilities; and the heightened expression and activity of metabolic enzymes such as aldehyde dehydrogenase results in the breakdown and inactivation of various chemotherapeutic agents (Visvader and Lindeman, 2012, Abdullah and Chow, 2013). Therefore, we were interested in isolating the putative CSCs from HL-

derived cell lines to determine whether they were resistant to the proteotoxic therapies explored in the Chapter 4. As reliable cell surface markers have yet to be identified to distinguish CSCs in HL from HRS cells, our efforts focused on other physical properties of CSCs, mainly the heightened efflux capacity, stem cell-associated enzyme activity and the ability to maintain low levels of ROS.

The first property examined was of heightened efflux capacity, which has been associated with drug resistance, and can be measured using fluorescent dyes such as Hoechst 33342. This dye binds to A-T regions in DNA and fluoresces under UV light (Lalande and Miller, 1979). It is also actively pumped out of cells by ATP-binding cassette (ABC) transporters associated with multi-drug resistance, such as MDR1 (Golebiewska et al., 2011). Following excitation by ultraviolet (UV), Hoechst 33342 emits predominantly in the blue range of the spectrum (with maximum emission at approximately 450 nm), described as Hoechst blue, but also emits in the far-red range (at wavelengths greater than 675 nm), described as Hoechst red. Side-population analysis using Hoechst is examined on a bivariate dot plot by plotting Hoechst blue against Hoechst red (Figure 6-1). As emissions in both the blue and red ranges increase with dye concentration, this allows easy discrimination between cells that are actively pumping the dye out versus those that are not. This process can be inhibited by Verapamil, allowing the presence of SP cells to be confirmed by the disappearance of Hoechst blue or red emission (Goodell et al., 1996).

UV light sources on flow cytometers have become rare and are often replaced by violet laser diodes as they are cheaper and more reliable. While Hoechst exhibits poor excitation by violet lasers, a violet dye called Vybrant® DyeCycle Violet (DCV), which is excluded from stem-like cells by the same mechanism as Hoechst 33342, has been developed and displays greater excitation by Violet laser sources (Telford et al., 2007). SP populations are examined in the same way using the two dyes and when compared in mouse bone marrow have been found to correspond to the same lineage negative Ska-1⁺c-kit⁺ SP population associated with pluripotent progenitor cells (Telford et al., 2007).

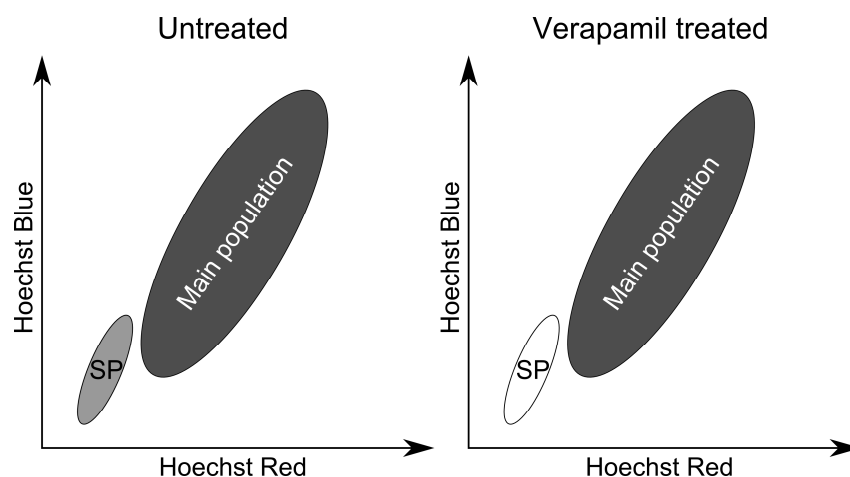


Figure 6-1 Example of side population analysis.

Dark grey areas represent the main cell population. The light grey area indicates the side population. This is lost following incubation with the ABC transporter inhibitor Verapamil.

Another dye-based method of identifying stem-like cells is the ALDELFUOR™ Assay (Stem Cell Technologies). This exploits the heightened activity of aldehyde dehydrogenase (ALDH) enzymes in primitive/ stem cells which can be used to identify ALDH^{hi} cells using a fluorescent substrate. Briefly, the fluorescent substrate boron-dipyrromethene (BODIPY) aminoacetaldehyde (BAAA) passively diffuses into the cells of interest and is cleaved by ALDH into BODIPY-aminoacetate (BAA⁻), which is retained inside the cells due to its negative charge (Ma and Allan, 2011). This results in the accumulation of fluorescent dye in cells with high ALDH activity. These ALDH^{hi} cells are lost with the inclusion of an ALDH inhibitor diethylamino-benzaldehyde (DEAB), thus allowing easy identification of this population (Figure 6-2).

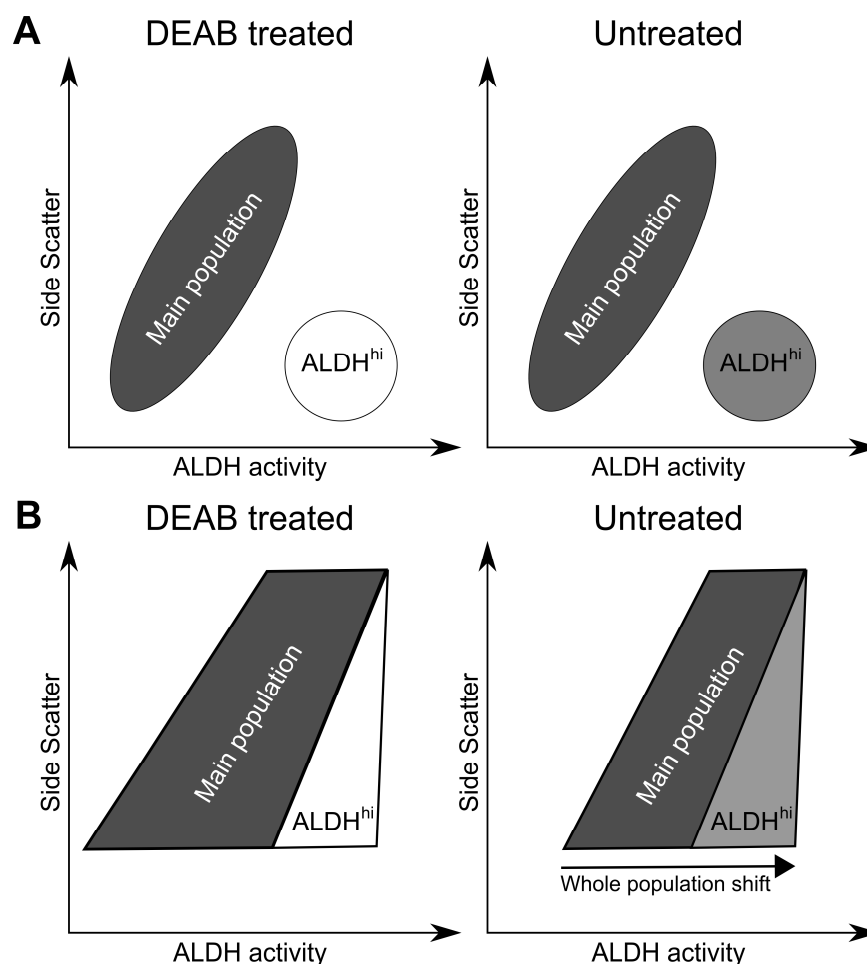


Figure 6-2 Example of ALDEFLUOR™ analysis.

Examples of common ALDH expression patterns of (A) haematopoietic stem cells isolated from bone marrow and (B) cancer stem cells in cancer cell lines such as breast cancer line SKBR1 as measured using the ALDEFLUOR™ assay. Dark grey areas represent the main cell population. The light grey area indicates cells expressing high levels of ALDH activity (ALDH^{hi}). This is lost following incubation with ALDH inhibitor DEAB. Adapted from Technical Bulletins “Identification of viable stem and progenitor cells with ALDEFLUOR™” and “Identification of ALDH-expressing cancer stem cells using ALDEFLUOR™” (Stem Cell Technologies, www.stemcell.com).

Another feature of stem cells that can be exploited using fluorescent dyes is their ability to maintain low levels of reactive oxygen species (ROS). Intracellular ROS can be measured using non-fluorescent dyes that become fluorescent upon oxidation by ROS (Chen et al., 2010). In this study a green fluorescent dye, CM-H₂DCFDA, and a red fluorescent dye, CellROX® Deep Red

Reagent, were used. Regulation of ROS levels is important to maintain genomic integrity as ROS has been found to induce DNA damage by oxidising DNA bases and hydrolysing nucleotides (Nagaria et al., 2013). Throughout the life of an organism, the stem cell niche is responsible for its own self-renewal and for the maintenance and repair of tissue through terminal differentiation. It would therefore be detrimental to the organism for these cells to acquire genomic damage as this could impact tissue function and ultimately reduce life-span.

ROS in a cell are principally generated by electron leakage from the electron transport chain in mitochondria. These harmful species are carefully eliminated by antioxidative enzyme systems including superoxide dismutase (SOD) 1/2/3, catalase, glutathione peroxidase (GPX) and peroxiredoxin (Shi et al., 2012). The regulation of ROS levels has been demonstrated to be vital in the maintenance of the stem cell niche as loss of any mechanism of regulation seems to result in dysregulation and exhaustion of the stem cell pool. For example, the FoxO transcription factors are responsible for the expression of ROS regulating genes such as superoxide dismutase and catalase (Shi et al., 2012). Triple knock-out of FoxO1, FoxO3a and FoxO4 results in increased proliferation and exhaustion of the haematopoietic stem cell (HSC) population in mice, which can be partially prevented by the addition of oxygen scavenger n-acetyl cysteine (NAC) (Tothova et al., 2007). Similarly knock-out of ROS regulators ATM kinase, MDM2 or Prdm16 also results in increased ROS and proliferation resulting in exhaustion of the stem cell population (Ito et al., 2004, Abbas et al., 2010, Chuikov et al., 2010). These effects could be at least partially alleviated by treatment with NAC, again highlighting the importance of the regulation of ROS levels.

There are only a few papers to date that specifically examine the potential existence of CSCs in HL. The first, published in 1988 by Newcom, Kadin and Phillips, described a clonal population of mononuclear cells that gave rise to both mono and multi-nuclear cells in the L-428 cell line (Newcom et al., 1988). Jones *et al.* identified a similar small mononuclear B-cell like subpopulation in L-428 and KM-H2 cell lines (Jones et al., 2009). These CD20⁺ cells were found to

express the memory B-cell marker CD27 and immunoglobulin light chain. Additionally they were found to express higher levels of aldehyde dehydrogenase (ALDH) activity than the remaining cell line population. Similar clonal cells possessing the same immunoglobulin gene rearrangements as the HRS cells were found circulating in the blood of a number of HL patients.

Shafer *et al.* identified side-population cells using the Hoechst method in HDLM-2 and L-428 but not in L-1236 or L-540 cell lines (Shafer et al., 2010). These SP cells proved resistant to Gemcitabine, a drug commonly used to treat refractory HL, and expressed higher levels than non-SP cells of ABC transporter proteins ABCG2 and MDR1, the latter only in L-428 SP cells. They were also able to identify a similar SP population in 6 primary lymph node biopsies from HL patients.

Nakashima *et al.* also identified SP cells in HL cell lines KM-H2 and L-428 (Nakashima et al., 2010). They detected similar levels of constitutive NF κ B and CD30 positivity between the SP and non-SP cells. They also found that SP cells could re-establish the original HRS population while maintaining a SP fraction, but this was not always the case for non-SP cells. In some instances non-SP cells were capable of generating both SP and non-SP populations, supporting the notion that cell sorting based on SP analysis merely enriches for CSCs and some may remain in the non-SP fraction. SP cells were also found to be positive for the proliferation marker Ki-67 while a number of non-SP cells were not, suggesting a greater proliferative potential for the SP cells. In agreement with Schafer *et al.* (2010) SP cells were found to be more resistant than non-SP cells when challenged with a chemotherapy agent, this time doxorubicin. They were, however, equally susceptible to inhibition of NF κ B by DHMEQ.

Ikeda *at al.* (2010) performed similar experiments to Newcom and colleagues (1988) by isolating mononuclear cells from L-428 and L-1236 and demonstrating that they can give rise to multi-nucleate cells (Ikeda et al., 2010). They then

took this further by demonstrating that culturing in methylcellulose or inoculation into NOD/SCID mice resulted in increased colony number and tumour size from their mononuclear cells versus multi-nuclear cells. On examining ROS levels in the mononuclear cells, they found a subpopulation that maintained low ROS levels following exposure to hydrogen peroxide and expressed higher levels of transcription factor FoxO3a. FoxO3a is involved in regulating the expression of ROS-degrading enzymes and is commonly elevated in hematopoietic stem cells. On examining paraffin-embedded HL biopsy samples, they found mononuclear Hodgkin cells expressing FoxO3a but this was not detected in RS cells.

In 2012, Ikeda *et al.* further examined this ROS-low population of cells in the L-428 cell line and its relation to the CD20⁺CD27⁺ALDH^{hi} population of Jones *et al.* (2009) (Ikeda *et al.*, 2012). They found an overlap between the ROS^{low} and ALDH^{hi} cells in that ROS^{low} cells had higher ALDH activity than ROS^{hi} cells and expressed higher levels of ALDH1A1. They also showed that ROS^{low} and ALDH^{hi} cells formed more colonies in methylcellulose and larger tumour masses in NOD/SCID mice than their counterparts. The main difference they found between ROS^{low} and ALDH^{hi} was in terms of cell cycle status. In order to maintain themselves and the relevant tissue throughout the lifetime of the organism, stem cells are generally thought to exist in a quiescent state to prevent accumulation of genomic damage through replicative stress and the shortening of telomeres associated with replicative age (Harrington, 2004). In fact, some stem cell populations have been found to express telomerase in order to maintain their chromosome ends, thus prolonging the life of the cells (Harrington, 2004). Ikeda *et al.* (2012) found that ROS^{low} cells had a higher proportion of cells in the G₀/G₁ phase of cell cycle than ROS^{hi} cells, whereas ALDH^{hi} and ALDH^{low} cells did not differ greatly in this respect. This suggested that ROS^{low} cells were more likely candidates for CSC than ALDH^{hi} as the G₀/G₁ phase can be associated with a quiescent state.

The primary aim of this chapter was to identify putative stem cell populations in HL-derived cell lines using Hoechst 33342 and DCV SP analysis, ALDH activity,

and ROS levels as described above. Having identified candidate CSC populations the second aim was to separate them from main cell population by fluorescence-activated cell sorting (FACS) and to challenge them with the protein degradation inhibitors examined in Chapter 4. This was of interest as any therapy displaying activity against the main cell population would also have to be effective against the CSC fraction to prevent treatment resistance or relapse. A number of potential CSC populations were identified, in accordance with published work; however following cell sorting we were unable to maintain cell viability for further studies.

6.3 Results

6.3.1 CD30⁻CD20⁺CD27⁺ Cells in KM-H2 and L-428

Initial experiments focused on the KM-H2 and L-428 HL-derived cell lines as these were the subjects of investigation by Jones *et al.* (2009). KM-H2 was of additional interest as it has low levels of DNA damage compared to the other HL-derived cell lines (Chapter 4, Figure 4-17B) and was not found to stain positively for senescence-associated β -galactosidase during my MRES project (Nuclear stress responses in Hodgkin's Lymphoma, 2009), both of which are consistent with a CSC phenotype. In contrast to the publication of Jones *et al.* (2009) we were unable to identify a CD30⁻CD20⁺CD27⁺ population within the KM-H2 cell line (Figure 6-3). On incubation with anti-CD30 antibody, the live cells, identified by PI negativity, were found to be CD30 positive. Using anti-CD20 or anti-CD27 antibodies, no differences in event distribution in the dot blots were found between those cells incubated with antibody or those not, suggesting the absence of these CD20⁺CD27⁺ populations. It was concluded that the population of CD20⁺ cells that most closely resembled those described by Jones *et al.* (2009) were excluded from the PI negative gate and were therefore dead cells (experiments were performed in collaboration with D. Montgomery). Similarly, in L-428 cells no CD20 or CD27 positive cells could be identified in the live cell gate (Figure 6-4). Consequently, in the absence of a reliable cell surface marker, we focused on the other aspects of CSCs described briefly in the Introduction to this Chapter.

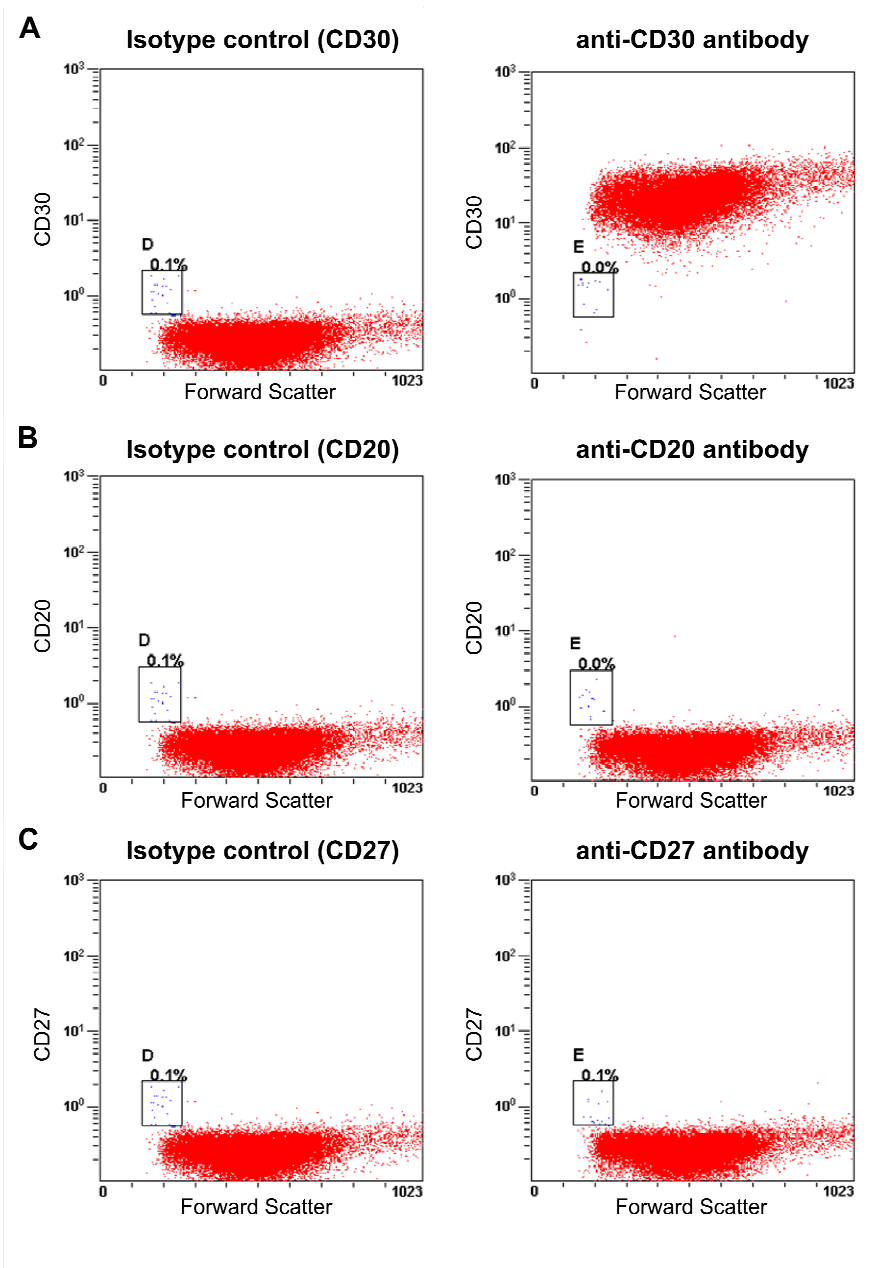


Figure 6-3 CD30⁺ but not CD20⁺ or CD27⁺ cells were detected in the KM-H2 cell line.

KM-H2 cells were incubated with (A) anti-CD30, (B) anti-CD20 and (C) anti-CD27 antibodies and the relevant isotype controls. Live cells were identified by propidium iodide exclusion. The boxed regions D and E were positioned according to Jones *et al.* and represent the putative CD30⁻CD20⁺CD27⁺ cells. For analysis, 10,000 events were collected.

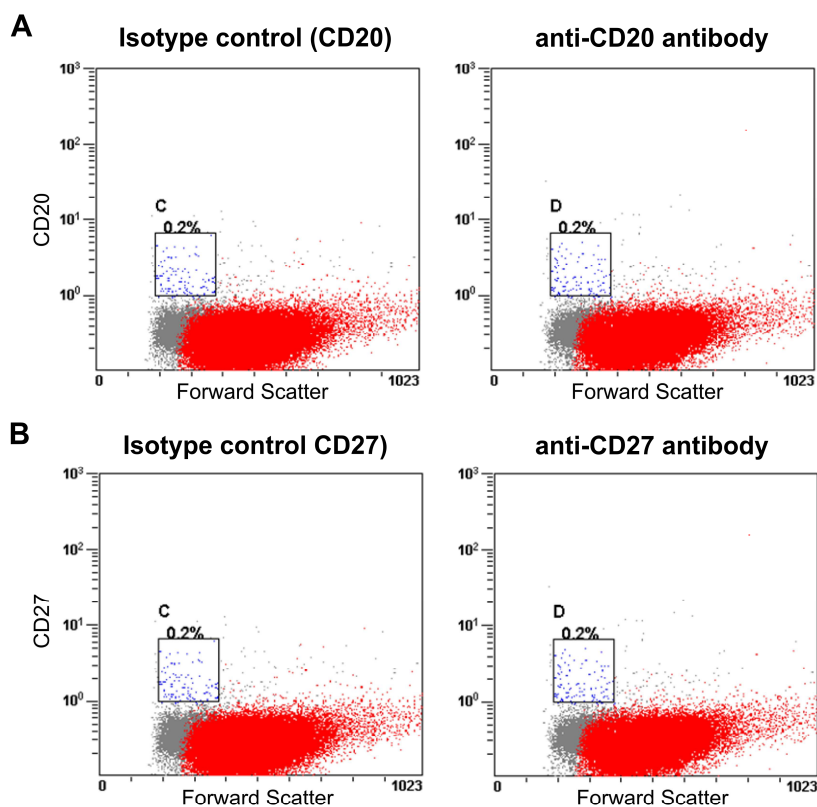


Figure 6-4 CD20⁺ and CD27⁺ cells were not detected in the L-428 cell line.

L-428 cells were incubated with (A) anti-CD20 and (B) anti-CD27 antibodies and the relevant isotype controls. Live cells were identified by propidium iodide (PI) exclusion and are indicated by red events. Grey events represent PI positive dead cells. The boxed regions C and D were positioned according to Jones *et al.* and represent the putative CD20⁺CD27⁺ cells. For analysis, 10,000 events were collected.

6.3.2 Hoechst 33342 Side Population

The gold standard method for the identification of SP cells has for many years been the Hoechst 33342 dye assay (Golebiewska *et al.*, 2011). We therefore began our investigation of putative CSCs in HL-derived cell lines using this dye, although the flow cytometric cell sorter that we had access to (BD FACSAria™) did not possess a UV laser source. Instead we relied on the limited excitation of Hoechst 33342 by a violet diode. The KM-H2 and L-428 cell lines were incubated with the dye, with and without the ABC transporter inhibitor, Verapamil in order

to identify SP cells. In KM-H2, a small SP was identified by this method (Figure 6-5); however no SP fraction was detected in L-428 cells. SP cells made up approximately 0.1% of the cell population; however, they were not exclusively small cells but were heterogeneous in size and scattered throughout the whole cell population. SP cells were sorted from bulk KM-H2 populations, and found by trypan blue exclusion to be 70% viable. Approximately 10,000 SP cells were seeded in 2 batches into a 96 well plate, however none survived overnight. *In vivo* there is a high degree of cross talk between HRS cells and the surrounding immune infiltrate that this is thought to promote the survival of HRS cells (Section 1.1.5). When removed from this environment and into culture HRS cells do not thrive as evidenced by the low number of HL-derived cell lines (Section 1.1.7.1). HL-derived cell lines express a large number of cytokines, chemokines and their receptors and seem reliant on tumour necrosis factor (TNF) family members and their receptors to maintain NF κ B signalling (Section 1.1.6). It was proposed that SP cells may not produce or secrete these signalling molecules to the same extent as HRS cells, although they may still be required for survival. Therefore, KM-H2 SP cells were cultured with preconditioned cell-free media collected from unsorted KM-H2 cells; however this did not improve viability.

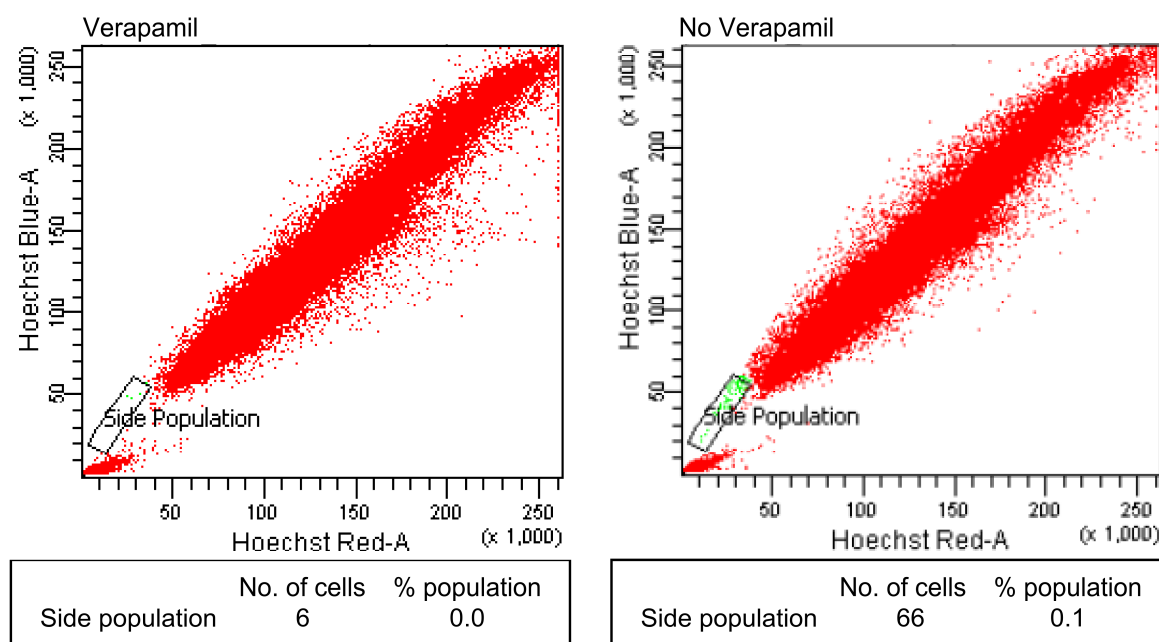


Figure 6-5 SP cells were identified in the KM-H2 cell line using Hoechst 33342 dye efflux.

KM-H2 cells were treated with or without 50 μM Verapamil in the presence of 5 $\mu\text{g/ml}$ Hoechst 33342 dye for 105 minutes at 37°C. The general cell population is indicated by red events while the Hoechst 33342 extruding side population cells are indicated by green events in the labelled boxed region. For analysis, 100,000 events were collected.

6.3.3 DyeCycle Violet (DCV) Side population

In an effort to improve SP detection, we performed further experiments using DyeCycle Violet (DCV), which displays more efficient excitation by a violet light source (Telford et al., 2007). Using the same methodology as for Hoechst 33342 SP analysis, DCV SP cells were identified in L-428 (Figure 6-6) and KM-H2 (Figure 6-7) cell lines. The cytometer used for cell sorting is used by multiple groups for a diverse range of experiments and is constantly recalibrated to fit requirements. Consequently, SP cells were often presented in different ways (Figure 6-7). KM-H2 SP and non-SP cells were sorted and seeded into 96-well plates. There were very few SP cells so they were maintained in RPMI 1640 containing 20% FBS and 2 μM β -mercaptoethanol to create a reducing environment as this has been found to prevent stem cell differentiation. Non-SP

cells were also sorted into a 96-well plate and maintained in complete medium. Following 2 weeks of growth, sufficient numbers of SP cells were achieved to allow cytopins to be prepared in order to briefly assess protein handling stress via distribution of p62. The distributions of vimentin and mitochondria (by Tom20 immunostaining) were also examined to determine whether SP cells displayed the MTOC-like polarisation described in Chapter 4. The expression of promyelocytic leukemia protein (PML), which is implicated in DNA damage repair and stem cell differentiation among other processes (Zhou and Bao, 2013), and the levels of DNA damage, by γ H2AX expression, were also assessed. No differences were observed in the expression or distribution of any of the above (Figure 6-8). As stem cells are also presumed to be smaller in size than their differentiated counterparts, it was also noted that there were no obvious differences in cell size between SP and non-SP cells. Some stem cells have been reported to stain faintly with DAPI compared to differentiated cells as they express greater levels of euchromatin than heterochromatin (Zhou et al., 2011). However, DAPI staining of nuclei was comparable in SP and non-SP cells.

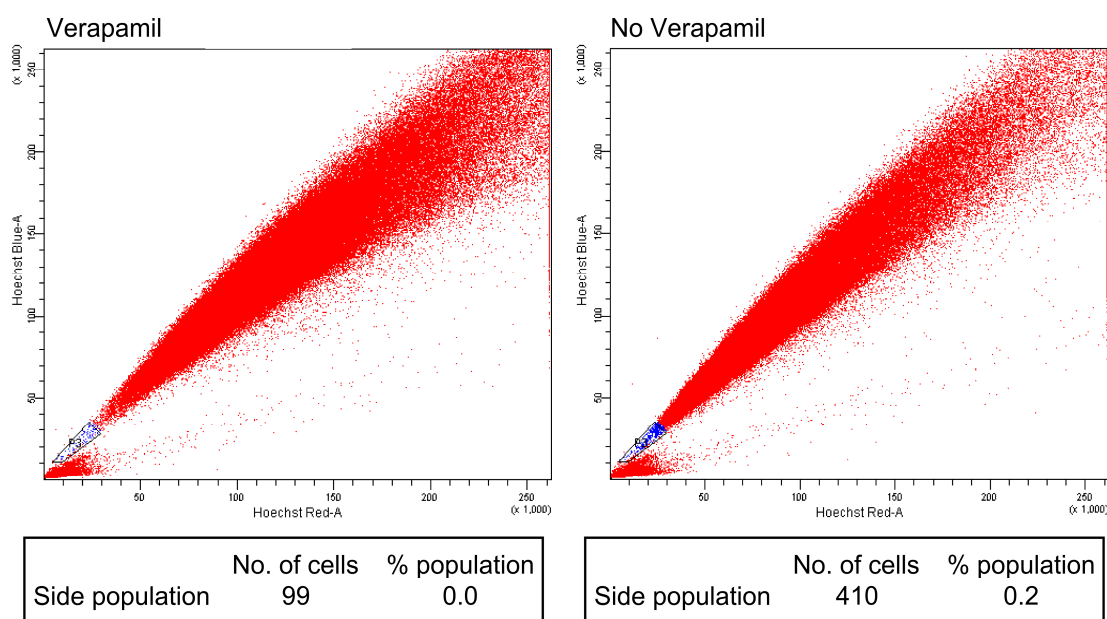


Figure 6-6 Vybrant® DyeCycle Violet SP cells were detected in the L-428 cell line.

L-428 cells were treated with or without 50 μ M Verapamil in the presence of 5 μ M Vybrant® DyeCycle violet stain for 30 minutes at 37°C before 200,000 events were collected for analysis. The general cell population is indicated by red events while the dye extruding side population cells are indicated by blue events in the boxed region.

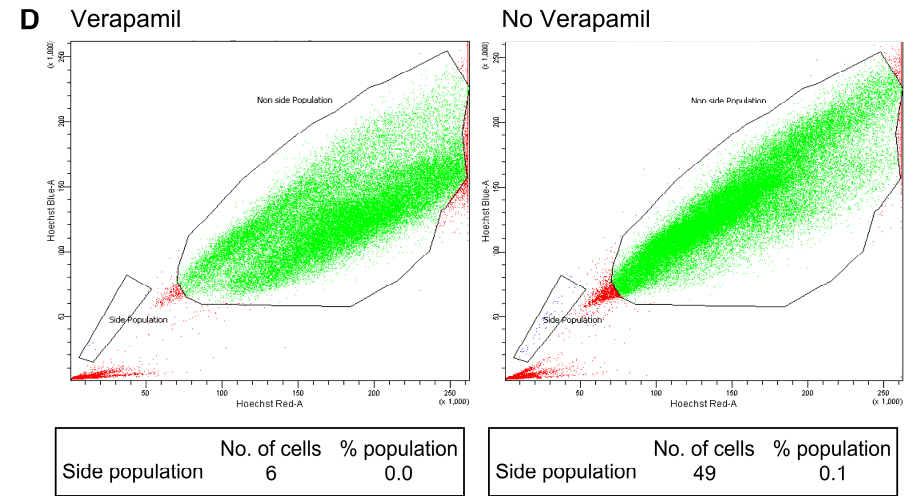
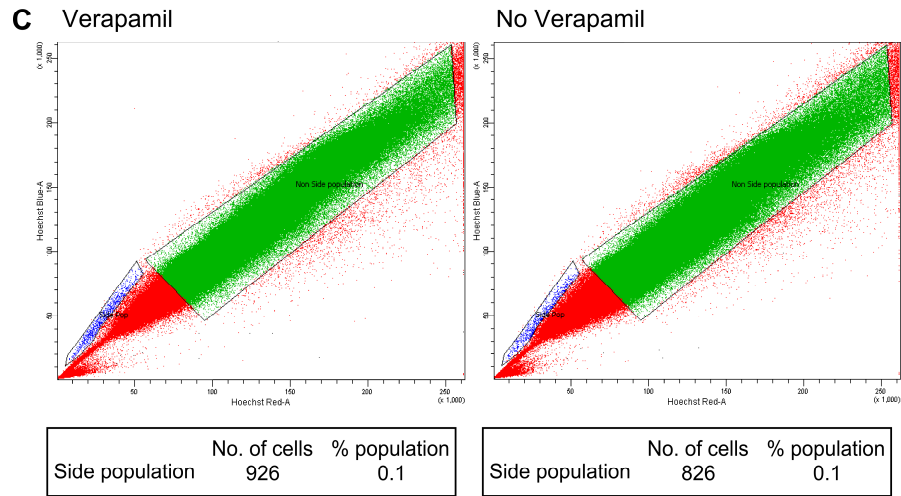
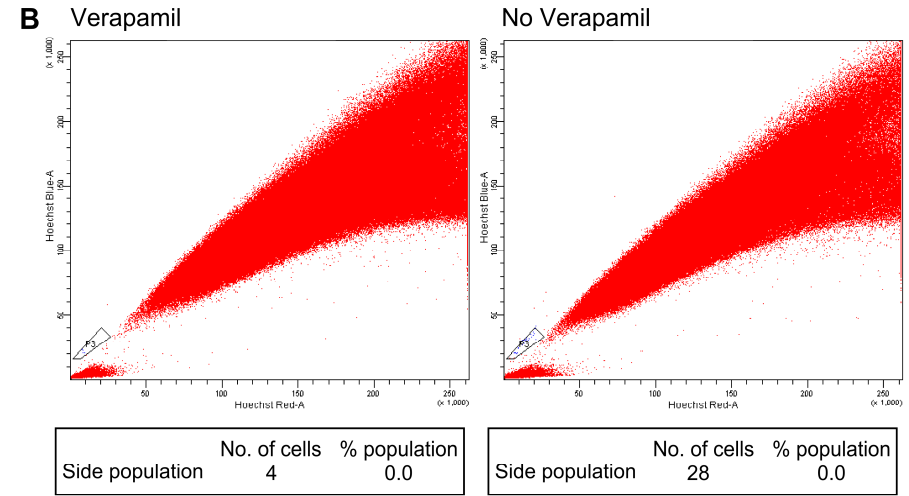
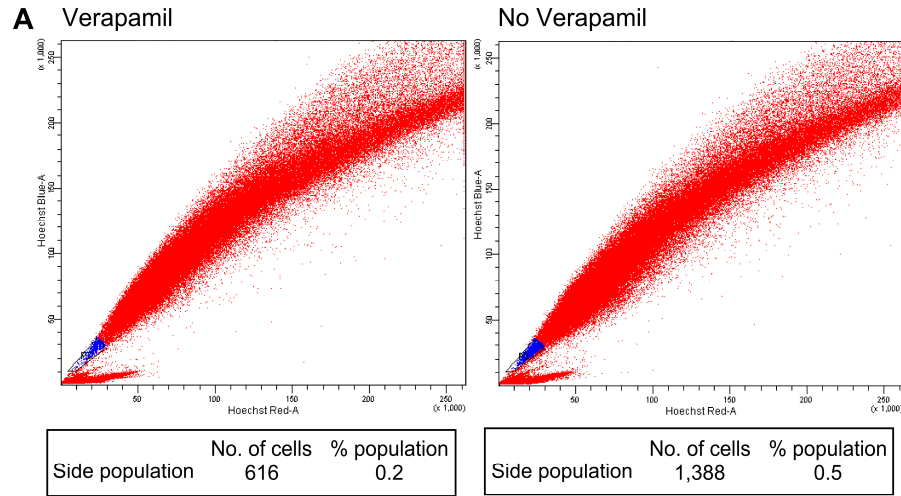


Figure 6-7 Vybrant® DyeCycle Violet SP was detected in the KM-H2 cell line.

KM-H2 cells were treated with or without 50 μ M Verapamil in the presence of 5 μ M Vybrant® DyeCycle violet stain for 30 minutes at 37°C before 100 000 events were collected for analysis. **A, B, C** and **D** represent 4 separate experiments. The general cell population is indicated by red events while the dye extruding side population cells are indicated by blue events in the boxed region. In **C** and **D**, an arbitrary region was created for non-side population cells (green events) in an effort to ensure a greater distinction between side population and non-side population cells when sorting.

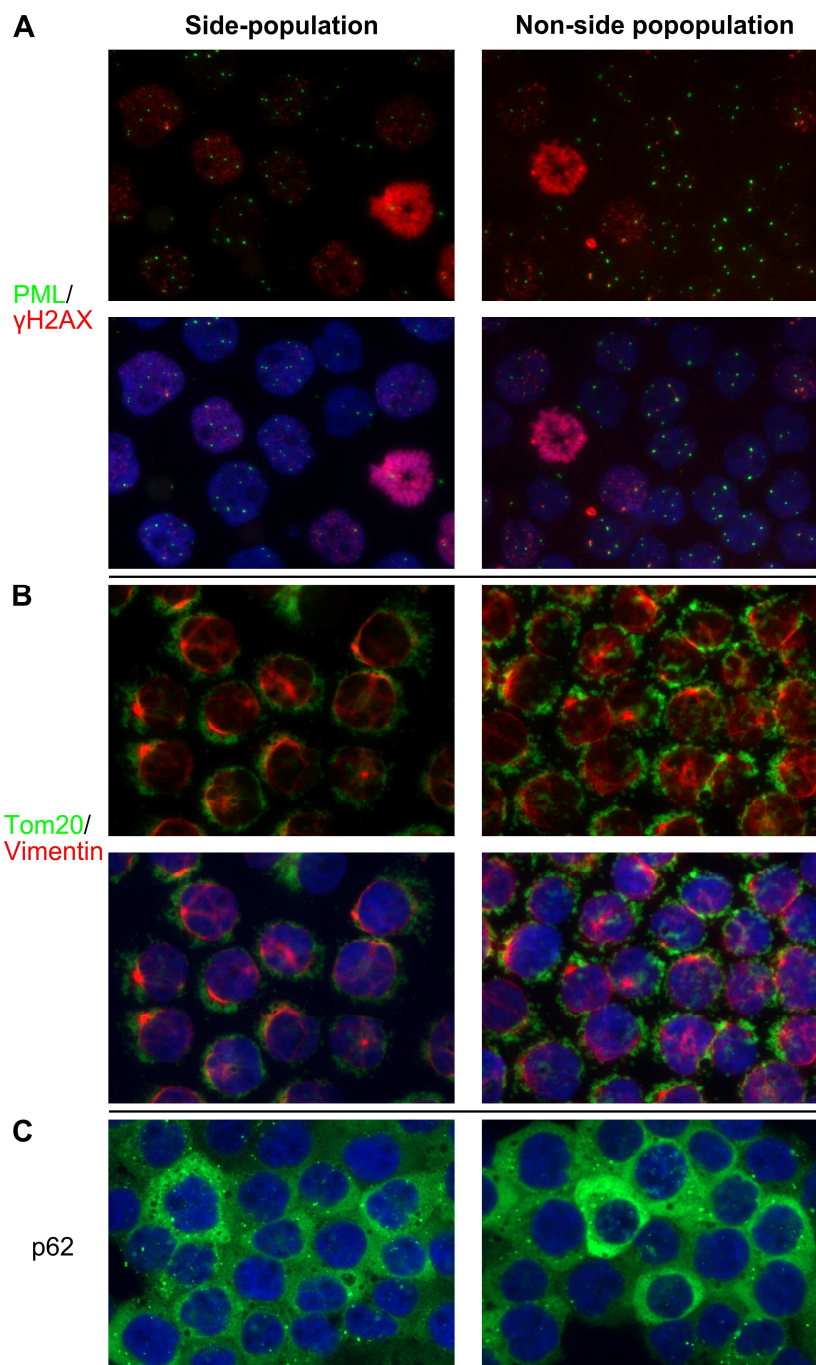


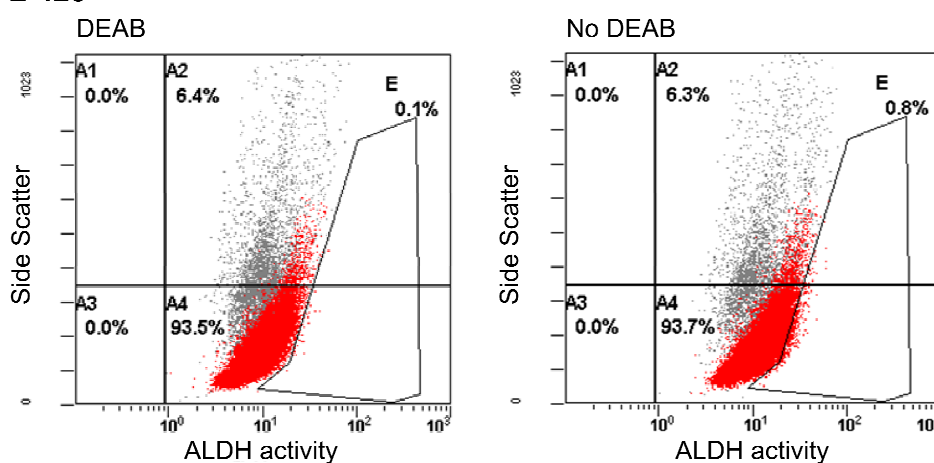
Figure 6-8 No differences were observed in the expression of PML, γ H2AX, Tom20, Vimentin or p62 in SP vs. non-SP cells.

Following sorting based on Vybrant® DyeCycle Violet side population analysis, cytopins were prepared from SP and non-SP cells and the distributions of **(A)** PML (green) and γ H2AX (red), **(B)** Tom20 (green) and Vimentin (red) and **(C)** p62 (green) were examined by immunocytochemistry. A DAPI stain was included to identify nuclei (blue).

6.3.4 ALDEFLUOR™ Assay

In initial experiments we were aiming to replicate the results of others, consequently we focused on the L-428 and L-1236 cell lines as an ALDH^{hi} population had been previously identified in these cell lines (Ikeda et al., 2012). ALDH^{hi} populations were identified in both cell lines, although they made up a very small proportion of the total cell population (Figure 6-9). In contrast to the findings of Ikeda *et al.* (2012) we found a higher percentage of ALDH^{hi} cells in the L-1236 cell line compared to L-428.

A L-428



B L-1236

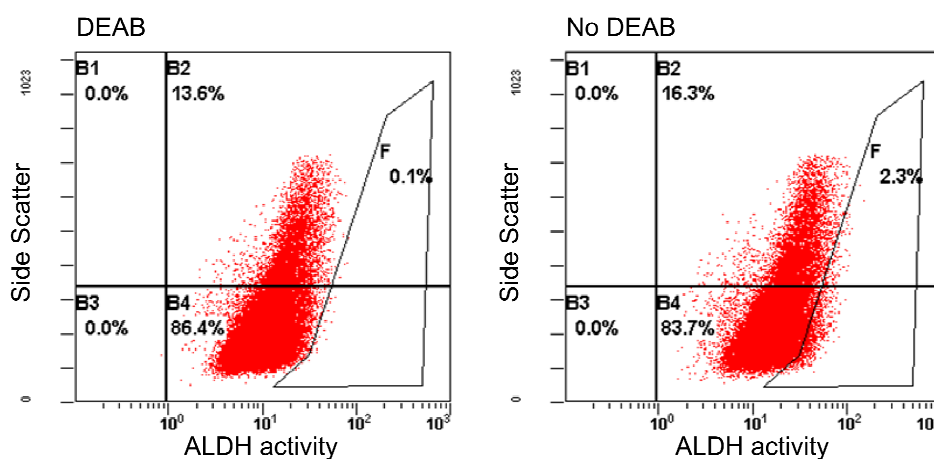


Figure 6-9 A small population of ALDH^{hi} cells were identified in the L-428 and L-1236 cell lines.

(A) L-428 and (B) L-1236 cells were incubated with the ALDEFLUOR™ dye in the presence or absence of the ALDH inhibitor DEAB for 30 minutes at 37°C. Red events represent live cells identified by propidium iodide exclusion. The boxed regions indicate ALDH^{hi} cells in L-428 (E) and L-1236 (F). All dot blots represent 100,000 events.

6.3.5 Reactive Oxygen Species

ROS levels were also easier for us to measure as again these could be analysed in-house. L-428 and L-1236 cells displayed heterogeneous levels of ROS identified using fluorescent dyes CM-H₂DCFDA (green fluorescence) and CellROX® Deep Red reagent (red fluorescence). A major concern with this assay was that ROS levels would be cell size dependent, with larger cells displaying higher levels of ROS. When L-1236 cells were examined by fluorescent microscopy, ROS bright cells were not found to be exclusively large cells. Some large cells did not staining positively for ROS at all, and no ROS positive cells, even the least bright, were found to be PI positive, meaning ROS^{low} cells were unlikely to be dead (Figure 6-10). Analysis of ROS levels by flow cytometry revealed that while there was overlap between the two populations, ROS^{low} cells (lowest 10% of the total population) did tend to be smaller in size, with ROS^{hi} cells (highest 10% of total population) interspersed with the main cell population (Figure 6-11).

L1236

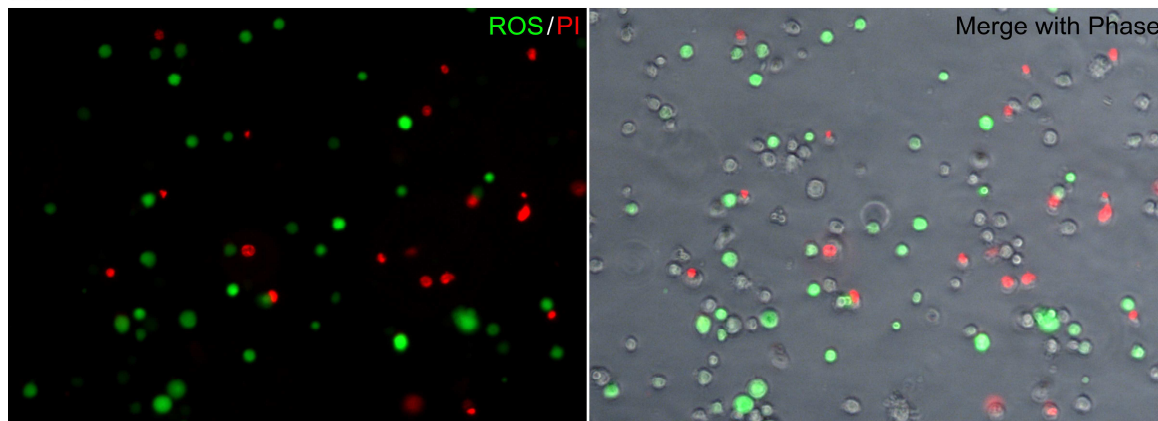


Figure 6-10 ROS expression is not cell size dependent.

L1236 cells were incubated with 10 μ M ROS dye CM-H₂DCFDA for 20 minutes at 37°C. Cells were washed and resuspended in PBS (to prevent auto-fluorescence from the media) with 1 μ g/ml propidium iodide (PI) before analysis. Left hand panel shows ROS expression by CM-H₂DCFDA (green). Dead cells were identified by PI positivity (red). Right hand panel shows left panel merged with a phase contrast image.

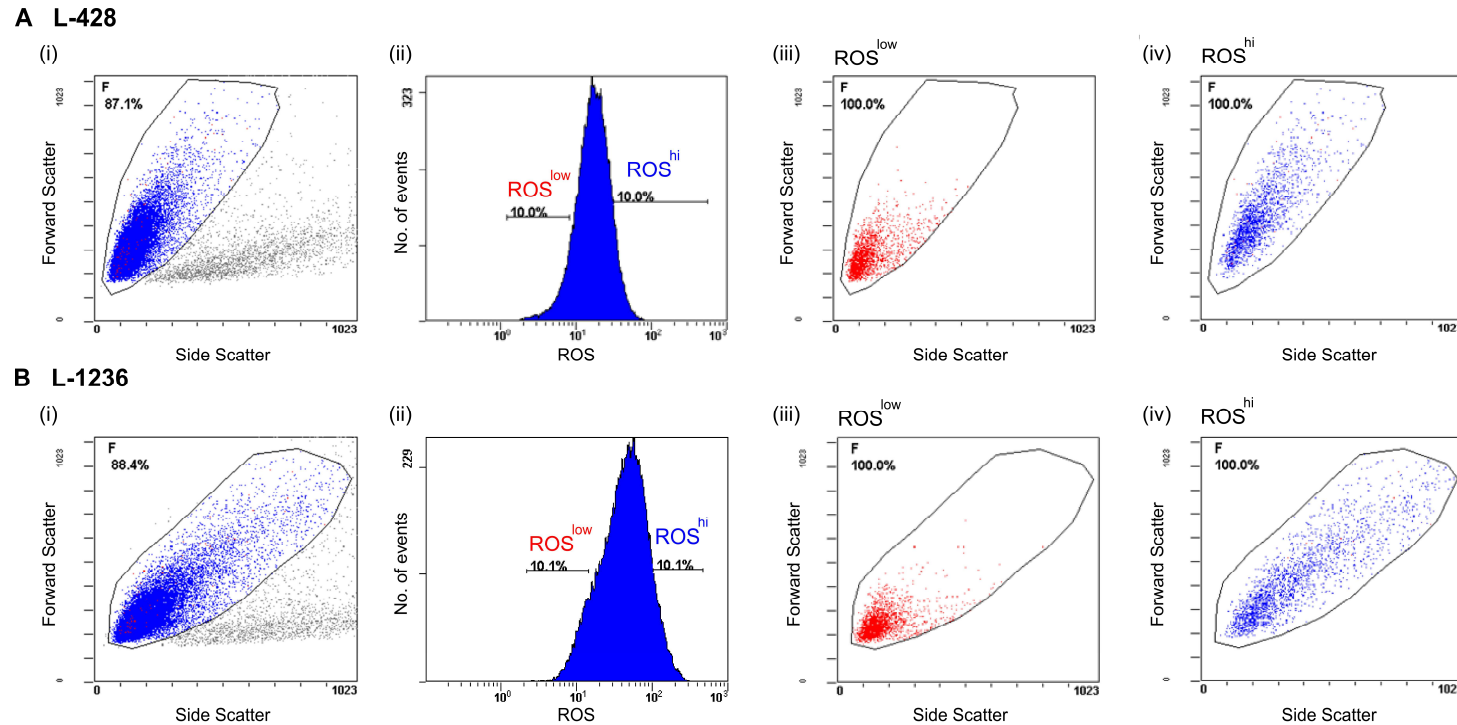


Figure 6-11 ROS^{low} cells in L-428 and L-1236 cell lines tend to be smaller cells while ROS^{hi} cells are heterogeneous in size.

(A) L-428 and (B) L-1236 cells were incubated with 5 μ M CellROX® Deep Red reagent for 20 minutes at 37°C and 100,000 events were analysed. (i) Live cells were identified by propidium iodide exclusion and are represented by blue events in region F. Grey events represent PI positive dead cells. (ii) ROS expression of the total cell population. ROS^{low} and ROS^{hi} cells were selected based on the lower or upper 10% of ROS expression in the total cell population. (iii) ROS^{low} cells (red) analysed by forward and side scatter were found to be relatively small cells compared to the total cell population (blue events in (i)). (iv) ROS^{hi} cells (blue) analysed by forward and side scatter were found to be heterogeneous in size and interspersed within the total cell population in size.

The majority of ROS dyes emit in the green range of the spectrum (at approximately 488 nm), however, CellROX® Deep Red reagent (Life Technologies, C10422) emits in the far red range (at approximately 665nm) allowing double-staining with green fluorescent dyes. Thus using the CellROX® Deep Red reagent we were able to identify the ALDH^{hi} and ROS^{low} populations simultaneously. ALDH^{hi} cells did not appear either ROS^{hi} or ROS^{low} but displayed heterogeneous levels of ROS (Figure 6-12). Similarly neither the main population of ROS^{hi} or ROS^{low} cells appeared within the ALDH^{hi} gate in L-428 (Figure 6-13) or L-1236 (Figure 6-14), although a higher percentage of ROS^{hi} cells fell within this gate in L-428 cells while the opposite was true of L-1236 cells.

These findings suggested that the ROS^{low} cells were a better candidate for CSCs, as their small size fits with the accepted models of CSCs. These conclusions are similar to those of Ikeda *et al.* (2012). Consequently, ROS^{low} and ROS^{hi} cells (the lowest and highest 10% of the total population, respectively) were sorted from the L-428 and L-1236 cell lines. The intention was to cytopsin 50,000 cells and retain a further 50,000 cells for drug treatment to determine whether these cells would be sensitive to a combination of Bortezomib and BML-281, as the total cell population proved to be in Chapter 4. While the ROS^{hi} cells were sorted with no difficulty, ROS^{low} cells took approximately 1 hour to sort 50,000 cells. This resulted in very poor viability and rendered further experiments unsuccessful.

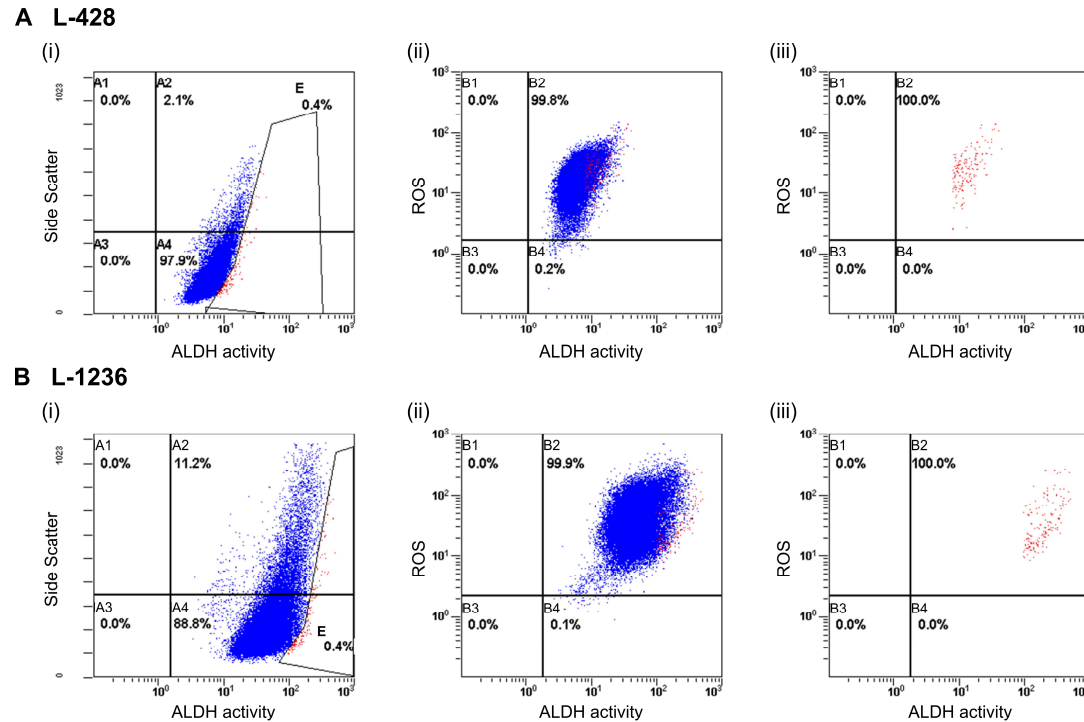


Figure 6-12 ALDH^{hi} cells displayed heterogeneous ROS levels.

(A) L-428 and (B) L-1236 cells were incubated with ALDEFLUOR™ dye and CellROX® deep red reagent for 30 minutes at 37°C and 100,000 events were analysed. (i) ALDH activity as measured by the ALDEFLUOR™ assay. ALDH^{hi} cells are represented as red events in region E. Blue events represent the remaining cell population. Region E was selected based on cells incubated with ALDEFLUOR™ dye in the presence of DEAB as in Figure 6-9. (ii) ROS expression of ALDH^{hi} cells compared to total cell population. Red events represent ALDH^{hi} cells from region E (i). Blue events represent the remaining cell population. (iii) ROS expression of ALDH^{hi} cells from region E (i) alone.

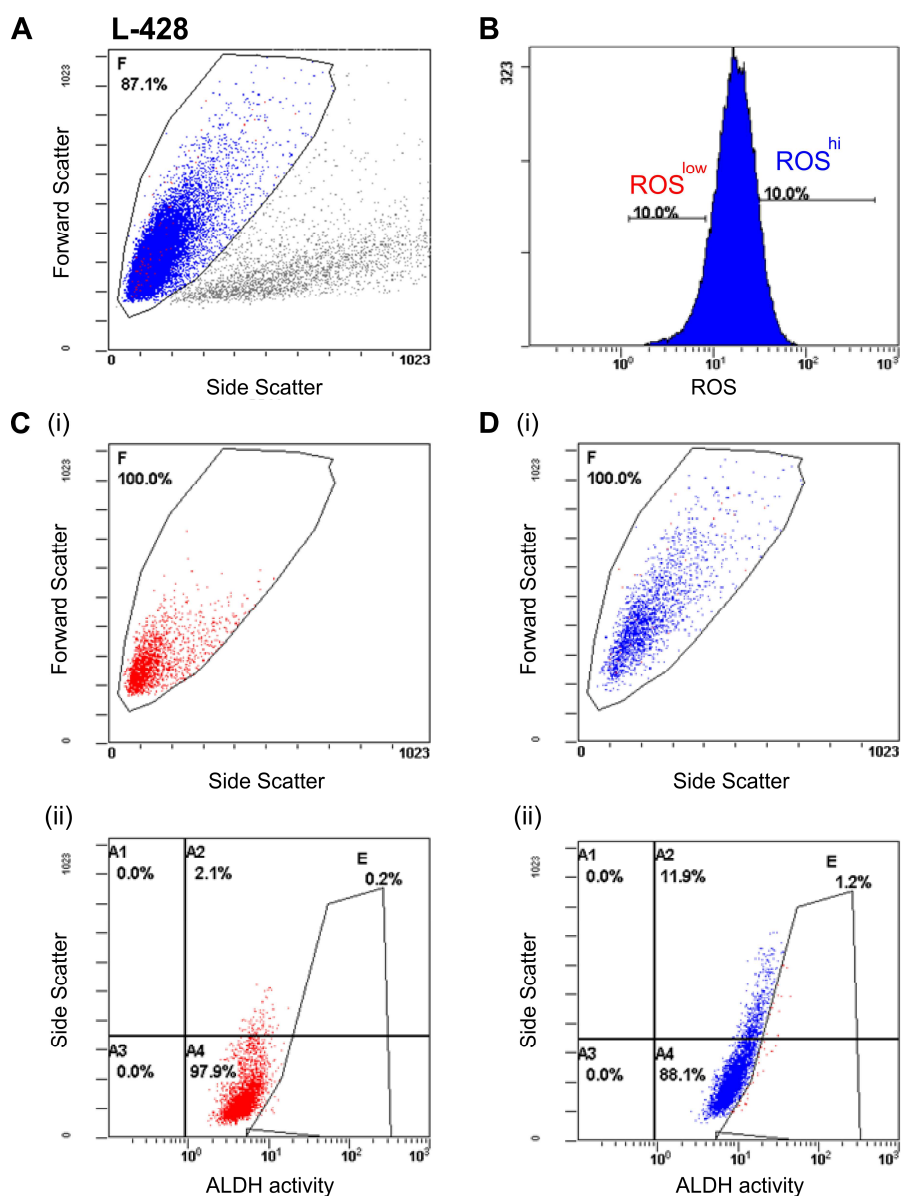


Figure 6-13 ROS^{low} cells do not fall within the ALDH^{hi} population in the L-428 cell line.

L-428 cells were incubated with ALDEFLUOR™ dye and CellROX® deep red reagent for 30 minutes at 37°C and 100,000 events were analysed. **(A)** Live cells were identified by propidium iodide exclusion and are represented by blue events in region F. Grey events represent PI positive dead cells. **(B)** ROS^{low} and ROS^{hi} cells were selected based on the lower or upper 10% of ROS expression in the total cell population. **(C)** ROS^{low} cells (red events) and **(D)** ROS^{hi} cells (blue events) were analysed by (i) forward and side scatter to assess size and (ii) ALDEFLUOR™ assay to assess ALDH activity. ROS^{low} cells were found to be relatively small in size while ROS^{hi} cells were heterogeneous in size. Neither population fell within the ALDH^{hi} gate (region E); although a higher percentage of ROS^{hi} cells were present within this region.

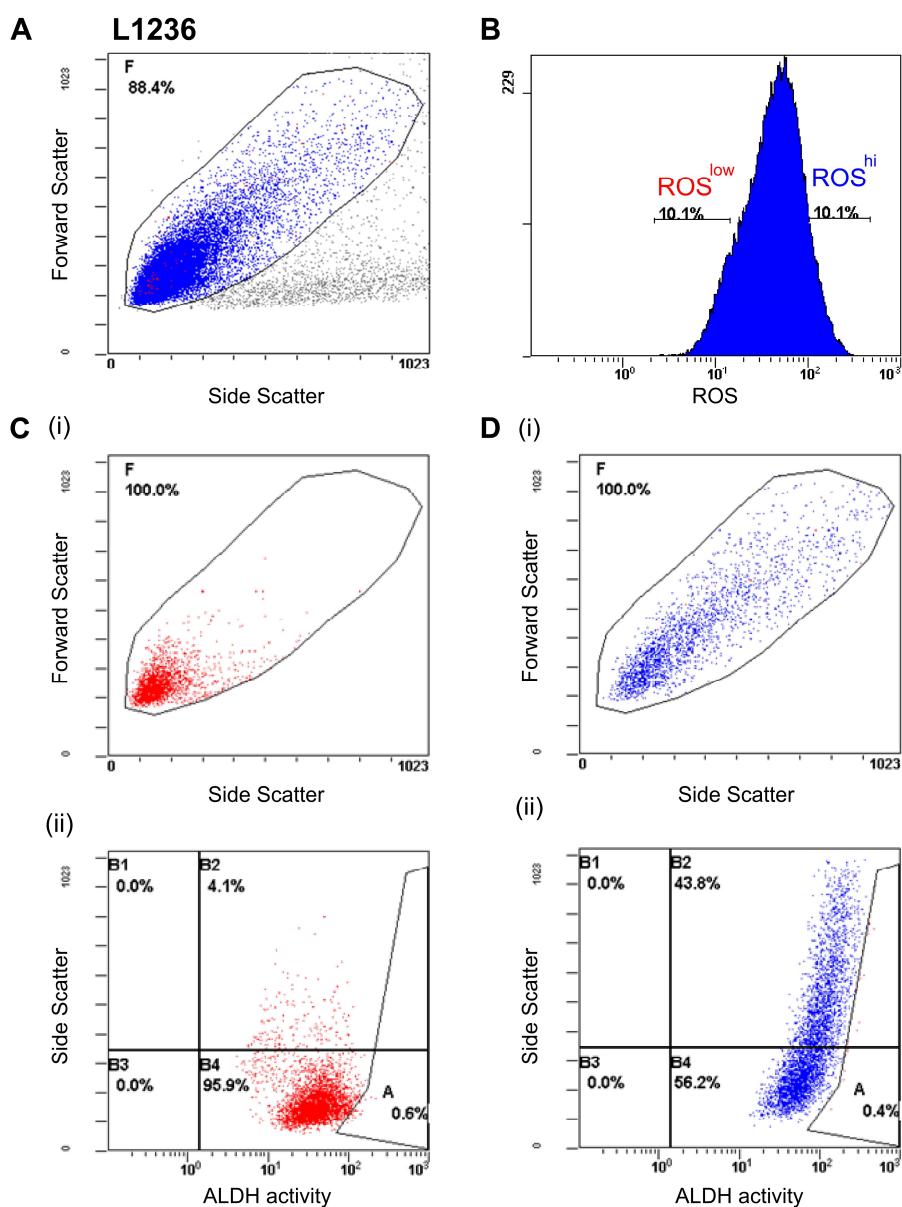


Figure 6-14 ROS^{low} cells do not fall within the ALDH^{hi} population in the L-1236 cell line.

L-1236 cells were incubated with ALDEFLUOR™ dye and CellROX® deep red reagent for 30 minutes at 37°C and 100,000 events were analysed. (A) Live cells were identified by propidium iodide exclusion and are represented by blue events in region F. Grey events represent PI positive dead cells. (B) ROS^{low} and ROS^{hi} cells were selected based on the lower or upper 10% of ROS expression in the total cell population. (C) ROS^{low} cells (red events) and (D) ROS^{hi} cells (blue events) were analysed by (i) forward and side scatter to assess size and (ii) ALDEFLUOR™ assay to assess ALDH activity. ROS^{low} cells were found to be relatively small in size while ROS^{hi} cells were heterogeneous in size. Neither population fell within the ALDH^{hi} gate (region E); although a higher percentage of ROS^{hi} cells were present within this region.

6.4 Discussion

Here the presence of Hoechst 33342 and Vybrant® DyeCycle Violet excluding side population cells, ALDH^{hi} and ROS^{low} cells were confirmed in a selection of HL-derived cell lines. Although these populations each shared a phenotypic characteristic with CSCs, there did not appear to be any correlation between each population suggesting that they require further characterisation to confirm their status as CSCs.

The side population cells identified by both Hoechst 33342 and Vybrant® DyeCycle violet were both promising candidates for our CSCs. Our clearest side population was obtained on the first sort with Hoechst 33342 in KM-H2 (Figure 6-5) however we were unable to find a similar population in L-428 cells. An explanation for this may be the poor excitation of this dye by the violet laser installed on the cytometer. Indeed, on switching to Vybrant® DyeCycle violet a side population was identified in L-428 cells and a population similar to that observed using the Hoechst dye was also observed in KM-H2 cells. While we were able to sort DyeCycle violet SP cells from KM-H2, they were very few in number and had to be cultured for an extended period of time before there were sufficient numbers to cytopspin. Although this culture was conducted under reducing conditions to prevent differentiation, there is no guarantee that this did not occur. As has been found by other groups, these SP cells are perfectly capable of reconstituting the HRS cell population (Nakashima et al., 2010). Indeed, on examining the expression of a number of proteins, no differences were observed between our SP and non-SP cells. The tumour suppressor PML was examined in conjunction with DNA damage marker γ H2AX. It was thought that SP cells may harbour less endogenous DNA damage than non-SP cells, as stem-like cells are generally under less replicative stress than cycling counterparts (Nagaria et al., 2013). Similarly, working on the assumption that stem-like cells are better at maintaining low levels of ROS, which can cause genomic damage, SP cells may have less ROS-induced damage (Shi et al., 2012). This did not prove to be the case with similar expression levels of punctate γ H2AX, indicating

double-strand DNA breaks (Bonner et al., 2008), observed in interphase cells and the same diffuse staining in mitotic cells seen in both SP and non-SP KM-H2 cells. Expression of PML was examined as it is involved in the DNA damage response and a difference in PML expression in terms of DNA damage recognition it would have been of interest (Zhou and Bao, 2013). PML was also of interest in SP cells as it is involved in the regulation of progenitor cell replication (Zhou and Bao, 2013). In both SP and non-SP cells the majority of PML bodies did not appear to co-localise with γ H2AX, with only a small number displaying clear juxtaposition or co-localisation with larger γ H2AX puncta. This suggested a degree of damage recognition, however, no differences were observed. PML expression was also of interest, due to its multi-functional role as a tumour suppressor involved in regulation of numerous post-translational modifications affecting transcription, cell proliferation and cell fate (Bernardi and Pandolfi, 2007). Specifically, in haematopoietic stem cells, loss of PML was found to lead to a loss of the quiescent state required to maintain the stem cell niche and subsequently these cells replicated and the niche was exhausted (Ito et al., 2008). Similarly in a model of chronic myeloid leukaemia, in which PML over-expression is associated with poor outcome, depletion of PML resulted in expansion and exhaustion of the leukaemia-initiating cells (Ito et al., 2008).

The expression patterns of Tom20, Vimentin and p62 were also of interest in terms of determining whether there was any evidence of differences in protein handling stress between the SP and non-SP cells. All 3 proteins displayed similar patterns of expression and were similar to those described in Chapters 3 and 4, with the MTOC-polarisation of Vimentin and Tom20 suggesting similar degrees of polarisation of protein degradation in SP and non-SP cells. Again, p62 appeared in a diffuse cytoplasmic pattern in both populations with a number of small cytoplasmic puncta in each. As discussed in Chapters 3 and 4, the interpretation of p62 expression in relation to pathway activity is complicated. Therefore, in order to fully examine pathway activity in SP and non-SP cells using similar methods to those used in Chapter 4, many more cells would be required than we were able to viably purify by FACS.

Although an ALDH^{hi} population seemed to be present in L-428 and L-1236, the very slight shift indicating ALDH activity when the ALDH inhibitor DEAB was not present was not convincing. Often ALDH activity profiles generated from genuine haematopoietic stem cells resemble the example shown in Figure 6-2A, while profiles generated from cancer cell lines resemble the example in Figure 6-2B and the profiles we observed. However, published ALDH profiles, including those observed by Ikeda *et al.* (2012) in the same cell lines, show a much more significant increase in ALDH activity in the absence of DEAB. It is possible that changes in cell metabolism during various stages of growth may affect ALDH expression and activity and we merely caught our cells at stages when their activity was low. It may be of interest to synchronise the cell population at various stages of cell cycle to determine whether ALDH display different activities at each stage. Additionally, growing the cells under different growth conditions, such as low serum or increased cell density may change ALDH expression. It may also be possible to enrich for ALDH^{hi} cells by pretreating cells with Cyclophosphamide. ALDH has been found to metabolise this drug (Magni *et al.*, 1996) and its use enhanced the ALDH^{hi} CSC population in colorectal cancer xenograft tumours (Dylla *et al.*, 2008). Determining whether these factors would allow for better resolution of the ALDH population could be of use in the future.

Targeting ALDH^{hi} cells with agents that will reduce ALDH levels may also be of interest. An end product of metabolism by ALDH is retinoic acid (RA), which through interaction with its receptor (RAR) and retinoid x receptor (RXR) acts as a transcription factor influencing numerous cellular processes including proliferation, differentiation and cell fate (Ma and Allan, 2011). Treatment with ALDH inhibitor DEAB has resulted in expansion of haematopoietic stem cells (Chute *et al.*, 2006), suggesting a role for this enzyme in the maintenance of the quiescent state. In haematopoietic stem cells and in breast cancer stem cells treatment with RA or all-trans-RA (ATRA) resulted in reduced ALDH levels and induced differentiation (Chute *et al.*, 2006, Moreb *et al.*, 2005). RA acts in a negative feedback loop to regulate ALDH levels. In conditions of low retinoic acid (RA) concentration, RA receptor (RAR) binds retinoic acid receptor element

(RARE), CCAAT/enhancer-binding protein- β (C/EBP β) binds to CCAAT box upstream of *Aldh1* gene to transactivate *Aldh1* (Ma and Allan, 2011). High concentrations of RA result in enhanced production of C/EBP β and GADD153 which form a complex, reducing the ability of C/EBP β to bind to the CCAAT box upstream of the *Aldh1* promoter, thus reducing its transcription and reducing ALDH levels (Ma and Allan, 2011). ATRA induces apoptosis or differentiation in a number of cancers and is used in the treatment of acute promyelocytic leukaemia where it results in the terminal differentiation and ultimately apoptosis of the malignant cells (Elliott et al., 1992, Gianni et al., 2000). Similarly in breast cancer cells ATRA has been used to induce cancer stem cell differentiation and resulted in increased sensitivity to both radiation and chemotherapy (Ginestier et al., 2009, Croker and Allan, 2012).

The best candidates for CSC were thought to be the ROS^{low} cells detected in L-428 and L-1236 as they were also small cells. As stem cells are adept at regulating their ROS levels it may be beneficial in future to treat cells with a ROS inducing agent such as hydrogen peroxide in a manner similar to Ikeda *et al.* (2010). This should allow easier differentiation between putative ROS^{low} CSC and non-CSC, as CSC are capable of maintaining low levels of ROS while ROS levels in the remaining cell population would increase. Ikeda *et al.* (2012) identified higher levels of an ALDH isoform (ALDH1A1) in ROS^{low} cells compared to ROS^{hi}, and a greater proportion of ALDH^{hi} cells expressing the ROS-regulating transcription factor FoxO3a compared to ALDH^{low} cells, suggesting that ALDH^{hi} and ROS^{low} cells may be part of the same CSC population. In contrast, we saw no correlation between these populations when measured by ALDEFLUORTM assay and the ROS detecting CellROX[®] deep red reagent. As mentioned previously, the ALDH^{hi} populations detected by Ikeda *et al.* (2012) were more convincing in their ALDH levels as measured by the ALDEFLUORTM assay than those we observed despite using identical procedures.

In conclusion, a number of small populations were identified in a selection of HL-derived cell lines which shared properties with CSCs. These cells had heightened efflux capabilities, increased stem cell-related enzymatic activity or low ROS levels. These cell populations require further characterisation to fully elucidate their role as potential CSCs. The presence of an HL CSC is still a controversial topic and a CSC-like population has yet to be identified in all of the HL-derived cell lines. Future work would require the identification of a CSC-like population with shared characteristics in all HL-derived cell lines to confirm the presence of this putative population in HL.

Chapter 7. Concluding Remarks

7.1 Concluding remarks

HL is one of the most treatable human malignancies and the majority of patients are ultimately cured of their disease (Eichenauer and Engert, 2012). Patient treatment is largely dictated by the Ann Arbor staging system, which is based on the spread of the disease but does not address the biology of the tumour (Lister et al., 1989). Although highly successful against HL, the current treatment regimens are accompanied by a number of side-effects including infertility and potentially fatal secondary malignancies (Aleman et al., 2003). This is of particular importance to the younger patients, whose quality of life can be significantly affected as a result of the therapy. Furthermore, there are a small proportion of HL cases that do not respond to treatment, indicating that there is still a need to continue to improve primary therapies.

The current radiotherapy combined with multidrug treatment regimens focus largely on the use of genotoxic agents to cause intolerable DNA damage to the malignant cells (Eichenauer and Engert, 2012). The effect of the proteasome inhibitor Bortezomib has previously been examined in HL, in terms of cell death in HL-derived cell lines (Zheng et al., 2004, Kashkar et al., 2007) and in disease responses following treatment of patients refractile to primary therapy (Younes et al., 2006, Strauss et al., 2006, Blum et al., 2007). Similarly, HDAC inhibitors have also been trialled in non-responsive HL cases (Kirschbaum et al., 2012, Younes et al., 2011, Younes et al., 2012b). However, these studies have not addressed the affects of these treatments on protein degradation pathways and the activities of these pathways in HL have not previously been reported. Knowledge of the pathway activity would allow correlates to be drawn between activity and sensitivity to therapy. This, in turn would allow the possibility of predicting sensitivity using HL biopsy material.

The primary focus of this thesis was to assess the activities of the proteasome and autophagy pathways in HL-derived cell lines and their responses to inhibition of these pathways. These studies were initiated due to the unusually high levels

of p62 expression observed in HL-derived cell lines and are discussed in Chapters 3 and 4. All the cell lines exhibited varying degrees of proteasome activity, although the three cell lines with lower proteasome activity (L-540, KM-H2 and HDLM-2) also expressed the highest levels of proteasome substrate K48-linked polyubiquitin. This suggested that they were struggling with their protein load, which was confirmed when L-540 and HDLM-2 cells were found to be highly susceptible to proteasome inhibition, while KM-H2 cells were able to compensate by increasing the activity of the autophagy pathway. The cell lines with the higher activity, L-1236, L-428 and particularly HD-MyZ, were less sensitive to proteasome inhibition. These measured sensitivities go against the conventional wisdom that high pathway activity implies an over-reliance and therefore sensitivity to inhibition.

With the exception of HD-MyZ, autophagy activity was detected by LC3B flux assays in all of the HL-derived cell lines. Autophagy inhibition alone or in combination with proteasome inhibition, did not greatly affect cell viability. Combined treatment with the proteasome inhibitor Bortezomib and the HDAC6-specific inhibitor BML-281, on the other hand, resulted in reduced cell viability compared to Bortezomib or BML-281 treatment alone. The L-1236 cell line was an exception to this as it was more sensitive to BML-281 treatment alone than it was to BML-281 in combination with Bortezomib. This sensitivity was found to be due to DNA damage caused by BML-281 in mitotic cells. While BML-281 appeared to cause cell cycle arrest at prophase in KM-H2 cells, L-1236 cells displayed no such arrest and cell death was the prominent phenotype. The different cell fates may be due to the p53 status of the cell lines, as KM-H2 expresses wild type p53 and L-1236 expresses a transcriptionally inactive truncated form of the protein (Janz et al., 2007). The protective effect of the combined Bortezomib and BML-281 treatment was suggested to be due to cell cycle arrest at G1 caused by Bortezomib preventing the formation of DSBs in response to BML-281 during mitosis. Therefore, Bortezomib and BML-281 displayed anti-proliferative effects against HL-derived cell lines, both as single agents and in combination. These

agents may be effective against HL; however, a reliable biomarker is required to indicate which pathway(s) to target.

Originally, p62 was intended as a biomarker to inform on the activity and susceptibility of cells to inhibition of protein degradation pathways. The expression patterns in the HL-derived cell lines were too complex, however, and did not reliably correlate with pathway activity or sensitivity to inhibition. In response to proteasome inhibition, p62 was observed to aggregate in HL-derived cell lines regardless of their proteasome activity. In the case of L-540 cells, this was to the detriment of the diffuse expression pattern, while in KM-H2, HDLM-2, L-1236 and L-428 cells the diffuse fraction of p62 did not diminish but increased, particularly in L-428 and L-1236 cells. In contrast, in HD-MyZ cells, p62 expression did not change following proteasome inhibition. When autophagy was inhibited, p62 formed numerous small aggregates in the HL-derived cell lines, with larger irregular aggregates formed in HDLM-2. With the exception of HD-MyZ, all the cell lines tested positive for LC3B flux removing any correlation between autophagy activity and p62 aggregation. Therefore, the aggregation of p62 did not necessarily indicate the failure of a specific pathway but occurred during inhibition of both the proteasome and autophagy pathways. The expression patterns of p62 observed in paraffin-embedded HL biopsy samples, which were comparable to those observed in the cell lines, suggested that interpretation of pathway activity using p62 as a biomarker would be similarly complex in patients.

p62 may be of use in determining the primary location of protein handling stress in a cell, as evidenced by the L-1236 cell line. This cell line predominantly expressed p62 in the nucleus yet following proteasome or autophagy inhibition, p62 was observed as multiple aggregates in the cytoplasm. Therefore, p62 may be of use as a marker in malignancies in which disease progression involves the generation of or changes in a protein handling stress. In all of the HL-derived cell lines, there appeared to be a high degree of p62 traffic between the cytoplasm and nucleus. The exact role of nuclear p62 is unclear, although the

previously unreported association of p62 with DNA-damage associated γ H2AX in both the nucleus and cytoplasm would suggest a chaperone function for the degradation of nuclear proteins in the cytoplasm.

Throughout this project HD-MyZ differed greatly from the other HL-derived cell lines. It is no longer thought to be a genuine HL cell line, although it was established from the pleural effusion of a HL patient (Kuppers and Re, 2007). It does not express the cell surface markers characteristic of HL and instead expresses macrophage and myeloid-associated markers, suggesting a different cellular origin from conventional HL cells (Bargou et al., 1993). Additionally, unlike the other HL-derived cell lines, HD-MyZ cells are exclusively adherent and express vimentin in an unusual distribution, reminiscent of that observed in myeloid leukaemia (Dellagi et al., 1985). This cell line was the only cell line, in which we were unable to demonstrate autophagy flux using LC3B turnover yet p62 formed multiple cytoplasmic aggregates following autophagy inhibition indicating there was activity in lysosome-associated degradative pathways. The discovery of an alternative form of macroautophagy in $ATG5^{-/-}ATG7^{-/-}$ mice, which acted independently of the ubiquitin-like conjugation systems, may be of relevance to this cell line (Nishida et al., 2009). Although in the $Atg5/Atg7$ -independent system, there was no evidence of LC3B lipidation; LC3BII was present in HD-MyZ. This may represent an attempt and failure to use the conventional autophagy pathway and a compensatory switch to an alternative pathway. As there have been differences observed in cytoskeletal interaction depending on the type of autophagy (quality control or starvation-induced) (Lee et al., 2010) this failure in the conventional pathway may be caused by the large irregular vimentin expression pattern observed in HD-MyZ. Furthermore, the lack of p62 aggregation following inhibition of chymotrypsin-like proteasome activity despite a comparable increase in K48-linked polyubiquitinated proteins to that observed in cell lines in which p62 did aggregate implies an efficient alternative means of dealing with protein waste. Additionally, in Chapter 5, proteasome inhibition with WFA, a proteasome inhibitor with specific anti-vimentin activity, did not result in build up of K48-linked polyubiquitin in HD-MyZ unlike in other

HL-derived cell lines, although it did result in p62 aggregation at higher concentrations. Taken together these data suggest that HD-MyZ would make an attractive model in which to examine alternative protein degradation pathways in the future.

The unexpected nuclear expression of the lysosomal enzyme cathepsin B observed in HL-derived cell lines in Chapter 5 has not previously been reported and may be of relevance to the transcriptional reprogramming characteristic of HL. Other members of this family of lysosomal proteases have been implicated in transcriptional regulation (Duncan et al., 2008, Goulet et al., 2004), suggesting that cathepsin B could play a similar role in HL cells. The identification of cathepsin B nuclear targets in the future could be informative for HL. The nuclear activity of this protease warrants further investigation as cathepsin B-specific inhibitors exist and may be of use in alleviating the aberrant transcriptional profile of HL cells.

In Chapter 6 the presence of CSCs in HL-derived cell lines was examined. CSCs have been associated with resistance to therapy in other malignancies and may be responsible for treatment failure in HL (Abdullah and Chow, 2013). Therefore, it is important to understand their biology and the mechanisms by which they escape primary therapy. The HL CSC is a controversial topic as evidenced by the limited number of studies into this intriguing cell population. Furthermore, a population with CSC-like properties has yet to be identified in all of the HL-derived cell lines. This would seem a prerequisite for the acceptance of this cell population. Nevertheless, the discovery of putative CSCs in HL-derived cell lines has important implications for HL treatment, particularly for patients who relapse. A number of small populations of cells that shared properties with stem-like cells were detected in HL-derived cell lines. Side population cells were detected based on Hoechst 33342 or Vybrant® DyeCycle Violet efflux in the KM-H2 and L-428 cell lines. ALDH^{hi} and ROS^{low} populations were also detected in L-428 and L-1236, although these populations did not appear to be the same (i.e. not ALDH^{hi}ROS^{low}). These assays require further

optimisation to allow the characterisation of these putative CSCs. A reliable cell surface marker would be preferable to the above assays, as this would require minimal manipulation of the cells prior to their isolation from the main cell population. This would allow more reliable testing of the efficacies of novel therapies against HL CSCs in the future.

As discussed throughout this thesis, the HL-derived cell lines differed greatly in terms of their protein degradation pathway activities and their responses to inhibition of these pathways. These cell lines are often used in a panel to assess gene expression, and pathway and drug activity, as in this study. The majority of the currently available HL-derived cell lines were generated many years ago from patients with advanced stage disease. They were all established from extranodal sites, such as the peripheral blood, bone marrow or plural effusions, suggesting that they had adapted to survive outside of their usual lymph node-associated HL microenvironment (Kuppers and Re, 2007). This is likely to be the main reason they were successfully cultured. The advanced stage of disease and decreased reliance on interactions with the immune system may diminish the value of these cell lines as representations of HL. Therefore, there is an argument for the generation of new HL-derived cell lines. With the increased understanding of the complex interactions between HRS cells and the immune system and advances in 3D culturing techniques it is likely that fresh attempts to culture cells from primary material would see greater success than in the past. Of course, this would still be hampered by the scarcity of patient material, as patients are generally diagnosed based on needle biopsies and physicians would be understandably reluctant to undertake more invasive procedures which would not be directly beneficial to the patient. It would therefore perhaps be best to further explore animal models.

The recent generation of an autoimmune mouse model expressing an ubiquitin-binding deficient form of the NF κ B-regulator ABIN1 showed some promise in this field. ABIN1 is an A20 binding protein, required for the deubiquitinating activity of A20 in NF κ B regulation (Mauro et al., 2006). Knock-in of mutant ABIN1

resulted in the enlargement of lymph nodes with increased germinal centre formation in the spleen (Nanda et al., 2011). This was accompanied by increased numbers of follicular helper T cells and cytokine producing germinal centre B cells. Following receptor stimulation, these B cells displayed heightened IKK activity, as well as increased JNK and p38 MAPK activity, all of which are of relevance to HL. Although this particular model was of autoimmunity, it is feasible that further exploration of mutations of NF κ B regulators may result in Hodgkin-like disease.

The discovery of Hodgkin-like lymphoma in domestic ferrets is of great significance to this field (Ammersbach et al., 2008). Further characterisation of this malignancy in the ferret could lead to the generation of a promising animal model of HL. Epidemiological data of out breaks of this devastating malignancy in ferrets implicates an infectious agent and represents a promising opportunity in viral discovery for those pursuing the hunt for an additional viral involvement in HL.

This project has not addressed the activity of protein degradation pathways in EBV-infected HL cells and future work would be needed to rectify this omission. The activities of these pathways are likely to differ from those in uninfected cells, as EBV is known to modulate both the UPS and the autophagy pathway (Masucci, 2004, Williams and Taylor, 2012). This is largely to prevent antigen presentation and to escape viral recognition by the immune system. This could have important implications for the treatment of EBV-positive HL patients if protein degradation pathways were to be pursued as a therapeutic target. Future work may also focus on alternative malignancies with similar multinucleate properties and an immune system involvement. For example, p62 may be useful as a biomarker in mast cell tumours in which the immune interaction is much less complex than that of HL and the tumour cells are more abundant (Welle et al., 2008). This would allow the isolation of primary tumour cells for functional studies into pathway activity and may inform treatment options in the future.

References

- ABBAS, H. A., MACCIO, D. R., COSKUN, S., JACKSON, J. G., HAZEN, A. L., SILLS, T. M., YOU, M. J., HIRSCHI, K. K. & LOZANO, G. 2010. Mdm2 is required for survival of hematopoietic stem cells/progenitors via dampening of ROS-induced p53 activity. *Cell Stem Cell*, 7, 606-17.
- ABDULLAH, L. N. & CHOW, E. K. 2013. Mechanisms of chemoresistance in cancer stem cells. *Clin Transl Med*, 2, 3.
- ALDINUCCI, D., LORENZON, D., CATTARUZZA, L., PINTO, A., GLOGHINI, A., CARBONE, A. & COLOMBATTI, A. 2008. Expression of CCR5 receptors on Reed-Sternberg cells and Hodgkin lymphoma cell lines: involvement of CCL5/Rantes in tumor cell growth and microenvironmental interactions. *Int J Cancer*, 122, 769-76.
- ALDINUCCI, D., LORENZON, D., OLIVO, K., RAPANA, B. & GATTEI, V. 2004. Interactions between tissue fibroblasts in lymph nodes and Hodgkin/Reed-Sternberg cells. *Leuk Lymphoma*, 45, 1731-9.
- ALEMAN, B. M., VAN DEN BELT-DUSEBOUT, A. W., KLOKMAN, W. J., VAN'T VEER, M. B., BARTELINK, H. & VAN LEEUWEN, F. E. 2003. Long-term cause-specific mortality of patients treated for Hodgkin's disease. *J Clin Oncol*, 21, 3431-9.
- AMMERSBACH, M., DELAY, J., CASWELL, J. L., SMITH, D. A., TAYLOR, W. M. & BIENZLE, D. 2008. Laboratory findings, histopathology, and immunophenotype of lymphoma in domestic ferrets. *Vet Pathol*, 45, 663-73.
- ANGEL, C. A., CULLEN, R. A., PRINGLE, J. H. & LAUDER, I. 1992. Vimentin expression by Reed-Sternberg cells in Hodgkin's disease. *Virchows Arch A Pathol Anat Histopathol*, 421, 9-11.
- BABU, J. R., GEETHA, T. & WOOTEN, M. W. 2005. Sequestosome 1/p62 shuttles polyubiquitinated tau for proteasomal degradation. *J Neurochem*, 94, 192-203.
- BAI, D., UENO, L. & VOGT, P. K. 2009. Akt-mediated regulation of NFkappaB and the essentialness of NFkappaB for the oncogenicity of PI3K and Akt. *Int J Cancer*, 125, 2863-70.
- BALL, E. H. & SINGER, S. J. 1981. Association of microtubules and intermediate filaments in normal fibroblasts and its disruption upon transformation by a temperature-sensitive mutant of Rous sarcoma virus. *Proc Natl Acad Sci U S A*, 78, 6986-90.
- BARGAGNA-MOHAN, P., HAMZA, A., KIM, Y. E., KHUAN ABBY HO, Y., MOR-VAKNIN, N., WENDSCHLAG, N., LIU, J., EVANS, R. M., MARKOVITZ, D. M., ZHAN, C. G., KIM, K. B. & MOHAN, R. 2007. The tumor inhibitor and antiangiogenic agent withaferin A targets the intermediate filament protein vimentin. *Chem Biol*, 14, 623-34.
- BARGAGNA-MOHAN, P., PARANTHAN, R. R., HAMZA, A., DIMOVA, N., TRUCCHI, B., SRINIVASAN, C., ELLIOTT, G. I., ZHAN, C. G., LAU, D. L., ZHU, H., KASAHARA, K., INAGAKI, M., CAMBI, F. & MOHAN, R. 2010. Withaferin A targets intermediate filaments glial fibrillary acidic protein and vimentin in a model of retinal gliosis. *J Biol Chem*, 285, 7657-69.
- BARGOU, R. C., EMMERICH, F., KRAPPMANN, D., BOMMERT, K., MAPARA, M. Y., ARNOLD, W., ROYER, H. D., GRINSTEIN, E., GREINER, A., SCHEIDEREIT, C. & DORKEN, B. 1997. Constitutive nuclear factor-kappaB-RelA activation is required for proliferation and survival of Hodgkin's disease tumor cells. *J Clin Invest*, 100, 2961-9.
- BARGOU, R. C., MAPARA, M. Y., ZUGCK, C., DANIEL, P. T., PAWLITA, M., DOHNER, H. & DORKEN, B. 1993. Characterization of a novel Hodgkin cell line, HD-MyZ, with myelomonocytic features mimicking Hodgkin's disease in severe combined immunodeficient mice. *J Exp Med*, 177, 1257-68.
- BASSERMANN, F., EICHNER, R. & PAGANO, M. 2013. The ubiquitin proteasome system - Implications for cell cycle control and the targeted treatment of cancer. *Biochim Biophys Acta*.

- BEHRINGER, K., BREUER, K., REINEKE, T., MAY, M., NOGOVA, L., KLIMM, B., SCHMITZ, T., WILDT, L., DIEHL, V. & ENGERT, A. 2005. Secondary amenorrhea after Hodgkin's lymphoma is influenced by age at treatment, stage of disease, chemotherapy regimen, and the use of oral contraceptives during therapy: a report from the German Hodgkin's Lymphoma Study Group. *J Clin Oncol*, 23, 7555-64.
- BELLODI, C., LIDONNICI, M. R., HAMILTON, A., HELGASON, G. V., SOLIERA, A. R., RONCHETTI, M., GALAVOTTI, S., YOUNG, K. W., SELMI, T., YACOBI, R., VAN ETTEN, R. A., DONATO, N., HUNTER, A., DINSDALE, D., TIRRO, E., VIGNERI, P., NICOTERA, P., DYER, M. J., HOLYOAKE, T., SALOMONI, P. & CALABRETTA, B. 2009. Targeting autophagy potentiates tyrosine kinase inhibitor-induced cell death in Philadelphia chromosome-positive cells, including primary CML stem cells. *J Clin Invest*, 119, 1109-23.
- BERNARDI, R. & PANDOLFI, P. P. 2007. Structure, dynamics and functions of promyelocytic leukaemia nuclear bodies. *Nat Rev Mol Cell Biol*, 8, 1006-16.
- BESTVATER, F., DALLNER, C. & SPIESS, E. 2005. The C-terminal subunit of artificially truncated human cathepsin B mediates its nuclear targeting and contributes to cell viability. *BMC Cell Biol*, 6, 16.
- BLOMMAART, E. F., KRAUSE, U., SCHELLENS, J. P., VREELING-SINDELAROVA, H. & MEIJER, A. J. 1997. The phosphatidylinositol 3-kinase inhibitors wortmannin and LY294002 inhibit autophagy in isolated rat hepatocytes. *Eur J Biochem*, 243, 240-6.
- BLUM, K. A., JOHNSON, J. L., NIEDZWIECKI, D., CANELLOS, G. P., CHESON, B. D. & BARTLETT, N. L. 2007. Single agent bortezomib in the treatment of relapsed and refractory Hodgkin lymphoma: cancer and leukemia Group B protocol 50206. *Leuk Lymphoma*, 48, 1313-9.
- BOMONT, P. & KOENIG, M. 2003. Intermediate filament aggregation in fibroblasts of giant axonal neuropathy patients is aggravated in non dividing cells and by microtubule destabilization. *Hum Mol Genet*, 12, 813-22.
- BONADONNA, G., ZUCALI, R., MONFARDINI, S., DE LENA, M. & USLENGHI, C. 1975. Combination chemotherapy of Hodgkin's disease with adriamycin, bleomycin, vinblastine, and imidazole carboxamide versus MOPP. *Cancer*, 36, 252-9.
- BONNER, W. M., REDON, C. E., DICKEY, J. S., NAKAMURA, A. J., SEDELNIKOVA, O. A., SOLIER, S. & POMMIER, Y. 2008. GammaH2AX and cancer. *Nat Rev Cancer*, 8, 957-67.
- BOYA, P., REGGIORI, F. & CODOGNO, P. 2013. Emerging regulation and functions of autophagy. *Nat Cell Biol*, 15, 713-20.
- BRAUNINGER, A., SCHMITZ, R., BECHTEL, D., RENNE, C., HANSMANN, M. L. & KUPPERS, R. 2006. Molecular biology of Hodgkin's and Reed/Sternberg cells in Hodgkin's lymphoma. *Int J Cancer*, 118, 1853-61.
- BRAUNINGER, A., WACKER, H. H., RAJEWSKY, K., KUPPERS, R. & HANSMANN, M. L. 2003. Typing the histogenetic origin of the tumor cells of lymphocyte-rich classical Hodgkin's lymphoma in relation to tumor cells of classical and lymphocyte-predominance Hodgkin's lymphoma. *Cancer Res*, 63, 1644-51.
- BUGLIO, D., MAMIDIPUDI, V., KHASKHELY, N. M., BRADY, H., HEISE, C., BESTERMAN, J., MARTELL, R. E., MACBETH, K. & YOUNES, A. 2010. The class-I HDAC inhibitor MGCD0103 induces apoptosis in Hodgkin lymphoma cell lines and synergizes with proteasome inhibitors by an HDAC6-independent mechanism. *Br J Haematol*, 151, 387-96.
- BYUN, Y., CHEN, F., CHANG, R., TRIVEDI, M., GREEN, K. J. & CRYNS, V. L. 2001. Caspase cleavage of vimentin disrupts intermediate filaments and promotes apoptosis. *Cell Death Differ*, 8, 443-50.
- CADWELL, K., LIU, J. Y., BROWN, S. L., MIYOSHI, H., LOH, J., LENNERZ, J. K., KISHI, C., KC, W., CARRERO, J. A., HUNT, S., STONE, C. D., BRUNT, E. M., XAVIER, R. J., SLECKMAN, B. P., LI, E., MIZUSHIMA, N., STAPPENBECK, T. S. & VIRGIN, H. W. T. 2008. A key role for autophagy and the autophagy gene Atg16l1 in mouse and human intestinal Paneth cells. *Nature*, 456, 259-63.

- CARBONE, A., GLOGHINI, A., GRUSS, H. J. & PINTO, A. 1995. CD40 ligand is constitutively expressed in a subset of T cell lymphomas and on the microenvironmental reactive T cells of follicular lymphomas and Hodgkin's disease. *Am J Pathol*, 147, 912-22.
- CHEN, L., SMITH, L., WANG, Z. & SMITH, J. B. 2003. Preservation of caspase-3 subunits from degradation contributes to apoptosis evoked by lactacystin: any single lysine or lysine pair of the small subunit is sufficient for ubiquitination. *Mol Pharmacol*, 64, 334-45.
- CHEN, X., ZHONG, Z., XU, Z., CHEN, L. & WANG, Y. 2010. 2',7'-Dichlorodihydrofluorescein as a fluorescent probe for reactive oxygen species measurement: Forty years of application and controversy. *Free Radic Res*, 44, 587-604.
- CHEN, Z. J. 2005. Ubiquitin signalling in the NF-kappaB pathway. *Nat Cell Biol*, 7, 758-65.
- CHHABRA, E. S. & HIGGS, H. N. 2007. The many faces of actin: matching assembly factors with cellular structures. *Nat Cell Biol*, 9, 1110-21.
- CHIU, A., XU, W., HE, B., DILLON, S. R., GROSS, J. A., SIEVERS, E., QIAO, X., SANTINI, P., HYJEK, E., LEE, J. W., CESARMAN, E., CHADBURN, A., KNOWLES, D. M. & CERUTTI, A. 2007. Hodgkin lymphoma cells express TACI and BCMA receptors and generate survival and proliferation signals in response to BAFF and APRIL. *Blood*, 109, 729-39.
- CHOI, A. M., RYTER, S. W. & LEVINE, B. 2013. Autophagy in human health and disease. *N Engl J Med*, 368, 1845-6.
- CHUIKOV, S., LEVI, B. P., SMITH, M. L. & MORRISON, S. J. 2010. Prdm16 promotes stem cell maintenance in multiple tissues, partly by regulating oxidative stress. *Nat Cell Biol*, 12, 999-1006.
- CHUTE, J. P., MURAMOTO, G. G., WHITESIDES, J., COLVIN, M., SAFI, R., CHAO, N. J. & MCDONNELL, D. P. 2006. Inhibition of aldehyde dehydrogenase and retinoid signaling induces the expansion of human hematopoietic stem cells. *Proc Natl Acad Sci U S A*, 103, 11707-12.
- CLAGUE, M. J. & URBE, S. 2010. Ubiquitin: same molecule, different degradation pathways. *Cell*, 143, 682-5.
- CLEVELAND, D. W., YAMANAKA, K. & BOMONT, P. 2009. Gigaxonin controls vimentin organization through a tubulin chaperone-independent pathway. *Hum Mol Genet*, 18, 1384-94.
- COLE, N. B. & LIPPINCOTT-SCHWARTZ, J. 1995. Organization of organelles and membrane traffic by microtubules. *Curr Opin Cell Biol*, 7, 55-64.
- COPPE, J. P., DESPREZ, P. Y., KRTOLICA, A. & CAMPISI, J. 2010. The senescence-associated secretory phenotype: the dark side of tumor suppression. *Annu Rev Pathol*, 5, 99-118.
- CROKER, A. K. & ALLAN, A. L. 2012. Inhibition of aldehyde dehydrogenase (ALDH) activity reduces chemotherapy and radiation resistance of stem-like ALDHhiCD44(+) human breast cancer cells. *Breast Cancer Res Treat*, 133, 75-87.
- CROSAS, B., HANNA, J., KIRKPATRICK, D. S., ZHANG, D. P., TONE, Y., HATHAWAY, N. A., BUECKER, C., LEGGETT, D. S., SCHMIDT, M., KING, R. W., GYGI, S. P. & FINLEY, D. 2006. Ubiquitin chains are remodeled at the proteasome by opposing ubiquitin ligase and deubiquitinating activities. *Cell*, 127, 1401-13.
- DATTA, S. R., DUDEK, H., TAO, X., MASTERS, S., FU, H., GOTOH, Y. & GREENBERG, M. E. 1997. Akt phosphorylation of BAD couples survival signals to the cell-intrinsic death machinery. *Cell*, 91, 231-41.
- DEGENHARDT, K., MATHEW, R., BEAUDOIN, B., BRAY, K., ANDERSON, D., CHEN, G., MUKHERJEE, C., SHI, Y., GELINAS, C., FAN, Y., NELSON, D. A., JIN, S. & WHITE, E. 2006. Autophagy promotes tumor cell survival and restricts necrosis, inflammation, and tumorigenesis. *Cancer Cell*, 10, 51-64.
- DELLAGI, K., TABILIO, A., PORTIER, M. M., VAINCHENKER, W., CASTAIGNE, S., GUICHARD, J., BRETON-GORIUS, J. & BROUET, J. C. 1985. Expression of vimentin intermediate filament cytoskeleton in acute nonlymphoblastic leukemias. *Blood*, 65, 1444-52.

- DESHAIES, R. J. & JOAZEIRO, C. A. 2009. RING domain E3 ubiquitin ligases. *Annu Rev Biochem*, 78, 399-434.
- DEVERAUX, Q., USTRELL, V., PICKART, C. & RECHSTEINER, M. 1994. A 26 S protease subunit that binds ubiquitin conjugates. *J Biol Chem*, 269, 7059-61.
- DICE, J. F. 2007. Chaperone-mediated autophagy. *Autophagy*, 3, 295-9.
- DIEPSTRA, A., POPPEMA, S., BOOT, M., VISSER, L., NOLTE, I. M., NIENS, M., TE MEERMAN, G. J. & VAN DEN BERG, A. 2008. HLA-G protein expression as a potential immune escape mechanism in classical Hodgkin's lymphoma. *Tissue Antigens*, 71, 219-26.
- DIMRI, G. P., LEE, X., BASILE, G., ACOSTA, M., SCOTT, G., ROSKELLEY, C., MEDRANO, E. E., LINSKENS, M., RUBELJ, I., PEREIRA-SMITH, O. & ET AL. 1995. A biomarker that identifies senescent human cells in culture and in aging skin in vivo. *Proc Natl Acad Sci U S A*, 92, 9363-7.
- DOERR, J. R., MALONE, C. S., FIKE, F. M., GORDON, M. S., SOGHOMONIAN, S. V., THOMAS, R. K., TAO, Q., MURRAY, P. G., DIEHL, V., TEITELL, M. A. & WALL, R. 2005. Patterned CpG methylation of silenced B cell gene promoters in classical Hodgkin lymphoma-derived and primary effusion lymphoma cell lines. *J Mol Biol*, 350, 631-40.
- DRAKE, K. R., KANG, M. & KENWORTHY, A. K. 2010. Nucleocytoplasmic distribution and dynamics of the autophagosome marker EGFP-LC3. *PLoS One*, 5, e9806.
- DREXLER, H. G. 1993. Recent results on the biology of Hodgkin and Reed-Sternberg cells. II. Continuous cell lines. *Leuk Lymphoma*, 9, 1-25.
- DUBREUIL, V., MARZESCO, A. M., CORBEIL, D., HUTTNER, W. B. & WILSCH-BRAUNINGER, M. 2007. Midbody and primary cilium of neural progenitors release extracellular membrane particles enriched in the stem cell marker prominin-1. *J Cell Biol*, 176, 483-95.
- DUKERS, D. F., VAN GALEN, J. C., GIROTH, C., JANSEN, P., SEWALT, R. G., OTTE, A. P., KLUIN-NELEMANS, H. C., MEIJER, C. J. & RAAPHORST, F. M. 2004. Unique polycomb gene expression pattern in Hodgkin's lymphoma and Hodgkin's lymphoma-derived cell lines. *Am J Pathol*, 164, 873-81.
- DUNCAN, E. M., MURATORE-SCHROEDER, T. L., COOK, R. G., GARCIA, B. A., SHABANOWITZ, J., HUNT, D. F. & ALLIS, C. D. 2008. Cathepsin L proteolytically processes histone H3 during mouse embryonic stem cell differentiation. *Cell*, 135, 284-94.
- DURAN, A., SERRANO, M., LEITGES, M., FLORES, J. M., PICARD, S., BROWN, J. P., MOSCAT, J. & DIAZ-MECO, M. T. 2004. The atypical PKC-interacting protein p62 is an important mediator of RANK-activated osteoclastogenesis. *Dev Cell*, 6, 303-9.
- DUTTON, A., REYNOLDS, G. M., DAWSON, C. W., YOUNG, L. S. & MURRAY, P. G. 2005. Constitutive activation of phosphatidylinositol 3 kinase contributes to the survival of Hodgkin's lymphoma cells through a mechanism involving Akt kinase and mTOR. *J Pathol*, 205, 498-506.
- DYLLA, S. J., BEVIGLIA, L., PARK, I. K., CHARTIER, C., RAVAL, J., NGAN, L., PICKELL, K., AGUILAR, J., LAZETIC, S., SMITH-BERDAN, S., CLARKE, M. F., HOEY, T., LEWICKI, J. & GURNEY, A. L. 2008. Colorectal cancer stem cells are enriched in xenogeneic tumors following chemotherapy. *PLoS One*, 3, e2428.
- EICHENAUER, D. A. & ENGERT, A. 2011. One size for all in Hodgkin lymphoma? *Blood*, 117, 2557-8.
- EICHENAUER, D. A. & ENGERT, A. 2012. Advances in the treatment of Hodgkin lymphoma. *Int J Hematol*, 96, 535-43.
- ELLIOTT, S., TAYLOR, K., WHITE, S., RODWELL, R., MARLTON, P., MEAGHER, D., WILEY, J., TAYLOR, D., WRIGHT, S. & TIMMS, P. 1992. Proof of differentiative mode of action of all-trans retinoic acid in acute promyelocytic leukemia using X-linked clonal analysis. *Blood*, 79, 1916-9.
- EMMERICH, F., MEISER, M., HUMMEL, M., DEMEL, G., FOSS, H. D., JUNDT, F., MATHAS, S., KRAPPMANN, D., SCHEIDEREIT, C., STEIN, H. & DORKEN, B. 1999. Overexpression of I kappa B alpha without inhibition of NF-kappaB activity and mutations in the I kappa B alpha gene in Reed-Sternberg cells. *Blood*, 94, 3129-34.

- EMMERICH, F., THEURICH, S., HUMMEL, M., HAEFFKER, A., VRY, M. S., DOHNER, K., BOMMERT, K., STEIN, H. & DORKEN, B. 2003. Inactivating I kappa B epsilon mutations in Hodgkin/Reed-Sternberg cells. *J Pathol*, 201, 413-20.
- ENGERT, A., DIEHL, V., FRANKLIN, J., LOHRI, A., DORKEN, B., LUDWIG, W. D., KOCH, P., HANEL, M., PFREUNDSCHUH, M., WILHELM, M., TRUMPER, L., AULITZKY, W. E., BENTZ, M., RUMMEL, M., SEZER, O., MULLER-HERMELINK, H. K., HASENCLEVER, D. & LOFFLER, M. 2009. Escalated-dose BEACOPP in the treatment of patients with advanced-stage Hodgkin's lymphoma: 10 years of follow-up of the GHSG HD9 study. *J Clin Oncol*, 27, 4548-54.
- ENGERT, A., PLUTSCHOW, A., EICH, H. T., LOHRI, A., DORKEN, B., BORCHMANN, P., BERGER, B., GREIL, R., WILLBORN, K. C., WILHELM, M., DEBUS, J., EBLE, M. J., SOKLER, M., HO, A., RANK, A., GANSER, A., TRUMPER, L., BOKEMEYER, C., KIRCHNER, H., SCHUBERT, J., KRAL, Z., FUCHS, M., MULLER-HERMELINK, H. K., MULLER, R. P. & DIEHL, V. 2010. Reduced treatment intensity in patients with early-stage Hodgkin's lymphoma. *N Engl J Med*, 363, 640-52.
- ERTMER, A., HUBER, V., GILCH, S., YOSHIMORI, T., ERFLE, V., DUUYSTER, J., ELSASSER, H. P. & SCHATZL, H. M. 2007. The anticancer drug imatinib induces cellular autophagy. *Leukemia*, 21, 936-42.
- FABUNMI, R. P., WIGLEY, W. C., THOMAS, P. J. & DEMARTINO, G. N. 2001. Interferon gamma regulates accumulation of the proteasome activator PA28 and immunoproteasomes at nuclear PML bodies. *J Cell Sci*, 114, 29-36.
- FADER, C. M., SANCHEZ, D., FURLAN, M. & COLOMBO, M. I. 2008. Induction of autophagy promotes fusion of multivesicular bodies with autophagic vacuoles in k562 cells. *Traffic*, 9, 230-50.
- FINLEY, D. 2009. Recognition and processing of ubiquitin-protein conjugates by the proteasome. *Annu Rev Biochem*, 78, 477-513.
- FISCHER, M., JUREMALM, M., OLSSON, N., BACKLIN, C., SUNDSTROM, C., NILSSON, K., ENBLAD, G. & NILSSON, G. 2003. Expression of CCL5/RANTES by Hodgkin and Reed-Sternberg cells and its possible role in the recruitment of mast cells into lymphomatous tissue. *Int J Cancer*, 107, 197-201.
- FIUMARA, P., SNELL, V., LI, Y., MUKHOPADHYAY, A., YOUNES, M., GILLENWATER, A. M., CABANILLAS, F., AGGARWAL, B. B. & YOUNES, A. 2001. Functional expression of receptor activator of nuclear factor kappaB in Hodgkin disease cell lines. *Blood*, 98, 2784-90.
- FLETCHER, D. A. & MULLINS, R. D. 2010. Cell mechanics and the cytoskeleton. *Nature*, 463, 485-92.
- FORTUN, J., DUNN, W. A., JR., JOY, S., LI, J. & NOTTERPEK, L. 2003. Emerging role for autophagy in the removal of aggresomes in Schwann cells. *J Neurosci*, 23, 10672-80.
- FOSS, H. D., HERBST, H., GOTTSTEIN, S., DEMEL, G., ARAUJO, I. & STEIN, H. 1996. Interleukin-8 in Hodgkin's disease. Preferential expression by reactive cells and association with neutrophil density. *Am J Pathol*, 148, 1229-36.
- FOSS, H. D., REUSCH, R., DEMEL, G., LENZ, G., ANAGNOSTOPOULOS, I., HUMMEL, M. & STEIN, H. 1999. Frequent expression of the B-cell-specific activator protein in Reed-Sternberg cells of classical Hodgkin's disease provides further evidence for its B-cell origin. *Blood*, 94, 3108-13.
- FRESNO VARA, J. A., CASADO, E., DE CASTRO, J., CEJAS, P., BELDA-INIESTA, C. & GONZALEZ-BARON, M. 2004. PI3K/Akt signalling pathway and cancer. *Cancer Treat Rev*, 30, 193-204.
- FUJITA, N., ITOH, T., OMORI, H., FUKUDA, M., NODA, T. & YOSHIMORI, T. 2008. The Atg16L complex specifies the site of LC3 lipidation for membrane biogenesis in autophagy. *Mol Biol Cell*, 19, 2092-100.
- FUNG, C., LOCK, R., GAO, S., SALAS, E. & DEBNATH, J. 2008. Induction of autophagy during extracellular matrix detachment promotes cell survival. *Mol Biol Cell*, 19, 797-806.
- FURST, D. E. 1996. Pharmacokinetics of hydroxychloroquine and chloroquine during treatment of rheumatic diseases. *Lupus*, 5 Suppl 1, S11-5.

- FURUTA, N. & AMANO, A. 2010. Cellular machinery to fuse antimicrobial autophagosome with lysosome. *Commun Integr Biol*, 3, 385-7.
- FURUTA, N., FUJITA, N., NODA, T., YOSHIMORI, T. & AMANO, A. 2010. Combinational soluble N-ethylmaleimide-sensitive factor attachment protein receptor proteins VAMP8 and Vti1b mediate fusion of antimicrobial and canonical autophagosomes with lysosomes. *Mol Biol Cell*, 21, 1001-10.
- GATTO, D. & BRINK, R. 2010. The germinal center reaction. *J Allergy Clin Immunol*, 126, 898-907; quiz 908-9.
- GEETHA, T., SEIBENHENER, M. L., CHEN, L., MADURA, K. & WOOTEN, M. W. 2008. p62 serves as a shuttling factor for TrkA interaction with the proteasome. *Biochem Biophys Res Commun*, 374, 33-7.
- GEISLER, S., HOLMSTROM, K. M., SKUJAT, D., FIESEL, F. C., ROTHFUSS, O. C., KAHLE, P. J. & SPRINGER, W. 2010. PINK1/Parkin-mediated mitophagy is dependent on VDAC1 and p62/SQSTM1. *Nat Cell Biol*, 12, 119-31.
- GHIAUR, G., GERBER, J. & JONES, R. J. 2012. Concise review: Cancer stem cells and minimal residual disease. *Stem Cells*, 30, 89-93.
- GIANNI, M., PONZANELLI, I., MOLOGNI, L., REICHERT, U., RAMBALDI, A., TERAIO, M. & GARATTINI, E. 2000. Retinoid-dependent growth inhibition, differentiation and apoptosis in acute promyelocytic leukemia cells. Expression and activation of caspases. *Cell Death Differ*, 7, 447-60.
- GINESTIER, C., WICINSKI, J., CERVERA, N., MONVILLE, F., FINETTI, P., BERTUCCI, F., WICHA, M. S., BIRNBAUM, D. & CHARAFE-JAUFFRET, E. 2009. Retinoid signaling regulates breast cancer stem cell differentiation. *Cell Cycle*, 8, 3297-302.
- GLICK, D., BARTH, S. & MACLEOD, K. F. 2010. Autophagy: cellular and molecular mechanisms. *J Pathol*, 221, 3-12.
- GLIMELIUS, I., EDSTROM, A., AMINI, R. M., FISCHER, M., NILSSON, G., SUNDSTROM, C., ENBLAD, G. & MOLIN, D. 2006. IL-9 expression contributes to the cellular composition in Hodgkin lymphoma. *Eur J Haematol*, 76, 278-83.
- GOCHEVA, V., ZENG, W., KE, D., KLIMSTRA, D., REINHECKEL, T., PETERS, C., HANAHAAN, D. & JOYCE, J. A. 2006. Distinct roles for cysteine cathepsin genes in multistage tumorigenesis. *Genes Dev*, 20, 543-56.
- GOLEBIEWSKA, A., BRONS, N. H., BJERKVIG, R. & NICLOU, S. P. 2011. Critical appraisal of the side population assay in stem cell and cancer stem cell research. *Cell Stem Cell*, 8, 136-47.
- GOODELL, M. A., BROSE, K., PARADIS, G., CONNER, A. S. & MULLIGAN, R. C. 1996. Isolation and functional properties of murine hematopoietic stem cells that are replicating in vivo. *J Exp Med*, 183, 1797-806.
- GORDON, D. J., RESIO, B. & PELLMAN, D. 2012. Causes and consequences of aneuploidy in cancer. *Nat Rev Genet*, 13, 189-203.
- GOULET, B., BARUCH, A., MOON, N. S., POIRIER, M., SANSREGRET, L. L., ERICKSON, A., BOGYO, M. & NEPVEU, A. 2004. A cathepsin L isoform that is devoid of a signal peptide localizes to the nucleus in S phase and processes the CDP/Cux transcription factor. *Mol Cell*, 14, 207-19.
- GOYAL, S. D. & BARTLETT, N. L. 2012. Where does brentuximab vedotin fit into the management of patients with Hodgkin lymphoma? *Curr Hematol Malig Rep*, 7, 179-85.
- GROETTRUP, M., KIRK, C. J. & BASLER, M. 2010. Proteasomes in immune cells: more than peptide producers? *Nat Rev Immunol*, 10, 73-8.
- GROUP, N. C. R. I. L. C. S. 2013. *NCRN487: A+AVD vs ABVD in first line advanced Hodgkin lymphoma*. [Online]. Available: <http://public.ukcrn.org.uk/Search/StudyDetail.aspx?StudyID=13505>.

- GROVER, A., SHANDILYA, A., PUNETHA, A., BISARIA, V. S. & SUNDAR, D. 2010. Inhibition of the NEMO/IKKbeta association complex formation, a novel mechanism associated with the NF-kappaB activation suppression by *Withania somnifera*'s key metabolite withaferin A. *BMC Genomics*, 11 Suppl 4, S25.
- GRUSS, H. J., SCHEFFRAHN, I., HUBINGER, G., DUYSER, J. & HERMANN, F. 1996. The CD30 ligand and CD40 ligand regulate CD54 surface expression and release of its soluble form by cultured Hodgkin and Reed-Sternberg cells. *Leukemia*, 10, 829-35.
- GUAN, H., XIE, L., LEITHAUSER, F., FLOSSBACH, L., MOLLER, P., WIRTH, T. & USHMOROV, A. 2010. KLF4 is a tumor suppressor in B-cell non-Hodgkin lymphoma and in classic Hodgkin lymphoma. *Blood*, 116, 1469-78.
- GUTIERREZ, M. G., MUNAFO, D. B., BERON, W. & COLOMBO, M. I. 2004. Rab7 is required for the normal progression of the autophagic pathway in mammalian cells. *J Cell Sci*, 117, 2687-97.
- HAMASAKI, M., SHIBUTANI, S. T. & YOSHIMORI, T. 2013. Up-to-date membrane biogenesis in the autophagosome formation. *Curr Opin Cell Biol*, 25, 455-60.
- HAMAZAKI, J., IEMURA, S., NATSUME, T., YASHIRODA, H., TANAKA, K. & MURATA, S. 2006. A novel proteasome interacting protein recruits the deubiquitinating enzyme UCH37 to 26S proteasomes. *EMBO J*, 25, 4524-36.
- HARRINGTON, L. 2004. Does the reservoir for self-renewal stem from the ends? *Oncogene*, 23, 7283-9.
- HARRIS, J. 2011. Autophagy and cytokines. *Cytokine*, 56, 140-4.
- HEDVAT, C. V., JAFFE, E. S., QIN, J., FILIPPA, D. A., CORDON-CARDO, C., TOSATO, G., NIMER, S. D. & TERUYA-FELDSTEIN, J. 2001. Macrophage-derived chemokine expression in classical Hodgkin's lymphoma: application of tissue microarrays. *Mod Pathol*, 14, 1270-6.
- HERBST, H., FOSS, H. D., SAMOL, J., ARAUJO, I., KLOTZBACH, H., KRAUSE, H., AGATHANGELOU, A., NIEDOBITEK, G. & STEIN, H. 1996. Frequent expression of interleukin-10 by Epstein-Barr virus-harboring tumor cells of Hodgkin's disease. *Blood*, 87, 2918-29.
- HERRMANN, H., BAR, H., KREPLAK, L., STRELKOV, S. V. & AEBI, U. 2007. Intermediate filaments: from cell architecture to nanomechanics. *Nat Rev Mol Cell Biol*, 8, 562-73.
- HERTEL, C. B., ZHOU, X. G., HAMILTON-DUTOIT, S. J. & JUNKER, S. 2002. Loss of B cell identity correlates with loss of B cell-specific transcription factors in Hodgkin/Reed-Sternberg cells of classical Hodgkin lymphoma. *Oncogene*, 21, 4908-20.
- HORWITZ, S. B. 1994. Taxol (paclitaxel): mechanisms of action. *Ann Oncol*, 5 Suppl 6, S3-6.
- HOUSLAY, M. D. & CHRISTIAN, F. 2010. p62 (SQSTM1) forms part of a novel, reversible aggregate containing a specific conformer of the cAMP degrading phosphodiesterase, PDE4A4. *Autophagy*, 6, 1198-200.
- HSU, P. L., LIN, Y. C. & HSU, S. M. 1991. Expression of macrophage colony-stimulating factor (M-CSF) in two Hodgkin's Reed-Sternberg (H-RS) cell lines, HDLM-1 and KM-H2, and in H-RS cells in tissues. *Int J Hematol*, 54, 315-26.
- HSU, S. M. & HSU, P. L. 1986. Phenotypes and phorbol ester-induced differentiation of human histiocytic lymphoma cell lines (U-937 and SU-DHL-1) and Reed-Sternberg cells. *Am J Pathol*, 122, 223-30.
- HSU, S. M. & HSU, P. L. 1994. The nature of Reed-Sternberg cells: phenotype, genotype, and other properties. *Crit Rev Oncog*, 5, 213-45.
- HSU, S. M., ZHAO, X., CHAKRABORTY, S., LIU, Y. F., WHANG-PENG, J., LOK, M. S. & FUKUHARA, S. 1988. Reed-Sternberg cells in Hodgkin's cell lines HDLM, L-428, and KM-H2 are not actively replicating: lack of bromodeoxyuridine uptake by multinuclear cells in culture. *Blood*, 71, 1382-9.
- HU, C. K., COUGHLIN, M. & MITCHISON, T. J. 2012. Midbody assembly and its regulation during cytokinesis. *Mol Biol Cell*, 23, 1024-34.

- HUSNJAK, K., ELSASSER, S., ZHANG, N., CHEN, X., RANGLES, L., SHI, Y., HOFMANN, K., WALTERS, K. J., FINLEY, D. & DIKIC, I. 2008. Proteasome subunit Rpn13 is a novel ubiquitin receptor. *Nature*, 453, 481-8.
- ICHIJIMA, Y., SAKASAI, R., OKITA, N., ASAHINA, K., MIZUTANI, S. & TERAOKA, H. 2005. Phosphorylation of histone H2AX at M phase in human cells without DNA damage response. *Biochem Biophys Res Commun*, 336, 807-12.
- IKEDA, J., MAMAT, S., TIAN, T., WANG, Y., LUO, W., RAHADIANI, N., AOZASA, K. & MORII, E. 2012. Reactive oxygen species and aldehyde dehydrogenase activity in Hodgkin lymphoma cells. *Lab Invest*, 92, 606-14.
- IKEDA, J., MAMAT, S., TIAN, T., WANG, Y., RAHADIANI, N., AOZASA, K. & MORII, E. 2010. Tumorigenic potential of mononucleated small cells of Hodgkin lymphoma cell lines. *Am J Pathol*, 177, 3081-8.
- INAMI, Y., WAGURI, S., SAKAMOTO, A., KOUNO, T., NAKADA, K., HINO, O., WATANABE, S., ANDO, J., IWADATE, M., YAMAMOTO, M., LEE, M. S., TANAKA, K. & KOMATSU, M. 2011. Persistent activation of Nrf2 through p62 in hepatocellular carcinoma cells. *J Cell Biol*, 193, 275-84.
- ITAKURA, E. & MIZUSHIMA, N. 2010. Characterization of autophagosome formation site by a hierarchical analysis of mammalian Atg proteins. *Autophagy*, 6, 764-76.
- ITO, K., BERNARDI, R., MOROTTI, A., MATSUOKA, S., SAGLIO, G., IKEDA, Y., ROSENBLATT, J., AVIGAN, D. E., TERUYA-FELDSTEIN, J. & PANDOLFI, P. P. 2008. PML targeting eradicates quiescent leukaemia-initiating cells. *Nature*, 453, 1072-8.
- ITO, K., HIRAO, A., ARAI, F., MATSUOKA, S., TAKUBO, K., HAMAGUCHI, I., NOMIYAMA, K., HOSOKAWA, K., SAKURADA, K., NAKAGATA, N., IKEDA, Y., MAK, T. W. & SUDA, T. 2004. Regulation of oxidative stress by ATM is required for self-renewal of haematopoietic stem cells. *Nature*, 431, 997-1002.
- ITOH, K., TONG, K. I. & YAMAMOTO, M. 2004. Molecular mechanism activating Nrf2-Keap1 pathway in regulation of adaptive response to electrophiles. *Free Radic Biol Med*, 36, 1208-13.
- IWATA, A., RILEY, B. E., JOHNSTON, J. A. & KOPITO, R. R. 2005. HDAC6 and microtubules are required for autophagic degradation of aggregated huntingtin. *J Biol Chem*, 280, 40282-92.
- IZBAN, K. F., WRONE-SMITH, T., HSI, E. D., SCHNITZER, B., QUEVEDO, M. E. & ALKAN, S. 1999. Characterization of the interleukin-1beta-converting enzyme/ced-3-family protease, caspase-3/ CPP32, in Hodgkin's disease: lack of caspase-3 expression in nodular lymphocyte predominance Hodgkin's disease. *Am J Pathol*, 154, 1439-47.
- JAGER, S., BUCCI, C., TANIDA, I., UENO, T., KOMINAMI, E., SAFTIG, P. & ESKELINEN, E. L. 2004. Role for Rab7 in maturation of late autophagic vacuoles. *J Cell Sci*, 117, 4837-48.
- JAIN, A., LAMARK, T., SJOTTEM, E., LARSEN, K. B., AWUH, J. A., OVERVATN, A., MCMAHON, M., HAYES, J. D. & JOHANSEN, T. 2010. p62/SQSTM1 is a target gene for transcription factor NRF2 and creates a positive feedback loop by inducing antioxidant response element-driven gene transcription. *J Biol Chem*, 285, 22576-91.
- JANER, A., MARTIN, E., MURIEL, M. P., LATOUCHE, M., FUJIGASAKI, H., RUBERG, M., BRICE, A., TROTTIER, Y. & SITTLER, A. 2006. PML clastosomes prevent nuclear accumulation of mutant ataxin-7 and other polyglutamine proteins. *J Cell Biol*, 174, 65-76.
- JANZ, M., STUHMER, T., VASSILEV, L. T. & BARGOU, R. C. 2007. Pharmacologic activation of p53-dependent and p53-independent apoptotic pathways in Hodgkin/Reed-Sternberg cells. *Leukemia*, 21, 772-9.
- JARRETT, R. F., KRAJEWSKI, A. S., ANGUS, B., FREELAND, J., TAYLOR, P. R., TAYLOR, G. M. & ALEXANDER, F. E. 2003. The Scotland and Newcastle epidemiological study of Hodgkin's disease: impact of histopathological review and EBV status on incidence estimates. *J Clin Pathol*, 56, 811-6.

- JIN, Z., LI, Y., PITTI, R., LAWRENCE, D., PHAM, V. C., LILL, J. R. & ASHKENAZI, A. 2009. Cullin3-based polyubiquitination and p62-dependent aggregation of caspase-8 mediate extrinsic apoptosis signaling. *Cell*, 137, 721-35.
- JOHANSEN, T. & LAMARK, T. 2011. Selective autophagy mediated by autophagic adapter proteins. *Autophagy*, 7, 279-96.
- JONES, R. J., GOCKE, C. D., KASAMON, Y. L., MILLER, C. B., PERKINS, B., BARBER, J. P., VALA, M. S., GERBER, J. M., GELLERT, L. L., SIEDNER, M., LEMAS, M. V., BRENNAN, S., AMBINDER, R. F. & MATSUI, W. 2009. Circulating clonotypic B cells in classic Hodgkin lymphoma. *Blood*, 113, 5920-6.
- JOOS, S., KUPPER, M., OHL, S., VON BONIN, F., MECHTERSHEIMER, G., BENTZ, M., MARYNEN, P., MOLLER, P., PFREUNDSCHUH, M., TRUMPER, L. & LICHTER, P. 2000. Genomic imbalances including amplification of the tyrosine kinase gene JAK2 in CD30+ Hodgkin cells. *Cancer Res*, 60, 549-52.
- JOOS, S., MENZ, C. K., WROBEL, G., SIEBERT, R., GESK, S., OHL, S., MECHTERSHEIMER, G., TRUMPER, L., MOLLER, P., LICHTER, P. & BARTH, T. F. 2002. Classical Hodgkin lymphoma is characterized by recurrent copy number gains of the short arm of chromosome 2. *Blood*, 99, 1381-7.
- JOSTING, A., FRANKLIN, J., MAY, M., KOCH, P., BEYKIRCH, M. K., HEINZ, J., RUDOLPH, C., DIEHL, V. & ENGERT, A. 2002. New prognostic score based on treatment outcome of patients with relapsed Hodgkin's lymphoma registered in the database of the German Hodgkin's lymphoma study group. *J Clin Oncol*, 20, 221-30.
- JOSTING, A., RUEFFER, U., FRANKLIN, J., SIEBER, M., DIEHL, V. & ENGERT, A. 2000. Prognostic factors and treatment outcome in primary progressive Hodgkin lymphoma: a report from the German Hodgkin Lymphoma Study Group. *Blood*, 96, 1280-6.
- JUNDT, F., ACIKGOZ, O., KWON, S. H., SCHWARZER, R., ANAGNOSTOPOULOS, I., WIESNER, B., MATHAS, S., HUMMEL, M., STEIN, H., REICHARDT, H. M. & DORKEN, B. 2008. Aberrant expression of Notch1 interferes with the B-lymphoid phenotype of neoplastic B cells in classical Hodgkin lymphoma. *Leukemia*, 22, 1587-94.
- JUNDT, F., ANAGNOSTOPOULOS, I., BOMMERT, K., EMMERICH, F., MULLER, G., FOSS, H. D., ROYER, H. D., STEIN, H. & DORKEN, B. 1999. Hodgkin/Reed-Sternberg cells induce fibroblasts to secrete eotaxin, a potent chemoattractant for T cells and eosinophils. *Blood*, 94, 2065-71.
- JUNGNICKEL, B., STARATSCHEK-JOX, A., BRAUNINGER, A., SPIEKER, T., WOLF, J., DIEHL, V., HANSMANN, M. L., RAJEWSKY, K. & KUPPERS, R. 2000. Clonal deleterious mutations in the I kappa B alpha gene in the malignant cells in Hodgkin's lymphoma. *J Exp Med*, 191, 395-402.
- JUNN, E., LEE, S. S., SUHR, U. T. & MOURADIAN, M. M. 2002. Parkin accumulation in aggresomes due to proteasome impairment. *J Biol Chem*, 277, 47870-7.
- JUSZCZYNSKI, P., OUYANG, J., MONTI, S., RODIG, S. J., TAKEYAMA, K., ABRAMSON, J., CHEN, W., KUTOK, J. L., RABINOVICH, G. A. & SHIPP, M. A. 2007. The AP1-dependent secretion of galectin-1 by Reed Sternberg cells fosters immune privilege in classical Hodgkin lymphoma. *Proc Natl Acad Sci U S A*, 104, 13134-9.
- KAILEH, M., VANDEN BERGHE, W., HEYERICK, A., HORION, J., PIETTE, J., LIBERT, C., DE KEUKELEIRE, D., ESSAWI, T. & HAEGEMAN, G. 2007. Withaferin A strongly elicits I kappa B kinase beta hyperphosphorylation concomitant with potent inhibition of its kinase activity. *J Biol Chem*, 282, 4253-64.
- KANZLER, H., KUPPERS, R., HANSMANN, M. L. & RAJEWSKY, K. 1996. Hodgkin and Reed-Sternberg cells in Hodgkin's disease represent the outgrowth of a dominant tumor clone derived from (crippled) germinal center B cells. *J Exp Med*, 184, 1495-505.
- KAPP, U., DUX, A., SCHELL-FREDERICK, E., BANIK, N., HUMMEL, M., MUCKE, S., FONATSCH, C., BULLERDIEK, J., GOTTSSTEIN, C., ENGERT, A. & ET AL. 1994. Disseminated growth of Hodgkin's-derived cell lines L540 and L540cy in immune-deficient SCID mice. *Ann Oncol*, 5 Suppl 1, 121-6.

- KAPP, U., WOLF, J., HUMMEL, M., PAWLITA, M., VON KALLE, C., DALLENBACH, F., SCHWONZEN, M., KRUEGER, G. R., MULLER-LANTZSCH, N., FONATSCH, C. & ET AL. 1993. Hodgkin's lymphoma-derived tissue serially transplanted into severe combined immunodeficient mice. *Blood*, 82, 1247-56.
- KAPP, U., WOLF, J., VON KALLE, C., TAWADROS, S., ROTTGEN, A., ENGERT, A., FONATSCH, C., STEIN, H. & DIEHL, V. 1992. Preliminary report: growth of Hodgkin's lymphoma derived cells in immune compromised mice. *Ann Oncol*, 3 Suppl 4, 21-3.
- KASAMON, Y. L., JACENE, H. A., GOCKE, C. D., SWINNEN, L. J., GLADSTONE, D. E., PERKINS, B., LINK, B. K., POPPLEWELL, L. L., HABERMANN, T. M., HERMAN, J. M., MATSUI, W. H., JONES, R. J. & AMBINDER, R. F. 2012. Phase 2 study of rituximab-ABVD in classical Hodgkin lymphoma. *Blood*, 119, 4129-32.
- KASHKAR, H., DEGGERICH, A., SEEGER, J. M., YAZDANPANAH, B., WIEGMANN, K., HAUBERT, D., PONGRATZ, C. & KRONKE, M. 2007. NF-kappaB-independent down-regulation of XIAP by bortezomib sensitizes HL B cells against cytotoxic drugs. *Blood*, 109, 3982-8.
- KATO, M., SANADA, M., KATO, I., SATO, Y., TAKITA, J., TAKEUCHI, K., NIWA, A., CHEN, Y., NAKAZAKI, K., NOMOTO, J., ASAKURA, Y., MUTO, S., TAMURA, A., IIO, M., AKATSUKA, Y., HAYASHI, Y., MORI, H., IGARASHI, T., KUROKAWA, M., CHIBA, S., MORI, S., ISHIKAWA, Y., OKAMOTO, K., TOBINAI, K., NAKAGAMA, H., NAKAHATA, T., YOSHINO, T., KOBAYASHI, Y. & OGAWA, S. 2009. Frequent inactivation of A20 in B-cell lymphomas. *Nature*, 459, 712-6.
- KATO, N., FUJIMOTO, H., YODA, A., OISHI, I., MATSUMURA, N., KONDO, T., TSUKADA, J., TANAKA, Y., IMAMURA, M. & MINAMI, Y. 2004. Regulation of Chk2 gene expression in lymphoid malignancies: involvement of epigenetic mechanisms in Hodgkin's lymphoma cell lines. *Cell Death Differ*, 11 Suppl 2, S153-61.
- KAWAGUCHI, Y., KOVACS, J. J., MCLAURIN, A., VANCE, J. M., ITO, A. & YAO, T. P. 2003. The deacetylase HDAC6 regulates aggresome formation and cell viability in response to misfolded protein stress. *Cell*, 115, 727-38.
- KAWAI, K., SAITO, A., SUDO, T. & OSADA, H. 2008. Specific regulation of cytokine-dependent p38 MAP kinase activation by p62/SQSTM1. *J Biochem*, 143, 765-72.
- KERPPOLA, T. K. 2009. Polycomb group complexes--many combinations, many functions. *Trends Cell Biol*, 19, 692-704.
- KILGER, E., KIESER, A., BAUMANN, M. & HAMMERSCHMIDT, W. 1998. Epstein-Barr virus-mediated B-cell proliferation is dependent upon latent membrane protein 1, which simulates an activated CD40 receptor. *EMBO J*, 17, 1700-9.
- KIM, J. Y. & OZATO, K. 2009. The sequestosome 1/p62 attenuates cytokine gene expression in activated macrophages by inhibiting IFN regulatory factor 8 and TNF receptor-associated factor 6/NF-kappaB activity. *J Immunol*, 182, 2131-40.
- KIMURA, S., NODA, T. & YOSHIMORI, T. 2008. Dynein-dependent movement of autophagosomes mediates efficient encounters with lysosomes. *Cell Struct Funct*, 33, 109-22.
- KIRKIN, V., LAMARK, T., SOU, Y. S., BJORKOY, G., NUNN, J. L., BRUUN, J. A., SHVETS, E., MCEWAN, D. G., CLAUSEN, T. H., WILD, P., BILUSIC, I., THEURILLAT, J. P., OVERVATN, A., ISHII, T., ELAZAR, Z., KOMATSU, M., DIKIC, I. & JOHANSEN, T. 2009. A role for NBR1 in autophagosomal degradation of ubiquitinated substrates. *Mol Cell*, 33, 505-16.
- KIRSCHBAUM, M. H., GOLDMAN, B. H., ZAIN, J. M., COOK, J. R., RIMSZA, L. M., FORMAN, S. J. & FISHER, R. I. 2012. A phase 2 study of vorinostat for treatment of relapsed or refractory Hodgkin lymphoma: Southwest Oncology Group Study S0517. *Leuk Lymphoma*, 53, 259-62.
- KLEIN, U. & DALLA-FAVERA, R. 2008. Germinal centres: role in B-cell physiology and malignancy. *Nat Rev Immunol*, 8, 22-33.
- KLIONSKY, D. J., ABDALLA, F. C., ABELIOVICH, H., ABRAHAM, R. T., ACEVEDO-ARZENA, A., ADELI, K., AGHOLME, L., AGNELLO, M., AGOSTINIS, P., AGUIRRE-GHISO, J. A., AHN, H. J., AIT-MOHAMED, O., AIT-SI-ALI, S., AKEMATSU, T., AKIRA, S., AL-YOUNES, H. M., AL-ZEER, M. A., ALBERT, M. L., ALBIN, R. L., ALEGRE-ABARRATEGUI, J., ALEO, M. F., ALIREZAEI, M., ALMASAN,

A., ALMONTE-BECERRIL, M., AMANO, A., AMARAVADI, R., AMARNATH, S., AMER, A. O., ANDRIEU-ABADIE, N., ANANTHARAM, V., ANN, D. K., ANOOPKUMAR-DUKIE, S., AOKI, H., APOSTOLOVA, N., ARANCIA, G., ARIS, J. P., ASANUMA, K., ASARE, N. Y., ASHIDA, H., ASKANAS, V., ASKEW, D. S., AUBERGER, P., BABA, M., BACKUES, S. K., BAEHRECKE, E. H., BAHR, B. A., BAI, X. Y., BAILLY, Y., BAIOCCHI, R., BALDINI, G., BALDUINI, W., BALLABIO, A., BAMBER, B. A., BAMPION, E. T., BANHEGYI, G., BARTHOLOMEW, C. R., BASSHAM, D. C., BAST, R. C., JR., BATOKO, H., BAY, B. H., BEAU, I., BECHET, D. M., BEGLEY, T. J., BEHL, C., BEHREND, C., BEKRI, S., BELLAIRE, B., BENDALL, L. J., BENETTI, L., BERLIOCCI, L., BERNARDI, H., BERNASSOLA, F., BESTEIRO, S., BHATIA-KISSOVA, I., BI, X., BIARD-PIECHACZYK, M., BLUM, J. S., BOISE, L. H., BONALDO, P., BOONE, D. L., BORNHAUSER, B. C., BORTOLUCI, K. R., BOSSIS, I., BOST, F., BOURQUIN, J. P., BOYA, P., BOYER-GUITTAUT, M., BOZHKO, P. V., BRADY, N. R., BRANCOLINI, C., BRECH, A., BRENNAN, J. E., BRENNAND, A., BRESNICK, E. H., BREST, P., BRIDGES, D., BRISTOL, M. L., BROOKES, P. S., BROWN, E. J., BRUMELL, J. H., et al. 2012. Guidelines for the use and interpretation of assays for monitoring autophagy. *Autophagy*, 8, 445-544.

KNECHT, H., SAWAN, B., LICHTENSZTEJN, D., LEMIEUX, B., WELLINGER, R. J. & MAI, S. 2009. The 3D nuclear organization of telomeres marks the transition from Hodgkin to Reed-Sternberg cells. *Leukemia*, 23, 565-73.

KOBAYASHI, A., KANG, M. I., OKAWA, H., OHTSUJI, M., ZENKE, Y., CHIBA, T., IGARASHI, K. & YAMAMOTO, M. 2004. Oxidative stress sensor Keap1 functions as an adaptor for Cul3-based E3 ligase to regulate proteasomal degradation of Nrf2. *Mol Cell Biol*, 24, 7130-9.

KOLCH, W. 2005. Coordinating ERK/MAPK signalling through scaffolds and inhibitors. *Nat Rev Mol Cell Biol*, 6, 827-37.

KOMANDER, D. & RAPE, M. 2012. The ubiquitin code. *Annu Rev Biochem*, 81, 203-29.

KOMATSU, M., KUROKAWA, H., WAGURI, S., TAGUCHI, K., KOBAYASHI, A., ICHIMURA, Y., SOU, Y. S., UENO, I., SAKAMOTO, A., TONG, K. I., KIM, M., NISHITO, Y., IEMURA, S., NATSUME, T., UENO, T., KOMINAMI, E., MOTOHASHI, H., TANAKA, K. & YAMAMOTO, M. 2010. The selective autophagy substrate p62 activates the stress responsive transcription factor Nrf2 through inactivation of Keap1. *Nat Cell Biol*, 12, 213-23.

KOMATSU, M., WAGURI, S., KOIKE, M., SOU, Y. S., UENO, T., HARA, T., MIZUSHIMA, N., IWATA, J., EZAKI, J., MURATA, S., HAMAZAKI, J., NISHITO, Y., IEMURA, S., NATSUME, T., YANAGAWA, T., UWAYAMA, J., WARABI, E., YOSHIDA, H., ISHII, T., KOBAYASHI, A., YAMAMOTO, M., YUE, Z., UCHIYAMA, Y., KOMINAMI, E. & TANAKA, K. 2007. Homeostatic levels of p62 control cytoplasmic inclusion body formation in autophagy-deficient mice. *Cell*, 131, 1149-63.

KOROLCHUK, V. I., MANSILLA, A., MENZIES, F. M. & RUBINSZTEIN, D. C. 2009. Autophagy inhibition compromises degradation of ubiquitin-proteasome pathway substrates. *Mol Cell*, 33, 517-27.

KOZIKOWSKI, A. P., TAPADAR, S., LUCHINI, D. N., KIM, K. H. & BILLADEAU, D. D. 2008. Use of the nitrile oxide cycloaddition (NOC) reaction for molecular probe generation: a new class of enzyme selective histone deacetylase inhibitors (HDACIs) showing picomolar activity at HDAC6. *J Med Chem*, 51, 4370-3.

KRETSCHMER, C., JONES, D. B., MORRISON, K., SCHLUTER, C., FEIST, W., ULMER, A. J., ARNOLDI, J., MATTHES, J., DIAMANTSTEIN, T., FLAD, H. D. & ET AL. 1990. Tumor necrosis factor alpha and lymphotoxin production in Hodgkin's disease. *Am J Pathol*, 137, 341-51.

KREUZALER, P. A., STANISZEWSKA, A. D., LI, W., OMIÐVAR, N., KEDJOUAR, B., TURKSON, J., POLI, V., FLAVELL, R. A., CLARKSON, R. W. & WATSON, C. J. 2011. Stat3 controls lysosomal-mediated cell death in vivo. *Nat Cell Biol*, 13, 303-9.

KROEMER, G., MARINO, G. & LEVINE, B. 2010. Autophagy and the integrated stress response. *Mol Cell*, 40, 280-93.

KUBE, D., HOLTICK, U., VOCKERODT, M., AHMADI, T., HAIER, B., BEHRMANN, I., HEINRICH, P. C., DIEHL, V. & TESCH, H. 2001. STAT3 is constitutively activated in Hodgkin cell lines. *Blood*, 98, 762-70.

- KUHN, D. J., HUNSUCKER, S. A., CHEN, Q., VOORHEES, P. M., ORLOWSKI, M. & ORLOWSKI, R. Z. 2009. Targeted inhibition of the immunoproteasome is a potent strategy against models of multiple myeloma that overcomes resistance to conventional drugs and nonspecific proteasome inhibitors. *Blood*, 113, 4667-76.
- KUHN, D. J. & ORLOWSKI, R. Z. 2012. The immunoproteasome as a target in hematologic malignancies. *Semin Hematol*, 49, 258-62.
- KULATHU, Y. & KOMANDER, D. 2012. Atypical ubiquitylation - the unexplored world of polyubiquitin beyond Lys48 and Lys63 linkages. *Nat Rev Mol Cell Biol*, 13, 508-23.
- KUPPERS, R. 2009. The biology of Hodgkin's lymphoma. *Nat Rev Cancer*, 9, 15-27.
- KUPPERS, R., ENGERT, A. & HANSMANN, M. L. 2012. Hodgkin lymphoma. *J Clin Invest*, 122, 3439-47.
- KUPPERS, R., KLEIN, U., SCHWERING, I., DISTLER, V., BRAUNINGER, A., CATTORETTI, G., TU, Y., STOLOVITZKY, G. A., CALIFANO, A., HANSMANN, M. L. & DALLA-FAVERA, R. 2003. Identification of Hodgkin and Reed-Sternberg cell-specific genes by gene expression profiling. *J Clin Invest*, 111, 529-37.
- KUPPERS, R., RAJEWSKY, K., ZHAO, M., SIMONS, G., LAUMANN, R., FISCHER, R. & HANSMANN, M. L. 1994. Hodgkin disease: Hodgkin and Reed-Sternberg cells picked from histological sections show clonal immunoglobulin gene rearrangements and appear to be derived from B cells at various stages of development. *Proc Natl Acad Sci U S A*, 91, 10962-6.
- KUPPERS, R. & RE, D. 2007. Nature of Reed-Sternberg and L & H cells, and their molecular biology in Hodgkin lymphoma. In: HOPPE, R. T., MAUCH, P. M., ARMITAGE, J. O., DIEHL, V. & WEISS, L. M. (eds.) *Hodgkin Lymphoma*. Second Edition ed.: Lippincott Williams & Wilkins.
- LAHAT, G., ZHU, Q. S., HUANG, K. L., WANG, S., BOLSHAKOV, S., LIU, J., TORRES, K., LANGLEY, R. R., LAZAR, A. J., HUNG, M. C. & LEV, D. 2010. Vimentin is a novel anti-cancer therapeutic target; insights from in vitro and in vivo mice xenograft studies. *PLoS One*, 5, e10105.
- LAKE, A., SHIELD, L. A., CORDANO, P., CHUI, D. T., OSBORNE, J., CRAE, S., WILSON, K. S., TOSI, S., KNIGHT, S. J., GESK, S., SIEBERT, R., HAY, R. T. & JARRETT, R. F. 2009. Mutations of NFKBIA, encoding I κ B α , are a recurrent finding in classical Hodgkin lymphoma but are not a unifying feature of non-EBV-associated cases. *Int J Cancer*, 125, 1334-42.
- LALANDE, M. E. & MILLER, R. G. 1979. Fluorescence flow analysis of lymphocyte activation using Hoechst 33342 dye. *J Histochem Cytochem*, 27, 394-7.
- LAMARK, T., KIRKIN, V., DIKIC, I. & JOHANSEN, T. 2009. NBR1 and p62 as cargo receptors for selective autophagy of ubiquitinated targets. *Cell Cycle*, 8, 1986-90.
- LAPLANTE, M. & SABATINI, D. M. 2009. mTOR signaling at a glance. *J Cell Sci*, 122, 3589-94.
- LATONEN, L. 2011. Nucleolar aggresomes as counterparts of cytoplasmic aggresomes in proteotoxic stress. Proteasome inhibitors induce nuclear ribonucleoprotein inclusions that accumulate several key factors of neurodegenerative diseases and cancer. *Bioessays*, 33, 386-95.
- LATONEN, L., MOORE, H. M., BAI, B., JAAMAA, S. & LAIHO, M. 2011. Proteasome inhibitors induce nucleolar aggregation of proteasome target proteins and polyadenylated RNA by altering ubiquitin availability. *Oncogene*, 30, 790-805.
- LAWASUT, P., CHAUHAN, D., LAUBACH, J., HAYES, C., FABRE, C., MAGLIO, M., MITSIADES, C., HIDESHIMA, T., ANDERSON, K. C. & RICHARDSON, P. G. 2012. New proteasome inhibitors in myeloma. *Curr Hematol Malig Rep*, 7, 258-66.
- LEE, J. Y., KOGA, H., KAWAGUCHI, Y., TANG, W., WONG, E., GAO, Y. S., PANDEY, U. B., KAUSHIK, S., TRESSE, E., LU, J., TAYLOR, J. P., CUERVO, A. M. & YAO, T. P. 2010. HDAC6 controls autophagosome maturation essential for ubiquitin-selective quality-control autophagy. *EMBO J*, 29, 969-80.
- LEGGETT, D. S., HANNA, J., BORODOVSKY, A., CROSAS, B., SCHMIDT, M., BAKER, R. T., WALZ, T., PLOEGH, H. & FINLEY, D. 2002. Multiple associated proteins regulate proteasome structure and function. *Mol Cell*, 10, 495-507.

- LENG, L., METZ, C. N., FANG, Y., XU, J., DONNELLY, S., BAUGH, J., DELOHERY, T., CHEN, Y., MITCHELL, R. A. & BUCALA, R. 2003. MIF signal transduction initiated by binding to CD74. *J Exp Med*, 197, 1467-76.
- LI, W. W., LI, J. & BAO, J. K. 2012. Microautophagy: lesser-known self-eating. *Cell Mol Life Sci*, 69, 1125-36.
- LI, Z., WOO, C. J., IGLESIAS-USSEL, M. D., RONAI, D. & SCHARFF, M. D. 2004. The generation of antibody diversity through somatic hypermutation and class switch recombination. *Genes Dev*, 18, 1-11.
- LIANG, J., ZUBOVITZ, J., PETROCELLI, T., KOTCHETKOV, R., CONNOR, M. K., HAN, K., LEE, J. H., CIARALLO, S., CATZAVELOS, C., BENISTON, R., FRANSSSEN, E. & SLINGERLAND, J. M. 2002. PKB/Akt phosphorylates p27, impairs nuclear import of p27 and opposes p27-mediated G1 arrest. *Nat Med*, 8, 1153-60.
- LISTER, T. A., CROWTHER, D., SUTCLIFFE, S. B., GLATSTEIN, E., CANELLOS, G. P., YOUNG, R. C., ROSENBERG, S. A., COLTMAN, C. A. & TUBIANA, M. 1989. Report of a committee convened to discuss the evaluation and staging of patients with Hodgkin's disease: Cotswolds meeting. *J Clin Oncol*, 7, 1630-6.
- LIU, C. W., LI, X., THOMPSON, D., WOODING, K., CHANG, T. L., TANG, Z., YU, H., THOMAS, P. J. & DEMARTINO, G. N. 2006. ATP binding and ATP hydrolysis play distinct roles in the function of 26S proteasome. *Mol Cell*, 24, 39-50.
- LIU, M., ANEJA, R., SUN, X., XIE, S., WANG, H., WU, X., DONG, J. T., LI, M., JOSHI, H. C. & ZHOU, J. 2008. Parkin regulates Eg5 expression by Hsp70 ubiquitination-dependent inactivation of c-Jun NH2-terminal kinase. *J Biol Chem*, 283, 35783-8.
- LONGO, D. L. 2013. Treatment of advanced Hodgkin lymphoma: the more things change, the more they stay the same. *J Clin Oncol*, 31, 660-2.
- LUCIANI, M. G., STOPPACCIARO, A., PERI, G., MANTOVANI, A. & RUCO, L. P. 1998. The monocyte chemotactic protein 1 (MCP-1) and interleukin 8 (IL-8) in Hodgkin's disease and in solid tumours. *Mol Pathol*, 51, 273-6.
- LUDERS, J. & STEARNS, T. 2007. Microtubule-organizing centres: a re-evaluation. *Nat Rev Mol Cell Biol*, 8, 161-7.
- LUM, J. J., DEBERARDINIS, R. J. & THOMPSON, C. B. 2005. Autophagy in metazoans: cell survival in the land of plenty. *Nat Rev Mol Cell Biol*, 6, 439-48.
- MA, I. & ALLAN, A. L. 2011. The role of human aldehyde dehydrogenase in normal and cancer stem cells. *Stem Cell Rev*, 7, 292-306.
- MA, Y., VISSER, L., BLOKZIJL, T., HARMS, G., ATAYAR, C., POPPEMA, S. & VAN DEN BERG, A. 2008a. The CD4+CD26- T-cell population in classical Hodgkin's lymphoma displays a distinctive regulatory T-cell profile. *Lab Invest*, 88, 482-90.
- MA, Y., VISSER, L., ROELOFSEN, H., DE VRIES, M., DIEPSTRA, A., VAN IMHOFF, G., VAN DER WAL, T., LUIINGE, M., ALVAREZ-LLAMAS, G., VOS, H., POPPEMA, S., VONK, R. & VAN DEN BERG, A. 2008b. Proteomics analysis of Hodgkin lymphoma: identification of new players involved in the cross-talk between HRS cells and infiltrating lymphocytes. *Blood*, 111, 2339-46.
- MADER, A., BRUDERLEIN, S., WEGENER, S., MELZNER, I., POPOV, S., MULLER-HERMELINK, H. K., BARTH, T. F., VIARDOT, A. & MOLLER, P. 2007. U-HO1, a new cell line derived from a primary refractory classical Hodgkin lymphoma. *Cytogenet Genome Res*, 119, 204-10.
- MAEDA, H., OZAKI, K., HONAGA, S. & NARAMA, I. 1993. Hodgkin's-like lymphoma in a dog. *Zentralbl Veterinarmed A*, 40, 200-4.
- MAGGIO, E. M., VAN DEN BERG, A., VISSER, L., DIEPSTRA, A., KLUIVER, J., EMMENS, R. & POPPEMA, S. 2002. Common and differential chemokine expression patterns in rs cells of NLP, EBV positive and negative classical Hodgkin lymphomas. *Int J Cancer*, 99, 665-72.

- MAGNI, M., SHAMMAH, S., SCHIRO, R., MELLADO, W., DALLA-FAVERA, R. & GIANNI, A. M. 1996. Induction of cyclophosphamide-resistance by aldehyde-dehydrogenase gene transfer. *Blood*, 87, 1097-103.
- MAJEED, S. K. & GOPINATH, C. 1985. Hodgkin's disease-like lesion in a rat. *J Comp Pathol*, 95, 123-6.
- MARAFIOTI, T., HUMMEL, M., FOSS, H. D., LAUMEN, H., KORBJUHN, P., ANAGNOSTOPOULOS, I., LAMMERT, H., DEMEL, G., THEIL, J., WIRTH, T. & STEIN, H. 2000. Hodgkin and reed-sternberg cells represent an expansion of a single clone originating from a germinal center B-cell with functional immunoglobulin gene rearrangements but defective immunoglobulin transcription. *Blood*, 95, 1443-50.
- MARSHALL, N. A., CHRISTIE, L. E., MUNRO, L. R., CULLIGAN, D. J., JOHNSTON, P. W., BARKER, R. N. & VICKERS, M. A. 2004. Immunosuppressive regulatory T cells are abundant in the reactive lymphocytes of Hodgkin lymphoma. *Blood*, 103, 1755-62.
- MARTIN-SUBERO, J. I., GESK, S., HARDER, L., SONOKI, T., TUCKER, P. W., SCHLEGELBERGER, B., GROTE, W., NOVO, F. J., CALASANZ, M. J., HANSMANN, M. L., DYER, M. J. & SIEBERT, R. 2002. Recurrent involvement of the REL and BCL11A loci in classical Hodgkin lymphoma. *Blood*, 99, 1474-7.
- MASUCCI, M. G. 2004. Epstein-Barr virus oncogenesis and the ubiquitin-proteasome system. *Oncogene*, 23, 2107-15.
- MATHAS, S., JANZ, M., HUMMEL, F., HUMMEL, M., WOLLERT-WULF, B., LUSATIS, S., ANAGNOSTOPOULOS, I., LIETZ, A., SIGVARDSSON, M., JUNDT, F., JOHRENS, K., BOMMERT, K., STEIN, H. & DORKEN, B. 2006. Intrinsic inhibition of transcription factor E2A by HLH proteins ABF-1 and Id2 mediates reprogramming of neoplastic B cells in Hodgkin lymphoma. *Nat Immunol*, 7, 207-15.
- MATHAS, S., LIETZ, A., JANZ, M., HINZ, M., JUNDT, F., SCHEIDEREIT, C., BOMMERT, K. & DORKEN, B. 2003. Inhibition of NF-kappaB essentially contributes to arsenic-induced apoptosis. *Blood*, 102, 1028-34.
- MATHEW, R., KARP, C. M., BEAUDOIN, B., VUONG, N., CHEN, G., CHEN, H. Y., BRAY, K., REDDY, A., BHANOT, G., GELINAS, C., DIPOLA, R. S., KARANTZA-WADSWORTH, V. & WHITE, E. 2009. Autophagy suppresses tumorigenesis through elimination of p62. *Cell*, 137, 1062-75.
- MATSUDA, N., SATO, S., SHIBA, K., OKATSU, K., SAISHO, K., GAUTIER, C. A., SOU, Y. S., SAIKI, S., KAWAJIRI, S., SATO, F., KIMURA, M., KOMATSU, M., HATTORI, N. & TANAKA, K. 2010. PINK1 stabilized by mitochondrial depolarization recruits Parkin to damaged mitochondria and activates latent Parkin for mitophagy. *J Cell Biol*, 189, 211-21.
- MATVEEVA, E. A., CHERNOIVANENKO, I. S. & MININ, A. A. 2010. Vimentin intermediate filaments protect mitochondria from oxidative stress. *Biochemistry (Moscow) Supplement Series A: Membrane and Cell Biology*, 4, 321-331.
- MAURO, C., PACIFICO, F., LAVORGNA, A., MELLONE, S., IANNETTI, A., ACQUAVIVA, R., FORMISANO, S., VITO, P. & LEONARDI, A. 2006. ABIN-1 binds to NEMO/IKKgamma and co-operates with A20 in inhibiting NF-kappaB. *J Biol Chem*, 281, 18482-8.
- MAYER, R. J., LOWE, J., LENNOX, G., DOHERTY, F. & LANDON, M. 1989. Intermediate filaments and ubiquitin: a new thread in the understanding of chronic neurodegenerative diseases. *Prog Clin Biol Res*, 317, 809-18.
- MAYO, L. D. & DONNER, D. B. 2001. A phosphatidylinositol 3-kinase/Akt pathway promotes translocation of Mdm2 from the cytoplasm to the nucleus. *Proc Natl Acad Sci U S A*, 98, 11598-603.
- MAZUMDER, A., VESOLE, D. H. & JAGANNATH, S. 2010. Vorinostat plus bortezomib for the treatment of relapsed/refractory multiple myeloma: a case series illustrating utility in clinical practice. *Clin Lymphoma Myeloma Leuk*, 10, 149-51.
- MCCONKEY, D. 2010. Proteasome and HDAC: who's zooming who? *Blood*, 116, 308-9.

- MIZUSHIMA, N., LEVINE, B., CUERVO, A. M. & KLIONSKY, D. J. 2008. Autophagy fights disease through cellular self-digestion. *Nature*, 451, 1069-75.
- MIZUSHIMA, N. & YOSHIMORI, T. 2007. How to interpret LC3 immunoblotting. *Autophagy*, 3, 542-5.
- MIZUSHIMA, N., YOSHIMORI, T. & OHSUMI, Y. 2011. The role of Atg proteins in autophagosome formation. *Annu Rev Cell Dev Biol*, 27, 107-32.
- MOLIN, D., FISCHER, M., XIANG, Z., LARSSON, U., HARVIMA, I., VENGE, P., NILSSON, K., SUNDSTROM, C., ENBLAD, G. & NILSSON, G. 2001. Mast cells express functional CD30 ligand and are the predominant CD30L-positive cells in Hodgkin's disease. *Br J Haematol*, 114, 616-23.
- MOREB, J. S., GABR, A., VARTIKAR, G. R., GOWDA, S., ZUCALI, J. R. & MOHUCZY, D. 2005. Retinoic acid down-regulates aldehyde dehydrogenase and increases cytotoxicity of 4-hydroperoxycyclophosphamide and acetaldehyde. *J Pharmacol Exp Ther*, 312, 339-45.
- MOSCAT, J. & DIAZ-MECO, M. T. 2009a. p62 at the crossroads of autophagy, apoptosis, and cancer. *Cell*, 137, 1001-4.
- MOSCAT, J. & DIAZ-MECO, M. T. 2009b. To aggregate or not to aggregate? A new role for p62. *EMBO Rep*, 10, 804.
- MOSCAT, J. & DIAZ-MECO, M. T. 2012. p62: a versatile multitasker takes on cancer. *Trends Biochem Sci*, 37, 230-6.
- MUQIT, M. M., DAVIDSON, S. M., PAYNE SMITH, M. D., MACCORMAC, L. P., KAHNS, S., JENSEN, P. H., WOOD, N. W. & LATCHMAN, D. S. 2004. Parkin is recruited into aggresomes in a stress-specific manner: over-expression of parkin reduces aggresome formation but can be dissociated from parkin's effect on neuronal survival. *Hum Mol Genet*, 13, 117-35.
- MURATA, S., TAKAHAMA, Y. & TANAKA, K. 2008. Thymoproteasome: probable role in generating positively selecting peptides. *Curr Opin Immunol*, 20, 192-6.
- MURRAY, P. G., QIU, G. H., FU, L., WAITES, E. R., SRIVASTAVA, G., HEYS, D., AGATHANGGELOU, A., LATIF, F., GRUNDY, R. G., MANN, J. R., STARCZYNSKI, J., CROCKER, J., PARKES, S. E., AMBINDER, R. F., YOUNG, L. S. & TAO, Q. 2004. Frequent epigenetic inactivation of the RASSF1A tumor suppressor gene in Hodgkin's lymphoma. *Oncogene*, 23, 1326-31.
- MUSCHEN, M., RAJEWSKY, K., BRAUNINGER, A., BAUR, A. S., OUDEJANS, J. J., ROERS, A., HANSMANN, M. L. & KUPPERS, R. 2000. Rare occurrence of classical Hodgkin's disease as a T cell lymphoma. *J Exp Med*, 191, 387-94.
- NAGARIA, P., ROBERT, C. & RASSOOL, F. V. 2013. DNA double-strand break response in stem cells: mechanisms to maintain genomic integrity. *Biochim Biophys Acta*, 1830, 2345-53.
- NAGEL, S., BUREK, C., VENTURINI, L., SCHERR, M., QUENTMEIER, H., MEYER, C., ROSENWALD, A., DREXLER, H. G. & MACLEOD, R. A. 2007. Comprehensive analysis of homeobox genes in Hodgkin lymphoma cell lines identifies dysregulated expression of HOXB9 mediated via ERK5 signaling and BMI1. *Blood*, 109, 3015-23.
- NAKASHIMA, M., ISHII, Y., WATANABE, M., TOGANO, T., UMEZAWA, K., HIGASHIHARA, M., WATANABE, T. & HORIE, R. 2010. The side population, as a precursor of Hodgkin and Reed-Sternberg cells and a target for nuclear factor-kappaB inhibitors in Hodgkin's lymphoma. *Cancer Sci*, 101, 2490-6.
- NANDA, S. K., VENIGALLA, R. K., ORDUREAU, A., PATTERSON-KANE, J. C., POWELL, D. W., TOTH, R., ARTHUR, J. S. & COHEN, P. 2011. Polyubiquitin binding to ABIN1 is required to prevent autoimmunity. *J Exp Med*, 208, 1215-28.
- NARENDRA, D., KANE, L. A., HAUSER, D. N., FEARNLEY, I. M. & YOULE, R. J. 2010. p62/SQSTM1 is required for Parkin-induced mitochondrial clustering but not mitophagy; VDAC1 is dispensable for both. *Autophagy*, 6, 1090-106.
- NAWROCKI, S. T., CAREW, J. S., PINO, M. S., HIGHSHAW, R. A., ANDTBACKA, R. H., DUNNER, K., JR., PAL, A., BORNMANN, W. G., CHIAO, P. J., HUANG, P., XIONG, H., ABBRUZZESE, J. L. &

- MCCONKEY, D. J. 2006. Aggresome disruption: a novel strategy to enhance bortezomib-induced apoptosis in pancreatic cancer cells. *Cancer Res*, 66, 3773-81.
- NEWCOM, S. R. & GU, L. 1995. Transforming growth factor beta 1 messenger RNA in Reed-Sternberg cells in nodular sclerosing Hodgkin's disease. *J Clin Pathol*, 48, 160-3.
- NEWCOM, S. R., KADIN, M. E. & PHILLIPS, C. 1988. L-428 Reed-Sternberg cells and mononuclear Hodgkin's cells arise from a single cloned mononuclear cell. *Int J Cell Cloning*, 6, 417-31.
- NEZIS, I. P. & STENMARK, H. 2012. p62 at the interface of autophagy, oxidative stress signaling, and cancer. *Antioxid Redox Signal*, 17, 786-93.
- NISHIDA, Y., ARAKAWA, S., FUJITANI, K., YAMAGUCHI, H., MIZUTA, T., KANASEKI, T., KOMATSU, M., OTSU, K., TSUJIMOTO, Y. & SHIMIZU, S. 2009. Discovery of Atg5/Atg7-independent alternative macroautophagy. *Nature*, 461, 654-8.
- O'NIONS, J., TURNER, A., CRAIG, R. & ALLDAY, M. J. 2006. Epstein-Barr virus selectively deregulates DNA damage responses in normal B cells but has no detectable effect on regulation of the tumor suppressor p53. *J Virol*, 80, 12408-13.
- OECKINGHAUS, A. & GHOSH, S. 2009. The NF-kappaB family of transcription factors and its regulation. *Cold Spring Harb Perspect Biol*, 1, a000034.
- OLZMANN, J. A., LI, L., CHUDAIEV, M. V., CHEN, J., PEREZ, F. A., PALMITER, R. D. & CHIN, L. S. 2007. Parkin-mediated K63-linked polyubiquitination targets misfolded DJ-1 to aggresomes via binding to HDAC6. *J Cell Biol*, 178, 1025-38.
- OTTO, C., GIEFING, M., MASSOW, A., VATER, I., GESK, S., SCHLESNER, M., RICHTER, J., KLAPPER, W., HANSMANN, M. L., SIEBERT, R. & KUPPERS, R. 2012. Genetic lesions of the TRAF3 and MAP3K14 genes in classical Hodgkin lymphoma. *Br J Haematol*, 157, 702-8.
- PANDEY, U. B., NIE, Z., BATLEVI, Y., MCCRAY, B. A., RITSON, G. P., NEDELSKY, N. B., SCHWARTZ, S. L., DIPROSPERO, N. A., KNIGHT, M. A., SCHULDINER, O., PADMANABHAN, R., HILD, M., BERRY, D. L., GARZA, D., HUBBERT, C. C., YAO, T. P., BAEHRECKE, E. H. & TAYLOR, J. P. 2007. HDAC6 rescues neurodegeneration and provides an essential link between autophagy and the UPS. *Nature*, 447, 859-63.
- PANKIV, S., CLAUSEN, T. H., LAMARK, T., BRECH, A., BRUUN, J. A., OUTZEN, H., OVERVATN, A., BJORKOY, G. & JOHANSEN, T. 2007. p62/SQSTM1 binds directly to Atg8/LC3 to facilitate degradation of ubiquitinated protein aggregates by autophagy. *J Biol Chem*, 282, 24131-45.
- PANKIV, S., LAMARK, T., BRUUN, J. A., OVERVATN, A., BJORKOY, G. & JOHANSEN, T. 2010. Nucleocytoplasmic shuttling of p62/SQSTM1 and its role in recruitment of nuclear polyubiquitinated proteins to promyelocytic leukemia bodies. *J Biol Chem*, 285, 5941-53.
- PEREZ-GALAN, P., MORA-JENSEN, H., WENIGER, M. A., SHAFFER, A. L., 3RD, RIZZATTI, E. G., CHAPMAN, C. M., MO, C. C., STENNETT, L. S., RADER, C., LIU, P., RAGHAVACHARI, N., STETLER-STEVENSON, M., YUAN, C., PITTALUGA, S., MARIC, I., DUNLEAVY, K. M., WILSON, W. H., STAUDT, L. M. & WIESTNER, A. 2011. Bortezomib resistance in mantle cell lymphoma is associated with plasmacytic differentiation. *Blood*, 117, 542-52.
- PHAN, R. T. & DALLA-FAVERA, R. 2004. The BCL6 proto-oncogene suppresses p53 expression in germinal-centre B cells. *Nature*, 432, 635-9.
- PINTO, A., ALDINUCCI, D., GLOGHINI, A., ZAGONEL, V., DEGAN, M., IMPROTA, S., JUZBASIC, S., TODESCO, M., PERIN, V., GATTEI, V., HERRMANN, F., GRUSS, H. J. & CARBONE, A. 1996. Human eosinophils express functional CD30 ligand and stimulate proliferation of a Hodgkin's disease cell line. *Blood*, 88, 3299-305.
- POHL, C. & JENTSCH, S. 2009. Midbody ring disposal by autophagy is a post-abscission event of cytokinesis. *Nat Cell Biol*, 11, 65-70.
- PONS, E., UPHOFF, C. C. & DREXLER, H. G. 1998. Expression of hepatocyte growth factor and its receptor c-met in human leukemia-lymphoma cell lines. *Leuk Res*, 22, 797-804.
- POOLE, B. & OHKUMA, S. 1981. Effect of weak bases on the intralysosomal pH in mouse peritoneal macrophages. *J Cell Biol*, 90, 665-9.

- POPPEMA, S., BHAN, A. K., REINHERZ, E. L., POSNER, M. R. & SCHLOSSMAN, S. F. 1982. In situ immunologic characterization of cellular constituents in lymph nodes and spleens involved by Hodgkin's disease. *Blood*, 59, 226-32.
- POPPEMA, S., LAI, R., VISSER, L. & YAN, X. J. 1996. CD45 (leucocyte common antigen) expression in T and B lymphocyte subsets. *Leuk Lymphoma*, 20, 217-22.
- QIAN, B. Z. & POLLARD, J. W. 2010. Macrophage diversity enhances tumor progression and metastasis. *Cell*, 141, 39-51.
- RAAPHORST, F. M., VAN KEMENADE, F. J., BLOKZIJL, T., FIERET, E., HAMER, K. M., SATIJN, D. P., OTTE, A. P. & MEIJER, C. J. 2000. Coexpression of BMI-1 and EZH2 polycomb group genes in Reed-Sternberg cells of Hodgkin's disease. *Am J Pathol*, 157, 709-15.
- RAO, L., PEREZ, D. & WHITE, E. 1996. Lamin proteolysis facilitates nuclear events during apoptosis. *J Cell Biol*, 135, 1441-55.
- RAVIKUMAR, B., VACHER, C., BERGER, Z., DAVIES, J. E., LUO, S., OROZ, L. G., SCARAVILLI, F., EASTON, D. F., DUDEN, R., O'KANE, C. J. & RUBINSZTEIN, D. C. 2004. Inhibition of mTOR induces autophagy and reduces toxicity of polyglutamine expansions in fly and mouse models of Huntington disease. *Nat Genet*, 36, 585-95.
- RAWLINGS, J. S., ROSLER, K. M. & HARRISON, D. A. 2004. The JAK/STAT signaling pathway. *J Cell Sci*, 117, 1281-3.
- REN, Y., ZHAO, J. & FENG, J. 2003. Parkin binds to alpha/beta tubulin and increases their ubiquitination and degradation. *J Neurosci*, 23, 3316-24.
- RENNE, C., MARTIN-SUBERO, J. I., EICKERNJAGER, M., HANSMANN, M. L., KUPPERS, R., SIEBERT, R. & BRAUNINGER, A. 2006. Aberrant expression of ID2, a suppressor of B-cell-specific gene expression, in Hodgkin's lymphoma. *Am J Pathol*, 169, 655-64.
- RENNE, C., MINNER, S., KUPPERS, R., HANSMANN, M. L. & BRAUNINGER, A. 2008. Autocrine NGFbeta/TRKA signalling is an important survival factor for Hodgkin lymphoma derived cell lines. *Leuk Res*, 32, 163-7.
- RENNE, C., WILLENBROCK, K., KUPPERS, R., HANSMANN, M. L. & BRAUNINGER, A. 2005. Autocrine- and paracrine-activated receptor tyrosine kinases in classic Hodgkin lymphoma. *Blood*, 105, 4051-9.
- RICHARDSON, P. G., MITSIADES, C., HIDESHIMA, T. & ANDERSON, K. C. 2006. Bortezomib: proteasome inhibition as an effective anticancer therapy. *Annu Rev Med*, 57, 33-47.
- ROCCARO, A. M., SACCO, A., AUJAY, M., NGO, H. T., AZAB, A. K., AZAB, F., QUANG, P., MAISO, P., RUNNELS, J., ANDERSON, K. C., DEMO, S. & GHOBRIAL, I. M. 2010. Selective inhibition of chymotrypsin-like activity of the immunoproteasome and constitutive proteasome in Waldenstrom macroglobulinemia. *Blood*, 115, 4051-60.
- ROCKEL, T. D., STUHLMANN, D. & VON MIKECZ, A. 2005. Proteasomes degrade proteins in focal subdomains of the human cell nucleus. *J Cell Sci*, 118, 5231-42.
- ROTE, K. V. & RECHSTEINER, M. 1983. Degradation of microinjected proteins: effects of lysosomotropic agents and inhibitors of autophagy. *J Cell Physiol*, 116, 103-10.
- RUBIN, D. M., GLICKMAN, M. H., LARSEN, C. N., DHRUVAKUMAR, S. & FINLEY, D. 1998. Active site mutants in the six regulatory particle ATPases reveal multiple roles for ATP in the proteasome. *EMBO J*, 17, 4909-19.
- RUSSELL, R. C., TIAN, Y., YUAN, H., PARK, H. W., CHANG, Y. Y., KIM, J., KIM, H., NEUFELD, T. P., DILLIN, A. & GUAN, K. L. 2013. ULK1 induces autophagy by phosphorylating Beclin-1 and activating VPS34 lipid kinase. *Nat Cell Biol*, 15, 741-50.
- SAEKI, Y. & TANAKA, K. 2012. Assembly and function of the proteasome. *Methods Mol Biol*, 832, 315-37.

- SAMSON, F., DONOSO, J. A., HELLER-BETTINGER, I., WATSON, D. & HIMES, R. H. 1979. Nocodazole action on tubulin assembly, axonal ultrastructure and fast axoplasmic transport. *J Pharmacol Exp Ther*, 208, 411-7.
- SANCHEZ-AGUILERA, A., DELGADO, J., CAMACHO, F. I., SANCHEZ-BEATO, M., SANCHEZ, L., MONTALBAN, C., FRESNO, M. F., MARTIN, C., PIRIS, M. A. & GARCIA, J. F. 2004. Silencing of the p18INK4c gene by promoter hypermethylation in Reed-Sternberg cells in Hodgkin lymphomas. *Blood*, 103, 2351-7.
- SANZ, L., DIAZ-MECO, M. T., NAKANO, H. & MOSCAT, J. 2000. The atypical PKC-interacting protein p62 channels NF-kappaB activation by the IL-1-TRAF6 pathway. *EMBO J*, 19, 1576-86.
- SANZ, L., SANCHEZ, P., LALLENA, M. J., DIAZ-MECO, M. T. & MOSCAT, J. 1999. The interaction of p62 with RIP links the atypical PKCs to NF-kappaB activation. *EMBO J*, 18, 3044-53.
- SCHEEREN, F. A., DIEHL, S. A., SMIT, L. A., BEAUMONT, T., NASPETTI, M., BENDE, R. J., BLOM, B., KARUBE, K., OHSHIMA, K., VAN NOESEL, C. J. & SPITS, H. 2008. IL-21 is expressed in Hodgkin lymphoma and activates STAT5: evidence that activated STAT5 is required for Hodgkin lymphomagenesis. *Blood*, 111, 4706-15.
- SCHERZ-SHOVAL, R., WEIDBERG, H., GONEN, C., WILDER, S., ELAZAR, Z. & OREN, M. 2010. p53-dependent regulation of autophagy protein LC3 supports cancer cell survival under prolonged starvation. *Proc Natl Acad Sci U S A*, 107, 18511-6.
- SCHLIWA, M. & WOHLKE, G. 2003. Molecular motors. *Nature*, 422, 759-65.
- SCHMIDT, A., SCHMITZ, R., GIEFING, M., MARTIN-SUBERO, J. I., GESK, S., VATER, I., MASSOW, A., MAGGIO, E., SCHNEIDER, M., HANSMANN, M. L., SIEBERT, R. & KUPPERS, R. 2010. Rare occurrence of biallelic CYLD gene mutations in classical Hodgkin lymphoma. *Genes Chromosomes Cancer*, 49, 803-9.
- SCHMITZ, R., HANSMANN, M. L., BOHLE, V., MARTIN-SUBERO, J. I., HARTMANN, S., MECHTERSHEIMER, G., KLAPPER, W., VATER, I., GIEFING, M., GESK, S., STANELLE, J., SIEBERT, R. & KUPPERS, R. 2009a. TNFAIP3 (A20) is a tumor suppressor gene in Hodgkin lymphoma and primary mediastinal B cell lymphoma. *J Exp Med*, 206, 981-9.
- SCHMITZ, R., STANELLE, J., HANSMANN, M. L. & KUPPERS, R. 2009b. Pathogenesis of classical and lymphocyte-predominant Hodgkin lymphoma. *Annu Rev Pathol*, 4, 151-74.
- SCHWALLER, J., WENT, P., MATTHES, T., DIRNHOFER, S., DONZE, O., MHAWECH-FAUCEGLIA, P., MYIT, S. & HUARD, B. 2007. Paracrine promotion of tumor development by the TNF ligand APRIL in Hodgkin's Disease. *Leukemia*, 21, 1324-7.
- SCHWERING, I., BRAUNINGER, A., KLEIN, U., JUNGNIKEL, B., TINGUELY, M., DIEHL, V., HANSMANN, M. L., DALLA-FAVERA, R., RAJEWSKY, K. & KUPPERS, R. 2003. Loss of the B-lineage-specific gene expression program in Hodgkin and Reed-Sternberg cells of Hodgkin lymphoma. *Blood*, 101, 1505-12.
- SEIBENHENER, M. L., BABU, J. R., GEETHA, T., WONG, H. C., KRISHNA, N. R. & WOOTEN, M. W. 2004. Sequestosome 1/p62 is a polyubiquitin chain binding protein involved in ubiquitin proteasome degradation. *Mol Cell Biol*, 24, 8055-68.
- SEIBENHENER, M. L., GEETHA, T. & WOOTEN, M. W. 2007. Sequestosome 1/p62--more than just a scaffold. *FEBS Lett*, 581, 175-9.
- SEIFERT, U., BIALY, L. P., EBSTEIN, F., BECH-OTSCHIR, D., VOIGT, A., SCHROTER, F., PROZOROVSKI, T., LANGE, N., STEFFEN, J., RIEGER, M., KUCKELKORN, U., AKTAS, O., KLOETZEL, P. M. & KRUGER, E. 2010. Immunoproteasomes preserve protein homeostasis upon interferon-induced oxidative stress. *Cell*, 142, 613-24.
- SEITZ, V., HUMMEL, M., MARAFIOTI, T., ANAGNOSTOPOULOS, I., ASSAF, C. & STEIN, H. 2000. Detection of clonal T-cell receptor gamma-chain gene rearrangements in Reed-Sternberg cells of classic Hodgkin disease. *Blood*, 95, 3020-4.
- SEITZ, V., THOMAS, P. E., ZIMMERMANN, K., PAUL, U., EHLERS, A., JOOSTEN, M., DIMITROVA, L., LENZE, D., SOMMERFELD, A., OKER, E., LESER, U., STEIN, H. & HUMMEL, M. 2011. Classical

- Hodgkin's lymphoma shows epigenetic features of abortive plasma cell differentiation. *Haematologica*, 96, 863-70.
- SENER, P. D. & SIEVERS, E. L. 2012. The discovery and development of brentuximab vedotin for use in relapsed Hodgkin lymphoma and systemic anaplastic large cell lymphoma. *Nat Biotechnol*, 30, 631-7.
- SHAFER, J. A., CRUZ, C. R., LEEN, A. M., KU, S., LU, A., ROUSSEAU, A., HESLOP, H. E., ROONEY, C. M., BOLLARD, C. M. & FOSTER, A. E. 2010. Antigen-specific cytotoxic T lymphocytes can target chemoresistant side-population tumor cells in Hodgkin lymphoma. *Leuk Lymphoma*, 51, 870-80.
- SHI, X., ZHANG, Y., ZHENG, J. & PAN, J. 2012. Reactive oxygen species in cancer stem cells. *Antioxid Redox Signal*, 16, 1215-28.
- SKINNIDER, B. F., ELIA, A. J., GASCOYNE, R. D., PATTERSON, B., TRUMPER, L., KAPP, U. & MAK, T. W. 2002. Signal transducer and activator of transcription 6 is frequently activated in Hodgkin and Reed-Sternberg cells of Hodgkin lymphoma. *Blood*, 99, 618-26.
- SKINNIDER, B. F. & MAK, T. W. 2002. The role of cytokines in classical Hodgkin lymphoma. *Blood*, 99, 4283-97.
- SKULACHEV, V. P. 2001. Mitochondrial filaments and clusters as intracellular power-transmitting cables. *Trends Biochem Sci*, 26, 23-9.
- SMITH, D. A. & BARKER, I. K. 1983. Four cases of Hodgkin's disease in striped skunks (*Mephitis mephitis*). *Vet Pathol*, 20, 223-9.
- ST-GERMAIN, J. R., CHEN, J. & LI, Q. 2008. Involvement of PML nuclear bodies in CBP degradation through the ubiquitin-proteasome pathway. *Epigenetics*, 3, 342-9.
- STANELLE, J., DORING, C., HANSMANN, M. L. & KUPPERS, R. 2010. Mechanisms of aberrant GATA3 expression in classical Hodgkin lymphoma and its consequences for the cytokine profile of Hodgkin and Reed/Sternberg cells. *Blood*, 116, 4202-11.
- STEIDL, C., CONNORS, J. M. & GASCOYNE, R. D. 2011a. Molecular pathogenesis of Hodgkin's lymphoma: increasing evidence of the importance of the microenvironment. *J Clin Oncol*, 29, 1812-26.
- STEIDL, C., LEE, T., SHAH, S. P., FARINHA, P., HAN, G., NAYAR, T., DELANEY, A., JONES, S. J., IQBAL, J., WEISENBURGER, D. D., BAST, M. A., ROSENWALD, A., MULLER-HERMELINK, H. K., RIMSZA, L. M., CAMPO, E., DELABIE, J., BRAZIEL, R. M., COOK, J. R., TUBBS, R. R., JAFFE, E. S., LENZ, G., CONNORS, J. M., STAUDT, L. M., CHAN, W. C. & GASCOYNE, R. D. 2010a. Tumor-associated macrophages and survival in classic Hodgkin's lymphoma. *N Engl J Med*, 362, 875-85.
- STEIDL, C., SHAH, S. P., WOOLCOCK, B. W., RUI, L., KAWAHARA, M., FARINHA, P., JOHNSON, N. A., ZHAO, Y., TELENIUS, A., NERIAH, S. B., MCPHERSON, A., MEISSNER, B., OKOYE, U. C., DIEPSTRA, A., VAN DEN BERG, A., SUN, M., LEUNG, G., JONES, S. J., CONNORS, J. M., HUNTSMAN, D. G., SAVAGE, K. J., RIMSZA, L. M., HORSMAN, D. E., STAUDT, L. M., STEIDL, U., MARRA, M. A. & GASCOYNE, R. D. 2011b. MHC class II transactivator CIITA is a recurrent gene fusion partner in lymphoid cancers. *Nature*, 471, 377-81.
- STEIDL, C., TELENIUS, A., SHAH, S. P., FARINHA, P., BARCLAY, L., BOYLE, M., CONNORS, J. M., HORSMAN, D. E. & GASCOYNE, R. D. 2010b. Genome-wide copy number analysis of Hodgkin Reed-Sternberg cells identifies recurrent imbalances with correlations to treatment outcome. *Blood*, 116, 418-27.
- STEIN, H., MARAFIOTI, T., FOSS, H. D., LAUMEN, H., HUMMEL, M., ANAGNOSTOPOULOS, I., WIRTH, T., DEMEL, G. & FALINI, B. 2001. Down-regulation of BOB.1/OBF.1 and Oct2 in classical Hodgkin disease but not in lymphocyte predominant Hodgkin disease correlates with immunoglobulin transcription. *Blood*, 97, 496-501.
- STEIN, R., QU, Z., CARDILLO, T. M., CHEN, S., ROSARIO, A., HORAK, I. D., HANSEN, H. J. & GOLDENBERG, D. M. 2004. Antiproliferative activity of a humanized anti-CD74 monoclonal antibody, hLL1, on B-cell malignancies. *Blood*, 104, 3705-11.

- STRAUSS, S. J., MAHARAJ, L., HOARE, S., JOHNSON, P. W., RADFORD, J. A., VINNECOMBE, S., MILLARD, L., ROHATINER, A., BORAL, A., TREHU, E., SCHENKEIN, D., BALKWILL, F., JOEL, S. P. & LISTER, T. A. 2006. Bortezomib therapy in patients with relapsed or refractory lymphoma: potential correlation of in vitro sensitivity and tumor necrosis factor alpha response with clinical activity. *J Clin Oncol*, 24, 2105-12.
- SUI, X., CHEN, R., WANG, Z., HUANG, Z., KONG, N., ZHANG, M., HAN, W., LOU, F., YANG, J., ZHANG, Q., WANG, X., HE, C. & PAN, H. 2013. Autophagy and chemotherapy resistance: a promising therapeutic target for cancer treatment. *Cell Death Dis*, 4, e838.
- SUN, X., LIU, M., HAO, J., LI, D., LUO, Y., WANG, X., YANG, Y., LI, F., SHUI, W., CHEN, Q. & ZHOU, J. 2013. Parkin deficiency contributes to pancreatic tumorigenesis by inducing spindle multipolarity and misorientation. *Cell Cycle*, 12, 1133-41.
- SUZUKI, E., DEMO, S., DEU, E., KEATS, J., ARASTU-KAPUR, S., BERGSAGEL, P. L., BENNETT, M. K. & KIRK, C. J. 2011. Molecular mechanisms of bortezomib resistant adenocarcinoma cells. *PLoS One*, 6, e27996.
- SUZUKI, K., KIRISAKO, T., KAMADA, Y., MIZUSHIMA, N., NODA, T. & OHSUMI, Y. 2001. The pre-autophagosomal structure organized by concerted functions of APG genes is essential for autophagosome formation. *EMBO J*, 20, 5971-81.
- SZETO, J., KANIUK, N. A., CANADIEN, V., NISMAN, R., MIZUSHIMA, N., YOSHIMORI, T., BAZETT-JONES, D. P. & BRUMELL, J. H. 2006. ALIS are stress-induced protein storage compartments for substrates of the proteasome and autophagy. *Autophagy*, 2, 189-99.
- TABNER, B. J., EL-AGNAF, O. M., GERMAN, M. J., FULLWOOD, N. J. & ALLSOP, D. 2005. Protein aggregation, metals and oxidative stress in neurodegenerative diseases. *Biochem Soc Trans*, 33, 1082-6.
- TAGUCHI, K., MOTOHASHI, H. & YAMAMOTO, M. 2011. Molecular mechanisms of the Keap1-Nrf2 pathway in stress response and cancer evolution. *Genes Cells*, 16, 123-40.
- TAKAHASHI, J., FUJIGASAKI, H., IWABUCHI, K., BRUNI, A. C., UCHIHARA, T., EL HACHIMI, K. H., STEVANIN, G., DURR, A., LEBRE, A. S., TROTTIER, Y., DE THE, H., TANAKA, J., HAUW, J. J., DUYCKAERTS, C. & BRICE, A. 2003. PML nuclear bodies and neuronal intranuclear inclusion in polyglutamine diseases. *Neurobiol Dis*, 13, 230-7.
- TAN, J. M., WONG, E. S., KIRKPATRICK, D. S., PLETNIKOVA, O., KO, H. S., TAY, S. P., HO, M. W., TRONCOSO, J., GYGI, S. P., LEE, M. K., DAWSON, V. L., DAWSON, T. M. & LIM, K. L. 2008. Lysine 63-linked ubiquitination promotes the formation and autophagic clearance of protein inclusions associated with neurodegenerative diseases. *Hum Mol Genet*, 17, 431-9.
- TEDELIND, S., POLIAKOVA, K., VALETA, A., HUNEGNAW, R., YEMANABERHAN, E. L., HELDIN, N. E., KUREBAYASHI, J., WEBER, E., KOPITAR-JERALA, N., TURK, B., BOGYO, M. & BRIX, K. 2010. Nuclear cysteine cathepsin variants in thyroid carcinoma cells. *Biol Chem*, 391, 923-35.
- TELFORD, W. G., BRADFORD, J., GODFREY, W., ROBEY, R. W. & BATES, S. E. 2007. Side population analysis using a violet-excited cell-permeable DNA binding dye. *Stem Cells*, 25, 1029-36.
- TEOFILI, L., DI FEBBO, A. L., PIERCONTI, F., MAGGIANO, N., BENDANDI, M., RUTELLA, S., CINGOLANI, A., DI RENZO, N., MUSTO, P., PILERI, S., LEONE, G. & LARocca, L. M. 2001. Expression of the c-met proto-oncogene and its ligand, hepatocyte growth factor, in Hodgkin disease. *Blood*, 97, 1063-9.
- TERUYA-FELDSTEIN, J., JAFFE, E. S., BURD, P. R., KINGMA, D. W., SETSUDA, J. E. & TOSATO, G. 1999. Differential chemokine expression in tissues involved by Hodgkin's disease: direct correlation of eotaxin expression and tissue eosinophilia. *Blood*, 93, 2463-70.
- THROWER, J. S., HOFFMAN, L., RECHSTEINER, M. & PICKART, C. M. 2000. Recognition of the polyubiquitin proteolytic signal. *EMBO J*, 19, 94-102.
- TORLAKOVIC, E., TIERENS, A., DANG, H. D. & DELABIE, J. 2001. The transcription factor PU.1, necessary for B-cell development is expressed in lymphocyte predominance, but not classical Hodgkin's disease. *Am J Pathol*, 159, 1807-14.

- TOTHOVA, Z., KOLLIPARA, R., HUNTLY, B. J., LEE, B. H., CASTRILLON, D. H., CULLEN, D. E., MCDOWELL, E. P., LAZO-KALLANIAN, S., WILLIAMS, I. R., SEARS, C., ARMSTRONG, S. A., PASSEGUE, E., DEPINHO, R. A. & GILLILAND, D. G. 2007. FoxOs are critical mediators of hematopoietic stem cell resistance to physiologic oxidative stress. *Cell*, 128, 325-39.
- TRINCZEK, B., EBNETH, A., MANDELKOW, E. M. & MANDELKOW, E. 1999. Tau regulates the attachment/detachment but not the speed of motors in microtubule-dependent transport of single vesicles and organelles. *J Cell Sci*, 112 (Pt 14), 2355-67.
- TU, C., ORTEGA-CAVA, C. F., CHEN, G., FERNANDES, N. D., CAVALLO-MEDVED, D., SLOANE, B. F., BAND, V. & BAND, H. 2008. Lysosomal cathepsin B participates in the podosome-mediated extracellular matrix degradation and invasion via secreted lysosomes in v-Src fibroblasts. *Cancer Res*, 68, 9147-56.
- TYEDMERS, J., MOGK, A. & BUKAU, B. 2010. Cellular strategies for controlling protein aggregation. *Nat Rev Mol Cell Biol*, 11, 777-88.
- USHMOROV, A., LEITHAUSER, F., SAKK, O., WEINHAUSEL, A., POPOV, S. W., MOLLER, P. & WIRTH, T. 2006. Epigenetic processes play a major role in B-cell-specific gene silencing in classical Hodgkin lymphoma. *Blood*, 107, 2493-500.
- VAN DEN BERG, A., VISSER, L. & POPPEMA, S. 1999. High expression of the CC chemokine TARC in Reed-Sternberg cells. A possible explanation for the characteristic T-cell infiltrate in Hodgkin's lymphoma. *Am J Pathol*, 154, 1685-91.
- VAN DEVENTER, S. & NEEFJES, J. 2010. The Immunoproteasome Cleans up after Inflammation. *Cell*, 142, 517-8.
- VAN ROOSBROECK, K., COX, L., TOUSSEYN, T., LAHORTIGA, I., GIELEN, O., CAUWELIER, B., DE PAEPE, P., VERHOEF, G., MARYNEN, P., VANDENBERGHE, P., DE WOLF-PEETERS, C., COOLS, J. & WLODARSKA, I. 2011. JAK2 rearrangements, including the novel SEC31A-JAK2 fusion, are recurrent in classical Hodgkin lymphoma. *Blood*, 117, 4056-64.
- VANDEN BERGHE, W., SABBE, L., KAILEH, M., HAEGEMAN, G. & HEYNINCK, K. 2012. Molecular insight in the multifunctional activities of Withaferin A. *Biochem Pharmacol*, 84, 1282-91.
- VERDEL, A., SEIGNEURIN-BERNY, D., FAURE, A. K., EDDAHBI, M., KHOCHBIN, S. & NONCHEV, S. 2003. HDAC6-induced premature chromatin compaction in mouse oocytes and fertilised eggs. *Zygote*, 11, 323-8.
- VISVADER, J. E. & LINDEMAN, G. J. 2012. Cancer stem cells: current status and evolving complexities. *Cell Stem Cell*, 10, 717-28.
- VOCKERODT, M., SOARES, M., KANZLER, H., KUPPERS, R., KUBE, D., HANSMANN, M. L., DIEHL, V. & TESCH, H. 1998. Detection of clonal Hodgkin and Reed-Sternberg cells with identical somatically mutated and rearranged VH genes in different biopsies in relapsed Hodgkin's disease. *Blood*, 92, 2899-907.
- VON WASIELEWSKI, R., SETH, S., FRANKLIN, J., FISCHER, R., HUBNER, K., HANSMANN, M. L., DIEHL, V. & GEORGII, A. 2000. Tissue eosinophilia correlates strongly with poor prognosis in nodular sclerosing Hodgkin's disease, allowing for known prognostic factors. *Blood*, 95, 1207-13.
- WAHL, A. F., KLUSSMAN, K., THOMPSON, J. D., CHEN, J. H., FRANCISCO, L. V., RISDON, G., CHACE, D. F., SIEGALL, C. B. & FRANCISCO, J. A. 2002. The anti-CD30 monoclonal antibody SGN-30 promotes growth arrest and DNA fragmentation in vitro and affects antitumor activity in models of Hodgkin's disease. *Cancer Res*, 62, 3736-42.
- WALTON, R. M. & HENDRICK, M. J. 2001. Feline Hodgkin's-like lymphoma: 20 cases (1992-1999). *Vet Pathol*, 38, 504-11.
- WANG, H., LIU, B., ZHANG, C., PENG, G., LIU, M., LI, D., GU, F., CHEN, Q., DONG, J. T., FU, L. & ZHOU, J. 2009. Parkin regulates paclitaxel sensitivity in breast cancer via a microtubule-dependent mechanism. *J Pathol*, 218, 76-85.

- WANG, L., XIANG, S., WILLIAMS, K. A., DONG, H., BAI, W., NICOSIA, S. V., KHOCHBIN, S., BEPLER, G. & ZHANG, X. 2012. Depletion of HDAC6 enhances cisplatin-induced DNA damage and apoptosis in non-small cell lung cancer cells. *PLoS One*, 7, e44265.
- WEBB, J. L., RAVIKUMAR, B., ATKINS, J., SKEPPER, J. N. & RUBINSZTEIN, D. C. 2003. Alpha-Synuclein is degraded by both autophagy and the proteasome. *J Biol Chem*, 278, 25009-13.
- WELCHMAN, R. L., GORDON, C. & MAYER, R. J. 2005. Ubiquitin and ubiquitin-like proteins as multifunctional signals. *Nat Rev Mol Cell Biol*, 6, 599-609.
- WELLE, M. M., BLEY, C. R., HOWARD, J. & RUFENACHT, S. 2008. Canine mast cell tumours: a review of the pathogenesis, clinical features, pathology and treatment. *Vet Dermatol*, 19, 321-39.
- WENIGER, M. A., MELZNER, I., MENZ, C. K., WEGENER, S., BUCUR, A. J., DORSCH, K., MATTFELDT, T., BARTH, T. F. & MOLLER, P. 2006. Mutations of the tumor suppressor gene SOCS-1 in classical Hodgkin lymphoma are frequent and associated with nuclear phospho-STAT5 accumulation. *Oncogene*, 25, 2679-84.
- WHITE, E. 2012. Deconvoluting the context-dependent role for autophagy in cancer. *Nat Rev Cancer*, 12, 401-10.
- WILLIAMS, L. R. & TAYLOR, G. S. 2012. Autophagy and immunity - insights from human herpesviruses. *Front Immunol*, 3, 170.
- WONG, E. S., TAN, J. M., SOONG, W. E., HUSSEIN, K., NUKINA, N., DAWSON, V. L., DAWSON, T. M., CUERVO, A. M. & LIM, K. L. 2008. Autophagy-mediated clearance of aggresomes is not a universal phenomenon. *Hum Mol Genet*, 17, 2570-82.
- WOOTEN, M. W., GEETHA, T., BABU, J. R., SEIBENHENER, M. L., PENG, J., COX, N., DIAZ-MECO, M. T. & MOSCAT, J. 2008. Essential role of sequestosome 1/p62 in regulating accumulation of Lys63-ubiquitinated proteins. *J Biol Chem*, 283, 6783-9.
- WOOTEN, M. W., GEETHA, T., SEIBENHENER, M. L., BABU, J. R., DIAZ-MECO, M. T. & MOSCAT, J. 2005. The p62 scaffold regulates nerve growth factor-induced NF-kappaB activation by influencing TRAF6 polyubiquitination. *J Biol Chem*, 280, 35625-9.
- YAMAMOTO, A., TAGAWA, Y., YOSHIMORI, T., MORIYAMA, Y., MASAKI, R. & TASHIRO, Y. 1998. Bafilomycin A1 prevents maturation of autophagic vacuoles by inhibiting fusion between autophagosomes and lysosomes in rat hepatoma cell line, H-4-II-E cells. *Cell Struct Funct*, 23, 33-42.
- YAMAMOTO, R., NISHIKORI, M., KITAWAKI, T., SAKAI, T., HISHIZAWA, M., TASHIMA, M., KONDO, T., OHMORI, K., KURATA, M., HAYASHI, T. & UCHIYAMA, T. 2008. PD-1-PD-1 ligand interaction contributes to immunosuppressive microenvironment of Hodgkin lymphoma. *Blood*, 111, 3220-4.
- YANG, F., JIANG, Q., ZHAO, J., REN, Y., SUTTON, M. D. & FENG, J. 2005. Parkin stabilizes microtubules through strong binding mediated by three independent domains. *J Biol Chem*, 280, 17154-62.
- YANG, H., SHI, G. & DOU, Q. P. 2007. The tumor proteasome is a primary target for the natural anticancer compound Withaferin A isolated from "Indian winter cherry". *Mol Pharmacol*, 71, 426-37.
- YAO, T. & COHEN, R. E. 2002. A cryptic protease couples deubiquitination and degradation by the proteasome. *Nature*, 419, 403-7.
- YONEZAWA, M., NAKAMINE, H., TANAKA, T. & MIYAJI, T. 1989. Hodgkin's disease in a killer whale (*Orcinus orca*). *J Comp Pathol*, 100, 203-7.
- YOUNES, A., BARTLETT, N. L., LEONARD, J. P., KENNEDY, D. A., LYNCH, C. M., SIEVERS, E. L. & FORERO-TORRES, A. 2010. Brentuximab vedotin (SGN-35) for relapsed CD30-positive lymphomas. *N Engl J Med*, 363, 1812-21.
- YOUNES, A., OKI, Y., BOCIEK, R. G., KURUVILLA, J., FANALE, M., NEELAPU, S., COPELAND, A., BUGLIO, D., GALAL, A., BESTERMAN, J., LI, Z., DROUIN, M., PATTERSON, T., WARD, M. R.,

- PAULUS, J. K., JI, Y., MEDEIROS, L. J. & MARTELL, R. E. 2011. Mocetinostat for relapsed classical Hodgkin's lymphoma: an open-label, single-arm, phase 2 trial. *Lancet Oncol*, 12, 1222-8.
- YOUNES, A., OKI, Y., MCLAUGHLIN, P., COPELAND, A. R., GOY, A., PRO, B., FENG, L., YUAN, Y., CHUANG, H. H., MACAPINLAC, H. A., HAGEMEISTER, F., ROMAGUERA, J., SAMANIEGO, F., FANALE, M. A., DABAJA, B. S., RODRIGUEZ, M. A., DANG, N., KWAK, L. W., NEELAPU, S. S. & FAYAD, L. E. 2012a. Phase 2 study of rituximab plus ABVD in patients with newly diagnosed classical Hodgkin lymphoma. *Blood*, 119, 4123-8.
- YOUNES, A., PRO, B. & FAYAD, L. 2006. Experience with bortezomib for the treatment of patients with relapsed classical Hodgkin lymphoma. *Blood*, 107, 1731-2.
- YOUNES, A., SUREDA, A., BEN-YEHUDA, D., ZINZANI, P. L., ONG, T. C., PRINCE, H. M., HARRISON, S. J., KIRSCHBAUM, M., JOHNSTON, P., GALLAGHER, J., LE CORRE, C., SHEN, A. & ENGERT, A. 2012b. Panobinostat in patients with relapsed/refractory Hodgkin's lymphoma after autologous stem-cell transplantation: results of a phase II study. *J Clin Oncol*, 30, 2197-203.
- YOUNG, A. R., NARITA, M., FERREIRA, M., KIRSCHNER, K., SADAIE, M., DAROT, J. F., TAVARE, S., ARAKAWA, S., SHIMIZU, S. & WATT, F. M. 2009. Autophagy mediates the mitotic senescence transition. *Genes Dev*, 23, 798-803.
- YU, Y., DUMOLLARD, R., ROSSBACH, A., LAI, F. A. & SWANN, K. 2010. Redistribution of mitochondria leads to bursts of ATP production during spontaneous mouse oocyte maturation. *J Cell Physiol*, 224, 672-80.
- YUSEFF, M. I., REVERSAT, A., LANKAR, D., DIAZ, J., FANGET, I., PIEROBON, P., RANDRIAN, V., LAROCLETTE, N., VASCOTTO, F., DESDOUETS, C., JAUFFRED, B., BELLAICHE, Y., GASMAN, S., DARCHEN, F., DESNOS, C. & LENNON-DUMENIL, A. M. 2011. Polarized secretion of lysosomes at the B cell synapse couples antigen extraction to processing and presentation. *Immunity*, 35, 361-74.
- ZATLOUKAL, K., STUMPTNER, C., FUCHSBICHLER, A., HEID, H., SCHNOELZER, M., KENNER, L., KLEINERT, R., PRINZ, M., AGUZZI, A. & DENK, H. 2002. p62 is a common component of cytoplasmic inclusions in protein aggregation diseases. *Am J Pathol*, 160, 255-63.
- ZHANG, W., PENG, G., LIN, S. Y. & ZHANG, P. 2011. DNA damage response is suppressed by the high cyclin-dependent kinase 1 activity in mitotic mammalian cells. *J Biol Chem*, 286, 35899-905.
- ZHAO, J., REN, Y., JIANG, Q. & FENG, J. 2003. Parkin is recruited to the centrosome in response to inhibition of proteasomes. *J Cell Sci*, 116, 4011-9.
- ZHENG, B., FIUMARA, P., LI, Y. V., GEORGAKIS, G., SNELL, V., YOUNES, M., VAUTHEY, J. N., CARBONE, A. & YOUNES, A. 2003. MEK/ERK pathway is aberrantly active in Hodgkin disease: a signaling pathway shared by CD30, CD40, and RANK that regulates cell proliferation and survival. *Blood*, 102, 1019-27.
- ZHENG, B., GEORGAKIS, G. V., LI, Y., BHARTI, A., MCCONKEY, D., AGGARWAL, B. B. & YOUNES, A. 2004. Induction of cell cycle arrest and apoptosis by the proteasome inhibitor PS-341 in Hodgkin disease cell lines is independent of inhibitor of nuclear factor-kappaB mutations or activation of the CD30, CD40, and RANK receptors. *Clin Cancer Res*, 10, 3207-15.
- ZHOU, B. P., LIAO, Y., XIA, W., SPOHN, B., LEE, M. H. & HUNG, M. C. 2001. Cytoplasmic localization of p21Cip1/WAF1 by Akt-induced phosphorylation in HER-2/neu-overexpressing cells. *Nat Cell Biol*, 3, 245-52.
- ZHOU, W. & BAO, S. 2013. PML-mediated signaling and its role in cancer stem cells. *Oncogene*.
- ZHOU, Y., KIM, J., YUAN, X. & BRAUN, T. 2011. Epigenetic modifications of stem cells: a paradigm for the control of cardiac progenitor cells. *Circ Res*, 109, 1067-81.